Sea surface distribution of nitrous oxide and methane in European shelf seas and the Atlantic Ocean

Natalie Johanna Wager

Thesis submitted for the degree of Doctor of Philosophy

University of East Anglia

School of Environmental Sciences

September, 2015

Abstract

Human activities, including intensive agriculture and fertiliser use, are altering the radiative forcing on the planet by increasing the amount of the climatically active gases, nitrous oxide (N_2O) and methane (CH_4), in the troposphere. There are currently uncertainties in quantifying the natural sources and sinks of N_2O and CH_4 in the marine environment.

This thesis presents high-resolution surface-ocean and atmospheric data for N_2O, CH_4, CO_2 and CO, collected using Integrated Cavity Output Spectrometry (ICOS, *Los Gatos*) during the D366 (NW European shelf seas, June/ July, 2011) and Atlantic Meridional Transect 22 (Atlantic Ocean, October/November, 2012) cruises. Interpretation of the N_2O and CH_4 datasets revealed that shelf seas produced a greater atmospheric source of N_2O and CH_4 than the open ocean. Shelf sea surface waters were slightly supersaturated in N_2O at 102 %, but undersaturated in the open ocean at 97 %, acting as slight atmospheric sink. The cause of undersaturation in surface waters is unclear, but may be attributed to seasonal cooling and a potential microbial N_2O consumption pathway. The dominant pathway for N_2O formation in the open ocean is nitrification. Both nitrification and denitrification may be important in the production of N_2O in shelf seas. Vertical mixing processes and upwelling influence the surface concentration of N_2O. Surface waters in the shelf seas and the Atlantic Ocean were supersaturated in CH_4 at 118 % and 107 %. Methanogenesis, which occurs within anoxic sediments of shelf seas, rivers and estuaries, was the dominant source of CH_4 during D366. Freshwater inputs that were supersaturated in CH_4, and a fully mixed water column vertically mixing CH_4 from marine sediments, influenced the surface concentration of CH_4 in shelf seas. In the open ocean, methanogenesis occurs in-situ in the surface waters. Seasons influenced the surface concentration and saturation of N_2O and CH_4, with sea surface temperatures, seasonal effects, and stratification affecting these gases.

List of figures

Figure 1. 7: The major forms and transformations of nitrogen in the marine environment. The forms of nitrogen are plotted with their oxidation state. The processes in grey only occur in anoxic environments (Gruber, 2008).

Figure 1. 8: Longhurst provinces in the Atlantic Ocean. North Atlantic Drift Province (NADR), Gulf Stream Province (GFST), North Atlantic Subtropical Gyral Province (NAS), Eastern (Canary) Coastal Province (CNRY), North Atlantic Tropical Gyral Province (NATR), Western Tropical Atlantic Province (WTRA), South Atlantic Gyral province (SATL), South Subtropical Convergence Zone (SSTC) and Subantarctic Water Ring Province (SANT).

Figure 1. 9: Processes influencing the surface water concentration of N_2O. The mixed layer source may arise from in-situ nitrification.

Figure 1. 10: Globally averaged CH_4 dry mole fractions measured in the atmosphere, from University College London (UCL) (green; four values per year, except prior to 1984, when they are of lower and varying frequency), AGAGE (red; monthly), and NOAA/ERSL/GMD (blue; quasi-weekly). Figure from Hartmann et al., (2013).

Figure 1. 11: The excess CH_4 saturation (%). Excess CH_4 is defined here as the CH_4 saturation minus 100 % and is displayed with depth (m) in the Atlantic Ocean along 7°30' N (plus) and 4°30' S (cross). From Oudot et al. (2002).

Figure 2. 1: The D366 cruise track. The colour bar displays time in ordinal date. The contour lines show 1000m, 2000m, 3000m and 4000m depths.

Figure 2. 2: Cruise track for AMT22 from Southampton, UK to Punta Arenas, Chile.

Figure 2. 3: The set-up of the ICOS instruments on both cruises to measure seawater and atmospheric moist mole fractions of CO_2, N_2O, CH_4 and CO, as well as the calibration standards. Adapted from Grefe and Kaiser (2014).

Figure 2. 4: Mean measurements of the N_2O reference standard 25B22 (black dots) during the D366 OA cruise. Different interpolation methods were tested: linear (magenta), Spline (green) and pChip (cyan) to visualise the most accurate interpolation method to fit the data.

Figure 2. 5: Measurement of the two water reservoirs with different concentrations of a) N_2O, b) CO, c) CO_2 and d) CH_4. The x_{min} and x_{max} were calculated from the decay of N_2O and CO and the growth of CO_2 and CH_4 over time.

Figure 2. 6: Temperature calibration of the Pt100 temperature probes for the D366 cruise. A) Probe 1 pre-cruise calibration (temperature=9.7072*voltage-0.62219, R^2 = 0.99997), B) Probe 1 post-cruise calibration (R^2 = 0.99959), C) Probe 3 pre-cruise calibration (R^2 = 0.99992), and D) Probe 3 post-cruise calibration (R^2 = 0.99965). The red line is the line of best fit.

Figure 2. 7: Temperature calibration of the Pt100 temperature probes using a calibrated mercury thermometer for the known measurements for the AMT22 cruise. A) Probe A pre-cruise calibration (R^2 = 0.99919), B) Probe A post-cruise calibration (R^2 = 0.99996), C) Probe B pre-cruise calibration (R^2 = 0.99952) and D) Probe B post-cruise calibration (R^2 = 1.00000). The red line is the line of best fit.

Figure 2. 8: Atmospheric mean values (N=240) for each atmospheric run during the D366 cruise. Red is un-calibrated data. If the data was corrected using the four ship standards the offset lowers the values beyond what would be expected (blue). If an offset of +2.5 nmol mol^{-1} (magenta) is added to all data points to compensate for the lowering effect caused by the calibration, the values are more

inline with the atmospheric values of N_2O from Mace Head (Ireland) and Summit (Denmark).

Figure 2. 9: The N_2O atmospheric mean dry mole fraction of 324.28 ± 1 nmol mol $^{-1}$ (N=17) on the D366 cruise was calculated from the mean N_2O atmospheric value for the last five minutes of each run (blue) and excluded two unusually high values (cyan) and the initial five, unusually low, measurements (magenta). The error bars show the standard deviation of the measurements. The line displays the June/ July 2011 mean for atmospheric N_2O from Mace Head, Ireland.

Figure 2. 10: Mean atmospheric N_2O dry mole fractions (n=240) with latitude along the AMT22 transect from Southampton, UK, to Punta Arenas, Chile. The atmospheric mean values used (blue) excluded the data points contaminated by stack pollution (cyan) and unusually low values at the start of the cruise (magenta), which may have been caused by the instrument not having warmed up properly. Comparisons are made to Mace Head, Ireland, (monthly mean value from October 2012), Ridge Hill Tower, UK, (October 2012), Trinidad Head, October 2012), Izańa, Tenerife, (October 2012) and Cape Grim, Tasmania, (November 2012). The error bars show the standard deviation of the measurements.

Figure 2. 11: Sea surface saturation for N_2O with respect to the atmospheric value along the D366 cruise track. The mean sea surface saturation measured along the cruise track was slightly supersaturated at 102.25 ± 2.00 %. The red line shows 100% saturation. Atmospheric values used in the saturation were measured on the ship and discussed in section 2.6.2. Details of how surface saturation for N_2O was calculated are found in section 2.3.2.

Figure 2. 12: Sea surface concentration of N_2O measured along the D366 cruise track. The mean sea surface concentration measured along the cruise track was 9.47 ± 0.44 nmol L^{-1}. Details of how surface concentration for N_2O was calculated are found in section 2.3.2.

Figure 2. 13: Sea surface saturation for N_2O with respect to the atmospheric value along the AMT22 cruise track. The mean sea surface saturation measured along the cruise track was undersaturated at 97.50 ± 2.00 %. The red line shows 100% saturation. Atmospheric values used in the saturation were measured on the ship and discussed in section 2.6.2. Details of how surface saturation for N_2O was calculated are found in section 2.3.2.

Figure 2. 14: Sea surface concentration of N_2O measured along the AMT22 cruise track. The mean sea surface concentration measured along the cruise track was 6.91 ± 1.00 nmol L^{-1}. Details of how surface concentration for N_2O was calculated are found in section 2.3.2.

Figure 2. 15: Comparison of sea surface concentration (top left panel) and saturation (bottom left panel) measurements between the *Los Gatos* ICOS (blue) and GC (red) during the D366 OA transect. Differences in concentration and saturation between the two methods are plotted for concentration (top right panel) and saturation (bottom right panel) using samples that were collected at coinciding times (± 10 seconds).

Figure 2. 16: The overall CH_4 atmospheric mean dry mole fraction of 1855.60 ± 16 nmol mol^{-1} (N=23), with a range of 52.42 nmol mol^{-1} was calculated on the D366 cruise from the mean CH_4 atmospheric value for each run (N=240) (blue), excluding two unusually high values (cyan). The measurements were consistent with the Mace Head June and July 2011 mean atmospheric value of 1856.16 nmol mol^{-1}.

Figure 2. 17: Atmospheric CH_4 mean dry mole fractions (N= 240) with latitude along the AMT22 transect from Southampton, UK, to Punta Arenas, Chile. The atmospheric mean values used (blue) excluded the data points contaminated by stack pollution (cyan). Comparisons are made to Mace Head, Ireland, (monthly mean value from October 2012), Izańa, Tenerife (monthly mean value from October 2012), Ascension Island (monthly mean value for October/November 2012) and Cape Grim, Tasmania, (monthly mean value from November 2012).

Figure 2. 18: The sea surface saturation for CH_4 along the D366 shelf sea cruise track. The mean sea surface saturation was supersaturated in respect to the atmospheric equilibrium concentration at 118.38 ± 21.67 %. Details of how surface saturation for CH_4 was calculated are found in section 2.3.2. The red line shows 100 % saturation.

Figure 2. 19: The sea surface concentration of CH_4 along the D366 cruise track. The mean sea surface concentration was 3.05 ± 0.64 nmol L^{-1}. Details of how surface concentration for CH_4 was calculated are found in section 2.3.2.

Figure 2. 20: The sea surface saturation for CH_4 along the AMT22 cruise track. The mean sea surface saturation was supersaturated in respect to the atmospheric equilibrium concentration at 106.79 ± 4.61 %. The red line shows 100 % saturation. Details of how surface saturation for CH_4 was calculated are found in section 2.3.2.

Figure 2. 21: The sea surface concentration of CH_4 along the AMT22 cruise track. The mean sea surface concentration was 2.22 ± 0.19 nmol L^{-1}. Details of how surface concentration for CH_4 was calculated are found in section 2.3.2.

Figure 2. 22: The overall CO atmospheric mean value of 122.87 ± 10 nmol mol^{-1} (n=15) for the D366 cruise was calculated from the mean CO atmospheric value for each run selected (n=240) (blue) and excluded two unusually high values (cyan), the initial five, unusually low, measurements (magenta) and one stack contaminated run (red). Measurements were higher than the Mace Head mean atmospheric dry mole fraction for June and July 2011 at 93.76 nmol mol^{-1}.

Figure 2. 23: Atmospheric CO mean values (n=240) with latitude along the AMT22 transect from Southampton, UK, to Punta Arenas, Chile. The final atmospheric mean values used (blue) excluded the data points contaminated by stack pollution (cyan) and those unusually low for the N_2O measurements at the start of the cruise (same instrument) (magenta), which were assumed to be

caused by either the instrument not having warmed up properly or an issue to with the airline. Comparisons were made to Mace Head, Ireland, (October 2012 monthly mean), Trinidad Head, (October 2012 monthly mean), Ascension Island (October/November 2012 monthly mean) and Cape Grim, Tasmania, (November 2012 monthly mean).

Figure 2. 24: Kollumerwaard atmospheric station, The Netherlands, 2011 hourly atmospheric CO dataset. The variability in the months of June and July exceeded 250 nmol mol $^{-1}$.

Figure 2. 25: Sea surface saturation (%) for CO in respect to the atmospheric equilibrium concentration, along the D366 cruise track. The red line indicates 100 % saturation. The mean surface saturation for CO was 2342.20 ± 907.54 Details of how surface saturation for CO was calculated are found in section 2.3.2.

Figure 2. 26: Sea surface concentration of CO along the D366 cruise track. The mean surface concentration for CO was 2.56 ± 0.97 nmol L^{-1}. Details of how surface concentration for CO was calculated are found in section 2.3.2.

Figure 2. 27: Sea surface saturation (%) for CO in respect to the atmospheric equilibrium concentration, along the AMT22 cruise track. The red line indicates 100 % saturation. The mean surface saturation for CO was 951.05 ± 381.50 %. Details of how surface saturation for CO was calculated are found in section 2.3.2.

Figure 2. 28: Sea surface concentration for CO along the AMT22 cruise track. The mean surface concentration for CO was 0.62 ± 0.26 nmol L^{-1}. Details of how the surface concentration of CO was calculated are found in section 2.3.2.

Figure 2. 29: The CO_2 atmospheric mean value of 399.64 ± 5 µmol mol $^{-1}$ (n=21), with a range of 22.74 µmol mol $^{-1}$ was calculated from the D366 data from the mean value for CO_2 atmospheric value for each run selected (n=240) (blue),

excluding two unusually high values (cyan) and two stack contaminated runs (magenta) The measurements were higher than the Mace Head June and July mean atmospheric value of 390.68 μmol mol $^{-1}$.

Figure 2. 30: Atmospheric CO_2 mean values (n=240) with latitude along the AMT22 transect from Southampton, UK, to Punta Arenas, Chile. The atmospheric mean values used (blue) excluded the data points contaminated by stack pollution (cyan). Comparisons are made to Mace Head, Ireland, (monthly mean value from October 2012), Izańa, Tenerife, (October, 2012), Ascension Island (October and November, 2012) and Cape Grim, Tasmania, (November, 2012).

Figure 2. 31: Sea surface partial pressure of CO_2 (pCO_2) (μatm) along the D366 cruise track. The mean pCO_2 measured on the D366 cruise was 343.32 ± 31 μatm. The calculation for pCO_2 is found in section 2.3.3.

Figure 2. 32: Sea surface pCO_2 (μatm) along the AMT22 cruise track. The mean pCO_2 measured on the AMT22 cruise was 362.65 ± 24 μatm. The calculation for pCO_2 is found in section 2.3.3.

Figure 2. 33: Inter-comparison study between the pCO_2 measured by the UEA *Los Gatos* ICOS (black) a PML LI-COR (cyan) and a UEA LI-COR (red) instrument on the D366 cruise.

Figure 2. 34: (Left panel): Relationship between the pCO_2 ICOS and pCO_2 LI-COR (PML) datasets (Pearson's correlation: r = 0.978, p=<0.001) from the D366. (Right panel): Relationship between the pCO_2 ICOS and pCO_2 LI-COR (UEA) datasets (Pearson's correlation: r = 0.983, p=<0.001) from D366. The lines of perfect agreement (green) and least squares regression (red) are shown for each dataset comparison.

Figure 2. 35: (Left panel): Inter-comparison study between pCO_2 measured by the ICOS (black) and the LI-COR (PML) (cyan) instruments during the AMT22 cruise. (Right panel): Relationship between pCO_2 ICOS and pCO_2 LI-COR (PML)

datasets (Pearson's correlation: r = 0.989, p=<0.001) during AMT22. The lines of perfect agreement (green) and least squares regression (red) are shown.

Figure 3. 1: Sea surface saturation for N_2O with respect to the atmospheric value along the D366 cruise track. The mean sea surface saturation measured along the cruise track was slightly supersaturated at 102 ± 2 %. The red line shows 100% saturation. Atmospheric values used in the saturation were measured on the ship and discussed in section 2.6.2. Details of how surface saturation for N_2O was calculated are found in section 2.3.2.

Figure 3. 2: Sea surface concentration of N_2O measured along the D366 cruise track. The mean sea surface concentration measured along the cruise track was 9 ± 0 nmol L^{-1}. Details of how surface concentration for N_2O was calculated are found in section 2.3.2.

Figure 3. 3: The ocean-atmosphere flux of N_2O calculated along the OA D366 shelf seas cruise track. The surface water was a slight source of N_2O to the atmosphere at 997 ± 1250 nmol m^{-2} d^{-1}. Details of how the ocean to atmosphere flux is calculated are found in section 2.3.4.

Figure 3. 4: Surface water saturation (%) for N_2O with respect to the atmospheric value in the NW European shelf sea.

Figure 3. 5: Locations where surface water undersaturation (%) for N_2O occurred in the NW European shelf sea. Note: figures exclude saturations exceeding 100 %.

Figure 3. 6: Sea surface temperature distribution (°C) during D366.

Figure 3. 7: Sea surface salinity distribution during D366.

Figure 3. 8: Sea surface distribution of chl-a concentration (µg L^{-1}) during D366.

Figure 3. 9: The CTD stations around the NW European shelf seas that were fully mixed (red) and partially mixed (blue) during the OA D366 cruise. Mixed layer depth calculated based on a density criteria of 0.05 kg m-3 (Hickman et al., 2012).

Figure 3. 10: Nitrous oxide and SST over the entire NW European shelf sea region sampled.

Figure 3. 11: The distribution of the strength of both positive and negative correlations (displayed by the correlation coefficients (r-values)) between the sea surface saturation for N_2O and SST. All values plotted were significant to a p-value of <0.05. The colour bar shows the correlation coefficient (r) value.

Figure 3. 12: The distribution of the strength of both positive and negative correlations (displayed by the correlation coefficients (r-values)) between the sea surface saturation for N_2O and SSS. All values plotted were significant to a p-value of <0.05. The colour bar shows the correlation coefficient (r) value.

Figure 3. 13: The distribution of the strength of both positive and negative correlations (displayed by the correlation coefficients (r-values)) between the sea surface saturation for N_2O and surface chl-a concentration. All values plotted were significant to a p-value of <0.05.

Figure 3. 14: The distribution of the strength of both positive and negative correlations (displayed by the correlation coefficients (r-values)) between the sea surface saturation for N_2O and CH_4. All values plotted were significant to a p-value of <0.05.

Figure 3. 15: The distribution of the strength of both positive and negative correlations (displayed by the correlation coefficients (r-values)) between the sea surface saturation for N_2O and CO. All values plotted were significant to a p-value of <0.05.

Figure 3. 16: The distribution of the strength of both positive and negative correlations (displayed by the correlation coefficients (r-values)) between the sea surface saturation for N_2O and the surface partial pressure of CO_2. All values plotted were significant to a p-value of <0.05.

Figure 3. 17: The ventilation time of N_2O at a SST of 14.22 °C, at different mixed layer depths and wind speeds. On the D366 the mean mixed layer depth was calculated as 26.29 m, mean SST was measured at 14.22 °C and mean wind speed was 9.19 m s^{-1}. The ventilation time for N_2O using these mean values was approximately two weeks.

Figure 3. 18: The circulation in the Skagerrak region, with the six interacting water masses: BW= Baltic water, SNSW= South North Sea water, CNSW= Central North Sea water, KSW=Kattegat Water, JCW= Jutland Current Water, AW= Atlantic Water. From Svendsen et al., (1996).

Figure 3. 19: The SSS distribution in the Skagerrak region on the D366 cruise. The dashed boxes indicate transitional regions where vertical mixing occurs between more and less saline waters.

Figure 3. 20: The SST distribution (°C) in the Skagerrak region on D366.

Figure 3. 21: The distribution of surface chl-a concentration (µg l^{-1}) in the Skagerrak region on D366.

Figure 3. 22: The surface water distribution of saturation for N_2O (%) in the Skagerrak region. The black box indicates the location of a dying coccolithophorid bloom.

Figure 3. 23: The locations in which strong correlations, or rapid shifts, were found between sea surface saturation of N_2O and SST, SSS, surface chl-a concentration, saturation for CH_4 and the surface partial pressure of CO_2 (µatm) in the Skagerrak region (refer to Table 3. 2 for more details).

Figure 3. 24: Scatterplot showing the relationship between SST (°C), SSS and surface saturation for N_2O in the green region in Figure 3. 19. The colour bar displays the surface saturation of N_2O in respect to the atmospheric value (%).

Figure 3. 25: Scatterplot showing the relationship between the surface saturation of CH_4 (%), the surface partial pressure of CO_2 (µatm) and surface saturation of N_2O in the green region shown in Figure 3. 19. The colour bar displays the surface saturation of N_2O in respect to the atmospheric value (%).

Figure 3. 26: Scatterplot showing the relationship between surface chl-a concentration (µg l^{-1}), the surface partial pressure of CO_2 (µatm) and the surface saturation of N_2O (%) in the green region shown in Figure 3. 19.

Figure 3. 27: Circulation of the North Sea from Queste et al (2013). The shaded region in the south indicates the region usually well mixed throughout the year. The northern North Sea north of this shaded region displays seasonal stratification in the summer months. The colour bar shows the density difference (kg m^{-3}) between the surface and bottom mixed layers. DC: Dooley Current, SCC: Scottish Coastal Current, CNSC: Central North Sea Current, SNSC: Southern North Sea Current.

Figure 3. 28: The SSS distribution in the southern North Sea during the OA D366 cruise.

Figure 3. 29: The large river inputs into the southern North Sea. From Artioli et al., (2012).

Figure 3. 30: The SST distribution (°C) in the southern North Sea during D366.

Figure 3. 31: The surface chl-a concentration distribution (µg l^{-1}) in the southern North Sea during D366.

Figure 3. 32: The surface water distribution of N_2O saturation (%) with respect to the atmospheric value in the southern North Sea on D366.

Figure 3. 33: The regions in which positive and negative correlations were found between sea surface saturation of N_2O and SST, SSS, and surface chl-a concentration (refer to Table 3. 3 for more details).

Figure 3. 34: The SSS distribution in the English Channel during D366.

Figure 3. 35: The SST distribution (°C) in the English Channel during D366.

Figure 3. 36: The surface chl-a concentration distribution ($\mu g\ l^{-1}$) in the English Channel during D366.

Figure 3. 37: The surface water distribution of saturation for N_2O (%) in the English Channel during the D366.

Figure 3. 38: The regions in which strong correlations were found between sea surface N_2O saturation and SST, SSS, chl-a concentration, CH_4 and CO surface saturation, and the partial pressure of CO_2 during the D366 cruise (refer to Table 3. 4 for more details).

Figure 3. 39: The modelled locations of tidal fronts in the NW European shelf seas. The black line represents the mean frontal positions estimated from ICES data, and the red and green lines are from model outputs Exp 4 and Exp 5. The map is from Holt and Umlauf (2008).

Figure 3. 40: The Aqua MODIS monthly composite satellite image of surface water chl-a concentration across the study area in June 2011. The black circles indicate the location of tidal fronts. From Tyrrell and Achterberg (2014).

Figure 3. 41: The surface water distribution of saturation for N_2O (%) with respect to the atmospheric value in the NW European Shelf seas during D366.

The black circles highlight the locations where tidal frontal zones occur and the surface waters were supersaturated for N_2O.

Figure 3. 42: The regions in which either rapid transitions in SST, SSS and surface chl-a concentration occurred simultaneously with changes in surface N_2O saturation, or strong correlations between the sea surface parameters (Table 3. 5).

Figure 3. 43: The sea surface supersaturation for N_2O (%) calculated in the Malin Sea. The blue and red dots display CTD stations where the mixed layer depth was calculated. The blue dots indicate locations where the water column is partially mixed and the red dots fully mixed. The dashed line suggests the approximate location where the water column makes a transition from partially to fully mixed conditions, reflected as an increase in surface supersaturation for N_2O. The black arrows indicate the direction the ship was moving in. The CTD stations are not on the cruise track due to the CTD stations being sampled on the outbound journey and the ICOS measurements being made in the returning journey.

Figure 3. 44: The transition from lower to higher saturation for N_2O in surface waters as the ship crossed from a partially mixed water column to a fully mixed one in the Malin Sea (black region; Table 3. 5).

Figure 3. 45: The transition of surface waters from lower to higher saturation for N_2O and higher to lower SST, as the ship crossed from a partially mixed water column to a fully mixed one in the Malin Sea (black region; Table 3. 5).

Figure 3. 46: The transition of surface waters from lower to higher saturation for N_2O and concentration of chl-a, as the ship crossed from a partially mixed water column to a fully mixed one in the Malin Sea (black region; Table 3. 5).

Figure 3. 47: The circulation off the west coast of Scotland. From Inall et al., (2009). 1) The Scottish Coastal Current (SCC), and 2) the European Slope Current (ESC).

Figure 3. 48: The SSS distribution off the west coast of Scotland during the D366 cruise. The lines indicate the location of the shelf edge. The contour elevations are at 1000 m intervals.

Figure 3. 49: The bathymetry (m) off the west coast of Scotland. Data from General Bathymetric Chart of the Oceans (GEBCO, 2014).

Figure 3. 50: The SST (°C) distribution off the west coast of Scotland during D366. The lines indicate the location of the shelf edge. The contour elevations are at 1000 m intervals.

Figure 3. 51: The surface chl-a concentration distribution ($\mu g\ l^{-1}$) off the west coast of Scotland during D366. The lines indicate the location of the shelf edge. The contour elevations are at 1000 m intervals.

Figure 3. 52: The surface water distribution of N_2O saturation (%) with respect to the atmospheric value off the west coast of Scotland during the D366 OA research cruise. The dashed boxes indicate high surface N_2O assumed to be a result of mixing from internal waves. The lines indicate the location of the shelf edge. The contour elevations are at 1000 m intervals.

Figure 3. 53: The regions in which strong correlations were found between sea surface N_2O saturation and sea surface chl-a concentration, the partial pressure of CO_2 and CO saturation during the D366 OA research cruise (Table 3. 6). The lines indicate the location of the shelf edge. The contour elevations are at 1000 m intervals.

Figure 3. 54: The bathymetry around the Celtic Sea and the Bay of Biscay (m) (GEBCO, 2014).

Figure 3. 55: The SST distribution (°C) within the Celtic Sea and Bay of Biscay during D366. The lines indicate the location of the shelf edge. The contour elevations are at 1000 m intervals.

Figure 3. 56: The SSS distribution in the Celtic Sea and Bay of Biscay during D366. The lines indicate the location of the shelf edge. The contour elevations are at 1000 m intervals.

Figure 3. 57: The surface chl-a concentration distribution ($\mu g\ l^{-1}$) in the Celtic Sea and Bay of Biscay during D366. The lines indicate the location of the shelf edge. The contour elevations are at 1000 m intervals.

Figure 3. 58: The surface water saturation for N_2O (%) in the Celtic Sea and the Bay of Biscay. The lines indicate the location of the shelf edge. The dashed boxes indicate high surface N_2O assumed to be a result of mixing from internal waves. The lines indicate the location of the shelf edge. The contour elevations are at 1000 m intervals.

Figure 3. 59: The region within the Celtic Sea where strong correlations were established between sea surface saturation for N_2O and SST and SSS during D366 (Table 3. 7). The lines indicate the location of the shelf edge. The lines indicate the location of the shelf edge. The contour elevations are at 1000 m intervals.

Figure 4. 1: The sea surface saturation for CH_4 along the D366 cruise track. The mean sea surface saturation was supersaturated in respect to the atmospheric equilibrium concentration at 118.38 ± 21.67 %. The red line shows 100 % saturation. Details of how surface saturation for CH_4 was calculated are found in section 2.3.2.

Figure 4. 2: The sea surface concentration of CH_4 along the D366 cruise track. The mean sea surface concentration was 3.05 ± 0.64 nmol L^{-1}. Details of how the surface concentration for CH_4 was calculated are found in section 2.3.2.

Figure 4. 3: The ocean-atmosphere flux of CH_4 calculated along the D366 cruise track. The mean ocean-atmosphere flux of CH_4 was 2.32 x 10^3 ± 3.69 x 10^3 nmol m^{-2} d^{-1}, making the shelf seas a source to the atmosphere. Details of how the ocean to atmosphere flux is calculated are found in section 2.3.4.

Figure 4. 4: The D366 cruise track displaying the surface water saturation of CH_4 (%), with respect to the atmospheric value.

Figure 4. 5: The relationship between surface salinity and surface saturation for CH_4 across the NW European shelf seas during D366. The small map shows the location of the freshwater end-members of 1, 2 and 3. 1: SW Irish Sea in close proximity to Dublin Bay; 2: the Skagerrak, and 3: the Norwegian Trench.

Figure 4. 6: The distribution of the strength of positive and negative correlations (displayed by the correlation coefficients (r- values)) between the sea surface saturation of CH_4 and SST. All values plotted were significant to a p-value of ≤0.05.

Figure 4. 7: The distribution of the strength of positive and negative correlations (displayed by the correlation coefficients (r- values)) between the sea surface saturation of CH_4 and SSS. All values plotted were significant to a p-value of ≤0.05.

Figure 4. 8: The distribution of the strength of positive and negative correlations (displayed by the correlation coefficients (r- values)) between the sea surface saturation of CH_4 and surface chl-a concentration. All values plotted were significant to a p-value of ≤0.05.

Figure 4. 9: The distribution of the strength of positive and negative correlations (displayed by the correlation coefficients (r- values)) between the sea surface saturation of CH_4 and partial pressure of CO_2. All values plotted were significant to a p-value of ≤0.05.

Figure 4. 10: The distribution of the strength of positive and negative correlations (displayed by the correlation coefficients (r- values)) between the sea surface saturation of CH_4 and CO. All values plotted were significant to a p-value of ≤0.05.

Figure 4. 11: The ventilation time of CH_4 at a SST of 14.22 °C, at different mixed layer depths and wind speeds. On the D366 the mean mixed layer depth was calculated as 26.29 m, mean SST was measured at 14.22 °C and mean wind speed was 9.19 m s^{-1}. The ventilation time for CH_4 using these mean values was approximately two weeks.

Figure 4. 12: The distribution of surface water saturation of CH_4 (%) with respect to the atmospheric value in the NE North Sea, Skagerrak and Norwegian Trench.

Figure 4. 13: The inverse relationship between SSS and surface saturation of CH_4 over time in the NE North Sea, Skagerrak and Norwegian Trench (location displayed by the blue, red, green and magenta regions in Figure 4. 14).

Figure 4. 14: The regions in which correlations were found between SSS, surface chl-a concentration and surface saturation of CO_2 and CH_4. The majority of the blue, red and magenta regions displayed an inverse relationship between SSS and CH_4 saturation. Within both the red and magenta regions strong negative correlations were found between SSS and saturation of CH_4 and within the green region, a strong positive correlation was found between surface CO_2 and CH_4 saturation (refer to Table 4. 2 for more details).

Figure 4. 15: Sea surface salinity and surface saturation of CH_4 in the red region of the Skagerrak (Figure 4. 14; r=-0.88, p≤0.05).

Figure 4. 16: The locations where positive and negative correlations were located between sea surface saturation of CH_4 and surface chl-a concentration and saturation of CO in the Skagerrak, Norwegian Trench and NE North Sea (refer to Table 4. 2 for details).

Figure 4. 17: The relationship between surface saturation of CH_4 and the surface concentration of chl-a, over time, in the Skagerrak throughout the blue, red, green and magenta regions on map (refer to Figure 4. 14 for location).

Figure 4. 18: (Top panel): Surface saturation of CH_4 and surface chl-a concentration from south to north along part of the Norwegian Trench (green line in Figure 4. 14). (Bottom panel): Surface saturation of CO_2 and surface chl-a concentration from the south to north along part of the Norwegian Trench (green line in Figure 4. 14). The dashed grey lines indicate the transition out of the Norwegian Trench into the northern North Sea.

Figure 4. 19: The surface water distribution of saturation of CH_4 (%), with respect to the atmospheric value in the southern and central North Sea.

Figure 4. 20: Surface CH_4 saturation (blue) at locations A, B and C on Figure 4. 19 and surface salinity (green).

Figure 4. 21: (Large): the relationship between SSS and surface saturation of CH_4 within, and north of, the German Bight. (Small): a map showing the location of these measurements.

Figure 4. 22: The locations where positive correlations were found between sea surface saturation of CH_4 and SST, and surface saturation of CO and CO_2 in the central and southern North Sea (refer to Table 4. 3 for more details).

Figure 4. 23: CH_4 concentration (nM) measured in the German Bight, River Weser and the surrounding region. Squares: show data from cruise HE188 (May, 2003); circles display data from HE238 (September, 2005), and triangles: time-series data (October-November, 2005). From Grunwald et al., (2009). Contours are displayed for 50 – 400 nM CH_4.

Figure 4. 24: The surface water distribution of saturation of CH_4 (%), with respect to the atmospheric value in the SW Irish Sea. The red cross indicates the approximate location of Dublin Bay.

Figure 4. 25: Sea surface salinity and surface CH_4 saturation in the Irish Sea. The shaded area shows the inverse relationship found between SSS and surface CH_4 (which breaks down in the middle-at the most northern point) found in the green region (Figure 4. 26) of the SW Irish Sea.

Figure 4. 26: The green line shows the location of the inverse relationship found between SSS and surface saturation of CH_4 (shaded area in Figure 4. 25).

Figure 4. 27: The locations where positive correlations were identified between surface saturations of CH_4, CO and SST in the Irish Sea (Table 4. 4).

Figure 4. 28: The surface water saturation distribution of CH_4 (%), with respect to the atmospheric value in the English Channel.

Figure 4. 29: The relationship between SSS and surface saturation of CH_4 along the English Channel (west to east).

Figure 4. 30: The location where a positive correlation was found between surface CH_4 and CO saturation (Table 4. 5).

Figure 5. 1: The major circulation patterns in the Atlantic Ocean that influence the AMT cruise track. The black line shows the AMT-2 cruise track. The abbreviations are as follows: Gulf Stream (GS), North Atlantic Current (NAC),

Azores Current (AC), Portugal Current (PC), Canary Current (CC), North Equatorial Current (NEC), South Equatorial Current (SEC), the Brazil Current (BC), the South Atlantic Current (SAC) and the Benguela Current (BenC) and the North Equatorial Counter Current (NECC). The red dashed line indicates the equatorial upwelling, the red star the Guinea Dome upwelling region and the green star the western African Upwelling system. Adapted from Aiken et al., (2000) and Tomczak and Godfrey (1994).

Figure 5. 2: The cruise tracks for the five surface N_2O AMT datasets.

Figure 5. 3: (Top) The sea surface saturation of CH_4 along the AMT22 cruise track. Positive numbers indicate the NH and negative numbers the southern hemisphere. The mean sea surface saturation was supersaturated in respect to the atmospheric equilibrium concentration at 107 ± 5 %. (Middle) The sea surface concentration of CH_4 along the AMT22 cruise track. The mean sea surface concentration was 2 ± 0 nmol L^{-1}. (Bottom) The ocean to atmosphere flux of CH_4 along the AMT22 transect. The mean flux was 3.57 x 10^2 ± 3.28 x 10^2 nmol m^2 d^{-1}.

Figure 5. 4: (Top) Sea surface salinity along the AMT22 transect. (Middle) Sea surface temperature (°C) during AMT22. (Bottom) Windspeed during AMT22 (m s^{-1}).

Figure 5. 5: The sea surface saturation map for CH_4, in respect to the atmospheric equilibrium value, along the AMT22 transect (September-October, 2012). The colour bar shows the sea surface saturation for CH_4 (%).

Figure 5. 6: Sea surface temperature and salinity plot, with surface CH_4 saturation (between the latitudes of 0 to 20 °N) during the AMT22 cruise. The colour bar shows surface saturation of CH_4 (%).

Figure 5. 7: Sea surface temperature and salinity plot, with surface CH_4 saturation (between the latitudes of 15 to 35 °N) during the AMT22 cruise. The colour bar shows surface saturation of CH_4 (%).

Figure 5. 8: Sea surface temperature and surface CH_4 concentration across the AMT22 cruise track.

Figure 5. 9: The mean surface saturation for CH_4 (%) calculated in the northern hemisphere (15 to 41 °N) at 107 ± 3 %, and southern hemisphere (15 to 41 °S) at 105 ± 3 % was found to be significantly different from one another during the AMT22 cruise (unpaired t-test, p=0.05, n=17122). The mean is shown by the red and blue line in the centre of the box. The box indicates the 25th percentile and the black lines the 75th percentile. The red crosses are outliers larger than the 75th percentile.

Figure 5. 10: The mean flux of CH_4 from the ocean to the atmosphere calculated in the northern hemisphere (15 to 41 °N), at 426 ± 353 nmol m^2 d^{-1}, and in the southern hemisphere (15 to 41 °S) at 267 ± 318 nmol m^2 d^{-1} was found to be significantly different from one another during the AMT22 cruise (unpaired t-test, p=0.05, n=17122). The mean is shown by the red and blue line in the centre of the box. The box indicates the 25th percentile and the black lines the 75th percentile. The red crosses are outliers larger than the 75th percentile.

Figure 5. 11: Measured atmospheric values on (top left) AMT7, (top right) AMT20, (bottom left) AMT22, and (bottom right) AMT23. The red lines show the mean Mace Head (NH) and Cape Grim (SH) atmospheric values for the relevant months used in the comparison.

Figure 5. 12: (Top) surface concentration of N_2O (nmol kg^{-1}), and (bottom) estimated surface saturation for N_2O during all cruises with latitude, using Mace Head and Cape Grim monthly mean atmospheric values.

Figure 5. 13: Sea surface temperature and salinity plot, with surface N_2O saturation (between the latitudes of 0 and 20 °N) during the AMT22 cruise. The colour bar displays surface saturation for N_2O (%).

Figure 5. 14: The mean surface concentration for N_2O (nmol kg^{-1}) calculated in the northern hemisphere (15 to 45 °N) at 6 ± 0 nmol kg^{-1}, was significantly lower than that in the southern hemisphere (15 to 45 °S) at 8 ± 1 nmol kg^{-1}, during the AMT22 cruise (unpaired t-test, p=0.05, n=16980). The mean is shown by the red and blue line in the centre of the box. The box indicates the 25th percentile and the black lines the 75th percentile. The red crosses are outliers larger than the 75th percentile.

Figure 5. 15: The mean surface saturation for N_2O (%) calculated in the northern hemisphere (15 to 45 °N) at 96 ± 1 %, and southern hemisphere (15 to 45 °S) at 98 ± 1 % was found to be significantly different from one another during the AMT22 cruise (unpaired t-test, p=0.05, n=16980). The mean is shown by the red and blue line in the centre of the box. The box indicates the 25th percentile and the black lines the 75th percentile. The red crosses are outliers larger than the 75th percentile.

Figure 5. 16: The mean flux of N_2O from the atmosphere into the ocean calculated in the northern hemisphere (15 to 45 °N), at -963 ± 804 nmol m^2 d^{-1}, and southern hemisphere (15 to 45 °S) at -375± 697 nmol m^2 d^{-1}, was found to be significantly different from one another during the AMT22 cruise (unpaired t-test, p=0.05, n=16980). The mean is shown by the red and blue line in the centre of the box. The box indicates the 25th percentile and the black lines the 75th percentile. The red crosses are outliers larger than the 75th percentile.

Figure 5. 17: (Left column) Mean surface water concentration (nmol kg^{-1}), and (right column) the mean surface saturation for N_2O for the regions 30 - 40 °N (top), 10 °N - 10 °S (middle) and 10 – 30 °S (bottom), for each cruise where data was available. The error bars display the standard deviation of the data. The numbers in each column indicate the sample size (n).

Figure 5. 18: A MERIS/MODIS/SeaWiFS merged CHL1-/OC3V5/ GlobColour 8-day Level 3 product run from the 26/10/2012 to 03/11/2012. The product displays the average sea surface concentration of chl-a in the Atlantic Ocean between the latitudes of 30 °N and 30 °S during this time period. The colour bar displays the sea surface concentration of chl-a in mg/m^3. The red line shows the AMT22 cruise track.

Figure 5. 19: (Green dots) land-based N_2O measurements from Izana atmospheric centre, (black line) 'real time' atmospheric measurements during AMT22.

Figure 5. 20: Sea surface temperature with latitude, along the AMT22 transect. The northern hemisphere was warmer in boreal autumn than in the southern hemisphere in austral spring, at the same latitudes.

Figure 6. 1: (Top): the relationship between SST and the surface concentration of N_2O during D366. (Bottom): the relationship between SST and surface saturation of N_2O during D366.

Figure 6. 2: The mean saturation of surface N_2O was found to be significantly higher in the NW European shelf seas (D366), at 102 ± 2 %, than in the open ocean (AMT22), at 97 ± 1 %, during the AMT22 cruise (unpaired t-test, p=0.05, n=47330). The mean is shown by the red and blue line in the centre of the box. The box indicates the 25th percentile and the black lines the 75th percentile. The red crosses are outliers larger than the 75th percentile.

Figure 6. 3: The mean ocean to atmosphere flux of N_2O was found to be significantly different between the NW European shelf seas (D366), with an atmospheric source of 997 ± 1250 nmol m^2 d^{-1}, and the open ocean (AMT22), acting as a sink at -426 ± 554 nmol m^2 d^{-1} (unpaired t-test, p=0.05, n=47330). The mean is shown by the red and blue line in the centre of the box. The box

indicates the 25th percentile and the black lines the 75th percentile. The red crosses are outliers larger than the 75th percentile.

Figure 6. 4: The mean saturation for surface CH_4 was found to be significantly higher in the NW European shelf seas (D366), at 118 ± 22 %, than in the Atlantic Ocean (AMT22), at 107 ± 5 %, during the AMT22 cruise (unpaired t-test, p=0.05, n=47330). The mean is shown by the red and blue line in the centre of the box. The box indicates the 25th percentile and the black lines the 75th percentile. The red crosses are outliers larger than the 75th percentile.

Figure 6. 5: The mean ocean to atmosphere flux for CH_4 was found to be significantly greater in the NW European shelf seas (D366), with an atmospheric source of 2315.40 ± 3691.30 nmol m^{-2} d^{-1}, than in the Atlantic Ocean (AMT22) at 357.55 ± 308.42 nmol m^2 d^{-1} (unpaired t-test, p=0.05, n=47330). The mean is shown by the red and blue line in the centre of the box. The box indicates the 25th percentile and the black lines the 75th percentile. The red crosses are outliers larger than the 75th percentile.

Figure 3. A 1: Negative correlation found between SSS and saturation N_2O in the yellow and cyan regions of the Skagerrak (r=-0.75 p≤0.05) (Figure 3. 23; Table 3. 2).

Figure 3. A 2: Positive correlation found between surface chl-a concentration (µg l^{-1}) and saturation for N_2O in the red region of the Skagerrak (r=0.78 p≤0.05) (Figure 3. 23; Table 3. 2).

Figure 3. A 3: Positive correlation found between surface chl-a concentration (µg l^{-1}) and saturation for N_2O in the cyan region of the Skagerrak (r=0.91 p≤0.05) (Figure 3. 23; Table 3. 2).

Figure 3. A 4: Positive correlation found between SSS and saturation for N_2O in the black region of the southern North Sea (r=0.93 p≤0.05) (Figure 3. 33; Table 3. 3).

Figure 3. A 5: Negative correlation found between SST and saturation for N_2O in the red and blue regions of the southern North Sea (r=-0.73 p≤0.05) (Figure 3. 33; Table 3. 3).

Figure 3. A 6: Positive correlation found between SST and saturation for N_2O in the magenta region of the southern North Sea (r=0.88 p≤0.05) (Figure 3. 33; Table 3. 3).

Figure 3. A 7: Negative correlation found between surface chl-a concentration and saturation for N_2O in the blue region of the southern North Sea (r=-0.67 p≤0.05) (Figure 3. 33; Table 3. 3).

Figure 3. A 8: Negative correlation found between SSS and saturation for N_2O in the red region of the English Channel (r=-0.90 p≤0.05) (Figure 3. 38; Table 3. 4).

Figure 3. A 9: Negative correlation found between SST and saturation for N2O in the green, black and red regions of the English Channel (r=-0.85 p≤0.05) (Figure 3. 38; Table 3. 4).

Figure 3. A 10: Negative correlation found between surface Chl-a concentration and saturation for N_2O in the green region of the English Channel (r=-0.86 p≤0.05) (Figure 3. 38; Table 3. 4).

Figure 3. A 11: Negative correlation found between surface saturation for N_2O and CO in the green region of the English Channel (r=-0.88 p≤0.05) (Figure 3. 38; Table 3. 4).

Figure 3. A 12: Positive correlation found between surface saturation for N_2O and salinity in the blue region of the southern North Sea (Flamborough-Helgoland frontal zone) (r=0.93 p≤0.05) (Figure 3. 42; Table 3. 5).

Figure 3. A 13: Rapid transition from a partially to fully mixed water column south of the Shetland Islands. The higher SST's and lower saturation for N_2O in surface waters were located in the partially mixed region and the cooler temperatures and higher saturation for N_2O in the fully mixed (Figure 3. 42: red region; Table 3. 5).

Figure 3. A 14: Negative correlation found between surface saturation for N_2O and SST in the cyan region off the SW coast of England ($r=-0.80$ $p\leq0.05$) (Figure 3. 42; Table 3. 5).

Figure 3. A 15: Rapid transition from a partially to fully mixed water column south of the Shetland Islands. The lower saturation for N_2O and lower surface concentration of chl-a were located in surface waters in the partially mixed region and the higher supersaturation for N_2O and higher chl-a concentrations found in the fully mixed (Figure 3. 42: red region; Table 3. 5).

Figure 3. A 16: Rapid transition from a partially to fully mixed water column at St Georges Bank (Irish Sea). The lower saturation for N_2O and lower surface concentration of chl-a were located in surface waters in the partially mixed region and the higher saturation for N_2O and higher chl-a concentrations found in the fully mixed (Figure 3. 42: magenta region; Table 3. 5).

Figure 3. A 17: Positive correlation found between surface saturation for N_2O and surface chl-a concentration in the cyan region off the SW coast of England ($r=0.83$ $p\leq0.05$) (Figure 3. 42; Table 3. 5).

Figure 3. A 18: Negative correlation found between surface saturation for N_2O and CO in the green region off St Georges Bank (Irish Sea) ($r=-0.80$ $p\leq0.05$) (Figure 3. 42; Table 3. 5).

Figure 3. A 19: Rapid transition from a partially to fully mixed water column in the surface waters of the cyan region off the SW coast of England. The lower saturation for N_2O and higher saturation for CO were located in surface waters in

the partially mixed region and the higher saturation for N_2O and lower saturation for CO found in the fully mixed (Figure 3. 42: cyan region; Table 3. 5).

Figure 3. A 20: Positive correlation found between surface water saturation for N_2O and chl-a concentration in the green region (NE Atlantic) ($r=0.93$ $p\leq0.05$) (Figure 3. 53; Table 3. 6).

Figure 3. A 21: Positive correlation found between surface water saturation for N_2O and CO in the black region (NE Atlantic) ($r=0.92$ $p\leq0.05$) (Figure 3. 53; Table 3. 6).

Figure 3. A 22: Negative correlation found between surface water supersaturation for N_2O and pCO_2 in the black region (NE Atlantic) ($r=-0.91$ $p\leq0.05$) (Figure 3. 53; Table 3. 6).

Figure 3. A 23: Negative correlation found between surface water saturation for N_2O and SSS in the red region of the Bay of Biscay ($r=-0.78$ $p\leq0.05$) (Figure 3. 59; Table 3. 7).

Figure 3. A 24: Negative correlation found between surface water saturation for N_2O and SST in the red region of the Bay of Biscay ($r=-0.82$ $p\leq0.05$) (Figure 3. 59; Table 3. 7).

Figure 4.A 1: A negative correlation found between surface water saturation for CH_4 and salinity in the magenta region of the Skagerrak ($r=-0.94$, $p\leq0.05$) (Figure 4. 14; Table 4. 2).

Figure 4.A 2: A positive correlation found between surface water saturation for CH_4 and CO_2 in the green region of the Skagerrak ($r=0.86$, $p\leq0.05$) (Figure 4. 14; Table 4. 2).

Figure 4.A 3: A positive correlation found between surface water saturation for CH_4 and surface chl-a concentration in the blue region of the Skagerrak (r=0.87, p≤0.05) (Figure 4. 16; Table 4. 2).

Figure 4.A 4: A positive correlation found between surface water saturation for CH_4 and surface chl-a concentration in the red region of the Skagerrak (r=0.98, p≤0.05) (Figure 4. 16; Table 4. 2).

Figure 4.A 5: A positive correlation found between surface water saturation for CH_4 and surface chl-a concentration in the green region of the Norwegian Trench (r=0.95, p≤0.05) (Figure 4. 16; Table 4. 2).

Figure 4.A 6: A positive correlation found between surface water saturation for CH_4 and CO in the cyan region of the Skagerrak (r=0.96, p≤0.05) (Figure 4. 16; Table 4. 2).

Figure 4.A 7: A negative correlation found between surface water saturation for CH_4 and CO in the black and green region of the Norwegian Trench (r=-0.97, p≤0.05) (Figure 4. 16; Table 4. 2).

Figure 4.A 8: A positive correlation found between surface water saturation for CH_4 and SST in the blue and green region of the southern/central North Sea (r=0.93, p≤0.05) (Figure 4. 22; Table 4. 3).

Figure 4.A 9: A positive correlation found between surface water saturation for CH_4 and CO in the green region of the southern/central North Sea (r=0.98, p≤0.05) (Figure 4. 22; Table 4. 3).

Figure 4.A 10: A positive correlation found between surface water saturation for CH_4 and CO_2 in the magenta region of the southern/central North Sea (r=0.78, p≤0.05) (Figure 4. 22; Table 4. 3).

Figure 4.A 11: A positive correlation found between surface water saturation for CH_4 and SST in the red region of the Irish Sea ($r=0.66$, $p \leq 0.05$) (Figure 4. 27; Table 4. 4).

Figure 4.A 12: A positive correlation found between surface water saturation for CH_4 and CO in the blue region of the Irish Sea ($r=0.85$, $p \leq 0.05$) (Figure 4. 27; Table 4. 4).

Figure 4.A 13: A positive correlation found between surface water saturation for CH_4 and CO in the red region of the English Channel ($r=0.85$, $p \leq 0.05$) (Figure 4. 30; Table 4. 5).

List of tables

Table 2. 1: Mole fractions of the four gases in the working standards measured on the D366 OA cruise.

Table 2. 2: Mole fractions of the four gases in the reference standards used for the pre and post cruise calibrations at WAO for both cruises.

Table 2. 3: Mole fractions of the four gases in the working standards measured daily on the AMT22 cruise.

Table 2. 4: Atmospheric N_2O monthly mean values calculated at various global locations. NA: not available.

Table 2. 5: Atmospheric CH_4 monthly mean dry mole fractions calculated at various locations. The standard deviation of the mean measurement at each station, the sample size (n) and the range within the datasets was not available.

Table 2. 6: Atmospheric CO monthly mean values calculated at various global locations. Data available at: the World Data Centre for Greenhouse Gases. NA: data not available. Information on the sample size (n) and the range within the data was not available for any of the locations below therefore are not included in the table.

Table 2. 7: Atmospheric CO_2 monthly mean values calculated at various locations. The standard deviation of the mean measurement at each station, the sample size (n) and the range within the datasets was not available.

Table 3. 1: Spearman's correlations over the entire NW European shelf seas sampled, between the surface ocean N_2O concentration (nmol L^{-1}) and saturation (%), with surface chl-a concentration (µg L^{-1}), SST (°C), SSS, windspeed (m s^{-1}), surface CH_4 and CO concentration (nmol L^{-1}) and saturation (%) and the surface pCO_2 (µatm).

Table 3. 2: The coloured regions, located in Figure 3. 23, where strong correlations, or rapid transitional zones, were found between sea surface N_2O saturation and SST, SSS, chl-a concentration, saturation for CH_4 and the surface partial pressure of CO_2 during D366. The correlation coefficient (r) and the p values for the correlations are shown below. N/A: a correlation coefficient only occurs with correlations not where there is a transitional zone. The parameters tested had a non-normal distribution and therefore Spearman's correlations were used.

Table 3. 3: The coloured regions (displayed in Figure 3. 33) where strong correlations were found between sea surface water saturation for N_2O and SST, SSS and surface chl-a concentration. The correlation coefficient (r) and the p values for the correlations are shown below. The parameters tested had a non-normal distribution and therefore Spearman's correlations were used.

Table 3. 4: The coloured regions (Figure 3. 38) where strong correlations were found between sea surface saturation for N_2O and SST, SSS, surface chl-a concentration, and saturation for CO during D366. The correlation coefficient (r) and the p values for the correlations are shown below. The parameters tested had a non-normal distribution and therefore Spearman's correlations were used.

Table 3. 5: The coloured regions (Figure 3. 42) where strong correlations/rapid transitional regions were found between sea surface saturation for N_2O and SST, SSS, surface chl-a concentration and CO saturation during D366. The correlation coefficient (r) and the p values for the correlations are shown. The parameters tested had a non-normal distribution and therefore Spearman's correlations were used. N/A: a correlation coefficient only occurs with correlations not where there is a transitional zone.

Table 3. 6: The coloured regions (found in Figure 3. 53), with strong correlations between sea surface N_2O saturation and sea surface chl-a concentration, the partial pressure of CO_2 and CO saturation during D366. The correlation coefficient (r) and the p values for the correlations are shown. The

parameters tested had a non-normal distribution and therefore Spearman's correlations were used.

Table 3. 7: The coloured region (Figure 3. 59) where strong correlations were found between sea surface N_2O saturation and SST and SSS during D366. The correlation coefficient (r) and the p values for the correlations are shown. The parameters tested had a non-normal distribution and therefore Spearman's correlations were used.

Table 4. 1: Spearman's correlations over the entire NW European shelf seas sampled, between the surface ocean CH4 concentration (nmol L-1) and saturation (%), with surface chl-a concentration (µg L-1), SST (°C), SSS, windspeed (m s-1), surface CO concentration (nmol L-1) and saturation (%) and the surface pCO2 (µatm).

Table 4. 2: Relationships between surface saturation of CH_4 and other parameters in the NE North Sea, Skagerrak and Norwegian Trench (refer to Figures 4. 14 and 4. 16 for locations of the correlations). The parameters tested had a non-normal distribution and therefore Spearman's correlations were used.

Table 4. 3: The relationship between surface saturation of CH_4 and other parameters in the southern and central North Sea.

Table 4. 4: Relationships between surface saturation of CH_4 and other measured parameters in the SW Irish Sea. Refer to Figures 4. 26 and 4. 27 for the locations.

Table 4. 5: The relationship between surface CH_4 and CO saturation in the English Channel (refer to Figure 4. 32 for location).

Table 5. 1: Measurement characteristics for each research cruise.

Table 6. 1: Comparison of surface saturation and air- sea flux of N_2O and CH_4 between shelf seas, estuaries, rivers and the open ocean. The shelf and open

ocean estimates for both N_2O and CH_4 are from the D366 and AMT22 cruises. The estuary estimates are from Barnes and Upstill-Goddard (2011) for N_2O and Upstill-Goddard et al. (2000) for CH_4.

Acknowledgements

This PhD would not have been possible without the help of many people. I am grateful for all the supervision I have received throughout the past four years and constructive feedback on my PhD chapters. I have been involved in many interesting scientific discussions with Dorothee Bakker, Martin Johnson, Tim Jickells and Jan Kaiser, throughout my time at UEA, which guided me through the project. Many thanks to Dorothee Bakker and Gareth Lee for collecting the D366 surface datasets used for this PhD. Additional thanks to Gareth who explained the workings of the integrated cavity output spectrometers, helped me build the value board used for fieldwork and assisted with the set-up for the two cruises that I participated in during the project. Thanks also to Grant Forster for always having your door open for a chat, and supporting me throughout the PhD. I am grateful to all the technicians on floor 02 that helped me with many tasks throughout the project. I also appreciate the assistance from all the crew and mates on the D366 and AMT22 cruises for solving any problems that arose to ensure that good data was collected.

A massive thank you to my mum, dad, sister, Tom, Bob and my friends for all the support and assuring words during the tough points of the PhD, you all really helped me get through those challenging times, and for all the fun times we have shared during the past four years. I could not have done this without you all!

The work presented in this thesis was funded by the Natural Research Council (NERC), without which it would not exist.

Chapter 1: Introduction.

1. 1: Aims of this chapter

This chapter aims to provide important background information for the thesis by reviewing the research literature available for the climatically active gases nitrous oxide (N_2O) and methane (CH_4), with a focus on the role of the marine environment in the uptake or production of these trace gases. This chapter will initially introduce the topic of climate change, as well as the global nitrogen and carbon cycles, followed by the importance of studying N_2O and CH_4, and how their atmospheric concentration has increased over time. The natural and anthropogenic atmospheric sources and sinks of these greenhouse gases, along with the global influence the marine environment plays in the production or uptake of N_2O and CH_4 will then be reviewed, along with the pathways that produce and consume each gas in the marine environment, the organisms responsible, and the processes influencing the distribution of the climatically active gases. This chapter will also briefly review literature available on carbon dioxide (CO_2) and carbon monoxide (CO).

1. 2: Climate change: the problem

Human activities, such as the burning of fossil fuels, agriculture, waste, biomass burning, atmospheric deposition and fertiliser use, are altering the emissions of climatically active gases, such as carbon dioxide (CO_2), N_2O and CH_4, causing the climate to change across the planet (Cubasch et al., 2013). Observations across the atmosphere, oceans, land and cryosphere have indicated that over the past few centuries concentrations of these important greenhouse gases in the atmosphere have increased (Cubasch et al., 2013). Greenhouse gases alter the radiative forcing on the planet and are believed to have led to an increase in the global mean surface temperature over the land and ocean during the last century (Cubasch et al., 2013), and consequently produced an increase in the occurrence of extreme weather events, including drought, floods and intensified storms in various regions of the world. To predict future scenarios concerning the impacts of climate change the Intergovernmental Panel on Climate Change (IPCC) use

observations of climatically active gases, to understand how current and predicted future concentrations may affect the planet, for example their influence on the global surface temperature and sea level rise (Cubasch et al., 2013). Each climate projection has become more advanced, including a more accurate description of the global budget of these greenhouse gases, to understand and quantify the different natural and anthropogenic sources and sinks. This thesis aims to provide more understanding of the role of both shelf seas and open ocean environments in the production and/or uptake of N_2O and CH_4.

1. 3: The global nitrogen and carbon cycles

1.3. 1: The nitrogen cycle

Nitrogen is an essential nutrient in natural ecosystems, on land and in the ocean. Nitrogen is present in the natural environment in many different forms such as organic nitrogen, ammonium (NH_4^+), nitrite (NO_2^-), nitrate (NO_3^-), N_2O, nitric oxide (NO) and inorganic nitrogen gas (N_2). Transformation between the different forms is undertaken by microbes during the harvest of energy, or as nitrogen is taken up for growth (Figure 1. 1). Nitrogen gas makes up the largest constituent of the atmosphere at 78%. This form of unreactive nitrogen must be fixed before it can be taken up by biota in a reactive nitrogen (N_r) form (Figure 1. 1). Once converted, N_r can be used by biological systems until it is converted back into N_2. Two natural processes, biotic fixation and lightning, fix unreactive nitrogen with the former being the dominant process at about two orders of magnitude greater than the latter (Galloway et al., 1995). Human activities including energy production, the use of fertilisers, and the cultivation of legumes and other crops also fix N_2 at an estimated rate of 140 Tg N yr^{-1}. This rate is more than double of that estimated from preindustrial times at 90 – 130 Tg N yr^{-1} (Galloway et al., 1995). Transportation of N_r from terrestrial environments plays a significant role in redistributing N_r into aquatic systems. It has been estimated that between 50 – 80 Tg N yr^{-1} of N_r enters the marine environment via rivers (Duce et al., 2008). A large quantity of this N_r is however either lost to the atmosphere or buried in coastal sediments, and therefore does not reach

oceanic regions. Atmospheric transport and deposition acts as an important pathway for N_r to enter the marine environment and could account for up to a third of the oceans external non-recycled nitrogen supply (Duce et al., 2008). When N_r enters the marine environment, microorganisms utilise these compounds during various oxidation and reduction reactions in the provision of energy. The oxidation and reduction of the N_r compounds occur during the nitrification and denitrification pathways until the nitrogen is returned back to a non-reactive state (explained in more detail in sections 1.4.5. 1 and 1.4.5. 2). During these pathways the greenhouse gas N_2O is produced (Figure 1. 1).

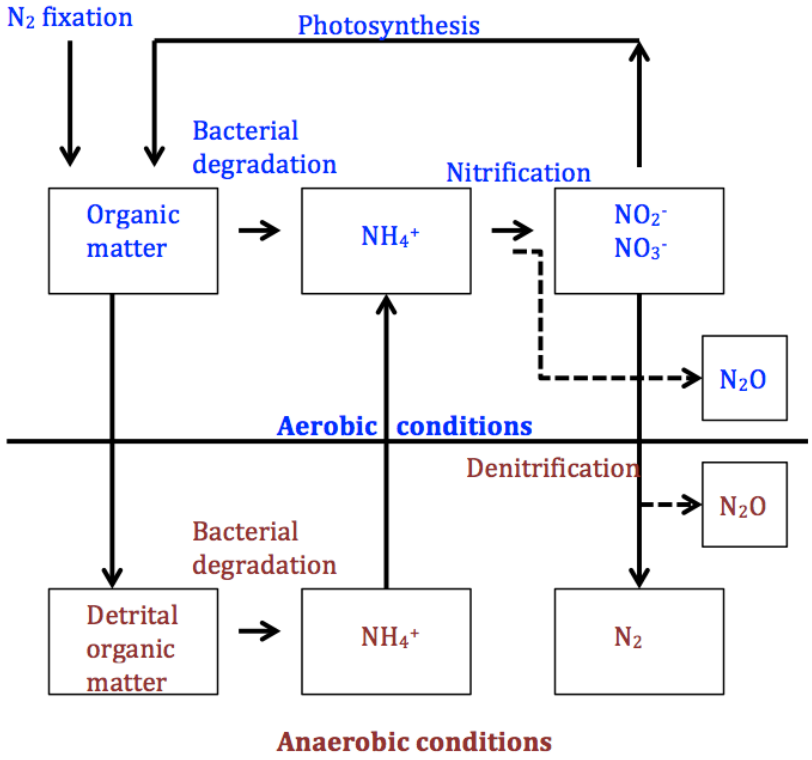

Figure 1. 1: Pathways and reactions involved in the nitrogen cycle. The pathways show N-fixation, whereby inorganic nitrogen (N_2) is fixed to organic nitrogen (organic-N) by nitrogen fixing biota and human activities; nitrogen mineralisation, where organic-N is converted to plant-available inorganic forms by bacteria and fungi; nitrification, where NH_4^+ is oxidised to NO_3^- via NO_2^- by nitrifying bacteria, this pathway releases N_2O; denitrification, where NO_3^- is reduced to N_2 via NO_2^- and N_2O by denitrifying bacteria, and finally photosynthesis, where NO_3^- and NH_4^+ are converted to organic-N by plants.

1.3. 2: The carbon cycle

Figure 1. 2 shows a generalised schematic of the global carbon cycle. Carbon dioxide in the atmosphere is converted to organic compounds by living organisms, for example during photosynthesis. The organic matter can decompose aerobically releasing CO_2 back into the atmosphere, or it can undergo fermentation. Fermentation occurs in the absence of oxygen and is a form of energy production undertaken by microorganisms, including bacteria and fungi. Products of fermentation including acetate, H_2+CO_2, formate, methanol, methylamines and methylsulphides can be reduced to CH_4 during methanogenesis, which is an anaerobic process that yields energy. Four per cent of all carbon is converted to methane by methanogens. The final step in the cycle is the oxidation of CH_4, yielding CO_2.

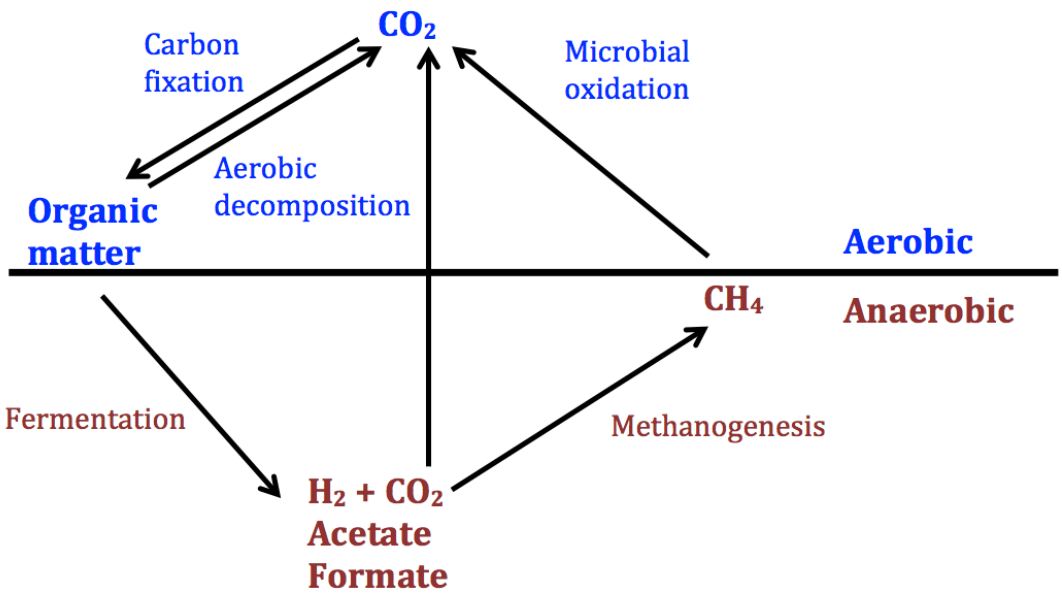

Figure 1. 2: A generalised schematic of the global carbon cycle. The schematic displays the cycling of different forms of carbon.

1. 4: Nitrous Oxide

This section discusses N_2O as an important greenhouse gas, examining global natural and anthropogenic sources and sinks. The text will discuss the uptake and production of this climatically active gas in the marine environment, examining the environments, pathways and processes in which N_2O is formed and consumed.

1.4. 1: Nitrous oxide as an important long-lived greenhouse gas

Nitrous oxide is an important long-lived greenhouse gas, with an atmospheric lifetime of approximately 114 years, that influences the earth's climate both directly and indirectly (Montzka et al., 2003). Nitrous oxide has a high global warming potential relative to both CO_2 and CH_4 (Table 1. 1) (Myhre et al., 2013). In the troposphere, N_2O directly contributes to radiative forcing. Indirectly, N_2O in the stratosphere is photochemically degraded producing the ozone depleting species nitric oxide (NO) and nitrogen dioxide (NO_2), as well as free radical reservoir species, such as nitric acid (HNO_3) and chlorine nitrate ($ClNO_3$) (Montzka and Reimann, 2011).

Table 1. 2: Global warming potential (GWP) with climate change feedbacks relative to CO_2 (adapted from Table 8. A. 1, IPCC Fifth Assessment Report). Methane lifetime values do not include CO_2 from CH_4 oxidation (Myhre et al., 2013) .

Chemical formula	Lifetime (years)	GWP for 100 year horizon
CO_2	1	1
N_2O	121.0	265
CH_4	12.4	28

The global average atmospheric concentration of N_2O in 2011 was calculated as [1]324.2 nmol mol^{-1} (Hartmann et al., 2013). This is a 20 % increase from estimates for the 1750's, which were obtained from ice core measurements (Prather et al., 2012). Atmospheric measurements of N_2O started in the late 1970's, with atmospheric concentrations increasing on average by 0.75 nmol mol^{-1} yr^{-1} (Hartmann et al., 2013) (Figure 1. 3). As the atmospheric concentration of dichlorodifluoromethane (CFC-12) has decreased over recent years, this places N_2O as the third most important, well mixed, greenhouse gas contributing to radiative forcing (not including water vapour) (Hartmann et al., 2013).

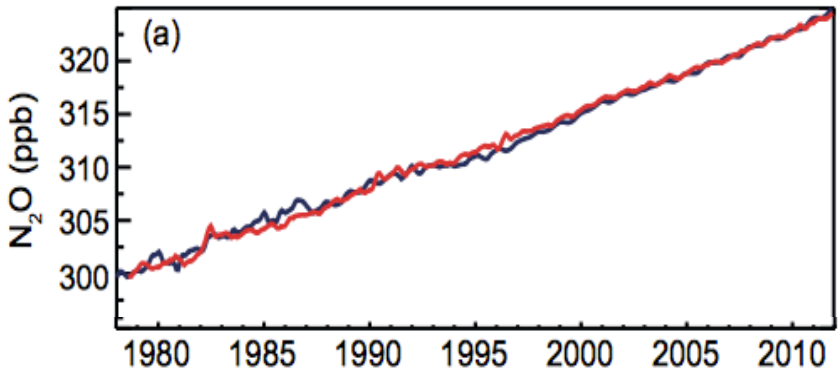

Figure 1. 3: Globally averaged atmospheric N_2O dry mole fractions from AGAGE [2](red) and NOAA/ESRL/GMD[3] (blue) at monthly resolution (ppb means one part in in one billion). Figure from Hartmann et al. (2013).

1.4. 2: Global atmospheric sources of nitrous oxide

Anthropogenic sources of N_2O include fossil fuel combustion, industrial processes, biomass burning, anthropogenic inputs into rivers, estuaries and coastal zones, atmospheric deposition on land and in the ocean, human and animal excreta, and agriculture. Natural emissions of N_2O arise from soils under natural vegetation, the ocean, and atmospheric chemistry (Ciais et al., 2013) (Table 1. 2). The most pronounced anthropogenic atmospheric N_2O source

[1] Atmospheric units are discussed in section 2.3.1.

[2] Advanced Global Atmospheric Gases Experiment (AGAGE)

[3] National Oceanic and Atmospheric Administration (NOAA)/ Earth System Research Laboratory (ESRL)/ Global Monitoring Division (GMD).

arises from agriculture (Menon et al., 2007), where increased fertiliser use has occurred in response to the growing food demand as the global population expanded (Kroeze et al., 1999) (Table 1. 2). With a future facing growing global food demand, quantifying the global N_2O budget is an essential area of research (Mosier et al., 1998).

Table 1. 3: The mean anthropogenic and natural atmospheric sources of N_2O from the IPCC report AR5 (2006 -2011). All units for N_2O fluxes are in Tg N (N_2O) yr^{-1}. Table adapted from Ciais et al. (2013).

Anthropogenic sources	**N_2O fluxes (Tg N (N_2O) yr^{-1})**
Fossil fuel combustion and industrial processes	0.7
Agriculture	4.1
Biomass and biofuel burning	0.7
Human excreta	0.2
Rivers estuaries, coastal zones	0.6
Atmospheric deposition on land	0.4
Atmospheric deposition on ocean	0.2
Surface sink	-0.01
Total anthropogenic sources	**6.9**
Natural sources	
Soils under natural vegetation	6.6
Oceans	3.8
Lightning	-
Atmospheric chemistry	0.6
Total natural sources	11.0
Total natural + anthropogenic sources	**17.9**

1.4. 3: Latitudinal gradients in atmospheric nitrous oxide

Annually averaged atmospheric N_2O concentrations show latitudinal gradients with the northern subtropical region displaying the atmospheric maximum, and concentrations around 1.70 nmol mol^{-1} and 0.40 nmol mol^{-1} lower in Antarctica and the Arctic (Figure 1. 4). These gradients may be linked to higher anthropogenic fertiliser use in the northern tropical to mid-latitude regions, and from natural emissions in the tropics arising from soils and oceanic upwelling (Hartmann et al., 2013).

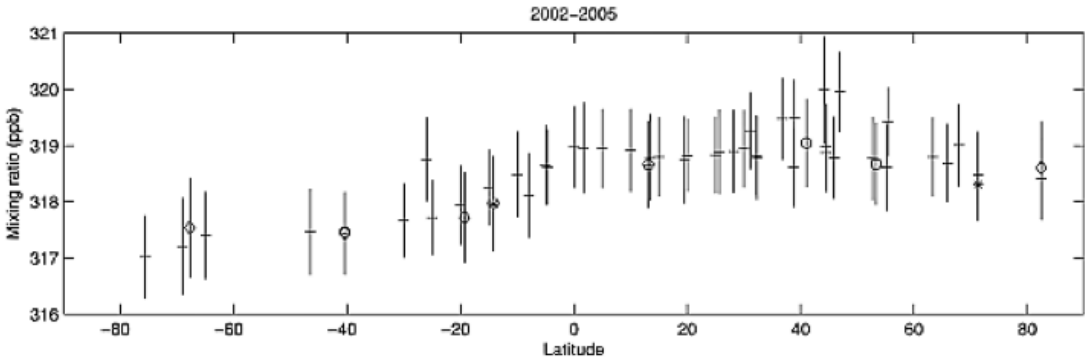

Figure 1. 4: Time-averaged latitudinal gradients of the observed N_2O mixing ratios (after scaling) from AGAGE (open circle), GMD/CCGG (plus), GMD/HATS (asterisk) and CSIRO (diamond) for 2002–2005. From Huang et al. (2008).

Seasonal variations (peak to peak) of atmospheric N_2O in the southern hemisphere (SH) are less pronounced, at 0.40 nmol mol^{-1}, than in the northern hemisphere (NH), at 1.00 nmol mol^{-1}. The seasonal variation observed in the NH is due to the air exchange between the stratosphere and troposphere, where stratospheric photochemical processes destroy N_2O (Jiang et al., 2007), (Equations 1. 1 and 1. 2 (Portmann et al., 2012)), rather than to the seasonality of N_2O emissions. In the SH the seasonal variation has been predominantly attributed to ventilation and thermal outgassing of the oceans, although stratospheric-tropospheric exchange also occurs (Hartmann et al., 2013).

$$\boldsymbol{N_2O + h\nu \rightarrow N_2 + O(1D)}$$

Equation 1. 1

$$\boldsymbol{N_2O + O(1D) \rightarrow N_2 + O_2}$$

Equation 1. 2

1.4. 4: The marine environment as a source of nitrous oxide

Nitrous oxide is biologically produced in the ocean, as well as in rivers, estuaries and coastal regions (Bange et al., 1996b, Bange, 2006, Forster et al., 2009, Barnes and Upstill-Goddard, 2011). The global average surface ocean saturation for N_2O was estimated as 103.5 %, showing that the global ocean acts as a net N_2O source to the atmosphere (Nevison et al., 1995). Saturation is defined as the extent to which a gas is dissolved into the ocean, compared with the atmospheric concentration at the same temperature. One hundred per cent saturation means both the concentration in the atmosphere and surface ocean are equal, 101 % means the surface waters are supersaturated in respect to the atmospheric value, and 99 % saturation means the surface waters are undersaturated in respect to the atmospheric value. This gives an indication of whether the gas will move into or out of the ocean, for example at 101 % saturation we would expect a net flux from the ocean to the atmosphere. According to the Fifth Assessment Report of the Intergovernmental Panel on Climate Change, the open ocean along with rivers, estuaries and coastal zones contribute approximately 24 % of the total global emissions of atmospheric N_2O of 17.9 Tg N yr^{-1}, respectively (Table 1. 2) (Ciais et al., 2013).

Suntharalingam and Sarmiento (2000) modelled the surface field of Δ pN_2O (natm) (difference in partial pressure between the surface water and atmospheric values), derived from the Weiss et al. (1992) database and binned to a 1 ° x 1° resolution. Their results showed that the global distribution of surface N_2O saturation is non-uniform, with 'hotspots' within regions of upwelling, including the equatorial upwelling and coastal upwelling off the Peruvian and NW African coasts, in the NW Indian Ocean (Arabian Sea), and off the west coast of both North and Central America (Figure 1. 5). Extremely high N_2O saturations have been observed in upwelling regions (Table 1. 3). Saturation values close to equilibrium with the atmospheric value were estimated in the northern and southern Atlantic Ocean and in the southern Indian Ocean (Suntharalingam and Sarmiento, 2000).

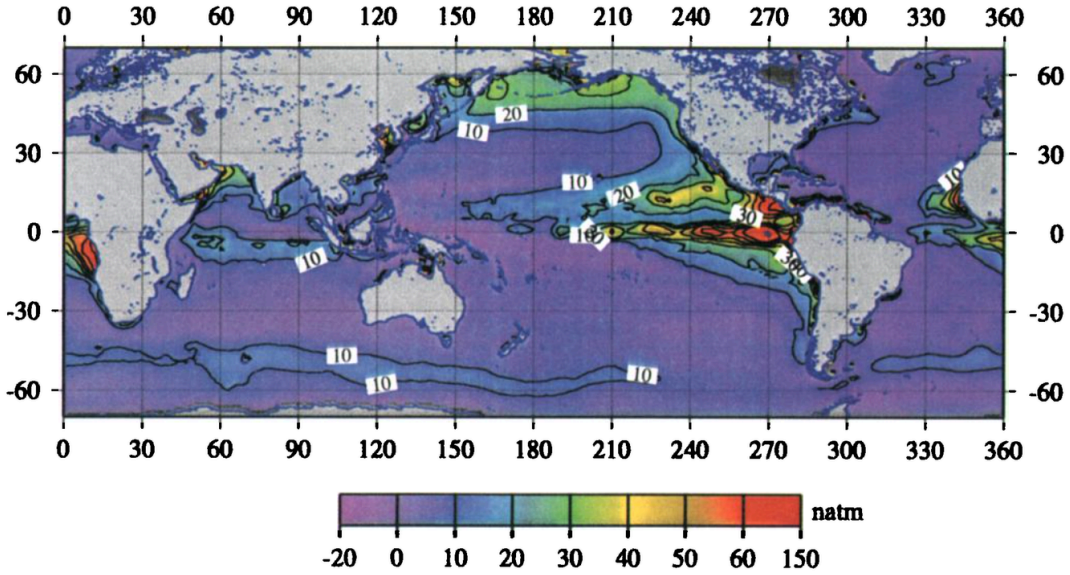

Figure 1. 5: Surface distribution of Δ pN_2O (natm) (difference in partial pressure between the surface water and atmospheric values), from Suntharalingam and Sarmiento (2000).

Table 1. 4 Nitrous oxide saturations observed in upwelling regions.

Region	N_2O saturation (%)	Reference
Arabian Sea	167 - 186	Law and Owens (1990b)
Arabian Sea (Off Oman)	230 ± 40	Naqvi and Noronha (1991)
Off Somalia	330	Bange et al. (1996a)
Off Somalia	1030	Bange et al. (1996a)
Indian shelf	8250	Naqvi et al. (2006)
Bay of Bengal	89 - 214	Naqvi et al. (1994)

1.4. 5: Which processes produce nitrous oxide in the ocean?

In the majority of the global ocean, the greatest concentration of N_2O has been suggested to occur in the oxic subsurface of the water column, as a result of nitrification (Figure 1. 6) (Freing et al., 2012)(refer to section 1.4.5. 1 for more details on nitrification). The yield of N_2O produced by nitrifying microbes in the ocean increases as the concentration of O_2 reduces, displaying an inverse linear relationship (Figure 1. 6) (Goreau et al., 1980, Hahn, 1974).

Approximately half the net production of N_2O in the open ocean arises from hypoxic (O_2<~2 mg l^{-1}/ O_2<~60 µM) and suboxic waters (O_2<~0.2 mg l^{-1}/

O_2<~5 µM (Naqvi et al., 2010)), at 3 Tg N yr^{-1}, respectively (Codispoti, 2010). Within hypoxic waters, where O_2 saturation is between 1 to 30 %, N_2O is produced rapidly as oxygen is consumed during the decomposition of organic matter, breaking down the inverse relationship with the O_2 concentration. Where a transition from hypoxic to suboxic seawater occurs, for example within the oxygen minimum zones (OMZ) of the eastern tropical North and South Pacific Ocean and the Arabian Sea, the saturation of O_2 can drop below 1 %. Different mechanisms of N_2O production and consumption, that are described below, are found throughout these regions depending on the concentration of O_2 present (Farías et al., 2009). Nitrous oxide is both consumed and produced during denitrification by denitrifying bacteria, which use the oxidised nitrogen source for respiration (refer to section 1.4.5. 2 for more details about denitrification). In the upper oxycline, the production of N_2O, via both partial denitrification and nitrification, leads to an accumulation of this trace gas. Moving downwards into the OMZ core consumption increases as N_2O is reduced to N_2. As a result, N_2O in suboxic zones can be depleted below saturation (Farías et al., 2009). This appears to take place within the working nitrite maximum of open water OMZ's, where N_2O is utilised by denitrifying organisms as an electron acceptor (Cohen and Gordon, 1978, Farías et al., 2009). Regardless of this sink, OMZ's act as overall net producers of this trace gas (Naqvi et al., 2010). The relative production of N_2O from nitrification and denitrification in the open ocean is currently uncertain. Denitrification has been estimated to contribute somewhere between 7 - 50 % of the amount of N_2O produced by nitrification, making the latter the dominant source (Bange and Andreae, 1999, Suntharalingam et al., 2000, Freing et al., 2012).

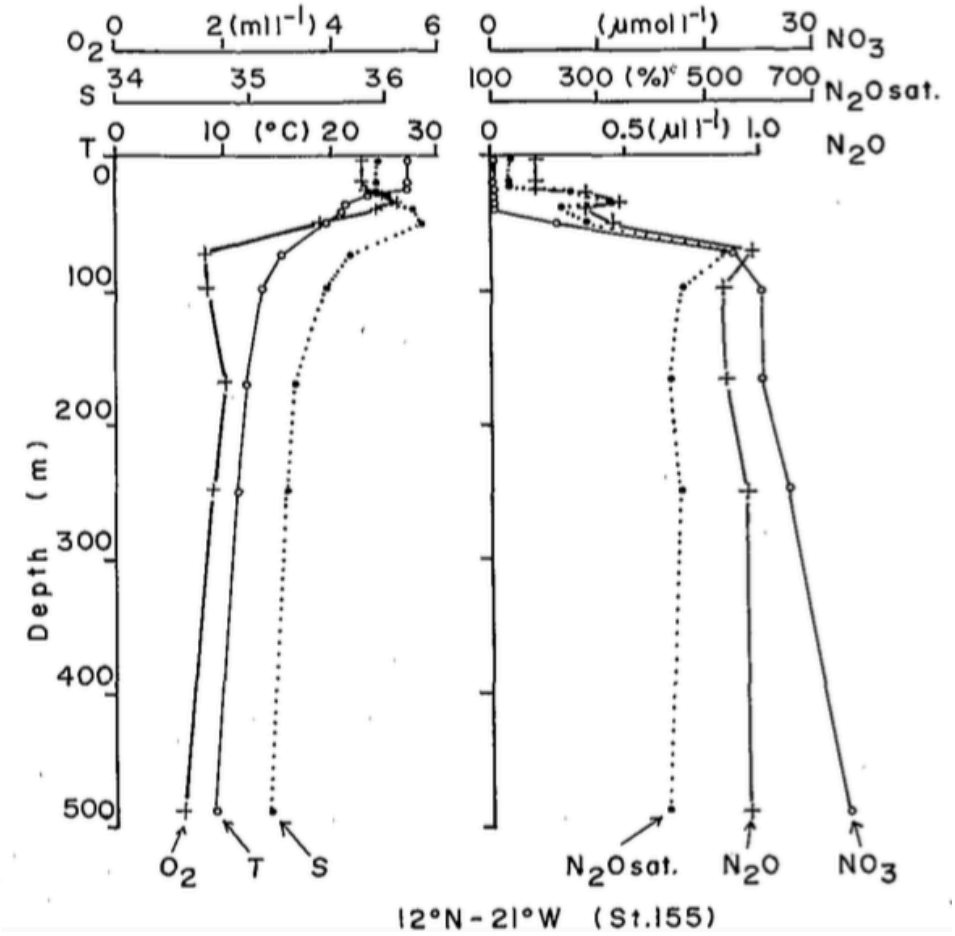

Figure 1. 6: Depth profile of oxygen (O_2), salinity (S), temperature (T), nitrate (NO_3^-), nitrous oxide saturation (N_2O sat) and nitrous oxide concentration (N_2O) from the centre of Guinea Dome in the Atlantic Ocean. The inverse relationship between the concentration of oxygen (O_2) (left panel) and the concentration of N_2O (right panel) is shown. From Oudot et al. (1990).

1.4.5. 1: Nitrification

Nitrification takes place under oxic conditions by ammonia oxidising bacteria (AOB) and archaea (AOA). Nitrification involves a series of oxidation reactions where ammonium is oxidised to nitrite and then nitrate ($NH_4^+ \rightarrow NO_2^- \rightarrow NO_3^-$) (Figure 1. 7). Nitrous oxide is produced as a by-product in the initial oxidation reaction from ammonium to nitrite (Capone et al., 2008). The nitrification pathway involves the oxidation of hydroxylamine (NH_2OH) by hydroxylamine oxidoreductase (HAO). The genes that control this reaction (haoAB) are regulated by the concentration of free ammonia in the environment (Desloover et al., 2012).

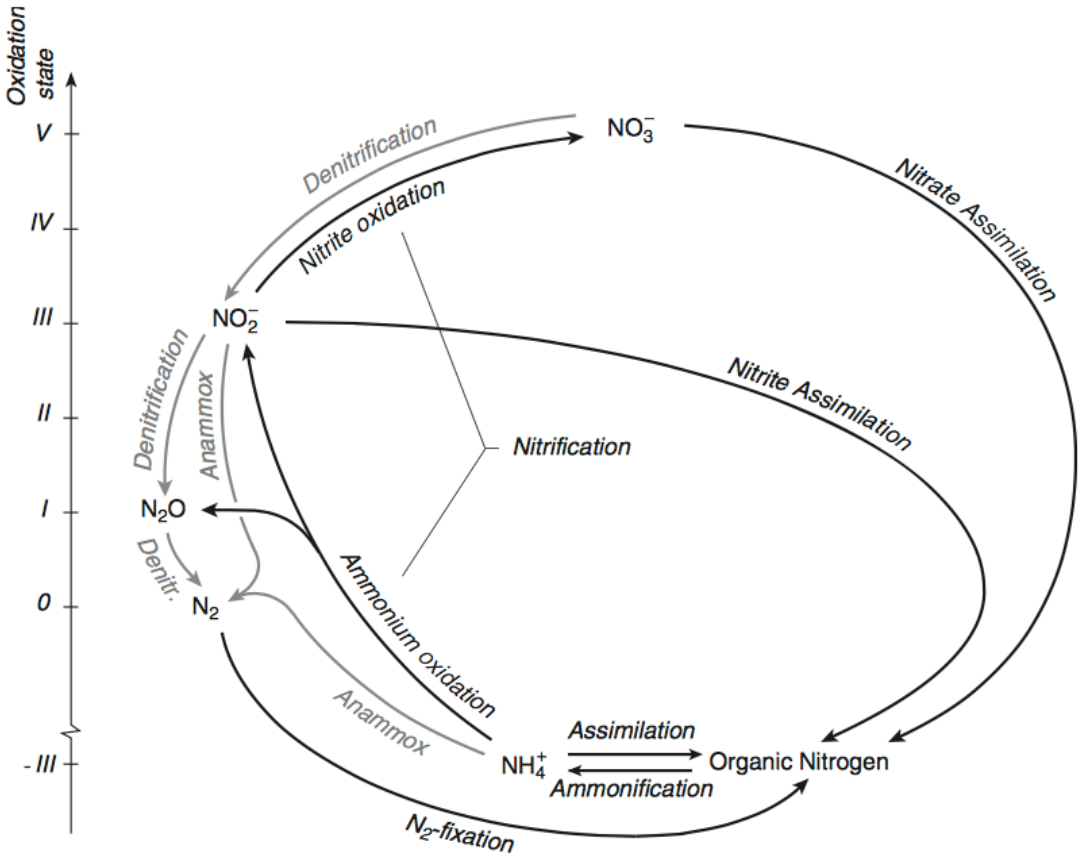

Figure 1. 7: The major forms and transformations of nitrogen in the marine environment. The forms of nitrogen are plotted with their oxidation state. The processes in grey only occur in anoxic environments (Gruber, 2008).

1.4.5. 2: Denitrification

The denitrification pathway can lead to the production or consumption of N_2O. Complete denitrification takes place under anoxic conditions, for example within marine sediments or within OMZ's, where very low oxygen concentrations are present. Complete denitrification involves a series of reduction reactions where nitrate is respired to nitrite, nitrous oxide and then finally to dinitrogen ($NO_3^- \rightarrow NO_2^- \rightarrow N_2O \rightarrow N_2$) (Figure 1. 7) (Capone et al., 2008). However, under certain conditions the final reduction reaction does not take place, leading to the production of N_2O. This is referred to as incomplete, or partial, denitrification (Capone et al., 2008). The production of N_2O from incomplete denitrification in the water column occurs under suboxic (O_2 concentrations below 5 µM) environmental conditions, such as in the Arabian Sea (Naqvi et al., 2005). Both the complete and incomplete denitrification pathways are undertaken by

heterotrophic denitrifying bacteria and archaea (Figure 1. 7) (Desloover et al., 2012).

1.4.5. 3: Nitrifier-denitrification, anammox and dissimilatory nitrate reduction to ammonium (DNRA)

The nitrification and denitrification pathways discussed above are the dominant pathways for N_2O production and consumption in the marine environment (Freing et al., 2012). Three other pathways that influence the production or consumption of N_2O are briefly described. The first pathway is called nitrifier-denitrification and involves the oxidation of ammonium (NH_4^+) to nitrite (NO_2^-), followed by the reduction of NO_2^- to nitric oxide (NO), N_2O and dinitrogen (N_2) (Figure 1. 7). The pathway is undertaken by autotrophic nitrifiers and therefore differs from the coupled nitrification-denitrification pathways, where denitrification is responsible for the reduction of NO_2^- (Wrage et al., 2001). A coupled pathway has also been identified in OMZ's between dissimilatory nitrate reduction to ammonium (DNRA) and anammox. DNRA is a nitrate reduction process that reduces nitrate (NO_3^-) to ammonium (NH_4^+), conserving nitrogen in the ecosystem. Anammox is a chemolithoautotrophic process whereby anaerobic ammonium oxidation by NO_2^- occurs yielding N_2 (van de Graaf et al., 1995) (Figure 1. 7). This pathway has been identified as the predominant pathway for reactive nitrogen loss in the Peruvian OMZ (Lam et al., 2009).

1.4. 6: Loss of nitrous oxide from the ocean.

The main known pathways for loss of N_2O from the marine environment are ocean to atmosphere fluxes (Bange, 2004) and N_2O consumption during complete denitrification.

1.4. 7: Nitrous oxide production in estuaries and shelf seas

Coastal regions are an important source of N_2O, with large quantities emitted from many riverine, estuarine and coastal upwelling regions (Bange et al., 1996b, Bange, 2006). This is a consequence of nitrogen enrichment arising from human activities, such as the addition of fertilisers to crops that run off into rivers and

enter the ocean (Mosier et al., 1998). Nitrous oxide concentration and saturation has been positively correlated to nitrate, nitrite and ammonium concentrations in English rivers and estuaries (Dong et al., 2005, Barnes and Upstill-Goddard, 2011). The main source of N_2O within estuaries appears to be nitrification in the water column (de Wilde and de Bie, 2000), but denitrification in soft sediments has also been reported (Garcia et al., 2004). Supersaturated surface waters of up to 6500 % have been reported in nitrogen-rich estuaries, such as the Humber (Barnes and Upstill-Goddard, 2011). The highest values for N_2O concentration and saturation tend to be found in at very low salinities within estuarine environments, in close vicinity of the turbidity maximum (Barnes and Upstill-Goddard, 2011). In the Schelde Estuary, NW Europe, nearly all N_2O produced was reported to be lost to the atmosphere rather than transported into the open sea (de Wilde and de Bie, 2000). Bange (2006) and Barnes and Upstill-Goddard (2011) found that within coastal regions, that are not influenced by coastal upwelling activity, N_2O production occurs predominantly in the estuarine and riverine environments rather than within shelf seas. Shelf seas have been suggested to account for less than 0.5 % of global oceanic N_2O subsurface production (Freing et al., 2012).

Surface saturations of N_2O in the NW European shelf sea have been observed at 99 to 130 %, with most estimates being at the lower end of this range (Table 1. 4). Comparing the NW European shelf sea observations to saturations reported in various other shelf sea regions, it is evident that globally there is a great variation in the range of N_2O saturation in surface waters, from 112 to 191 ± 74 (Table 1. 4). The NW European shelf seas are at the lower end of this range.

Table 1. 5: Mean surface saturations of N_2O measured within regions of the NW European shelf seas and other shelf seas.

Surface saturation of N_2O (%)	Region	Date	Source
104 ± 1	Central North Sea	September, 1992	Bange (1996b)
101 ± 2	German Bight	September, 1991	Bange (1996b)
99 ± 1	German Bight	September 1992	Bange (1996b)
130	German Bight	July, 1987	Law and Owens (1990a)
108 ± 10	NW European shelf seas	June, 2011	Rees and Brown- personal communication (2014)
191 ± 74	East China Sea	September, 2003	Zhang et al. (2008)
113	Continental shelves of the Bering and Chukchi Seas.	August/ September, 2006	Hirota et al. (2009)
112	Shelf of NW Black Sea	July/August, 1995	Amouroux et al. (2002)

1.4. 8: Nitrous oxide production in the Atlantic Ocean

Table 1. 5 shows the surface saturation of N_2O observed on various cruises in the Atlantic Ocean. Surface waters of the Atlantic Ocean are mostly slightly supersaturated, ranging between 99.7 and 102.5 %. In the Atlantic Ocean the highest surface concentrations and saturations of N_2O are found overlying regions of upwelling, including the west African upwelling and the equatorial upwelling regions. The source of N_2O in these regions arises from nitrification at depth, with N_2O-rich water being vertically mixed from depth to the surface (Yoshinari, 1976, Walter et al., 2006, Forster et al., 2009, Rhee et al., 2009). In the CNRY Longhurst province (Longhurst, 1998) (Figure 1. 8), high surface N_2O saturations have been reported at ~150 % within the Mauritanian upwelling region (Forster et al., 2009), 130 – 140 % around 20 °N (Weiss et al., 1992), and 113 – 118 % between 7 and 10 ° N (Oudot et al., 2002, Walter et al., 2006). In at SATL province mixed layer N_2O was reported at saturations between 98 – 108 %. Depth profiles have shown an increase in N_2O concentration towards the northern boundary, which was also found in both the NATR and WTRA provinces (Forster et al., 2009). Throughout the WTRA province N_2O saturations

reported during AMT12 and 13 from depth profiles were consistently high, at 240 – 360%. In the NAS(E) region N_2O saturations were reported close to the atmospheric equilibrium value (Weiss et al., 1992). The surface distribution of N_2O in the Atlantic Ocean still remains incompletely described.

Table 1. 6: Mean surface saturations of N_2O measured in the Atlantic Ocean on different cruises.

Mean surface saturation of N_2O (%)	**Cruise**	**Date**	**Source**
101.4 (open ocean) 102.3 (coastal)	AMT 7	September-October, 1998	Rhee et al. (2009)
100.8	CITHER-1	January-March, 1993	Oudot et al. (2002)
102.5	AMT13	September-October, 2003	Foster: personal communication (2015).
101.3	Gauss 384-1; M55-SOLAS; Meteor 55	October – November 2002, May 2002 and March-April 2004	Walter et al. (2004)
99.7	AMT20	October-November, 2010	Grefe, (2013)

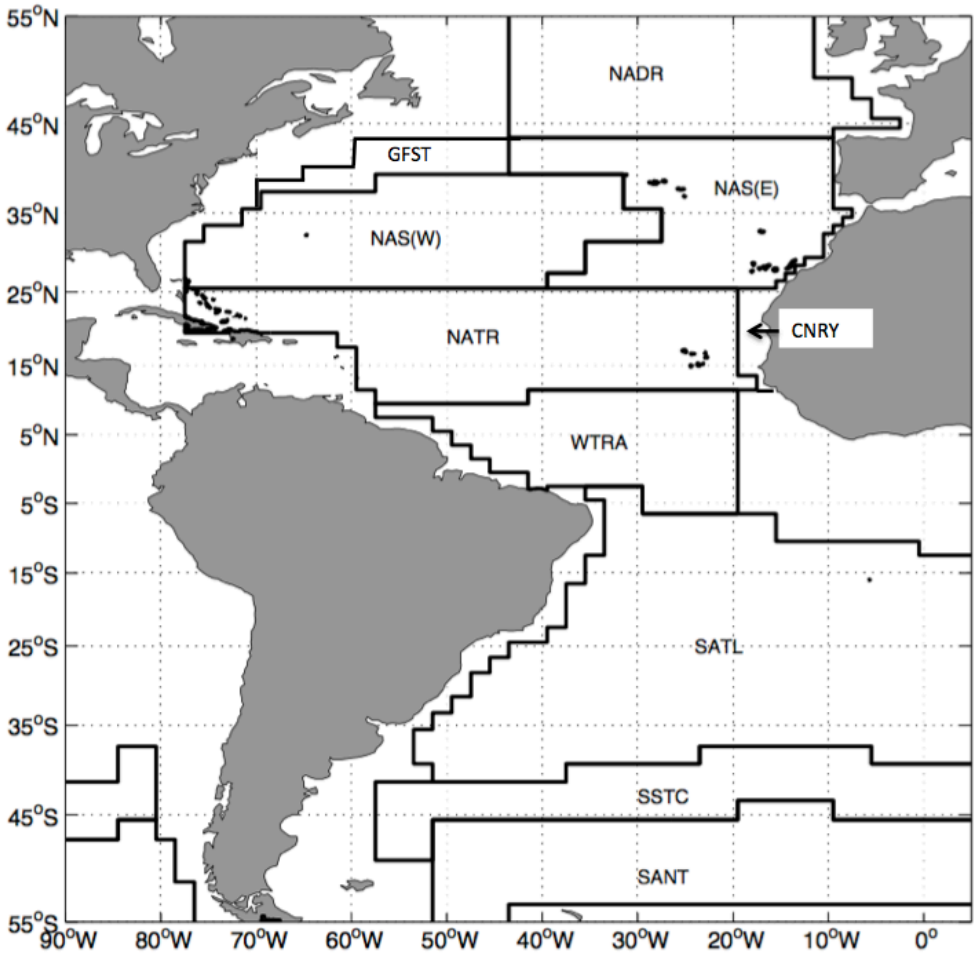

Figure 1. 8: Longhurst provinces in the Atlantic Ocean. North Atlantic Drift Province (NADR), Gulf Stream Province (GFST), North Atlantic Subtropical Gyral Province (NAS), Eastern (Canary) Coastal Province (CNRY), North Atlantic Tropical Gyral Province (NATR), Western Tropical Atlantic Province (WTRA), South Atlantic Gyral province (SATL), South Subtropical Convergence Zone (SSTC) and Subantarctic Water Ring Province (SANT).

1.4. 9: What influences the concentration of nitrous oxide in the surface ocean?

The ventilation time of N_2O in surface waters has been estimated at approximately three weeks (Najjar, 1992). Bange (2004) proposed that the predominant controls on the surface water N_2O saturation in the Arabian Sea were air-sea exchange, the entrainment of N_2O produced at depth to the surface, and the influence of changing sea surface temperatures on the solubility of the trace gas (Figure 1. 9). Based on the observations shown in Table 1. 5, away from highly productive areas, such as upwelling regions and shelf seas, the surface waters of the Atlantic Ocean are not more than 3 % out of equilibrium

with the atmosphere. As a result of this, we would expect to find the concentration of N_2O in the surface layer to be dominated by seasonal changes.

In addition to the controls discussed above, the possibility of a mixed layer source of N_2O has come to light (Dore and Karl, 1996, Law and Ling, 2001, Morell et al., 2001, Wankel et al., 2007, Clark et al., 2008). Ammonia-oxidising bacteria (AOB) biologically produce N_2O in the ocean during nitrification. Because AOB are inhibited by light the euphotic zone was never considered as an environment where nitrification may take place. Recent studies, however, have found that oceanic nitrification is also undertaken by ammonia-oxidising archaea (AOA), and in fact, AOA maybe the dominant contributor to the oceanic N_2O source by nitrification (Santoro et al., 2011, Löscher et al., 2012) Euphotic nitrification has the potential to influence the surface water N_2O concentration in the ocean (Figure 1. 9). There is, however, controversy over the prospect of in-situ nitrification in the euphotic zone of the ocean. Various studies have found the air-sea flux of N_2O to exceed the cross thermocline flux (Law and Ling, 2001, Morell et al., 2001, Freing et al., 2009, Charpentier et al., 2010, Kock et al., 2012). This difference has been attributed by some to nitrification taking place in the euphotic zone (Law and Ling, 2001, Morell et al., 2001) but others have assigned this discrepancy to the influence of surfactants in surface waters and vertical gradients of N_2O in near surface waters, making the air-sea exchange estimates incorrect (Kock et al., 2012). Further support for in-situ nitrification, arises from Clark et al. (2008), who found sufficient nitrification activity to completely turn over the nitrate pool in under eight hours in the euphotic zone of the oligotrophic Atlantic Ocean. In addition, Wankel et al. (2007) found 15 -27 % of nitrate-based productivity in Monterey Bay to be supported by surface water nitrification, and Dore and Karl (1996) estimated the euphotic zone nitrification rate as 47 to 142 % of the nitrate assimilation rate at the North Pacific time-series station ALOHA.

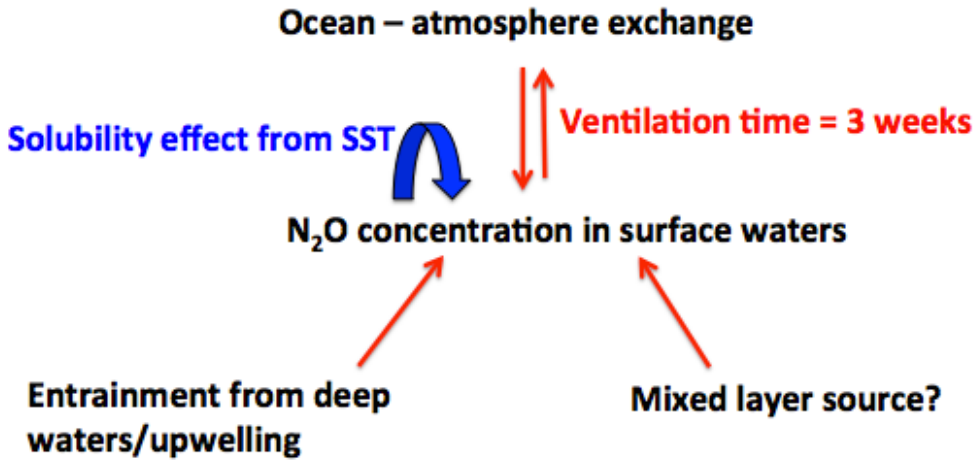

Figure 1. 9: Processes influencing the surface water concentration of N_2O. The mixed layer source may arise from in-situ nitrification.

1.4. 10: Future uncertainties over marine N_2O

Uncertainties over future changes in marine N_2O in response to an expanding O_2 minima, warming of the oceans, and ocean acidification are discussed in Section 6. 10: bullet points 7, 8 and 9.

1. 5: Methane

1.5. 1: Methane as an important long-lived greenhouse gas

Methane is currently the second most prevalent greenhouse gas globally emitted. Methane is a long-lived greenhouse gas, that plays an important role in both stratospheric and tropospheric chemistry (Cicerone and Oremland, 1988). In comparison to N_2O, CH_4 is short-lived, remaining in the troposphere for less than 10 years (Prather et al., 2012). However, CH_4 is a potent greenhouse gas with a high potential to trap heat. The estimated global warming potential of CH_4 in this coming century is 28 times that of CO_2 (Table 1. 1) (Myhre et al., 2013) . Atmospheric CH_4 has increased by 1081 nmol mol^{-1}, over a 261-year period, from 722 ± 25 nmol mol^{-1} in 1750 (considered the pre-industrial atmospheric value) to 1803 ± 2 nmol mol^{-1} in 2011 (Figure 1. 10)

(Etheridge et al., 1998, Dlugokencky et al., 2005, Hartmann et al., 2013). However, the amount of CH_4 in the air has not remained constant over time, with growth slowing in the 1990's, remaining relatively constant between 1999 to 2006, and increasing once again in 2007 (Nisbet et al., 2014). Both high temperatures in the Arctic and high rates of precipitation in the tropics have been linked to years with high atmospheric CH_4 concentrations (Dlugokencky et al., 2009, Bousquet et al., 2011, Nisbet et al., 2014). The main sink for atmospheric CH_4 is by reaction with the hydroxyl radical (OH) in the troposphere and stratosphere. Therefore, inter-annual trends in OH concentrations also significantly influence atmospheric CH_4 concentrations (Hartmann et al., 2013). Seasonal latitudinal differences are also caused by variations in OH in the atmosphere.

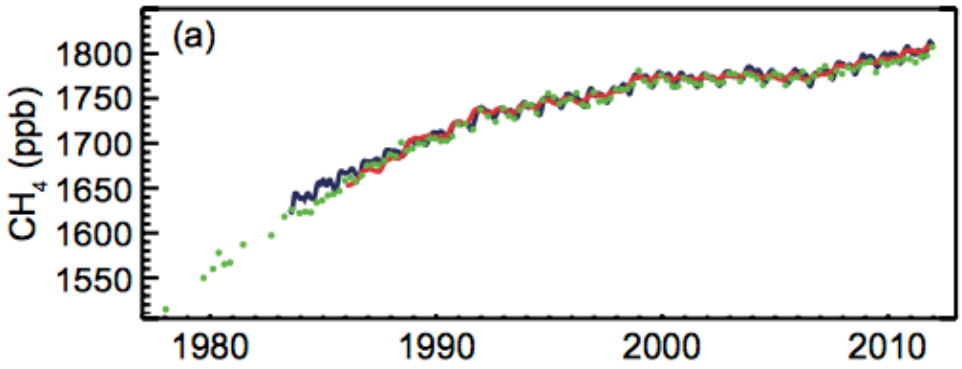

Figure 1. 10: Globally averaged CH_4 dry mole fractions measured in the atmosphere, from University College London (UCL) (green; four values per year, except prior to 1984, when they are of lower and varying frequency), AGAGE (red; monthly), and NOAA/ERSL/GMD (blue; quasi-weekly). Figure from Hartmann et al., (2013).

1.5. 2: Global atmospheric sources of methane

The fifth assessment report (AR5) is the first IPCC assessment that has synthesised the CH_4 budget per decade (Ciais et al., 2013). The report has two types of source measurements referred to as "bottom up" and "top down". Bottom up sources are derived directly from studies of CH_4–producing processes, and values tend to be higher than the top down estimates, which arise

from air observations. The top down estimates for 2011 showed that approximately two thirds of the global emissions of CH_4 to the atmosphere arise from anthropogenic sources and one third from natural sources during that year (Table 1. 6). There is currently no estimate for the oceanic source of CH_4 in this report, but this has been estimated between 1 to 4 % of annual global emissions (Cicerone and Oremland, 1988, Bange et al., 1994).

Methane emissions arise from three types of source: 1) thermogenic, where CH_4 is released during the slow transformation of organic matter into fossils fuels over millions of years, 2) pyrogenic sources, where CH_4 is produced from incomplete combustion, for example during the burning of biomass and biofuels, and 3) from biogenic sources (Neef et al., 2010). Biogenic global CH_4 emissions originate predominantly from the land, with wetlands acting as the greatest natural atmospheric source of CH_4 and agriculture and waste as the greatest anthropogenic source (Table 1. 7) (Ehhalt and Schmidt, 1978, Watson et al., 1992).

Table 1. 7: The 2011 estimates for global "top down" atmospheric CH_4 sources. Top-down refers to estimates from direct observations from air. Table adapted from Ciais et al. (2013).

Global top-down (year 2011)	2011 (AR5)
Atmospheric loss (Tg CH_4 yr^{-1})	542 ± 56
Atmospheric increase (Tg CH_4 yr^{-1})	14 ± 3
Total source (Tg CH_4 yr^{-1})	556 ± 56
Anthropogenic source (Tg CH_4 yr^{-1})	354 ± 45
Natural source (Tg CH_4 yr^{-1})	202 ± 35

Table 1. 8: The anthropogenic and natural atmospheric sources and sinks of CH_4 from the IPCC report AR5 (2000 -2009). "Bottom up" refers to measurements of CH_4-producing sources, and "top-down" to direct observations from air. Table adapted from Ciais et al. (2013).

Tg (CH_4) yr^{-1}	**Top-Down**	**Bottom-up**
Natural sources	218 (179 – 273)	347 (238 -484)
Natural wetlands	175 (142 – 208)	217 (177 – 284)
Other sources	43 (37 – 65)	130 (61 – 200)
Freshwater (lakes and rivers)		40 (8- 73)
Wild animals		15 (15 -15)
Wildfires		3 (1-5)
Termites		11 (2 – 22)
Geological (incl. oceans)		54 (33 – 75)
Hydrates		6 (2 -9)
Permafrost (excl. lakes and wetlands)		1 (0-1)
Anthropogenic sources	335 (273 – 409)	331 (304 – 368)
Agriculture and waste	209 (180 – 241)	200 (187 - 224)
Rice		36 (33 – 40)
Ruminants		89 (87 – 94)
Landfill and waste		75 (67 – 90)
Biomass burning (incl. biofuels)	30 (24 -45)	35 (32 -39)
Fossil fuels	96 (77 – 123)	96 (85 -105)

1.5. 3: Which processes produce methane in the marine environment?

Methane in the marine environment is produced by methanogenesis within anoxic marine sediments and OMZs subjected to vast inputs of organic matter (Levipan et al., 2007, Ferry and Lessner, 2008). Methanogenesis is a form of anaerobic respiration, which involves the conversion of complex organic matter to CH_4, using carbon as the final electron acceptor instead of O_2. Most commonly used electron acceptors include CO_2 and the methyl group of acetate (Ferry and Lessner, 2008). However, formic acid (HCOOH), methanol (CH_3OH) and methanthiol (CH_3SH) can also be used (Oremland and Polcin, 1982, Gupta et al., 1994).

1.5. 4: Methane loss in the marine environment

The main losses of CH_4 in the ocean are air-sea exchange and microbial consumption. Microbial oxidation occurs under oxic conditions, including well-oxygenated sediments and water columns, where CH_4 is oxidised to CO_2 (Equation 1. 3). The microbial oxidation of CH_4 can also occur in anoxic

environments, where sulphate acts as the terminal electron acceptor in the anaerobic oxidation of CH_4 (Equation 1. 4) (Boetius et al., 2000, Knittel and Boetius, 2009). During this process, archaebacteria interact with SRB under anoxic conditions reversing the process of methanogenesis (Hinrichs et al., 1999). Microbial oxidation, at low salinities, has a significant impact on reducing the emission of CH_4 to the atmosphere (Abril and Borges, 2005). Ward et al., (1987) and Jones (1991) estimated the turnover time of microbial consumption of CH_4 in the open ocean as averaging at around 65 years. Tilbrook and Karl (1995) used this average turnover time to calculate a consumption rate in the Pacific Ocean of CH_4 of 0.01µmol m^{-2} d^{-1} and concluded that this rate was negligible in comparison to the loss of CH_4 associated to air-sea exchange. The dominant sink for CH_4 in the open ocean is therefore the ocean to atmosphere flux of this trace gas.

$$\boldsymbol{CH_4 + 2O_2 \rightarrow CO_2 + 2H_2O}$$

Equation 1. 3

$$\boldsymbol{CH_4 + SO_4^{2-} \rightarrow HCO_3^- + HS^- + H_2O}$$

Equation 1. 4

1.5. 5: The marine environment as a source of methane

The marine environment contributes between 1 – 4 % of the global atmospheric CH_4 budget, with global ocean to atmosphere fluxes estimated at around 11-18 Tg CH_4 yr^{-1} and subject to seasonal variation (Bange et al., 1994). Global open ocean surface waters are usually supersaturated. As with N_2O, the global distribution of CH_4 in surface waters of the ocean is non-uniform with regions of high biological productivity, such as shelf sea regions and OMZ's, dominating the oceanic source. Shelf seas cover approximately 16 % of the global oceans, and have been proposed to account for around 75 % of the oceanic emission of CH_4 (Bange et al., 1994). The primary pathway by which CH_4 is produced in these regions is methanogenesis, which occurs predominantly within organically enriched coastal, estuarine and riverine systems and sediments, under anoxic conditions (Lamontagne et al., 1973, Scranton and McShane, 1991, Bange et al.,

1994, Bange et al., 1996b, Upstill-Goddard et al., 2000, Bange, 2006, Grunwald et al., 2009). The major ocean OMZ's, including the Arabian Sea and the eastern tropical South Pacific, also act as hotspots for CH_4 production in the ocean (Naqvi et al., 2010). In these regions the upwelling of nutrient-rich deep waters stimulates primary productivity, producing a downward flux of organic particles. As these particles reach sub-oxic intermediate waters, at around 500 – 1000 m depth, they are subject to methanogenesis, producing CH_4 (Rixen et al., 1996). The CH_4 concentration of surface waters overlying OMZ's, has been shown as highly influenced by upwelling of CH_4-rich waters, produced within the O_2-deficient waters below (Bange et al., 1998, Upstill-Goddard et al., 1999). Other oceanic sources of CH_4 include thermogenic CH_4 seepages and CH_4 hydrate dissolution (Bussmann and Suess, 1998, Kvenvolden and Rogers, 2005, Westbrook et al., 2009).

Methanogenesis is influenced by sulphate-reducing bacteria (SRB), because the process is generally inhibited in substrates due to the ability of SRB to outcompete methanogens for hydrogen (H_2) and acetate. Hydrogen is sourced from H_2 donating organotrophs in marine sediments (Abram and Nedwell, 1978). As a consequence of this, methane concentrations are mostly low in regions where sulphate-reduction occurs, and increase in sediments and the water column where sulphate is depleted, such as within freshwater environments and in regions that receive high organic loading, such as many shelf environments (Ferry and Lessner, 2008). This produces a gradient of CH_4 production by methanogenesis, of up to two orders of magnitude, within estuarine systems (Abril and Borges, 2005). However, a small fraction of CH_4 produced by methanogenesis has been found to occur in the presence of SRB's when substrates such as methylamines, which are not utilised by sulphate reducers, are present (Capone and Kiene, 1988).

Ebullition, where small bubbles of CH_4 gas form in the sediments and travel through the water column to the surface, is considered a major mechanism for transporting methane from anoxic sediments to the surface water and eventually

to the atmosphere (Walter et al. 2007). High intensity methane seeps have been detected in global oceans and may act as sources of CH_4 to the atmosphere (Holzner et al., 2005, Westbrook et al., 2009).

Although methanogenesis is an anaerobic process, supersaturation for CH_4 in oxic surface waters is a persistent feature in most oceans (Scranton and Brewer, 1977, Ward et al., 1987, Cicerone and Oremland, 1988, Bange et al., 1998, Forster et al., 2009), with a maximum at the base of the mixed layer and concentration decreasing with depth (Figure 1. 11) (Oudot et al., 2002, Forster et al., 2009). This phenomenon is referred to as the 'methane paradox' as the anoxic process of methanogenesis occurs within the 'oxic' surface waters of the ocean. Although coastal waters may be influenced by supplies from estuaries and marshlands (Bange et al., 1994), this can not explain the open ocean mixed layer source widely reported. The production of CH_4 in an oxic environment was originally believed to arise from small anoxic micro-niches found within decaying organic particles, faecal pellets, as well as in fish and zooplankton intestines (Lamontagne et al., 1973, Karl and Tilbrook, 1994, Van der Maarel et al., 1999). Further support for these theories arose from De Angelis and Lee (1994) who measured CH_4 release from both zooplankton and phytoplankton cultures. More recently however, the CH_4 cycle has been shown to be more complex with new findings revealing two pathways, which allow certain species to exploit oceanic phosphorus and nitrogen stores, releasing CH_4 in the process (Karl et al., 2008, Damm et al., 2010). Phytoplankton actively release various compounds, such as methylated substrates. Both methylphosphonate (Mpn) and dimethylsulfoniopropionate (DMSP) are used by bacteria during methylotrophic methanogenesis for energy supply in aerobic systems (Karl et al., 2008, Damm et al., 2010). During the decomposition of Mpn, CH_4 is produced as a by-product. This pathway occurs within phosphate-limited waters (Karl et al., 2008). The second pathway occurs in nitrate-limited waters, where phosphate is widely available. In such conditions, Damm et al. (2010) described bacteria as displaying an enhanced ability to compete for the phosphate, using DMSP as a carbon source, and producing CH_4 during the process. There is also potential for other currently unknown pathways, for example Tang et al. (2014) found CH_4

production in Lake Stechlin, northeast Germany, to be significantly related to photosynthesis and/or nitrogen fixation in the oxygen-rich upper layer. They hypothesised that methanogens were using substrates released by the photo-autotrophs in the production of CH_4. Neither dimethylphosphonate or trimethylamine were found to stimulate the production of CH_4 (Grossart et al., 2011), leading to the proposal that acetate maybe supporting methanogenesis in the oxic waters instead (Tang et al., 2014).

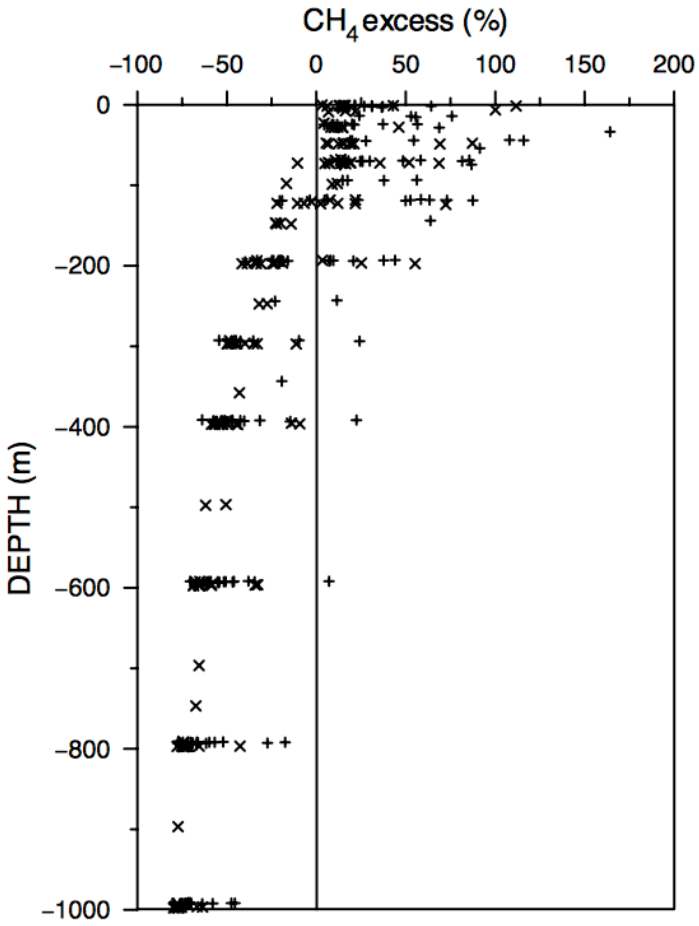

Figure 1. 11: The excess CH_4 saturation (%). Excess CH_4 is defined here as the CH_4 saturation minus 100 % and is displayed with depth (m) in the Atlantic Ocean along 7°30' N (plus) and 4°30' S (cross). From Oudot et al. (2002).

In the NW European shelf seas surface CH_4 saturation has been reported between 113 and 332 % with the higher values in the central North Sea, which is subjected to freshwater inputs from large rivers and estuaries (Table 1. 8). In comparison to other shelf seas, the NW European shelf sea has lower surface CH_4

saturations. For example, mean surface saturations have been reported in the NW Black Sea at 930 % (173 – 10500 %) (Amouroux et al., 2002), in the East Siberian Arctic shelf at 800 % in 2003 and 2500 % in 2004 (Shakhova and Semiletov, 2007), and 134 ± 22 % (110 to 222 %), in the Yellow Sea and East China Sea (Zhang et al., 2004) (Table 1. 8). The highest saturations have been associated with CH_4 seeps from the marine sediments (Shakhova and Semiletov, 2007).

Table 1. 9: Surface saturation of CH_4 reported in the NW European shelf seas and other shelf sea regions.

Surface saturation of CH_4 (%)	**Region**	**Date**	**Source**
126 ± 8	German Bight	September, 1991	Bange (1994)
140	Southern North Sea	November, 1980	Conrad and Seiler (1988)
100	NE Atlantic Bay of Biscay	November, 1980	Conrad and Seiler (1988)
113 (95 – 130)	Southern Bight	March, 1989	Scranton and McShane (1991)
120 - 332	Central North Sea	May, 1994	Rehder et al (1998)
129 (112 - 136)	Off the east coast of UK	1995 to 1999	Upstill-Goddard et al. (2000)
930 (173 – 10500)	NW Black Sea	July, 1995	Amouroux et al. (2002)
800 % 2500 %	East Siberian Arctic shelf	September, 2003 September, 2004	Shakhova and Semiletov (2007)
134 ± 22 (110 to 222)	Yellow Sea and East China Sea	March – May 2001	Zhang et al. (2004)

1. 6: Carbon dioxide (CO_2) and Carbon monoxide (CO)

Carbon dioxide and CO are briefly discussed below. These climatically relevant gases are not the main focus of the thesis, but are used in the interpretation of the N_2O and CH_4 datasets.

Atmospheric concentrations of CO_2 have increased by 40 % since 1750, at a rate of 2.0 +- 0.1 ppm yr^{-1} between 2002 and 2011(Pachauri and Meyer, 2014). The main contributors to increasing CO_2 atmospheric concentrations are fossil fuel combustion and land use change (Pachauri and Meyer, 2014). During the period of 1750 to 2011, CO_2 has acted as the largest contributor to radiative forcing (Pachauri and Meyer, 2014). The ocean contains the largest carbon reservoir for CO_2, holding approximately 93 % of carbon (Feely et al., 2001), taking up around a third of anthropogenic emissions (Siegenthaler and Sarmiento, 1993). The ocean has the capacity to store more CO_2 than the atmosphere and terrestrial biosphere because CO_2 that enters the ocean reacts with seawater producing carbonic acid, which dissociates to bicarbonate and carbonate ions (Feely et al., 2001). The exchange of carbon dioxide between the ocean and atmosphere takes place via gas transfer. Carbon dioxide is then transferred between the marine biota and other oceanic reservoirs during photosynthesis and respiration. Marine biota act as a carbon pump through the production of particulate and dissolved organic carbon, which is exported to the deep ocean (Siegenthaler and Sarmiento, 1993).

Carbon monoxide is a primary determinant in the production of tropospheric hydroxyl radical (OH), and as a result indirectly influences the atmospheric lifetimes of greenhouse gases such as methane, which are oxidised in the atmosphere (Isaksen and Hov, 1987), and can also lead to the formation of ozone. More than half of CO emissions arise from human activities, including deforestation, savannah, waste burning, fossil and domestic fuel use. (Prather et al., 2001). Observations indicate a decrease in atmospheric CO levels since the late 1980s (Khalil and Rasmussen, 1994), which may be attributed to the introduction of catalytic converters, reducing emissions from vehicles (Bakwin et al., 1994).

In the ocean carbon monoxide displays a strong diurnal cycle in sea surface CO concentrations (Stubbins et al., 2006). This arises predominantly from the sunlight-initiated photolysis of chromophoric dissolved organic matter (CDOM)(Wilson et al., 1970, Conrad et al., 1982) and the removal by microbial oxidation (Conrad et al., 1982). Carbon monoxide photoproduction is an important source, equivalent to 16 - 350 % of carbon burial in marine sediments (Hedges et al., 1997).

1. 7: Aims of this thesis

The sections above describe the vast amount of research already undertaken to understand the global sources and sinks of N_2O and CH_4. However, in the ocean there are still great uncertainties surrounding the ability of the marine environment to produce and/or consume these climatically important gases.

There have been many observational studies for N_2O and CH_4 in estuarine and riverine environments because high emissions of both gases are produced in these regions. There are however, limited measurements in the shelf seas that the estuaries discharge into. The high-resolution surface measurements of N_2O and CH_4 made during this project provide highly accurate coverage of the NW European shelf sea region. Most measurements that have been made within shelf seas have been discrete, so few and far apart, making it difficult to establish relationships with important parameters, to understand the fundamental processes affecting each trace gases surface distribution. During this project, four high-resolution datasets for surface N_2O, CH_4, CO_2 and carbon monoxide (CO) were collected in the summer of 2011. The relationships between surface N_2O and CH_4 and high-resolution underway measurements of sea surface temperature (SST), salinity (SSS) and chlorophyll-a (chl-a) concentrations were examined, along with the interaction with surface CO_2 and CO. This provided insight into relationships influencing the surface distribution of these gases within the NW European shelf seas in summer.

There are currently limited studies examining the effects of seasons on surface water N_2O and CH_4 concentrations. The high-resolution surface N_2O and CH_4 datasets collected across the Atlantic Meridional Transect (AMT) offer the potential to study this. In addition, as yet there have been no studies that have examined whether the surface ocean concentration and saturation of N_2O has changed over time, and if so, whether a change in source-sink characteristic has occurred. The comparison of the AMT dataset collected for this project, in conjunction with four other high-resolution AMT surface N_2O datasets over an eighteen-year time period, provides an opportunity to investigate this in the Atlantic Ocean. A comparison of surface concentration, saturation and air-sea flux for N_2O and CH_4 will also be made between the shelf sea and open ocean environment to determine which environment is the greatest source of N_2O and CH_4 to the atmosphere, and how the processes and sources differ between the two environments.

1.6. 1: Questions this thesis aims to address

This thesis aims to address the questions below:

- What are the mean surface concentration, saturation and air-sea fluxes of N_2O and CH_4 across the NW European shelf seas in the summertime, and what ranges are we seeing within these observations/estimates?
- Are these values comparable to other surface measurements made in this region?
- In the summertime, do the NW European shelf seas act as an atmospheric source or sink for N_2O and CH_4?
- Which processes influence the sea surface N_2O and CH_4 on the NW European shelf seas?
- Using high-resolution ICOS measurements, what are the mean surface concentration, saturation and air-sea flux of N_2O and CH_4 air-sea fluxes of N_2O across the Atlantic Ocean during boreal autumn and austral spring, and what ranges are we seeing within these observations/estimates?
- Are these values comparable to other surface measurements made in this region?

- In boreal autumn and austral spring does the Atlantic Ocean act as an atmospheric source or sink for N_2O and CH_4?
- Is there a difference between the surface saturation, concentration and ocean to atmosphere flux for N_2O and CH_4 between the northern hemisphere and southern hemisphere, and if so what causes this difference?
- Which processes influence the sea surface N_2O and CH_4 in the Atlantic Ocean?
- What are the sources of N_2O and CH_4 in shelf seas and open ocean environments, and do these sources differ in each environment?
- Is there a difference in surface saturation and the ocean to atmospheric flux of N_2O and CH_4 between open water and shelf sea environments, and if so, what causes this difference?
- Has there been a temporal change in surface N_2O in the Atlantic Ocean over the past eighteen years?

1. 8: Structure of the thesis

The paragraphs below describe the objectives of each chapter in the thesis.

Chapter 2 contains details of the methodology used in this study. This includes the set up of equipment on two research cruises (D366 and AMT22) and validation of the atmospheric and seawater measurements.

Chapter 3 presents and interprets the surface water N_2O data collected on the D366 ocean acidification cruise across the NW European shelf seas in June and July, 2011. The chapter describes the dataset, quantifying the mean surface concentration, saturation and ocean to atmosphere flux of N_2O in the region, and identifies the influential processes on the surface distribution of this climatically active gas.

Chapter 4 presents and interprets the surface water CH_4 data collected on the D366 ocean acidification cruise across the NW European shelf seas in June and July, 2011. The chapter quantifies the mean surface concentration, saturation and ocean to atmosphere flux of CH_4, identifies the influential processes affecting the surface distribution of this potent greenhouse gas.

Chapter 5 describes and interprets the surface N_2O and CH_4 measurements made on the Atlantic Meridional Transect 22 (AMT22). This chapter describes both datasets and identifies the important processes in the Atlantic Ocean that influence the surface distribution of these gases. Chapter 5 examines the effect of seasons on surface N_2O and CH_4 by investigating whether there is difference in surface saturation and the ocean to atmosphere flux between the NH and SH. Finally, this chapter draws a comparison between the AMT22 N_2O dataset and an additional four high-resolution surface water N_2O datasets made from 1996 to 2013, along the AMT transect, to determine whether a change in source-sink characteristic has occurred during that time period.

Chapter 6 discusses the general conclusions from the thesis, drawing together the chapters to identify whether there is a difference in the surface saturation

and air-sea fluxes calculated in the shelf sea and open ocean environments, and discussing reasons for this difference, as well as comparing the different processes and pathways between the two different environments. This chapter finishes by making suggestions for future work.

Chapter 2: Methodologies.

2. 1: Cruise specifics

The data collected for my thesis was obtained from two research cruises, the D366 Ocean Acidification (OA) cruise and the Atlantic Meridional Transect 22 (AMT22) cruise. The specifics are described below:

2.1. 1: D366 OA cruise

The D366 OA cruise, part of the UK Ocean Acidification Research Program, took place on *RRS* Discovery in the summer of 2011 (June 6th –July 9th, 2011) travelling around the Northwestern European Shelf seas. The cruise departed from Liverpool Bay on June 6th 2011 and arrived back at the same port on the 9th of July, 34 days later (Figure 2. 1). The cruise track covered 4730 nautical miles across a range of shelf and coastal environments within the Irish Sea, the North-East Atlantic, the Bay of Biscay, the English Channel, the North Sea and the Skagerrak. Dorothee Bakker (UEA) and Gareth Lee (UEA) undertook measurements using two Los Gatos off axis Integrated Cavity Output Spectrometers (ICOS) measuring sea surface and atmospheric N_2O, CH_4, CO_2 and CO on-board the research ship (instrumentation discussed in detail in section 2.2). Once the data were collected, I undertook the analysis of the data.

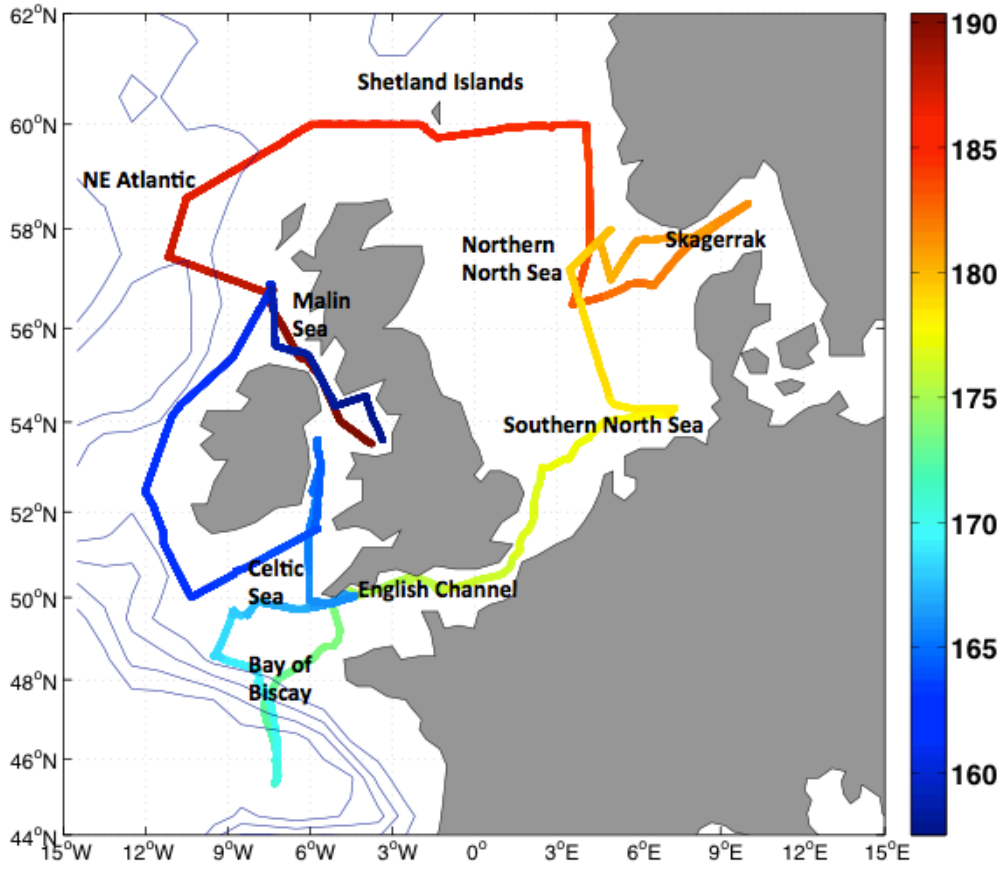

Figure 2. 1: The D366 cruise track. The colour bar displays time in ordinal date. The contour lines show 1000m, 2000m, 3000m and 4000m depths.

2.1. 2: AMT22

The AMT22 research cruise took place on the *RRS* James Cook, during the northern hemisphere autumn and the southern hemisphere spring period (October/November), 2012. The ship left Southampton Port, UK, on the 10th October, arriving into Punta Arenas Port, Chile on 23rd November 2012 (Figure 2. 2). The cruise track enabled sampling during two seasons, from coastal regions, to open ocean waters, across the oligotrophic North Atlantic Gyre (NAG) and the South Atlantic Gyre (SAG) and across the equator, sampling regions of upwelling. The vast diversity of environmental conditions during the cruise allowed an exploration of the controls and influences on the sea surface distribution of N2O and CH_4. The ship passed through several biogeochemical provinces, including NADR, NAST(E), NAST(W), NATR, WTRA, SATL, and SSTC (Figure 1. 8).

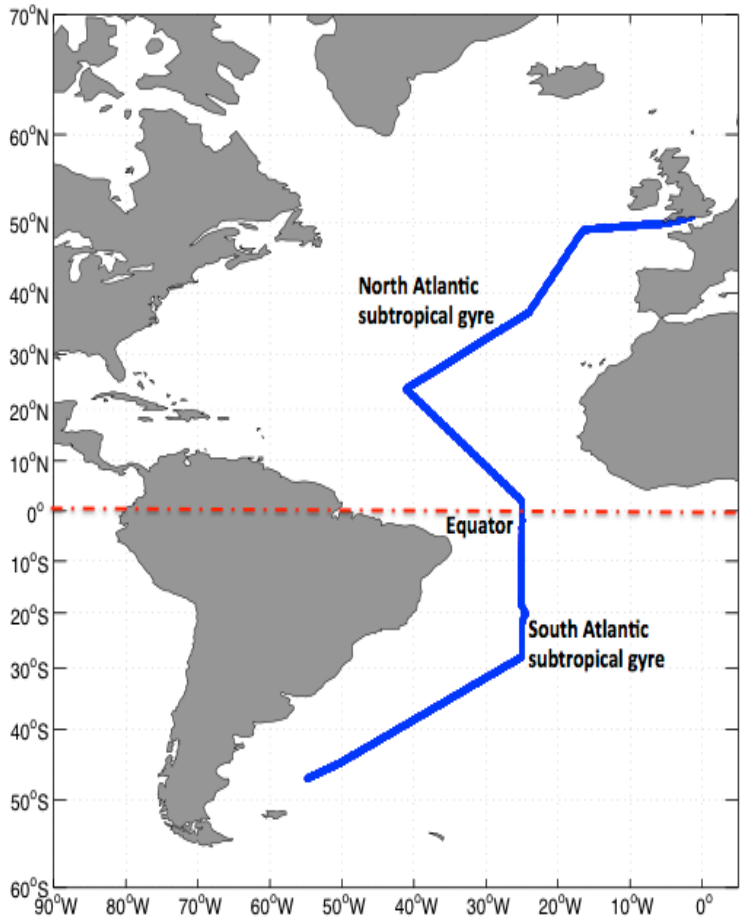

Figure 2. 2: Cruise track for AMT22 from Southampton, UK to Punta Arenas, Chile.

2. 2: Instrumentation

2.2. 1: Los Gatos off axis Integrated Cavity Output Spectrometers (ICOS)

Surface N_2O and CH_4 measurements currently and in the past have been made either discretely by sampling water from a conductivity, temperature and depth (CTD) instrument and measuring using an initial separation stage, usually gas chromatography (GC) followed by Electron Capture Detection (ECD) for N_2O, or Flame Ionisation Detection (FID) for CH_4, or have been made at high-resolution with the incorporation of an equilibrator into the system. The high-resolution systems have the advantage when studying the surface ocean of being able to capture high spatial and temporal coverage. This system for example has a resolution of 10 samples per nautical mile, allowing the detection of important

patterns to be identified. There are however disadvantages with these systems in comparison to GC-ECD/FID instrumentation, for example, they are unable to sample depth profiles, which are important in our understanding of the distribution of these important gases. This highlights the on-going importance of GC-ECD/FID method, which if used alongside ICOS would allowed the collection of both depth profiles and high-resolution surface datasets. The recent development of stable, high precision and resolution optical-based ICOS analysers, combined with an equilibration system, have further advantages over the previous high-resolution systems including:

1) Two ICOS instruments can be connected allowing the simultaneous measurement of N_2O and CH_4, as well as CO_2 and CO, in sea surface waters and in the atmosphere.
2) The system does not require a carrier gas, radioactive components, or the target gas to be separated or cryo-trapped.
3) Within a 5 minute ($1\ \sigma$) average precision (n=300) of the ICOS instruments for N_2O for a 103.90 nmol mol^{-1} standard was 0.29 nmol mol^{-1} and for a 2515.56 nmol mol^{-1} standard for CH_4 was 18.45 nmol mol^{-1}. These instruments demonstrate much better precision at 0.3 % (N_2O) and 0.7 % (CH_4) than the GC-ECD/FID instrumentation, e.g. Forster et al. (2009) at 5 %.

Integrated cavity output spectrometry instruments measure the moist mole fraction (X (gas, moist)) of a sample in the equilibrator headspace and atmosphere and report the dry mole fractions (X (gas, dry)) by correcting for water vapour (*Equation 2. 1*). (Units: (X (gas, moist)): µmol mol $^{-1}$ for CO_2 and nmol mol $^{-1}$ for N_2O, CH_4 and CO). The mole fraction (mixing ratio) of a gas is defined as the number of moles of Xgas per mole of air, and is given in the units of mol mol^{-1}, which represents the volume of gas per volume of air. The presence of water vapour reduces the concentration of a gas in a sample. If water vapour is not removed important features of the spatial and temporal distribution of a trace gas maybe affected, as water vapour is highly variable. Grefe (2014) found

the instrument's correction from moist to dry mole fractions to be accurate and therefore no further correction for water vapour was required.

$$\boldsymbol{X(gas, dry) = \frac{X(gas, moist)}{1 - X(gas, moist)}}$$

Equation 2. 1

The instruments require partially dry gas samples (to avoid condensation), to be continuously pumped through an optical cavity, which has highly reflective mirrors. A light source, in the form of a diode laser beam, is reflected back and forth in the cavity creating long pathways, 1000's of meters in length (Becker et al., 2012). A combination of scattering and absorption in the cavity, along with the reflectivity of the mirrors, influence the laser beam and produce an output intensity that decays over time due to absorption in the analysers. The mole fraction of the gas measured is calculated from this 'ring-down signal'.

2.2. 2: Instrumentation set-up at sea

The following information describes the set-up for simultaneously taking continuous, high resolution, sea surface and atmospheric measurements of N_2O, CH_4, CO_2 and CO during the two research cruises described above, using two *Los Gatos* ICOS analysers. The setup was based on Grefe and Kaiser (2014), who used a *Los Gatos* ICOS N_2O/CO analyser, but incorporated an additional *Los Gatos* ICOS CO_2/CH_4 Instrument 'daisy-chained' to the first instrument.

2.2. 3: Seawater measurements

For the seawater measurements (see Figure 2. 3 for a diagram of the setup), a glass-bed equilibrator was connected to the ICOS instruments (Schuster and Watson, 2007). The equilibrator was filled with glass rashig rings (Hilgenberg GmbH), leaving a small headspace at the top, to create a high surface area enabling equilibration between the seawater and gas phases. A constant seawater flow, from the ship's uncontaminated seawater supply, fed into the

top of the equilibrator (sourced from 5 m water depth), and drained from the bottom. Biological growth in the equilibrator could potentially lead to N_2O and CH_4 production through methanogenesis and denitrification undertaken by microorganisms within anoxic microsites. To avoid this the equilibrator and glass raschig rings were cleaned before and after each cruise with a weak acid wash to remove any algal growth. Biological growth in the equilibrator was visually minimal throughout the cruises. The sample was removed from the headspace at a rate of 100 ml min^{-1} by an internal diaphragm pump in the instruments. The headspace was maintained at ambient air pressure, with a venting tube (1/8" Dekabon tubing) open to the laboratory air. The venting tube held approximately 10% of the headspace volume so that small fluctuations in air pressure could move the headspace in and out the tube without any outside air being drawn in. A water trap at the base of the equilibrator minimised the air exchange between the laboratory air and the equilibrator headspace. As the partial pressure of gases is highly sensitive to temperature, the equilibrator temperature was continuously recorded onto a laptop using Omega V2.07.1 software, from two Pt100 temperature probes (discussed in more detail in the temperature calibration section), so any temperature changes could be corrected for during later analysis of the data. The gas headspace was sampled at a frequency of 1 Hz, with the sample being removed from the headspace and passing through a thermoelectric cool-box (T08 DC, Mobicool), set a 5 °C, to remove water vapour from the sample. Condensation from the cool box was regularly removed manually. A custom-built water safety valve, consisting of a Swagelok stainless steel tee and a water-watcher, was positioned prior to the instruments, to prevent any water entering the measuring cell. The safety valve closed to prevent gas flow to the instruments if water was detected in the line. The headspace sample, once measured, was returned back to the headspace of the equilibrator to maintain constant pressure.

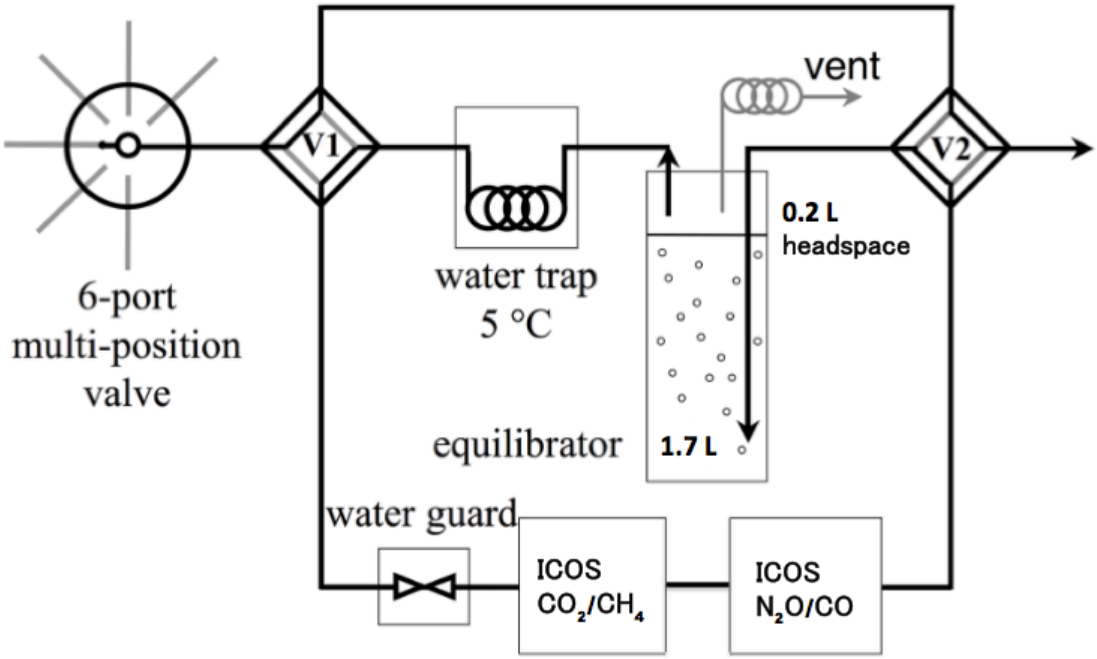

Figure 2. 3: The set-up of the ICOS instruments on both cruises to measure seawater and atmospheric moist mole fractions of CO_2, N_2O, CH_4 and CO, as well as the calibration standards. Adapted from Grefe and Kaiser (2014).

A constant flow of seawater, at a rate of 1.8 L min^{-1}, was aimed for throughout all the cruises. However, on the D366 OA cruise the water-flow from the underway system was often variable which lead to a lot of spikes in the trace gas datasets. These spikes were manually removed from the datasets by comparing the measured underway sea surface temperature (SST) and the equilibrator temperature and identifying inconsistencies where the equilibrator temperature suddenly changed in comparison to the sea surface temperature. These changes were indicative of sudden surges of water flow or reductions in water-flow and therefore the data were removed. To help eliminate the water flow problem during the AMT22 cruise, a water-flow controller was used (Robert Pearson & Company Ltd, 1/2 inch diameter tap tail flow regulator, orange). This was effective in controlling the water flow at a rate of 1.8 L min^{-1}, but did require cleaning every few days.

2.2. 4: Valves

Two valves were used to allow a fast switch to be made between measuring the headspace (seawater), atmospheric air and the calibration standards (Figure 2. 3). A 6-port multi-position valve, attached to the calibration standards used on each cruise, as well as the atmospheric airline. This attached to a 2-way, 8-port valve connecting to the equilibrator, thermoelectric cool-box and the water safety valve.

2.2. 5: Atmospheric measurements

A 1/4" Dekabon tube ran from the monkey island of each ship (18 m height on *RRS* Discovery and 15 m height on *RRS* James Cook), through the thermoelectric cool-box and the water safety valve and into the 6-port multi-position valve. The ICOS analysers sampled the atmospheric air regularly. On D366, 40 minute long atmospheric runs were recorded daily with higher frequencies at the start of the cruise when stability checks were being made. On AMT22 cruise this frequency was increased, sampling the atmospheric air approximately every 4 - 6 hours for 5 minutes. The airline was pumped at a rate of 100 ml min^{-1} to ensure constant flushing of the tubing. The data from the atmospheric runs were visually assessed to remove any samples that were considered contaminated by stack pollution from the ship. Both the wind speed and direction were also used to help assess this. Contaminated samples that were removed displayed variability throughout the measurements and/or decreased or increased throughout the final five minutes of the measurement period.

2.2. 6: Calibration standards

The accuracy of the measurements is determined by the standards used to correct the data. The ICOS instruments are calibrated at manufacture and can be recalibrated at any point when a significant drift from known values is observed. Working standards were measured daily on each cruise to correct for instrumental drift that occurred throughout the weeks at sea. On both D366 and AMT22 the instrumental drift was minimal. Four working standards were taken on the D366 cruise (Table 2. 1). One third of the way through the cruise an additional working standard was borrowed (PML 1) and measured for the rest of the cruise, to provide a greater range of the trace gases being measured in the

atmosphere and seawater. Three working standards were used for the AMT22 cruise (Table 2. 3). Each working standard contained a mixture of CO_2, N_2O, CH_4 and CO in a mixture of oxygen (O_2) (20 %) and nitrogen (N_2) (80 %). The working standards were calibrated against a range of reference standards used at the Weybourne Atmospheric Observatory (WAO) (Table 2. 2). The WAO reference standards are produced, calibrated and supplied by the Max Planck Institute for Biogeochemistry (MPI-BGC) GasLab (https://www.bgc-jena.mpg.de/index.php/ServiceGroups/GasLab). Designated mole fractions of N_2O, CH_4, CO_2 and CO are referenced to WMO calibration scales using primary laboratory standards supplied by WMO-GAW Central Calibration Laboratories (CCL's). For the gases mentioned in Table 2.2, NOAA is the WMO-GAW recognized CCL. The accuracies of the WAO reference gases for N_2O, CH_4, CO_2 and CO are estimated as 0.02 μmol mol^{-1} at 390 μmol mol^{-1}, 0.1 nmol mol^{-1} at 2150 nmol mol^{-1}, 0.15 nmol mol^{-1} at 345 nmol mol^{-1} and 0.6 nmol mol^{-1} at 180 nmol mol^{-1}, respectively.

The gas concentrations in both the reference and working standards aimed to represent the range of expected concentrations in the samples being analysed at sea and in the atmosphere. The calibrations for each gas are discussed further in the following sections: N_2O: section 2. 7, CO: section 2. 8, CO_2: section 2. 9 and CH_4: section 2. 10.

Table 2. 1: Mole fractions of the four gases in the working standards measured on the D366 OA cruise.

Standard name	N_2O (nmol mol^{-1})	CO (nmol mol^{-1})	CO_2 (μmol mol^{-1})	CH_4 (nmol mol^{-1})
OBO1	4.90	146.81	--------	-------
25B22	103.90	111.89	268.07	2515.56
35B28	58.41	91.72	363.43	3081.32
45B24	47.63	154.75	468.80	3378.41
PML 1	-------	------	-------	2022.11

Table 2. 2: Mole fractions of the four gases in the reference standards used for the pre and post cruise calibrations at WAO for both cruises.

Tank	N_2O (WMO N2O X2006) (nmol mol $^{-1}$)	CO (WMO CO X2004) (nmol mol $^{-1}$)	CO_2 (WMO CO2 X2007) (µmol mol $^{-1}$)	CH_4 (WMO CH4 X2004) (nmol mol $^{-1}$)
D718844	314.10	61.80	426.16	1753.70
D718845	319.60	105.20	372.46	1849.50
D718846	324.90	162.90	393.83	1945.10
D718847	329.70	201.70	396.99	2048.10
D718848	324.20	192.90	398.55	1909.50

Table 2. 3: Mole fractions of the four gases in the working standards measured daily on the AMT22 cruise.

Standard	N_2O (nmol mol $^{-1}$)	(CO nmol mol $^{-1}$)	CO_2 (µmol mol $^{-1}$)	CH_4 (nmol mol $^{-1}$)
6045	325.47	1049.00	392.38	1873.80
6036	298.07	219.89	299.12	1550.80
6040	344.07	5604.12	492.61	2022.60

The full set of working standards was measured once every twenty-four hours for twenty minutes during the AMT22 cruise and for forty minutes during the D366. Mean values for each calibration run were calculated from the final five minutes of measurement. A linear regression, using the mean values for the standards, was used to calibrate the measurements. To ensure the most accurate calibration, the daily discrete mean values of the working standards were interpolated to allow a calibration curve to be produced at every minute time-step to calibrate each measurement in the dataset. Different interpolation methods were explored (Figure 2. 4), including Linear, Spline and pChip, to determine the most accurate interpolation method to fit the data. Both the Spline and pChip interpolation methods displayed overshoots (over or under estimations) between data points, with the former method overshooting the

most. The best fit was found using the linear interpolation, which did not over or under-estimate calibration values.

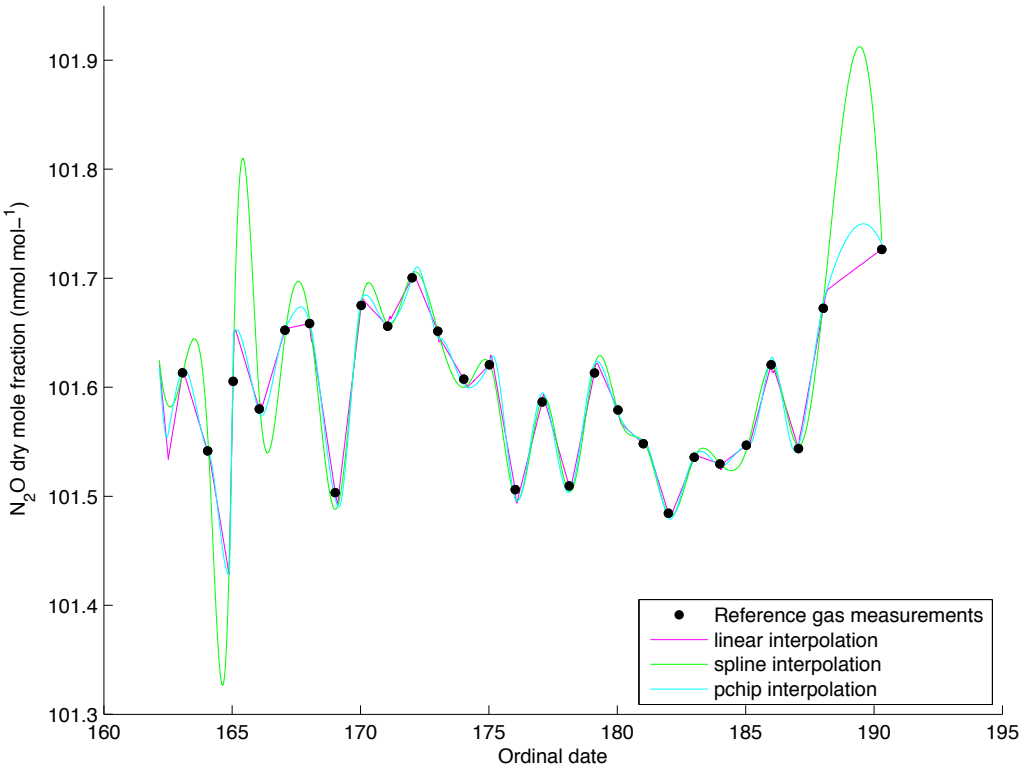

Figure 2. 4: Mean measurements of the N_2O reference standard 25B22 (black dots) during the D366 OA cruise. Different interpolation methods were tested: linear (magenta), Spline (green) and pChip (cyan) to visualise the most accurate interpolation method to fit the data.

2.2. 7: Spatial resolution of the measurements

At an assumed ship speed of 10 nautical miles (nm) the spatial resolution for the samples that were made (every minute) was 309 m min^{-1}. Each sample would therefore be a measurement of the previous 309 m (dependent on the ships speed). The spatial resolution would reduce at speeds slower than 10 nm and increase at faster speeds.

2. 3: Calculations

2.3. 1: Units of atmospheric measurements

All atmospheric measurements were measured during the two cruises in moist dry mole fractions converted to dry mole fractions by the ICOS instruments (Section 2.2.1, Equation 2. 1). The units for dry mole fractions for each gases measured are nmol mol^{-1} for N_2O CH_4 and CO and μmol mol^{-1} for CO_2.

2.3. 2: Concentration and sea surface saturation

The ICOS instruments measure moist mole fractions. Dry mole fractions are calculated from these moist mole fractions by the analysers (Equation 2. 1). Sea surface concentrations (Csw) for the gases were calculated from the dry mole fractions (x'), the solubility function '*f*' for N_2O (Weiss and Price, 1980) and the Bunsen solubility 'β' for CH_4 and CO (Wiesenburg and Guinasso, 1979) using the temperatures recorded in the equilibrator in Kelvin (Tequil), surface salinity (S) and the equilibrator pressure in atmospheres (assumed to be equal to atmospheric pressure) (Equations 2. 2 and 2. 3). Units for surface concentration for N_2O, CH_4 and CO are nmol L^{-1}; units for *f* are nmol L^{-1} atm, and atmospheric pressure (P) was converted from mbar to atmospheres.

$$\mathbf{Csw} = \mathbf{x'} * \boldsymbol{f}\ (\mathbf{Tequil}, \mathbf{S}) * \mathbf{P}$$

Equation 2. 2

$$\mathbf{Csw} = \mathbf{x'} * \boldsymbol{\beta}\ (\mathbf{Tequil}, \mathbf{S}) * \mathbf{P}$$

Equation 2. 3

The sea surface saturation (s) for each gas was calculated from the sea surface concentration (Csw) divided by the dry mole fraction of each gas measured in the atmosphere (x' (atmos)), the solubility function (*f)* or the Bunsen coefficient (β) (Wiesenburg and Guinasso, 1979, Weiss and Price, 1980), using the SST and SSS correcting for the difference in temperature between the seawater intake and equilibrator (Butler et al., 1988), and atmospheric pressure (P) (Equations 2. 4 and 2. 5).

$$s = \left(\frac{x'(sw) * f\ (Tequil, S) * P}{x'(atmos) * f\ (SST, S) * P}\right) * 100$$

Equation 2. 4

$$s = \left(\frac{x'(sw) * \beta(Tequil, S) * P}{x'(atmos) * \beta\ (SST, S) * P}\right) * 100$$

Equation 2. 5

2.3. 3: Partial pressure of CO_2

The partial pressure of CO_2 (µatm) was calculated from the dry mole fraction of CO_2 measured in the equilibrator (x') (µmol mol^{-1}), the equilibrator pressure (P) (in atmospheres) and the water vapour pressure (pH_2O) at the equilibrator temperature and surface salinity (in atmospheres) (Equation 2. 6) (Pierrot et al., 2009). An assumption of 100 % humidity is made for the air inside the equilibrator, however, the sample is dried when measured inside the ICOS instrument. The water vapour pressure is used to correct for this and calculate the wet pCO_2 (Equations 2. 6 and 2. 7) (Weiss and Price, 1980). To calculate the wet pCO_2 that would be in seawater at SST a temperature correction is made (Equation 2. 8) (Pierrot et al., 2009).

$$pCO_2(wet, Tequil) = x'[P - pH_2O(Tequil, SSS)]$$

Equation 2. 6

$$pH_2O(Tequil, SSS) = exp(24.4543 - 67.4509\left(\frac{100}{T}\right) - 4.8489\ ln\left(\frac{T}{100}\right) - 0.000544S)$$

Equation 2. 7

$$pCO_2(wet, SST) = (pCO_2(wet, Tequil) * exp(0.0423(SST - Tequil))$$

Equation 2. 8

2.3. 4: Ocean-atmosphere fluxes

The air-sea flux for each gas (F), was calculated at every minute time point from K, a gas transfer parameter, multiplied by the difference in concentration between sea surface waters and the equilibrium value (ΔCgas) (Equation 2. 9). The transfer parameter K (Equation 2. 10) is calculated from the Nightingale et al., (2000) transfer velocity (k_w), which itself is obtained from wind speed (u), corrected to 10 meter height, a Schmidt number for each gas measured (Wanninkhof, 1992), and the solubility coefficient *f* or β (calculated previously for each gas using SST) (Weiss and Price, 1980, Wiesenburg and Guinasso, 1979). The wind data were obtained underway on each ship. The Schmidt number is calculated from the relationship between the molecular diffusivity of the gas in the seawater and the kinematic viscosity of the seawater and is utilised as a scalar for different gases under different physical conditions. To assist in the comparison, under different physical conditions, Schmidt numbers are normalised to a common Sc. For seawater, at 20°C, this value is 660 (Equation 2. 11) (Le Quéré and Saltzman, 2013).

$$\mathbf{F = K\,(\Delta Cgas)}$$

Equation 2. 9

$$\mathbf{K = kw * f}$$

Equation 2. 10

$$\mathbf{k_w = (0.333 \cdot u + 0.222 \cdot u^2) \cdot (\frac{Sc}{660})^{-0.5}}$$

(Nightingale et al., 2000) ***Equation 2. 11***

2. 4: Equilibration time constant (τ) and the response time

Tests were carried out in the laboratory, based on Gülzow et al., (2011), Grefe (2013) and Grefe and Kaiser (2014) to determine the time constant (**τ**) of the system for each of the trace gases measured. The **τ** describes the time during which the difference in concentration between the water and gas phase decreases to 1/*e* (36.8%) of the initial value (Gülzow et al., 2011). Equilibration times for each of the four gases were calculated in experiments using two 220 L

water butts filled with Milli-Q water. The two water reservoirs contained water with different concentrations of each gas prior to the start of the tests. Water reservoir (A) was filled and left for 24 hours to equilibrate to concentrations of the gases in ambient laboratory air (or as close as possible to this within 24 hours). The water was pumped continuously from the water reservoir through the equilibrator and back again to achieve this. Water reservoir (B) in contrast was filled with water and left over-night undisturbed. The data from the experiments indicated that with these conditions reservoir A had higher concentrations of N_2O and CO and lower concentrations of CO_2 and CH_4 than reservoir (B).

To calculate the equilibration times of the gases, the water from reservoir (A) was passed through the equilibrator, where the headspace gas concentration gradually equilibrated to that in the water. The two ICOS instruments continuously sampled air from the headspace (initially with the CO_2/CH_4 analyser, followed by the N_2O/CO analyser). When the equilibration curve had plateaued for the gases (or the water ran out), the water flow to the equilibrator was switched to the water reservoir (B) until the equilibration curve reached a similar state. The lowest and highest dry mole fractions of each gas measured (x_{min} and x_{max}) were calculated from the decay of N_2O and CO and the growth of CO_2 and CH_4 over time (Figure 2. 5). The $\boldsymbol{\tau}$ for each gas was calculated from the slope of $-\ln\left[\frac{x_1-x_{min}}{x_{max}-x_{min}}\right]$ by rearranging Equation 2. 12 (Gülzow et al., 2011). Unfortunately the experiments were not run for long enough for CH_4 and CO to reach a complete plateau after the change of reservoirs, and consequently the calculated $\boldsymbol{\tau}$ would most likely be overestimated for these gases. In order to calculate the $\boldsymbol{\tau}$, the x_{max} for CH_4 and the x_{min} for CO were assumed to be where the last measurement was. If the experiment were to be repeated, it would be run for a longer duration to ensure a plateau was reached for both these slowly equilibrating gases.

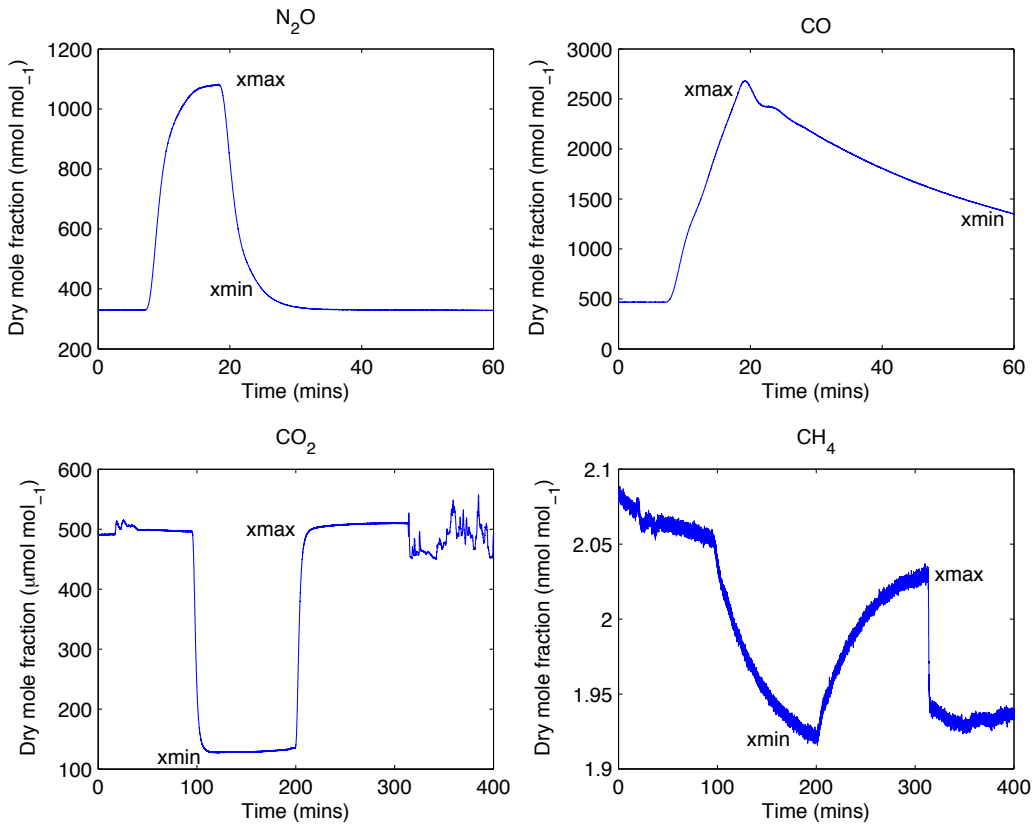

Figure 2. 5: Measurement of the two water reservoirs with different concentrations of a) N_2O, b) CO, c) CO_2 and d) CH_4. The x_{min} and x_{max} were calculated from the decay of N_2O and CO and the growth of CO_2 and CH_4 over time.

$$x_t = x_{min} + (x_{max} - x_{min})e^{-\frac{t}{\tau}}$$

Equation 2. 12

Using a water flow rate of 1.8 L min^{-1} and a gas flow of 100 mL min^{-1} throughout all the experiments, the τ for each trace gas measured for our equilibrator was as follows: CO_2 was (143 ± 1) seconds (n=4); N_2O was (150 ± 1) seconds (n=4); CH_4 was (42 ± 2) minutes (n=4) and CO was (62 ± 3) minutes (n=4). The 95 % relaxation time (3 x τ) was therefore calculated as approximately 7 minutes and 9 seconds for CO_2; 7 minutes and 30 seconds for N_2O; 2 hours and 6 minutes for CH_4 and 3 hours and 6 minutes for CO. The 95 % relaxation time calculated here for N_2O is consistent with Grefe and Kaiser (2014), who calculated approximately 7 minutes. The difference in τ and the 95 % relaxation time is due to the solubility of each gas, where N_2O and CO_2 are much more soluble in water than CO and CH_4.

During transit the ships were moving at varying speeds, during which the sea surface concentrations of each gas would be constantly changing producing a lagging effect in the signal received, unable to detect the areas where concentrations changed rapidly.

2. 5: Seawater temperature probe calibration

The seawater temperature in the equilibrator for the D366 and AMT22 cruises was measured using two Pt100 temperature probes (combined with a UEA electronics unit for the D366 and an OM-CP_PH101 Temperature Logger *Omega Engineering Limited* for AMT22). The probes, which measured approximately 1/4" in diameter, differed in lengths (one approximately 50 cm and the other 8 cm), and were placed into the top ¼ and bottom ¾ of each equilibrator to measure the temperature of the whole equilibrator. The temperature probes measured continuously at every second frequency throughout the cruise and averaged into minute means after the cruise. Precision for temperature measurements was better than 0.1 °C. The probes were calibrated before the cruise and afterwards to allow the temperature data to be corrected for drift. The probes responded quickly to temperature changes in the equilibrator. For the D366 cruise the bigger issue in accurately recording the equilibrator temperature was the time the water took to reach the equilibrator to be recorded when the ship was crossing such hydrographically diverse regions. During AMT22 this would not have been an issue as the SST change gradually.

2.5. 1: D366 OA cruise

For the D366 OA cruise, the pre-cruise calibration was undertaken by Gareth Lee, the post-calibration by Stephen Humphrey and the correction of the equilibrator temperature data by Dorothee Bakker. The post-cruise calibration indicated a major problem with the electronics unit, connected to the temperature probes, which gave a drift of around 4°C between the pre and post-cruise calibrations (Figure 2. 6: c and d). The effect of a 4 °C increase in seawater temperature would lead on average to a decrease in the surface concentration of

N_2O of 1.15 nmol mol^{-1}, alternatively, a 4 °C decrease in seawater temperature would lead to a 1.40 nmol mol^{-1} increase in the surface concentration of N_2O. To overcome this problem, the pre-cruise calibration was used. Readings from the 13th June 2011 09.57 to the 17th June 2011 17.12 have been decreased by 0.70 °C, with an introduction of this correction between 13th June 09.40 and 09.56. All readings after June 2011 21.57 have been increased by 0.70 °C to remove negative data points (Ribas-Ribas et al., 2014)

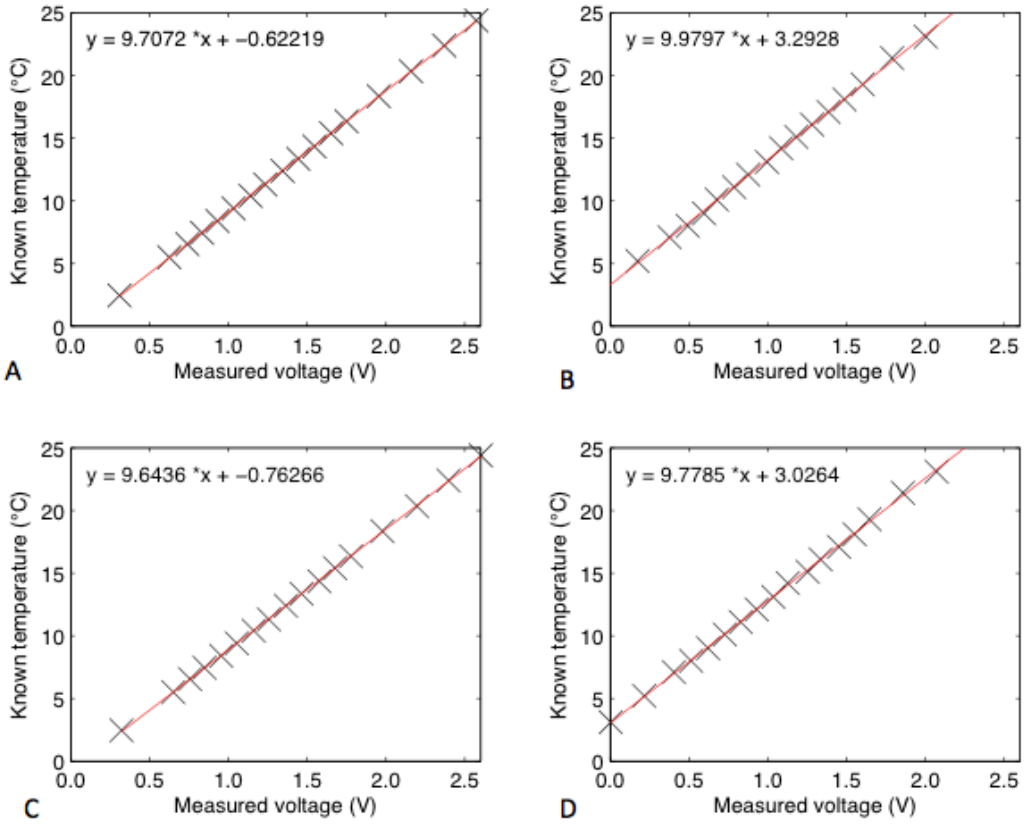

Figure 2. 6: Temperature calibration of the Pt100 temperature probes for the D366 cruise. A) Probe 1 pre-cruise calibration (temperature=9.7072*voltage-0.62219, R^2 = 0.99997), B) Probe 1 post-cruise calibration (R^2 = 0.99959), C) Probe 3 pre-cruise calibration (R^2 = 0.99992), and D) Probe 3 post-cruise calibration (R^2 = 0.99965). The red line is the line of best fit.

2.5. 2: AMT22 cruise

For the AMT22 cruise pre and post cruise calibrations were made with the two Pt100 probes. The regression fits were used to correct the equilibrator seawater temperatures recorded. The final equilibrator temperatures used were the mean values from the four corrected datasets (Figure 2. 7).

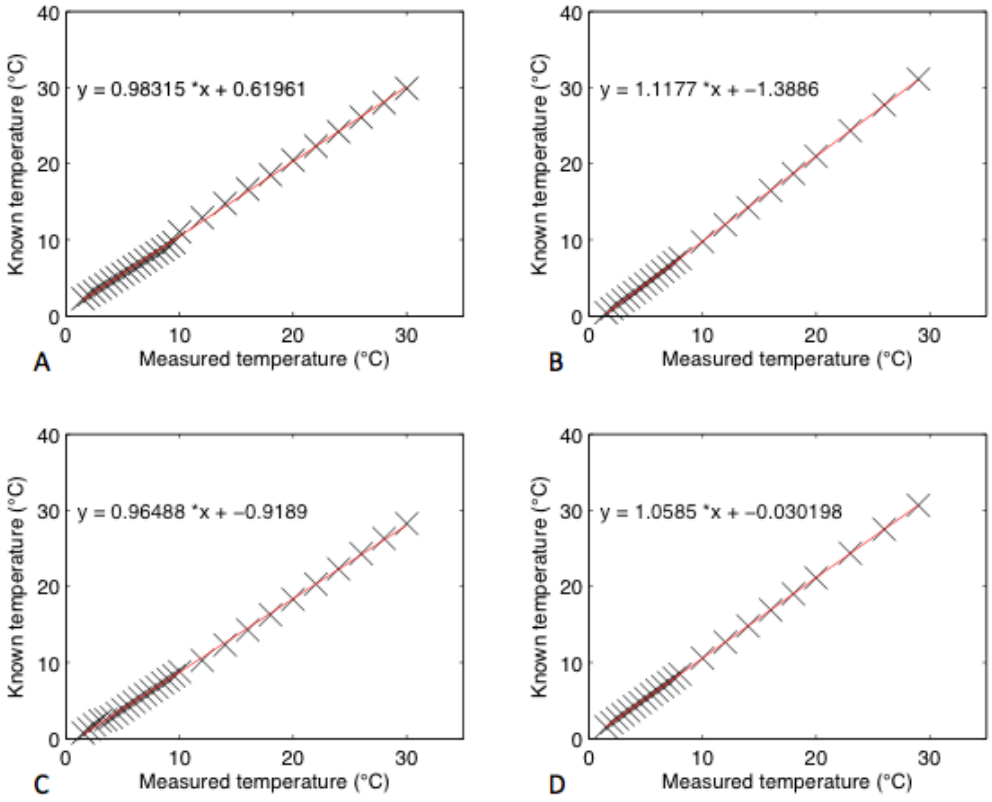

Figure 2. 7: Temperature calibration of the Pt100 temperature probes using a calibrated mercury thermometer for the known measurements for the AMT22 cruise. A) Probe A pre-cruise calibration (R^2 = 0.99919), B) Probe A post-cruise calibration (R^2 = 0.99996), C) Probe B pre-cruise calibration (R^2 = 0.99952) and D) Probe B post-cruise calibration (R^2 = 1.00000). The red line is the line of best fit.

2. 6: N_2O measurements

2.6. 1: Calibration

The N_2O values (Table 2. 1) of the four working N_2O calibration gases for the D366 were calculated from a post-cruise calibration using reference standards (Table 2. 2) at Weybourne Atmospheric Observatory (WAO), and used to calibrate the measurements at sea. The ICOS instruments were deployed at the last minute on the cruise and therefore a pre-cruise calibration against the reference standards was not possible. For the AMT22 cruise the values of three working standards (Table 2. 3) were calculated as a mean value from a pre and a post-cruise calibration against the same reference standards (Table 2. 2) at WAO. Linear regression, using the daily measurements of the working standards, was used to calibrate the measurements during the cruises.

2.6. 2: Atmospheric datasets: N_2O

2.6.2. 1: Atmospheric N_2O calibration for D366

The calibration, using the working N_2O standards, lowered atmospheric means to values that were lower than expected in the NW European Shelf sea region. This was based on a comparison to both Mace Head (Ireland) and Summit (Denmark) atmospheric values for the period of the 10th of June to the 10th July (Figure 2. 8), which were both higher than the calibrated values. The issue with the calibration is suspected to have been caused by the low values of the working standards in comparison to both the reference standards and the measurements in the atmosphere. Using working standards that were low introduced error into the calibration. Because N_2O in the atmosphere is relatively stable over a one-month period, this error was addressed by increasing each atmospheric mean value by an additional +2.5 nmol mol $^{-1}$ (Figure 2. 8). This correction brought the data values into the range of both the Mace Head and Summit atmospheric values (Figure 2. 8). With the correction an overall atmospheric N_2O mean value of 324.28 ± 1 nmol mol $^{-1}$ (n=17), with a range of 3.83 nmol mol $^{-1}$ (excluding 'unusual values', which will be explained in the next section) was calculated for the duration of the cruise (Figure 2. 9).

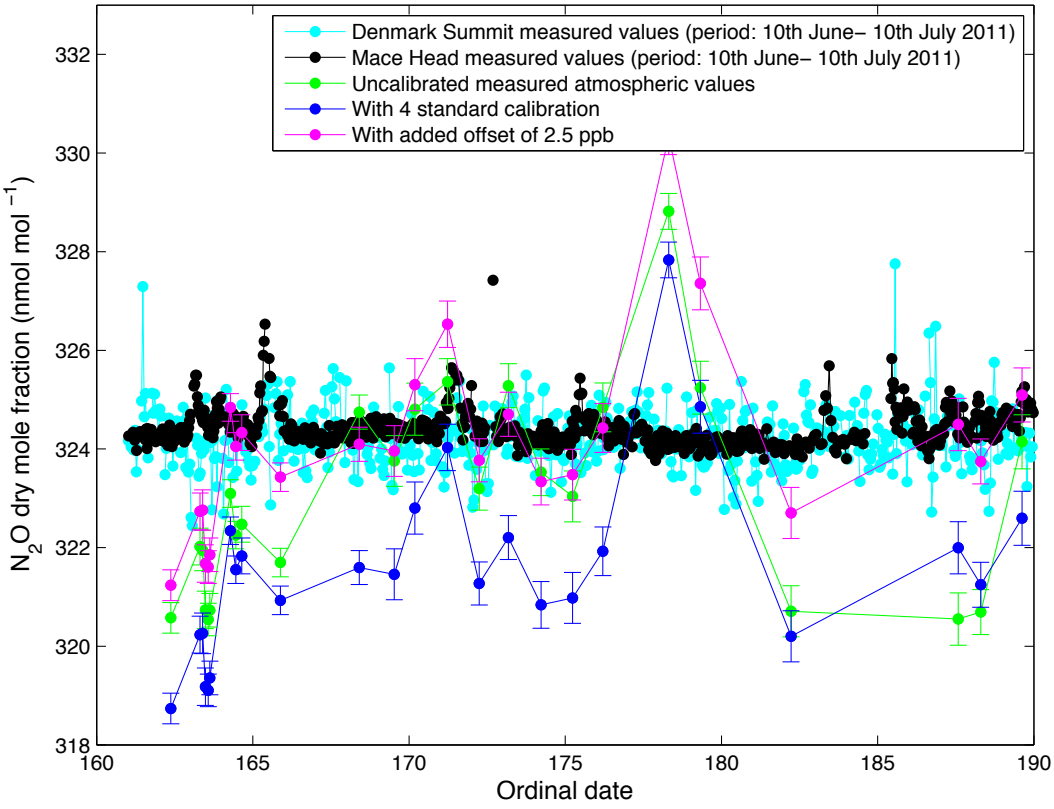

Figure 2. 8: Atmospheric mean values (n=240) for each atmospheric run during the D366 cruise. Red is un-calibrated data. If the data was corrected using the four ship standards the offset lowers the values beyond what would be expected (blue). If an offset of +2.5 nmol mol $^{-1}$ (magenta) is added to all data points to compensate for the lowering effect caused by the calibration, the values are more inline with the atmospheric values of N_2O from Mace Head (Ireland)[4] and Summit (Denmark)[5].

[4] **Data source: World Data Centre for Greenhouse Gases, Mace Head N_2O– Advanced Global Atmospheric Gases Experiment (AGAGE) (continuous, md) event, 1994-03-01 -2014-03-31. http://ds.data.jma.go.jp/gmd/wdcgg/pub/data/current/n2o/event/mhd653n00.agage.as.cn.n2o.md.ev.dat. Last accessed: June 2014.**

[5] **Data source: World Data Centre for Greenhouse Gases, Summit (Denmark) N_2O– NOAA (continuous, cats) hourly, 2011-01-01 -2011-12-31. http://ds.data.jma.go.jp/gmd/wdcgg/pub/data/current/n2o/hourly/y2011/sum672n00.noaa.as.cn.n2o.cats.hr2011.dat. Last accessed: January 2016.**

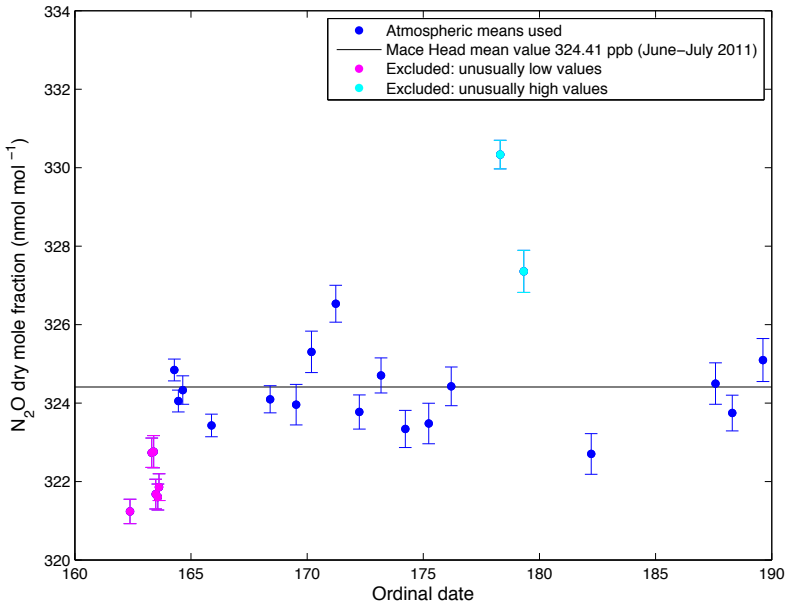

Figure 2. 9: The N_2O atmospheric mean dry mole fraction of 324.28 ± 1 nmol mol $^{-1}$ (n=17) on the D366 cruise was calculated from the mean N_2O atmospheric value for the last five minutes of each run (blue) and excluded two unusually high values (cyan) and the initial five, unusually low, measurements (magenta). The error bars show the standard deviation of the measurements. The line displays the June/ July 2011 mean for atmospheric N_2O from Mace Head[4], Ireland.

2.6.2. 2: Data points excluded from N_2O atmospheric dataset

For the D366 cruise the mean atmospheric value excluded two unusually high values at ordinal date 178 and 179 of the cruise (Figure 2. 9). Unusually high values were observed during the atmospheric measurement of all the four of the gases measured on these days and were all excluded as they indicated contamination by ships stack or another anthropogenic source, for example arising from industry or transport on land, and therefore were not representative of the actual atmospheric value for each gas. The initial five measurements were also excluded, as they were unusually low (Figure 2. 9). These low measurements may have been due to the instruments not having warmed up properly at the start of the cruise. Initial low mole fractions can also be seen at the start of the AMT22 cruise for N_2O, further reinforcing this idea. For the AMT22 cruise, out of the 216 mean atmospheric values eight were excluded due to contamination from stack pollution, as well as ten unusually low mean values at the start of the cruise (Figure 2. 10).

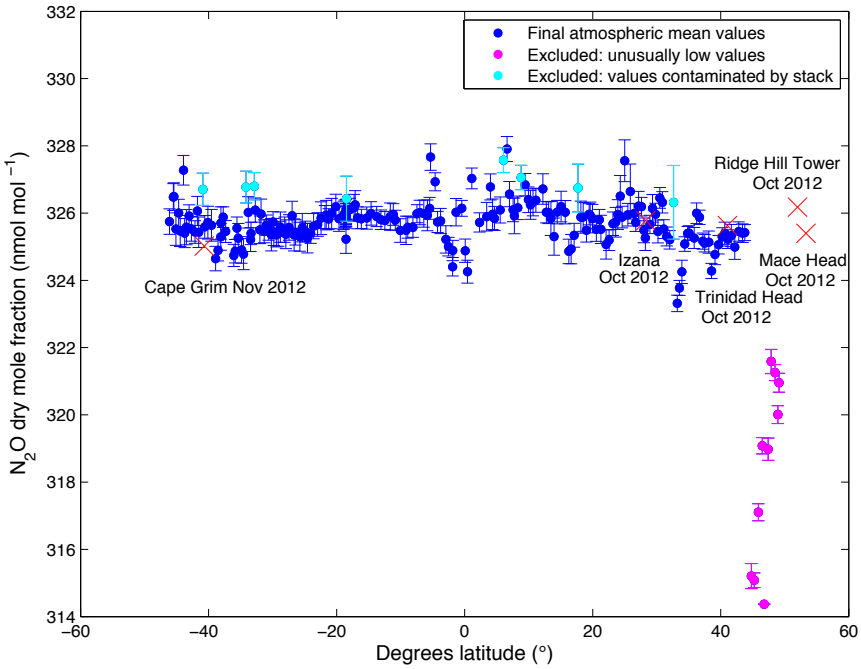

Figure 2. 10: Mean atmospheric N_2O dry mole fractions (n=240) with latitude along the AMT22 transect from Southampton, UK, to Punta Arenas, Chile. The atmospheric mean values used (blue) excluded the data points contaminated by stack pollution (cyan) and unusually low values at the start of the cruise (magenta), which may have been caused by the instrument not having warmed up properly. Comparisons are made to Mace Head[5], Ireland, (monthly mean value from October 2012), Ridge Hill Tower[6], UK, (October 2012), Trinidad Head[7], October 2012), Izańa[8], Tenerife, (October 2012) and Cape Grim[9], Tasmania, (November 2012). The error bars show the standard deviation of the measurements.

2.6.2. 3: Stack pollution

Each atmospheric run was visually assessed. As N_2O is stable in the atmosphere runs were discarded if the data points were fluctuating, creating a larger standard deviation than found on uncontaminated runs; or if the values were not stable throughout the run and, for example, were displaying a gradual increase or decrease throughout the measurement period. Under such conditions the runs were identified as contaminated by stack from the ship, or another source of pollution arising from land, and discarded. Figure 2. 9 shows the data points discarded due to contamination in cyan. The error bars show the standard deviation of the measurements.

Table 2. 4: Atmospheric N_2O monthly mean values calculated at various global locations. NA: not available.

Location	Lat/ lon of station	Month/ year	Mean (nmol mol $^{-1}$)	Standard deviation (nmol mol $^{-1}$)	Sample size (n)	Range of data (nmol mol $^{-1}$)	Contributor
Mace Head (Ireland)	53.32/ -9.90	October 2012	325.40	NA	2	NA	NOAA[6]/ESRL[2]
Ridge Hill Tower (UK)	52.00/ -2.54	October 2012	326.18	1.20	3040 (hourly)	7.29	University of Bristol[7]
Trinidad Head	41.05/ -124.15	October 2012	325.63	0.48	4	NA	NOAA/ESRL[8]
Izaña (Tenerife)	28.30/ -16.50	October 2012	325.57	0.30	23	1.02	AEMET[9]
Cape Grim (Australia)	-40.68/ 144.68	October 2012	324.78	0.11	NA	NA	CSIRO[10]
Cape Grim (Australia)	-40.68/ 144.68	Novembe r 2012	325.02	0.16	NA	NA	CSIRO[6]

[6] Data source: World Data Centre for Greenhouse Gases (WDCGG), Mace Head N_2O - National Oceanic and Atmospheric Administration (NOAA)/ Earth System Research Laboratory (ESRL) (flask, otto) event, 1998-10-12 -2013-12-31. http://ds.data.jma.go.jp/gmd/wdcgg/pub/data/current/n2o/event/mhd653n00.noaa.as.fl.n2o.otto.ev.dat Last accessed: June 2014.

[7] Data source: WDCGG, Ridge Hill Tower, UK N_2O – The University of Bristol, event 2012-03-01 -2012-11-21. Last accessed: http://ds.data.jma.go.jp/gmd/wdcgg/pub/data/current/n2o/event/rgl651n00.univbris.as.cn.n2o.nl.ev.dat Last accessed: June 2014.

[8] Data source: WDCGG, Trinidad Head N_2O, NOAA/ESRL (flask, otto) monthly 2002-01 – 2013-12. http://ds.data.jma.go.jp/gmd/wdcgg/pub/data/current/n2o/monthly/thd441n00.noaa.as.fl.n2o.otto.mo.dat Last accessed: June 2014.

[9] Data source: WDCGG, Izaña, Tenerife N_2O – Agencia Estatal de Meteorlogia (AEMET) (continuous) monthly 2007-01 – 2014-05. http://ds.data.jma.go.jp/gmd/wdcgg/pub/data/current/n2o/monthly/izo128n00.aemet.as.cn.n2o.nl.mo.dat Last accessed: June 2014.

[10] Data source: WDCGG, Cape Grim, Australia N_2O, Commonwealth Scientific and Industrial Research Organisation (CSIRO) (flask) monthly 1992-08 – 2013-12. http://ds.data.jma.go.jp/gmd/wdcgg/pub/data/current/n2o/monthly/cgo540s00.csiro.as.fl.n2o.nl.mo.dat Last accessed: June 2014.

2.6.2. 4: Data validation: comparing measurements to other N_2O atmospheric stations

The atmospheric N_2O dataset for the AMT22 transect had a mean dry mole fraction of 325.69 ± 1 nmol mol $^{-1}$ (n=189), displaying a range of 4.59 nmol mol $^{-1}$ between the data points. This agrees within the measurement uncertainties to the monthly mean dry mole fractions at Trinidad Head[7] (October 2012: 325.63 ± 0.48 nmol mol $^{-1}$) (n=4), Izaña[8], Tenerife (October 2012: 325.57 ± 0.30 nmol mol $^{-1}$) (n=23), and Cape Grim[9], Tasmania (November 2012: 325.02 ± 0.16 nmol mol $^{-1}$)(Figure 2. 10; Table 2. 4). The October 2012 monthly mean dry mole fractions for Mace Head[5], Ireland (325.40 nmol mol $^{-1}$), and Ridge Hill[6], UK, (326.18 ± 1.2 nmol mol $^{-1}$), are consistent to what we would have expected from our dataset if we had measured at those latitudes (Figure 2. 10).

2.6. 3: N_2O seawater datasets

2.6.3. 1: Data validation: comparing to other N_2O sea-surface measurements

Figures 2. 11 and 2. 13 display the sea surface saturation and Figures 2. 12 and 2. 14 the surface concentration for N_2O along the D366 and AMT22 cruise tracks. Bange (2006) estimated the average N_2O shelf sea surface saturation as 113%, which is consistent with the 97.5 - 110% range measured within the NW European shelf seas during D366 (Figure 3. 1). Grefe (2013) measured open ocean surface N_2O concentrations, between 24 °N and 39 °S, ranging from 5.5 - 8.6 nmol L^{-1}, with the lowest concentrations in the North Atlantic Gyre (NAG), during AMT20. Measurements from AMT22 were taken between 50 °N and 47 °S and showed consistency with Grefe (2013) at 5.5 - 10.5 nmol L^{-1}. The AMT22 and AMT20 surface waters were generally slightly undersaturated, increasing on some occasions, with the AMT22 measurements reaching 108 % at the equator and the AMT20 reaching 107 %. Forster et al (2009) and Grefe (2013) found 97 % and 99 % average N_2O sea surface saturations during the boreal autumn within the latitudinal band of 26 – 11 °N, which is consistent with the 97.87 % average measured during the AMT22 cruise in this NAG region.

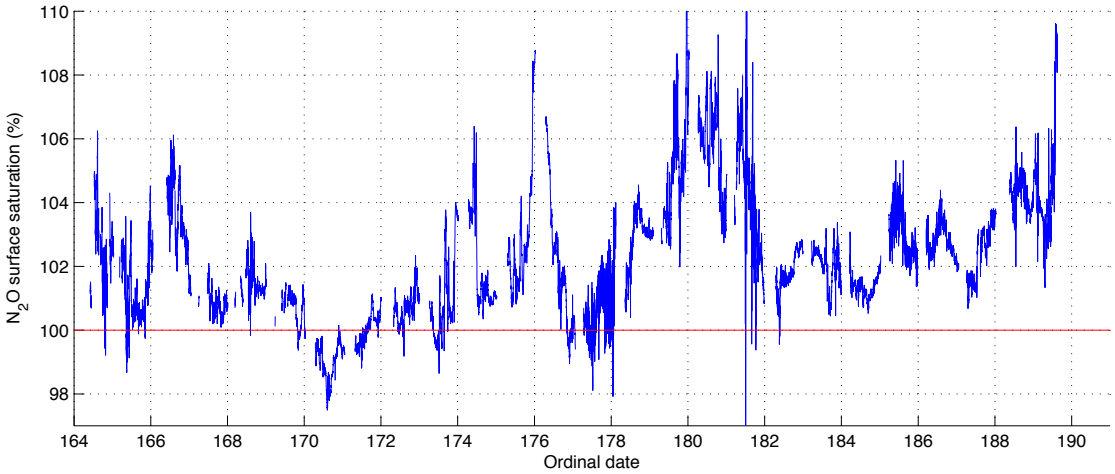

Figure 2. 11: Sea surface saturation for N_2O with respect to the atmospheric value along the D366 cruise track. The mean sea surface saturation measured along the cruise track was slightly supersaturated at 102.25 ± 2.00 %. The red line shows 100% saturation. Atmospheric values used in the saturation were measured on the ship and discussed in section 2.6.2. Details of how surface saturation for N_2O was calculated are found in section 2.3.2

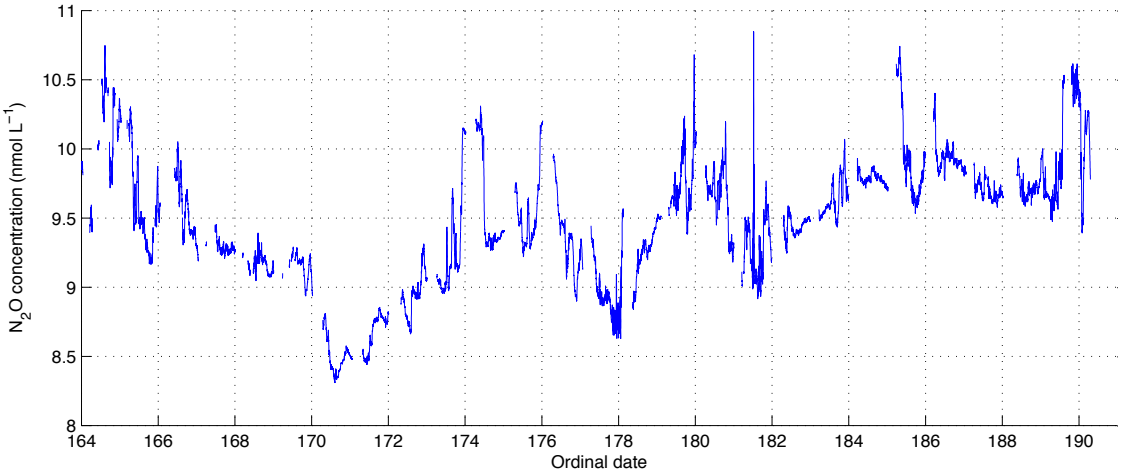

Figure 2. 12: Sea surface concentration of N_2O measured along the D366 cruise track. The mean sea surface concentration measured along the cruise track was 9.47 ± 0.44 nmol L^{-1}. Details of how surface concentration for N_2O was calculated are found in section 2.3.2

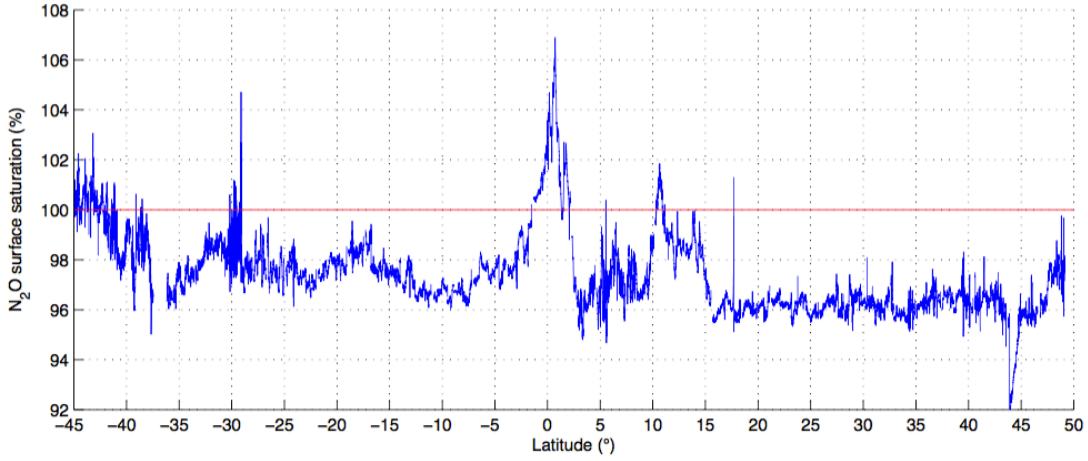

Figure 2. 13: Sea surface saturation for N_2O with respect to the atmospheric value along the AMT22 cruise track. The mean sea surface saturation measured along the cruise track was undersaturated at 97.50 ± 2.00 %. The red line shows 100% saturation. Atmospheric values used in the saturation were measured on the ship and discussed in section 2.6.2. Details of how surface saturation for N_2O was calculated are found in section 2.3.2

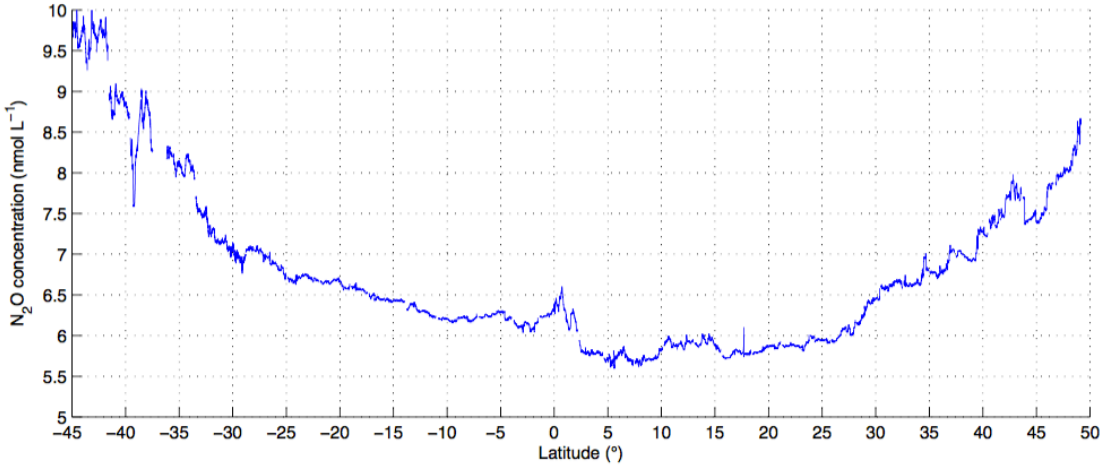

Figure 2. 14: Sea surface concentration of N_2O measured along the AMT22 cruise track. The mean sea surface concentration measured along the cruise track was 6.91 ± 1.00 nmol L^{-1}. Details of how surface concentration for N_2O was calculated are found in section 2.3.2

2.6.3. 2: Data validation: Inter-comparison study between continuous ICOS and discrete Gas Chromatography (GC) N_2O sea surface measurements during the D366.

An inter-comparison study was conducted comparing nine surface N_2O concentration and eight saturation samples between the *Los Gatos* ICOS (using the underway uncontaminated water supply), and the Gas Chromatography - Electron Capture Detection (GC-ECD) measurements from the same depth

(collected discretely from CTD rosette water samples) (Figure 2. 15). Andy Rees (Plymouth Marine Laboratory (PML)) and Ian Brown (PML) provided the GC measurements for comparison. Saturation, for both the ICOS and GC datasets, was calculated using the atmospheric mean value 325.69 ± 1 nmol mol $^{-1}$ (n = 189) measured using the ICOS instruments during the cruise. Using the same atmospheric value enabled as close a comparison as possible for the two datasets. Instrument precision for the GC of daily calibration standards was 95 % (n=81) (Clark et al., 2014) and 99.7 % for the ICOS (n= 300). Both datasets showed agreement in both the range of concentration (approximately 8.1 - 10.6 nmol L^{-1}) and saturation (approximately 88 – 116 %), as well as in the general pattern observed during the cruise, when both instruments were running. Both the mean surface N_2O concentration and saturation for GC measurements were significantly higher than for the ICOS measurements at 9.86 ± 1 nmol L $^{-1}$ and 9.47 ± 0 nmol L $^{-1}$, and 107.59 ± 10.31 % and 102.25 ± 2 % (unpaired t-test, h= 0, p= 0.58; h=0, p=0.80), but compared well considering the differences in methodologies.

Differences in concentration and saturation were calculated for coinciding times (± 10 seconds) between the ICOS data and the time the CTD entered the water for the GC samples. The mean difference in concentration and saturation between the collocated data points was found to be 0.15 ± 1 nmol L $^{-1}$ and 4.64 % (Figure 2. 15). Differences between the datasets may be attributed to the different methods with which the samples were collected and measured (i.e. the underway water system or CTD rosette, and ICOS or GC-ECD).

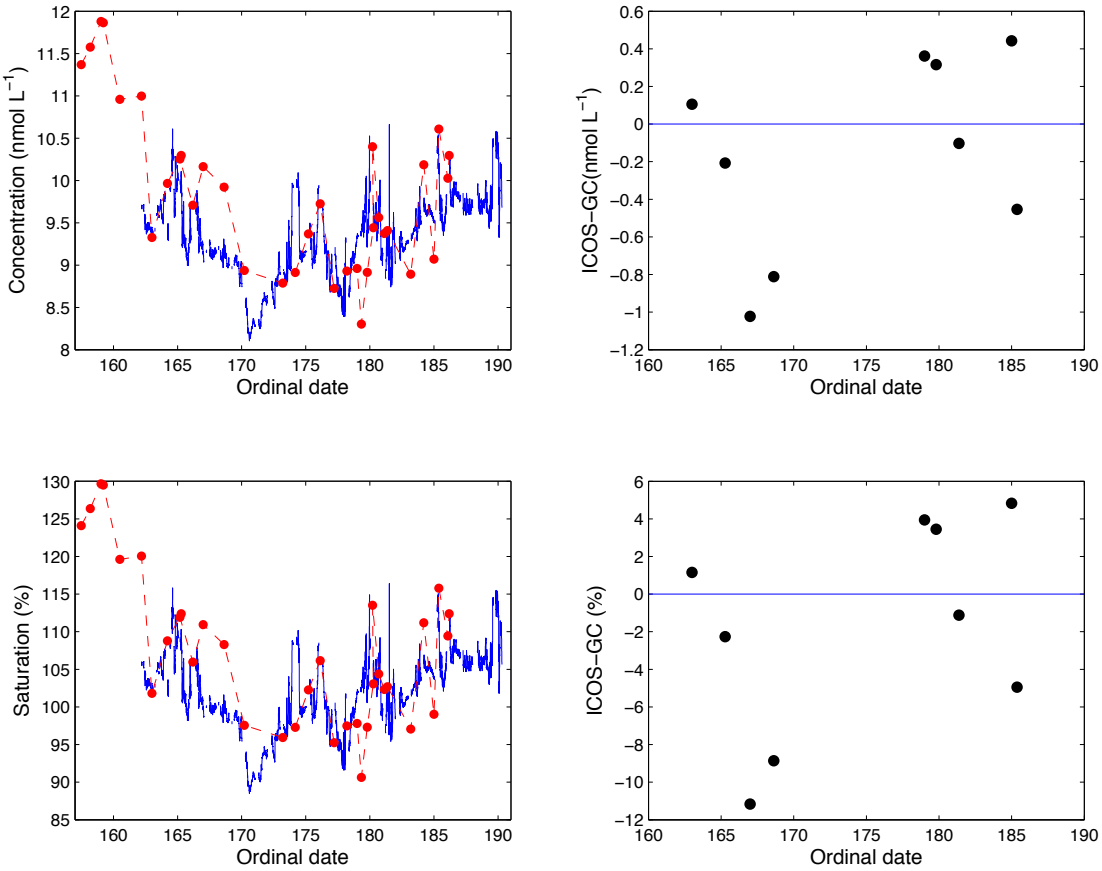

Figure 2. 15: Comparison of sea surface concentration (top left panel) and saturation (bottom left panel) measurements between the *Los Gatos* ICOS (blue) and GC (red) during the D366 OA transect. Differences in concentration and saturation between the two methods are plotted for concentration (top right panel) and saturation (bottom right panel) using samples that were collected at coinciding times (± 10 seconds).

2. 7: Measurements of CH_4

2.9. 1: Calibration

For the D366 cruise the CH_4 dry mole fractions (Table 2. 1) of the four working CH_4 standards were calculated from a post-cruise calibration using reference standards (Table 2. 2) at WAO. Some of the seawater measurements made on this cruise (between 3400 and 5000 nmol mol $^{-1}$), were extrapolated beyond the range of the working standards. The values of the three working CH_4 standards (Table 2. 3) were calculated for the AMT22 cruise, as a mean value from both a pre and a post cruise calibration against the reference standards.

2.9. 2: Atmospheric datasets for CH_4

2.9.2. 1: Data points excluded from the atmospheric datasets

The mean atmospheric dry mole fraction for CH_4 of 1855.60 ± 16.09 nmol mol $^{-1}$ (n=23) for the D366 excluded the two unusually high values at ordinal date 178 and 179 (Figure 2. 16). For the AMT22 cruise five mean atmospheric runs that were contaminated by stack pollution during the measurement were excluded (Figure 2. 17).

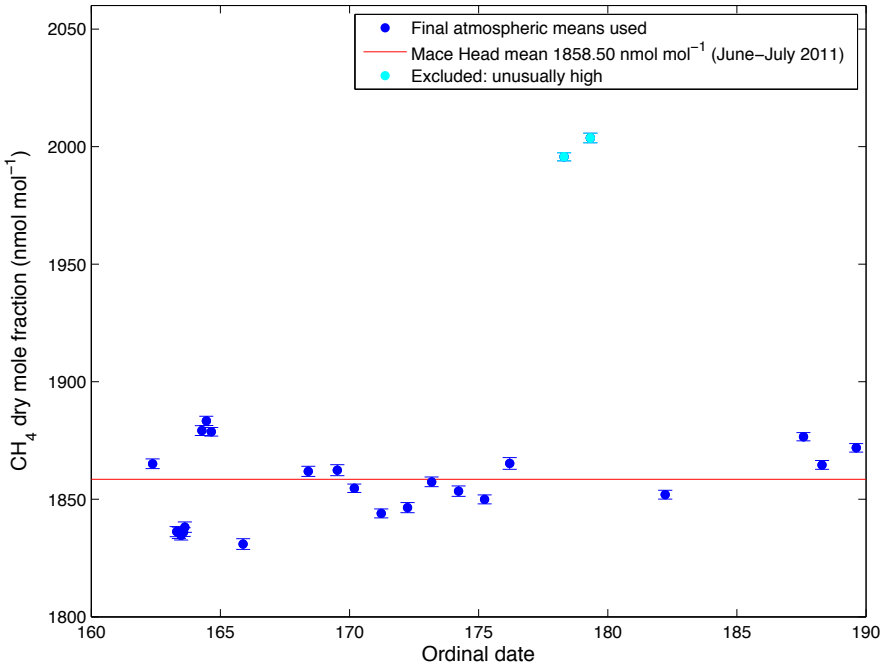

Figure 2. 16: The overall CH_4 atmospheric mean dry mole fraction of 1855.60 ± 16 nmol mol $^{-1}$ (n=23), with a range of 52.42 nmol mol $^{-1}$ was calculated on the D366 cruise from the mean CH_4 atmospheric value for each run (n=240) (blue), excluding two unusually high values (cyan). The measurements were consistent with the Mace Head[11] June and July 2011 mean atmospheric value of 1856.16 nmol mol $^{-1}$.

[11] **Data source: WDCGG, Mace Head CH_4– NOAA/ESRL (flask) monthly, 1991-06 -2013-12. http://ds.data.jma.go.jp/gmd/wdcgg/pub/data/current/ch4/monthly/mhd653n00.noaa.as.fl.ch4.nl.mo.dat Last accessed June 2014.**

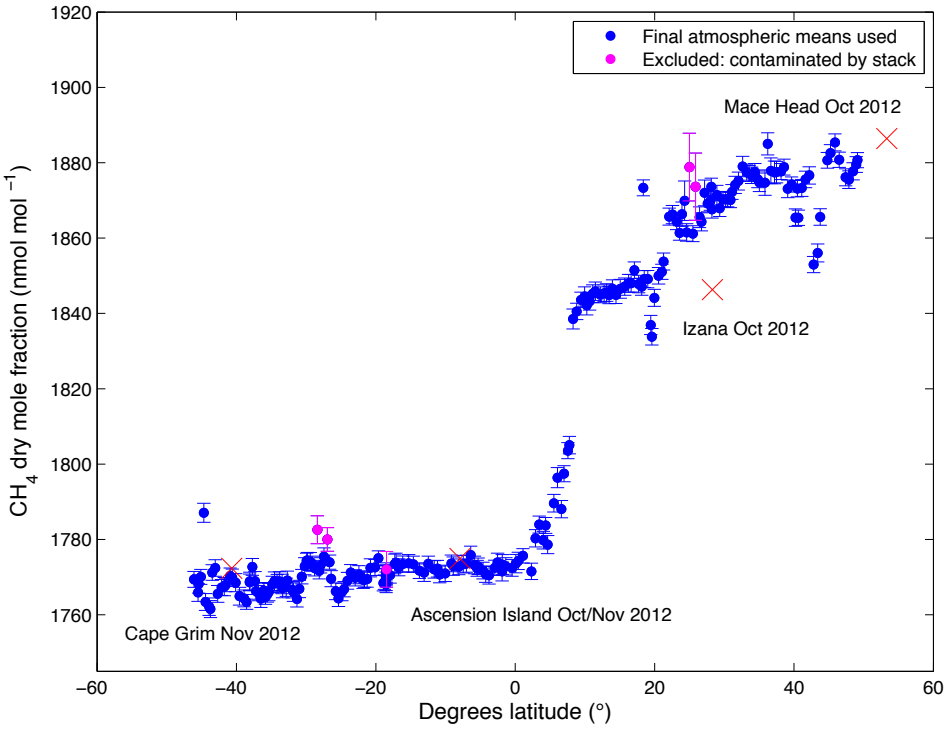

Figure 2. 17: Atmospheric CH_4 mean dry mole fractions (n= 240) with latitude along the AMT22 transect from Southampton, UK, to Punta Arenas, Chile. The atmospheric mean values used (blue) excluded the data points contaminated by stack pollution (cyan). Comparisons are made to Mace Head[11], Ireland, (monthly mean value from October 2012), Izańa[12], Tenerife (monthly mean value from October 2012), Ascension Island[13] (monthly mean value for October/November 2012) and Cape Grim[14], Tasmania, (monthly mean value from November 2012).

2.9.2. 2: Data validation: comparing measurements to other CH_4 atmospheric stations

The D366 cruise the mean atmospheric CH_4 dry mole fraction of 1855.60 ± 16 nmol mol $^{-1}$ (n=23), with a range of 52.42 nmol mol $^{-1}$ (Figure 2. 16) agrees within the measurement uncertainties to the Mace Head[11] June/July 2011 mean dry mole fraction of 1856.16 ± 11 nmol mol $^{-1}$ (n=820), with a range of 65.56 nmol mol $^{-1}$ (Figure 2. 16). The atmospheric CH_4 dry mole fractions measured during the AMT22 cruise were in agreement with the latitudinal trend displayed between different atmospheric stations, measuring CH_4, at varying latitudes (Figure 2. 17, Table 2. 5). The Izaña[12] (Tenerife) atmospheric CH_4 October monthly mean value of 1846.30 nmol mol $^{-1}$ was lower than what was measured on the AMT22 research cruise. The other atmospheric stations where comparisons were made were in line with the AMT22 measurements, with the

Mace Head[11] October 2012 mean at 1886.40 nmol mol $^{-1}$, the Ascension Island[13] October/November 2012 mean values at: 1774.95/1775.02 nmol mol $^{-1}$, and the Cape Grim[14] November 2012 mean at: 1772.46 nmol mol $^{-1}$.

Table 2. 5: Atmospheric CH_4 monthly mean dry mole fractions calculated at various locations. The standard deviation of the mean measurement at each station, the sample size (n) and the range within the datasets was not available.

Location	Lat/ lon of station	Month/ year	Mean (nmol mol $^{-1}$)	Contributor
Mace Head (Ireland)	53.32/ -9.90	October 2012	1886.40	NOAA/ESRL[11]
Izańa (Tenerife)	28.30/ -16.5	October 2012	1846.30	AEMET[12]
Ascension Island	-7.92/ -14.42	October 2012	1774.95	NOAA/ESRL[13]
Ascension Island	-7.92/ -14.42	November 2012	1775.02	NOAA/ESRL[13]
Cape Grim (Australia)	-40.68/ 144.68	November 2012	1772.46	CSIRO[14]

2.9. 3: Seawater datasets for CH_4

2.9.3. 1: Data validation: comparing to other CH_4 sea surface measurements

Figures 2. 18 and 2. 20 display the sea surface saturation and Figures 2. 19 and 2. 21 the concentration of CH_4 along the D366 and AMT22 cruise tracks. The sea

[12] Data source: WDCGG, Izańa Tenerife CH_4– AEMET (continuous) monthly, 1984-01 -2013-12. http://ds.data.jma.go.jp/gmd/wdcgg/pub/data/current/ch4/monthly/izo128n00.aemet.as.cn.ch4.nl.mo.dat Last accessed June 2014.

[13] Data source: WDCGG, Ascension Island CH_4– NOAA/ESRL (flask) monthly, 1983-05 - 2013-12. http://ds.data.jma.go.jp/gmd/wdcgg/pub/data/current/ch4/monthly/asc107s00.noaa.as.fl.ch4.nl.mo.dat Last accessed June 2014.

[14] Data source: WDCGG, Cape Grim CH_4– CSIRO (flask) monthly, 1984-08 -2013-12. http://ds.data.jma.go.jp/gmd/wdcgg/pub/data/current/ch4/monthly/cgo540s00.csiro.as.fl.ch4.nl.mo.dat Last accessed June 2014.

surface saturation of CH_4 measured in the NW European shelf seas was between 99.5 and 320.0 % (Figure 2. 18). These saturations are consistent with Conrad and Seiler (1988) who found 100 % in the Bay of Biscay, with 95 – 130 % in the southern North Sea (Scranton and McShane, 1991), 126 ± 8 % in the German Bight (Bange et al., 1994), 140 % in the southern North Sea (Conrad and Seiler, 1988), 120 – 332 % in the central North Sea (Rehder et al., 1998), 112 – 136 % off the east coast of the UK (Upstill-Goddard et al., 2000). The surface saturations measured during the AMT22 cruise ranged from 100 - 136 % in the open Atlantic Ocean (Figure 2. 20), which is consistent with the 105 - 130 % saturation measured by Conrad and Seiler (1988) in the Atlantic, and a range between 105 -175 % saturation observed between the coastal waters off central California and the oligotrophic waters in the central North Pacific Ocean (Tilbrook and Karl, 1995).

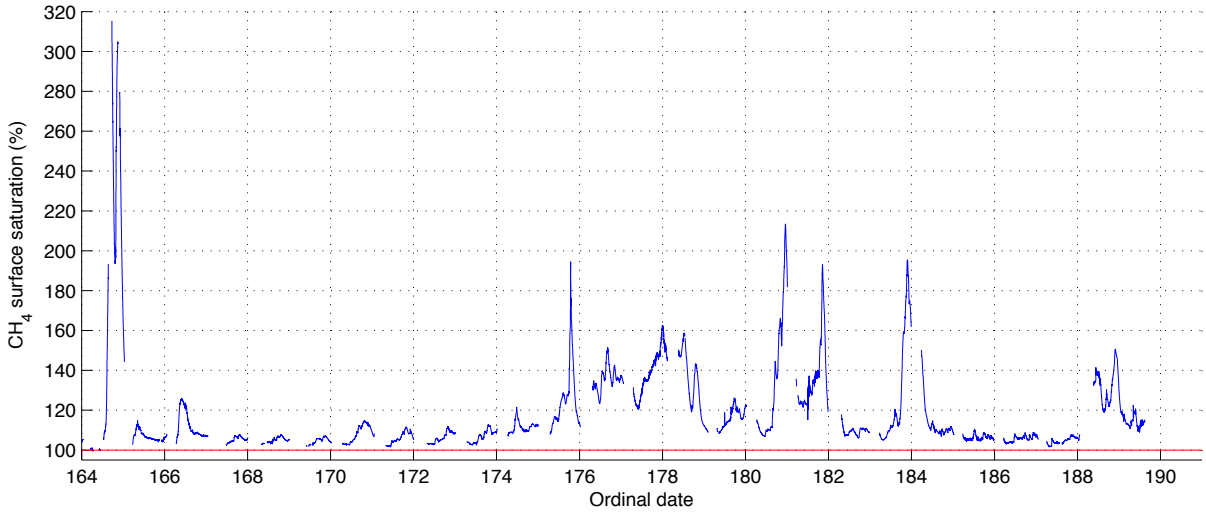

Figure 2. 18: The sea surface saturation for CH_4 along the D366 shelf sea cruise track. The mean sea surface saturation was supersaturated in respect to the atmospheric equilibrium concentration at 118.38 ± 21.67 %. Details of how surface saturation for CH_4 was calculated are found in section 2.3.2. The red line shows 100 % saturation.

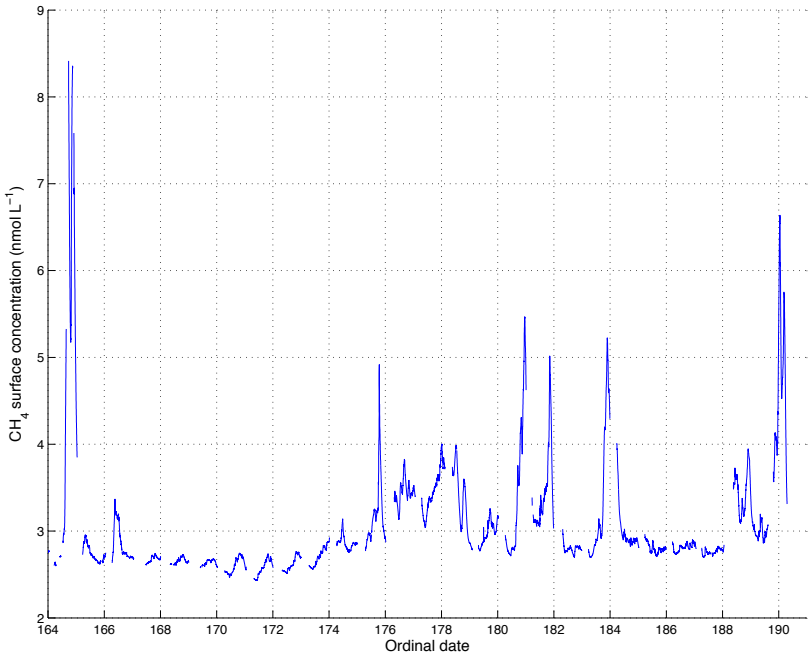

Figure 2. 19: The sea surface concentration of CH_4 along the D366 cruise track. The mean sea surface concentration was 3.05 ± 0.64 nmol L^{-1}. Details of how surface concentration for CH_4 was calculated are found in section 2.3.2.

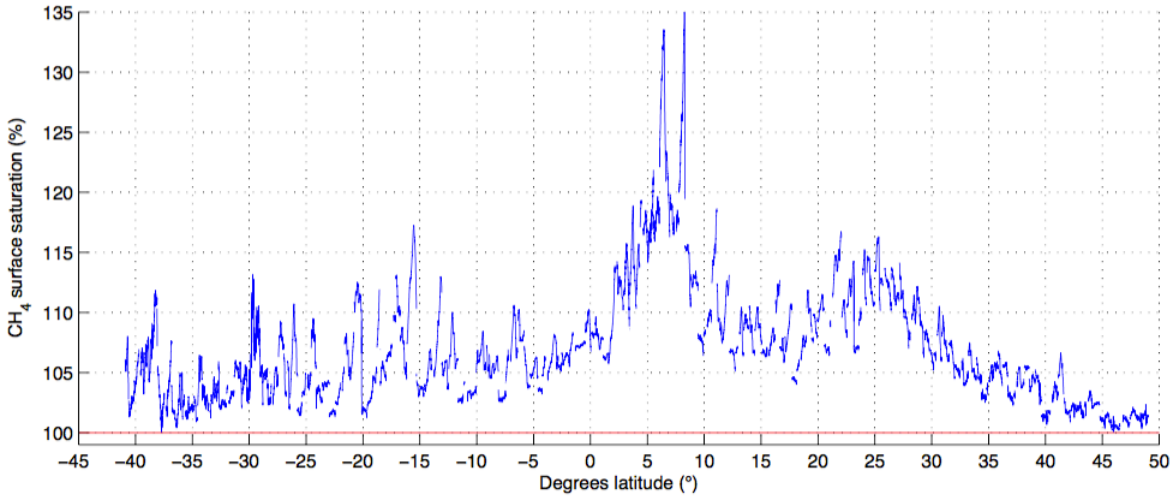

Figure 2. 20: The sea surface saturation for CH_4 along the AMT22 cruise track. The mean sea surface saturation was supersaturated in respect to the atmospheric equilibrium concentration at 106.79 ± 4.61 %. The red line shows 100 % saturation. Details of how surface saturation for CH_4 was calculated are found in section 2.3.2.

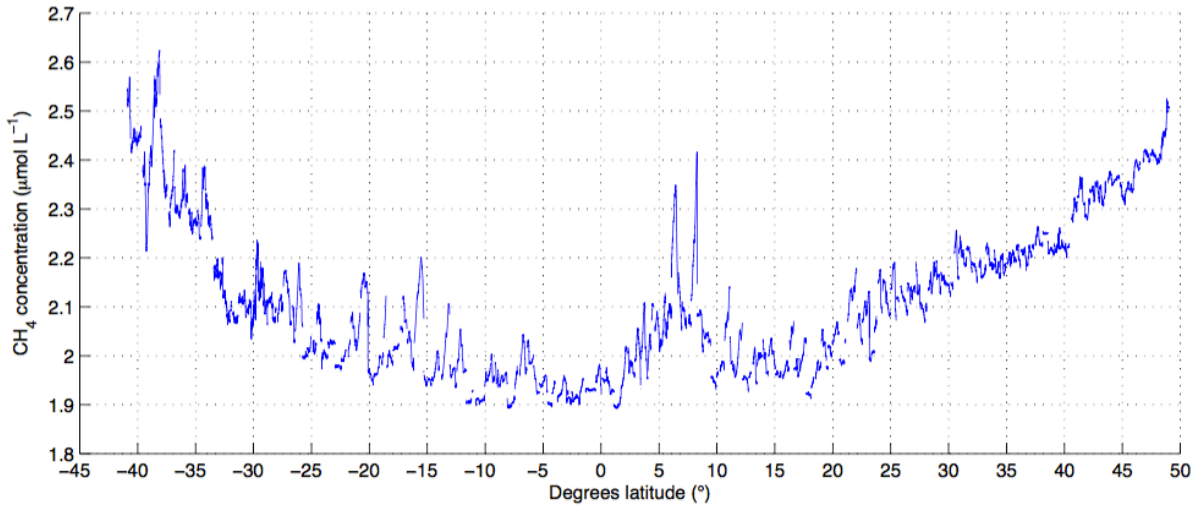

Figure 2. 21: The sea surface concentration of CH_4 along the AMT22 cruise track. The mean sea surface concentration was 2.22 ± 0.19 nmol L^{-1}. Details of how surface concentration for CH_4 was calculated are found in section 2.3.2.

2. 8: Measurements of CO

2.7. 1: Calibration

For the D366 OA cruise, the CO values (Table 2. 1) of the four working standards were calculated from a post-cruise calibration using reference standards (Table 2. 2) at WAO, and used to calibrate the measurements. For the AMT22 cruise the values of the three working standards were calculated, as a mean value from both a pre and a post cruise calibration against the same reference standards (Table 2. 3). Daily measurements of the working standards for both cruises were used to calibrate the measurements made at sea using linear regression. The seawater measurements made on the D366 cruise (1000 - 4000 nmol mol^{-1}) were extrapolated beyond the range of the working standards. Some error may have been introduced due to this. This error could be assessed by measuring a standard, with a known high concentration of CO standard (similar to that found in the atmosphere), and test the linear response of the ICOS instrument. These instruments are expected to respond linearly.

2.7. 2: Atmospheric CO datasets

2.7.2. 1: Data points excluded from the atmospheric datasets

The final mean atmospheric dry mole fraction calculated for the D366 cruise excluded two unusually high values at ordinal dates 178 and 179 as discussed in section 2.6.2.2. The initial five measurements were also excluded as a precautionary measure, as they were unusually low for the N_2O measurements (same instrument) and therefore may be indicative of problems with the instrument. One other measurement, at ordinal date 173, was also excluded as it was contaminated by stack pollution (Figure 2. 22). For the AMT22 cruise the final mean atmospheric values selected (Figure 2. 23 (blue)) excluded sixteen runs that were contaminated by stack pollution during the measurements (Figure 2. 23 (cyan)) and the five initial measurements that were unusually low for N_2O (Figure 2. 23 (magenta)). These were discarded from the CO dataset as precautionary measure in case this was an indication of a problem with the instrument.

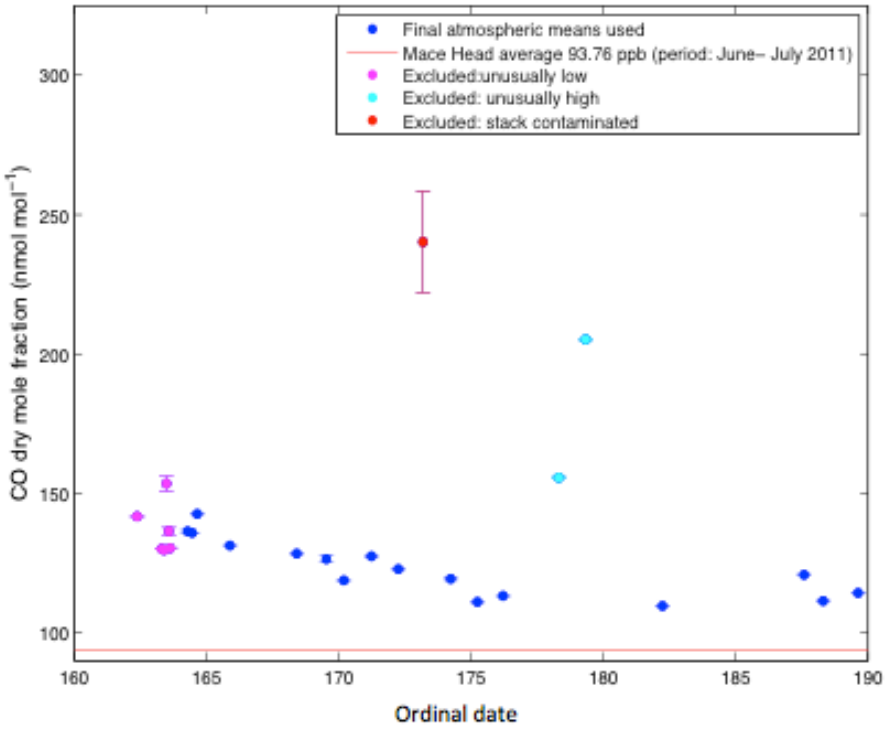

Figure 2. 22: The overall CO atmospheric mean value of 122.87 ± 10 nmol mol $^{-1}$ (n=15) for the D366 cruise was calculated from the mean CO atmospheric value for each run selected (n=240) (blue) and excluded two unusually high values (cyan), the initial five, unusually low, measurements (magenta) and one stack contaminated run (red). Measurements were higher than the Mace Head[15] mean atmospheric dry mole fraction for June and July 2011 at 93.76 nmol mol $^{-1}$.

[15] **Data source: World Data Centre for Greenhouse Gases, Mace Head CO– Advanced Global Atmospheric Gases Experiment (AGAGE) (continuous, md) event, 1994-03-01 -2014-03-31. http://ds.data.jma.go.jp/gmd/wdcgg/pub/data/current/co/event/mhd653n00.agage.as.cn.co.md.ev.dat Last accessed June 2014.**

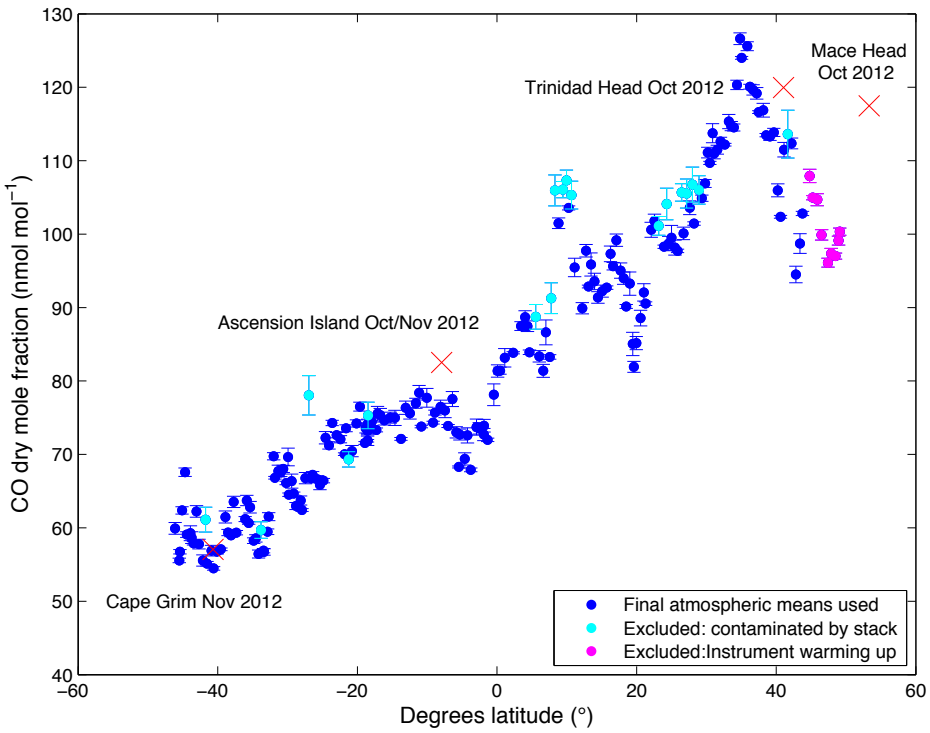

Figure 2. 23: Atmospheric CO mean values (n=240) with latitude along the AMT22 transect from Southampton, UK, to Punta Arenas, Chile. The final atmospheric mean values used (blue) excluded the data points contaminated by stack pollution (cyan) and those unusually low for the N_2O measurements at the start of the cruise (same instrument) (magenta), which were assumed to be caused by either the instrument not having warmed up properly or an issue to with the airline. Comparisons were made to Mace Head, Ireland, (October 2012 monthly mean), Trinidad Head, (October 2012 monthly mean), Ascension Island (October/November 2012 monthly mean) and Cape Grim, Tasmania, (November 2012 monthly mean).

2.7.2. 2: Data validation: comparing CO measurements to other CO atmospheric stations

Throughout the D366 cruise, a mean atmospheric CO dry mole fraction of 122.87 ± 10 nmol mol $^{-1}$ (n=15), with a range of 33.03 nmol mol $^{-1}$ was measured (Figure 2. 22). This value exceeds the measurement uncertainties of the Mace Head[15] CO monthly mean atmospheric values for both June and July 2011 at 99.33 ± 8 nmol mol $^{-1}$ (n=898) and 88.20 ± 4 nmol mol $^{-1}$ (n=725), respectively. However, atmospheric CO is highly variable and such differences could be explained by spatial and temporal differences. For example, the varying location of the ship may have introduced different wind driven atmospheric CO sources from inland. To more closely examine the range of atmospheric CO measurements that can be

found inland, an hourly data set from Kollumerwaard[16], The Netherlands, 2011 was studied (Figure 2. 24). Atmospheric CO from this region was found to exceed a range of 250 nmol mol $^{-1}$ throughout the June and July 2011 period (approximately 50-300 nmol mol $^{-1}$). Atmospheric inputs from inland sources may explain the higher mean obtained for the D366 OA cruise in comparison to the Mace Head mean.

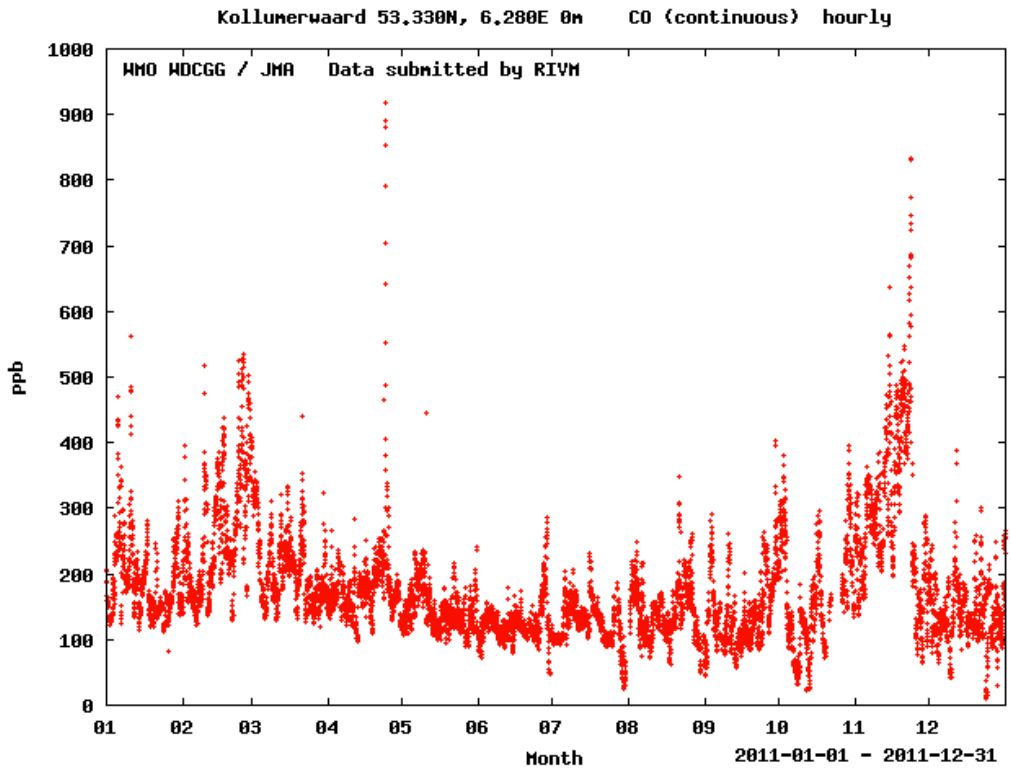

Figure 2. 24: Kollumerwaard[16] atmospheric station, The Netherlands, 2011 hourly atmospheric CO dataset. The variability in the months of June and July exceeded 250 nmol mol $^{-1}$.

[16] Data source: World Data Centre for Greenhouse Gases (WDCGG), Mace Head CO, Rijksinstituut voor volksgezondheid en milieu (RIVM) (continuous) hourly 2011-01-01 – 2011-12-31.
http://ds.data.jma.go.jp/gmd/wdcgg/cgi-bin/wdcgg/quick_plot.cgi?imagetype=png&dataid=201209210005 Last accessed June 2014.

Better comparisons were observed between the AMT22 atmospheric dataset and the monthly means from other atmospheric stations along the AMT latitudinal range. The AMT22 CO dataset had a mean atmospheric dry mole fraction of 82.55 ± 19 nmol mol $^{-1}$ (n=171), displaying a range of 72.14 nmol mol $^{-1}$ (Figure 2. 23). The AMT22 atmospheric CO dataset is consistent with the latitudinal trend in the dry mole fraction of CO, which increases towards the northern hemisphere, that is found between different atmospheric stations at varying latitudes (Mace Head[9] October 2012 monthly mean dry mole fraction: 117.47 nmol mol $^{-1}$, Trinidad Head[10] October 2012: 121.13 nmol mol $^{-1}$, Ascension Island[11] October/November 2012: 85.04 nmol mol $^{-1}$/80.00 nmol mol $^{-1}$ and Cape Grim[12] November 2012: 57.03 ± 2.21 nmol mol $^{-1}$ (Figure 2. 23; Table 2. 6).

Table 2. 6: Atmospheric CO monthly mean values calculated at various global locations. Data available at: the World Data Centre for Greenhouse Gases. NA: data not available. Information on the sample size (n) and the range within the data was not available for any of the locations below therefore are not included in the table.

Location	Lat/ lon of station	Month/ year	Mean (nmol mol $^{-1}$)	Standard deviation (nmol mol $^{-1}$)	Contributor
Mace Head (Ireland)	53.32/ -9.90	October 2012	117.47	NA	NOAA/ESRL[17]
Trinidad Head (Trinidad)	41.05/ -124.15	October 2012	121.13	NA	NOAA/ESRL[18]
Ascension Island	-7.92/ -14.42	October 2012	85.04	NA	NOAA/ESRL[19]
Ascension Island	-7.92/ -14.42	November 2012	80.00	NA	NOAA/ESRL[21]
Cape Grim (Australia)	-40.68/ 144.68	November 2012	57.03	2.21	CSIRO[20]

[17] Data source: World Data Centre for Greenhouse Gases (WDCGG), Mace Head CO– NOAA/ERSL (flask) monthly, 1991-06 -2013-12. http://ds.data.jma.go.jp/gmd/wdcgg/pub/data/current/co/monthly/mhd653n00.noaa.as.fl.co.nl.mo.dat Last accessed June 2014.

[18] Data source: WDCGG, Trinidad Head CO– NOAA/ERSL (flask) monthly, 2002-04 -2013-12. http://ds.data.jma.go.jp/gmd/wdcgg/pub/data/current/co/monthly/thd441n00.noaa.as.fl.co.nl.mo.dat Last accessed June 2014.

[19] Data source: WDCGG, Ascension Island CO– NOAA/ERSL (flask) monthly, 2002-04 -2013-12. http://ds.data.jma.go.jp/gmd/wdcgg/pub/data/current/co/monthly/asc107s00.noaa.as.fl.co.nl.mo.dat Last accessed June 2014.

[20] Data source: WDCGG, Cape Grim CO– CSIRO (flask) monthly, 1985-02 -2013-12. http://ds.data.jma.go.jp/gmd/wdcgg/pub/data/current/co/monthly/cgo540s00.csiro.as.fl.co.nl.mo.dat Last accessed June 2014.

2.7. 3: CO seawater datasets

2.7.3. 1: Data validation: comparing to other CO sea surface measurements

Figures 2. 25 and 2. 27 display the sea surface saturation and Figures 2. 26 and 2. 28 the concentration of CO measured along the D366 and AMT22 cruise transects. Although there is no direct concentration comparison for either the D366 or the AMT22 cruises, the open water sea surface concentrations during the AMT22 cruise found at a range between 0.2 and 1.6 nmol L^{-1} are consistent with measurements made by Stubbins et al. (2006) during AMT10, who found pronounced diurnal variations in surface-water CO ranging between 0.2-2.6 nmol L^{-1}, with afternoon maxima exceeding the pre-dawn minima. In the summertime in the NW European shelf seas, the surface-water CO concentration was far higher, and had a greater range (1.2- 8.0 nmol L^{-1}).

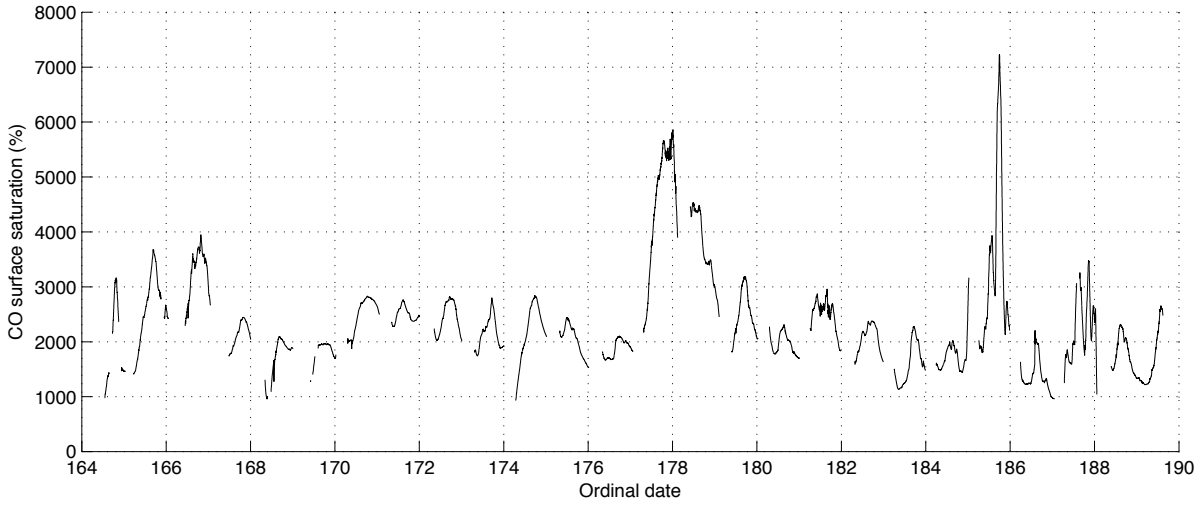

Figure 2. 25: Sea surface saturation (%) for CO in respect to the atmospheric equilibrium concentration, along the D366 cruise track. The red line indicates 100 % saturation. The mean surface saturation for CO was 2342.20 ± 907.54 Details of how surface saturation for CO was calculated are found in section 2.3.2.

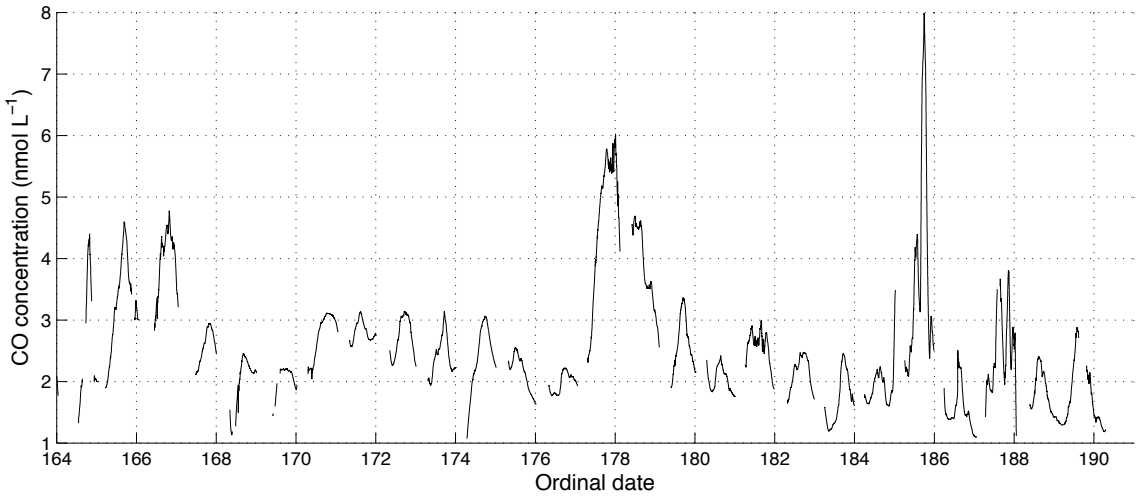

Figure 2. 26: Sea surface concentration of CO along the D366 cruise track. The mean surface concentration for CO was 2.56 ± 0.97 nmol L^{-1}. Details of how surface concentration for CO was calculated are found in section 2.3.2.

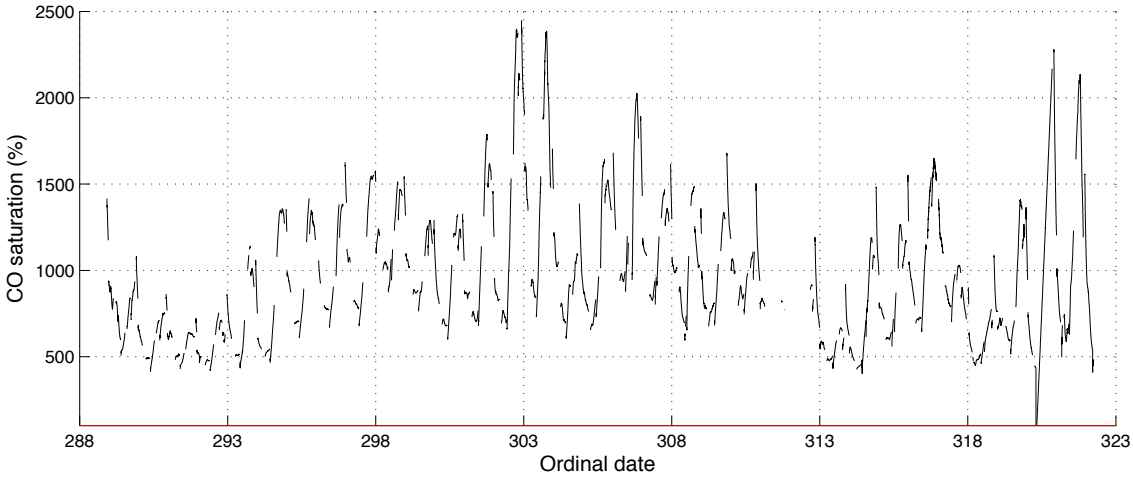

Figure 2. 27: Sea surface saturation (%) for CO in respect to the atmospheric equilibrium concentration, along the AMT22 cruise track. The red line indicates 100 % saturation. The mean surface saturation for CO was 951.05 ± 381.50 %. Details of how surface saturation for CO was calculated are found in section 2.3.2.

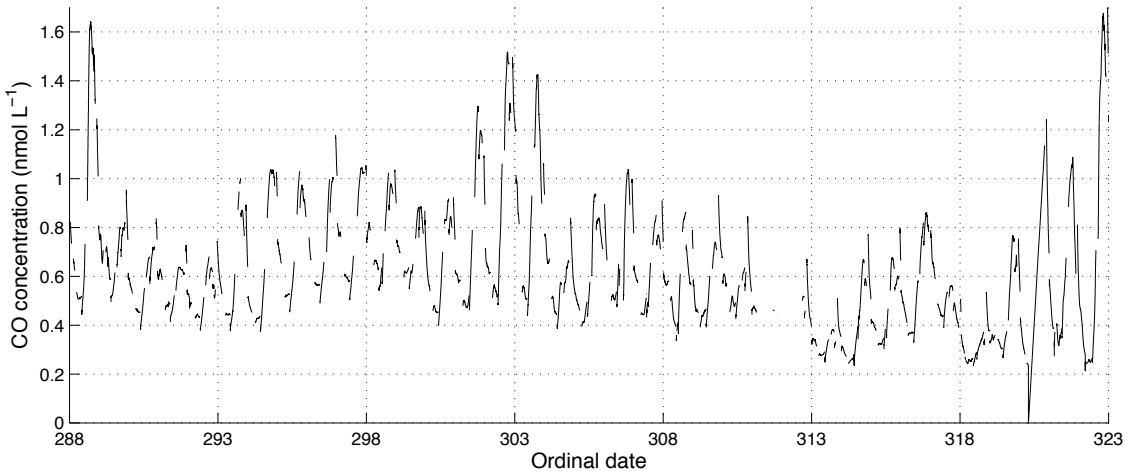

Figure 2. 28: Sea surface concentration for CO along the AMT22 cruise track. The mean surface concentration for CO was 0.62 ± 0.26 nmol L^{-1}. Details of how the surface concentration of CO was calculated are found in section 2.3.2.

2. 9: CO_2 measurements

2.8. 1: Calibration

For the D366 OA cruise the CO_2 values of the three CO_2 working standards (Table 2. 1) were calculated from a post-cruise calibration using reference standards (Table 2 .2) at WAO, and used to correct the offset of the measurements. The working standards were outside the range of the reference standards, which may have introduced marginal error in the calibration. For the AMT22 cruise the values of the three working CO_2 standards (Table 2 .3) were calculated as a mean value from a pre and a post cruise calibration against the same reference standards and used to correct the measurements for the offset. For both datasets a linear regression was used to correct the seawater measurements for both the offset and instrumental drift.

2.8. 2: CO_2 atmospheric datasets

2.8.2. 1: Data points excluded from the atmospheric datasets

The final mean atmospheric values selected excluded two unusually high values, at ordinal date 178 and 179 (Figure 2. 29 (cyan)) (discussed in section 2.6.2.2). Two additional atmospheric runs were excluded as they were contaminated by stack pollution (Figure 2. 29 (magenta)). For the AMT22 dataset the final mean

atmospheric values selected (Figure 2. 30 (blue)) excluded ten mean runs that were contaminated by stack pollution during the measurement (Figure 2. 30 (cyan)).

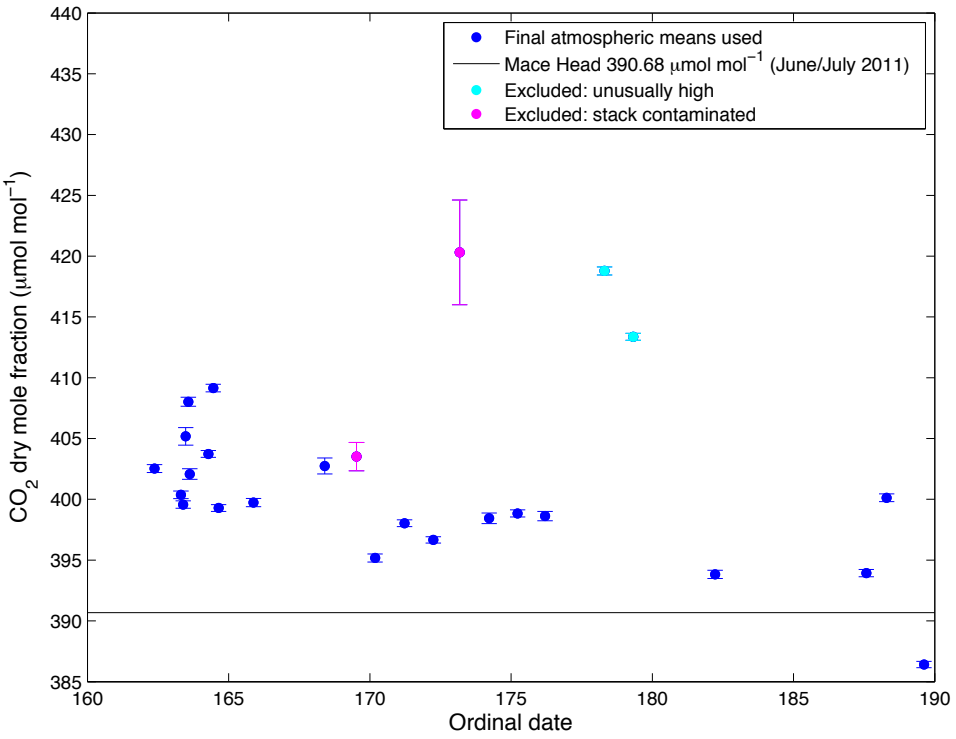

Figure 2. 29: The CO_2 atmospheric mean value of 399.64 ± 5 µmol mol $^{-1}$ (n=21), with a range of 22.74 µmol mol $^{-1}$ was calculated from the D366 data from the mean value for CO_2 atmospheric value for each run selected (n=240) (blue), excluding two unusually high values (cyan) and two stack contaminated runs (magenta) The measurements were higher than the Mace Head[21] June and July mean atmospheric value of 390.68 µmol mol $^{-1}$.

[21] **Data source: World Data Centre for Greenhouse Gases (WDCGG), Mace Head CO_2– NOAA/ERSL (flask) monthly, 1991-06 -2013-12. http://ds.data.jma.go.jp/gmd/wdcgg/pub/data/current/co2/monthly/mhd653n00.noaa.as.fl.co2.nl.mo.dat Last accessed June 2014.**

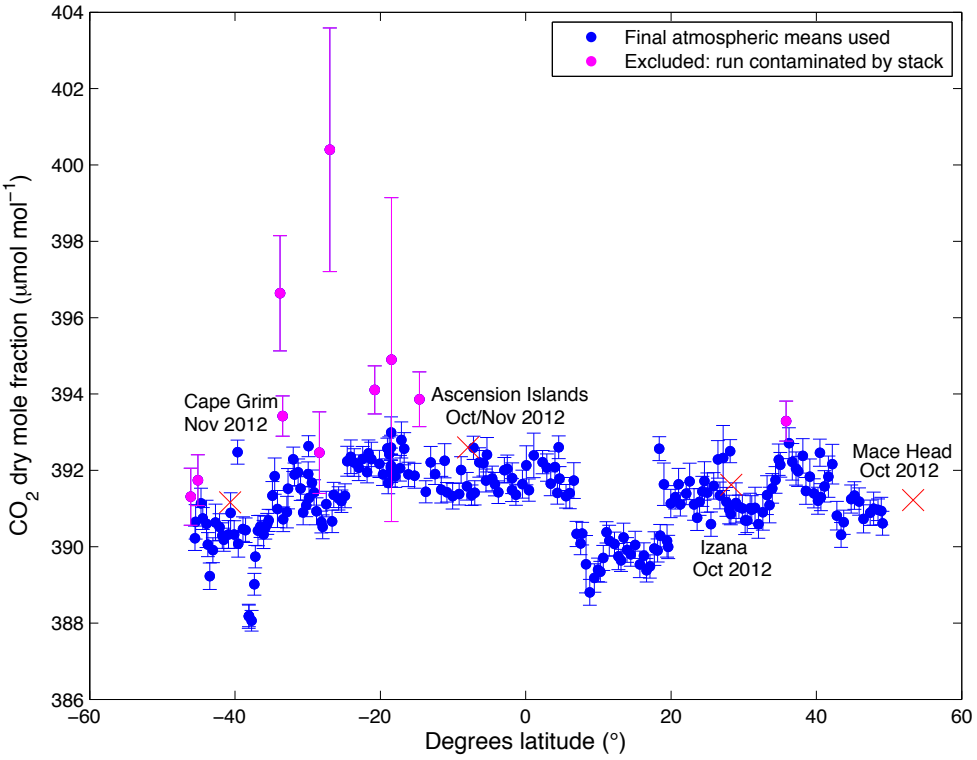

Figure 2. 30: Atmospheric CO_2 mean values (n=240) with latitude along the AMT22 transect from Southampton, UK, to Punta Arenas, Chile. The atmospheric mean values used (blue) excluded the data points contaminated by stack pollution (cyan). Comparisons are made to Mace Head[13], Ireland, (monthly mean value from October 2012), Izańa[14], Tenerife, (October, 2012), Ascension Island[15] (October and November, 2012) and Cape Grim[17], Tasmania, (November, 2012).

2.8.2. 2: Data validation: comparing measurements to other CO_2 atmospheric stations

During the D366 cruise a mean atmospheric CO_2 value of 399.64 ± 5 µmol mol $^{-1}$ (n=21), with a range of 22.74 µmol mol $^{-1}$ was measured (Figure 2. 29). This value exceeded the atmospheric CO_2 monthly mean value measured at Mace Head[13], for the June and July 2011 time period, at 393.59 µmol mol $^{-1}$ and 387.77 µmol mol $^{-1}$. However, Mace Head measurements are filtered and cleaned and occur at one location, where as on the ship measurements varied spatially and were not filtered.

Much closer correspondence was achieved between the AMT22 atmospheric CO_2 dataset and other stations. The mean atmospheric CO_2 value for the AMT22 cruise was 391.19 ± 1 µmol mol $^{-1}$ (n=213), with a range of 4.93 µmol mol $^{-1}$

(excluding the stack contaminated runs) (Figure 2. 30). The atmospheric CO_2 dataset from the AMT22 transect is consistent with the latitudinal trend found at different atmospheric stations at varying latitudes (Mace Head[21] October 2012 monthly mean value: 391.23 µmol mol $^{-1}$, Izaña[22], Tenerife, October 2012: 391.18 µmol mol $^{-1}$, Ascension Island[23] October/November 2012: 392.60 µmol mol $^{-1}$ and Cape Grim[24] November 2012: 391.18 µmol mol $^{-1}$ (Figure 2. 30; Table 2. 6).

2.8.2. 3: Comparing the D366 dataset to the AMT22 dataset

The atmospheric CO_2 measurements made on the D366 research cruise were much higher than those made on the AMT22 cruise, which took place a year later. When comparing these datasets, the large standard deviation and range found in the D366 atmospheric measurements (22.74 µmol mol $^{-1}$ and 5.04 µmol mol $^{-1}$) in comparison to the AMT22 measurements (4.93 µmol mol $^{-1}$ and 0.95 µmol mol $^{-1}$) suggests the D366 measurements have been influenced by anthropogenic sources. This is most likely due to the coastal location in which the D366 cruise took place, in comparison to the open ocean where the AMT22 measurements were made.

Table 2. 7: Atmospheric CO_2 monthly mean values calculated at various locations. The standard deviation of the mean measurement at each station, the sample size (n) and the range within the datasets was not available.

Location	Lat/ lon (°) of station	Month/ year	Mean (µmol mol $^{-1}$)	Contributor
Mace Head (Ireland)	53.32 °N/ 9.90 °W	October 2012	391.23	NOAA/ESRL[21]
Izaña (Tenerife)	28.30 °N /16.5 °W	October 2012	391.18	AEMET[22]
Ascension Island	7.92 °S/ 14.42 °W	October 2012	392.33	NOAA/ESRL[23]
Ascension Island	7.92 °S /14.42 °W	November 2012	392.86	NOAA/ESRL[23]
Cape Grim (Australia)	40.68 °S /144.68 °E	November 2012	391.18	CSIRO[24]

[22] Data source: World Data Centre for Greenhouse Gases (WDCGG), Izaña CO_2– AEMET (continuous) monthly, 1984-01 -2014-12. http://ds.data.jma.go.jp/gmd/wdcgg/pub/data/current/co2/monthly/izo128n00.aemet.as.cn.co2.nl.mo.dat Last accessed June 2014.

[23] Data source: WDCGG, Ascension Island CO_2– NOAA/ESRL (continuous) monthly, 1979-08 -2013-12. http://ds.data.jma.go.jp/gmd/wdcgg/pub/data/current/co2/monthly/asc107s00.noaa.as.fl.co2.nl.mo.dat Last accessed June 2014.

2.8. 3: CO_2 seawater datasets

Figures 2. 31 and 2. 32 show the partial pressure of CO_2 (pCO_2) at SST measured along the D366 and AMT22 cruise transects (section 2.3.3). The mean pCO_2 measured on the D366 cruise was 343.32 ± 31 µatm, and 362.65 ± 24 µatm on the AMT22.

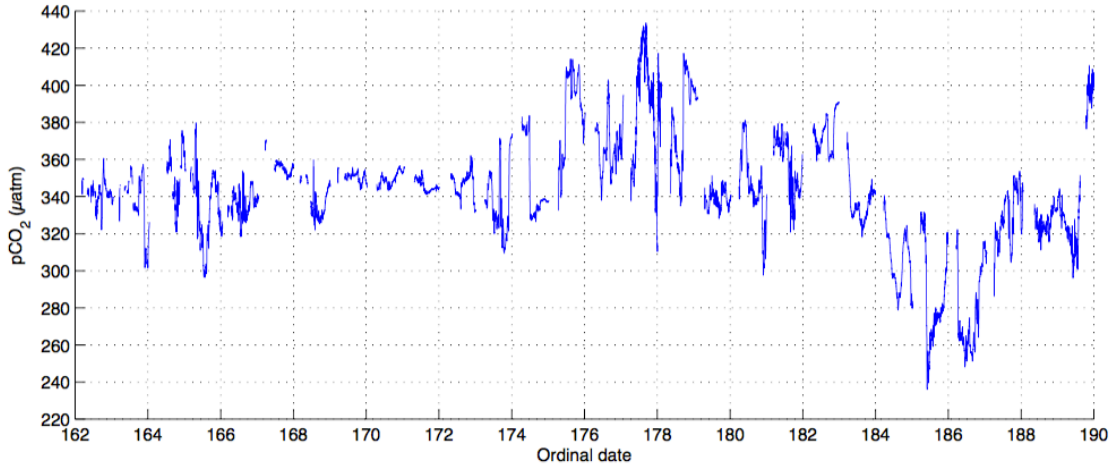

Figure 2. 31: Sea surface partial pressure of CO_2 (pCO_2) (µatm) along the D366 cruise track. The mean pCO_2 measured on the D366 cruise was 343.32 ± 31 µatm. The calculation for pCO_2 is found in section 2.3.3.

[24] **Data source: World Data Centre for Greenhouse Gases (WDCGG), Cape Grim CO_2– CSIRO (flask) monthly, 1991-06 -2013-12. http://ds.data.jma.go.jp/gmd/wdcgg/pub/data/current/co2/monthly/cgo540s00.csiro.as.fl.co2.nl.mo.dat Last accessed June 2014.**

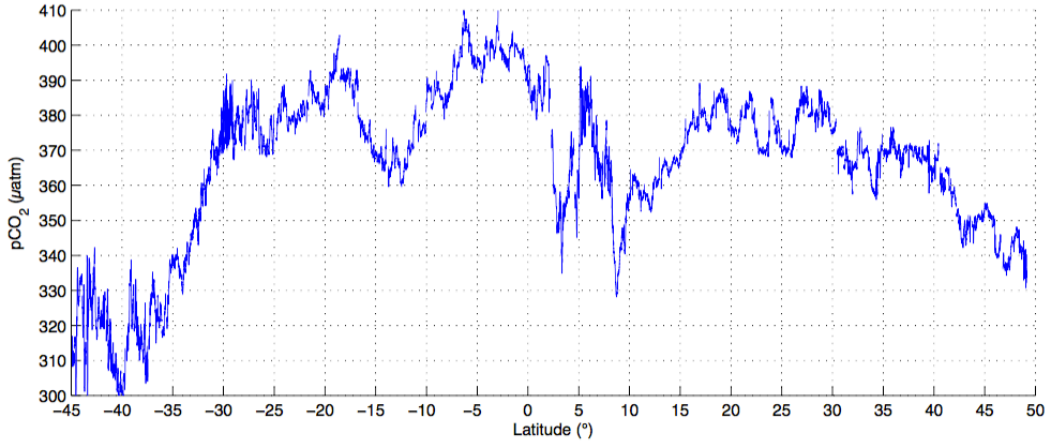

Figure 2. 32: Sea surface pCO_2 (µatm) along the AMT22 cruise track. The mean pCO_2 measured on the AMT22 cruise was 362.65 ± 24 µatm. The calculation for pCO_2 is found in section 2.3.3.

2.8.3. 1: Data validation: Inter-comparison studies between continuous the Los Gatos ICOS and LI-COR instruments during the D366 OA and AMT22 cruises.

Inter-comparison studies were conducted between the pCO_2 data measured with the *Los Gatos* ICOS and LI-COR instruments, on the D366 (Figures 2. 33 and 2. 34) and the AMT22 (Figure 2. 35) cruises. The ICOS D366 data was compared to two separate LI-COR analysers, one belonging to Plymouth Marine Laboratory (PML) and the other to the University of East Anglia (UEA) (Figure 2. 33). The ICOS AMT22 dataset was compared to the PML LI-COR dataset (Figure 2. 35 - left panel). Comparisons were made between datasets at collocated time points only, within approximately 10 seconds of one another. Pearson's correlations were used to assess the agreement between the datasets through their linear dependence. Ribas-Ribas et al. (2014) previously compared four carbonate system variables measured during the D366, including the PML and UEA LI-COR datasets, finding the two datasets to be significantly correlated (r=0.956, p<0.001). This study found a significant correlation between both the ICOS and PML LI-COR pCO_2 datasets (r = 0.978, p=<0.001) and the ICOS and UEA LI-COR datasets (r=0.983, p=<0.001) (Figure 2. 34: left and right panels). The agreement of the three datasets validates the pCO_2 ICOS dataset for the D366 cruise. The AMT22 ICOS pCO_2 dataset correlated significantly to the PML LI-COR dataset (r = 0.989, p=<0.001) (Figure 2. 35 - right panel), although there were greater differences between the line of perfect agreement (1: 1 green line) and

the line of best fit (red line) in this comparison than for the D366 comparison. This could be attributed to the different locations of the instruments on the RRS James Cook (AMT22) cruise leading to time differences in the water reaching each instrument for measurement.

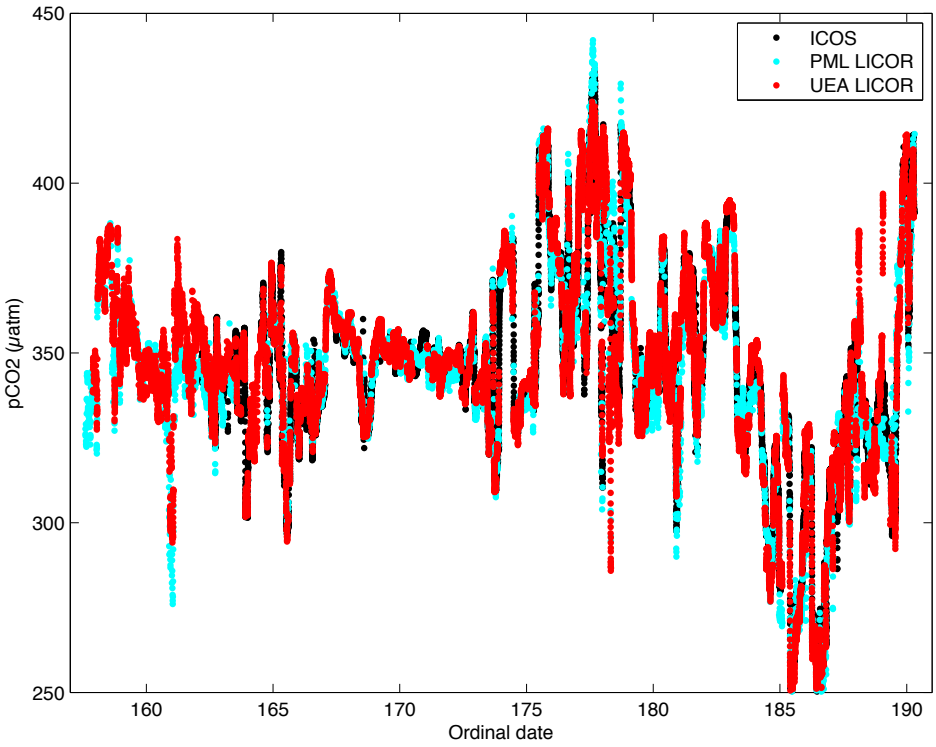

Figure 2. 33: Inter-comparison study between the pCO_2 measured by the UEA *Los Gatos* ICOS (black) a PML LI-COR (cyan) and a UEA LI-COR (red) instrument on the D366 cruise.

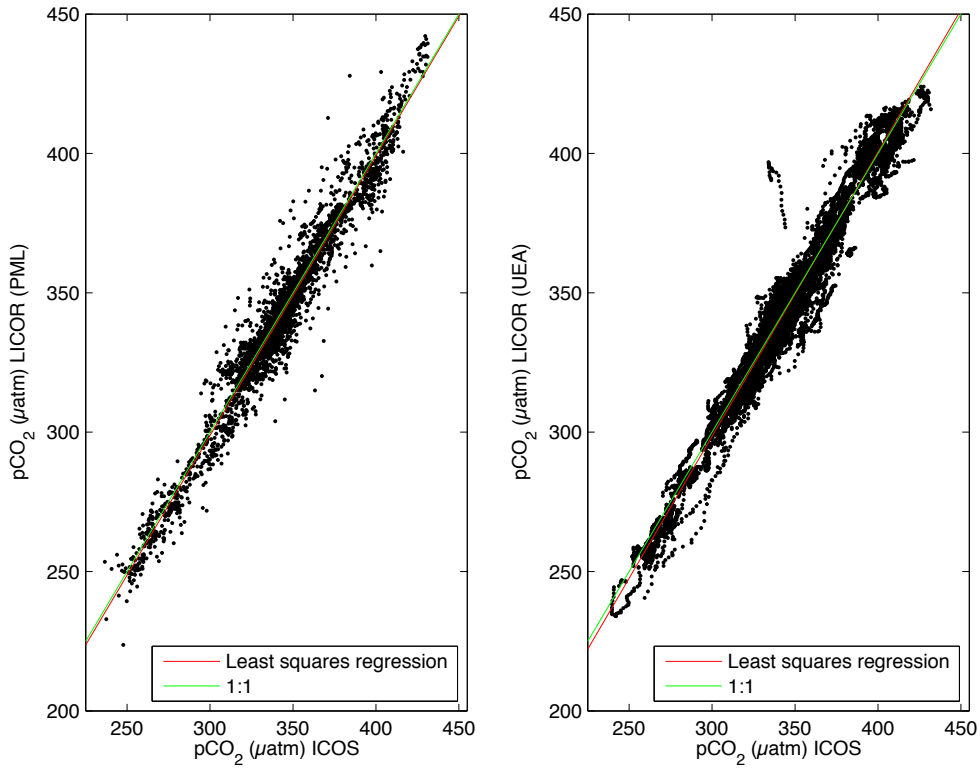

Figure 2. 34: (Left panel): Relationship between the pCO_2 ICOS and pCO_2 LI-COR (PML) datasets (Pearson's correlation: r = 0.978, p=<0.001) from the D366. (Right panel): Relationship between the pCO_2 ICOS and pCO_2 LI-COR (UEA) datasets (Pearson's correlation: r = 0.983, p=<0.001) from D366. The lines of perfect agreement (green) and least squares regression (red) are shown for each dataset comparison.

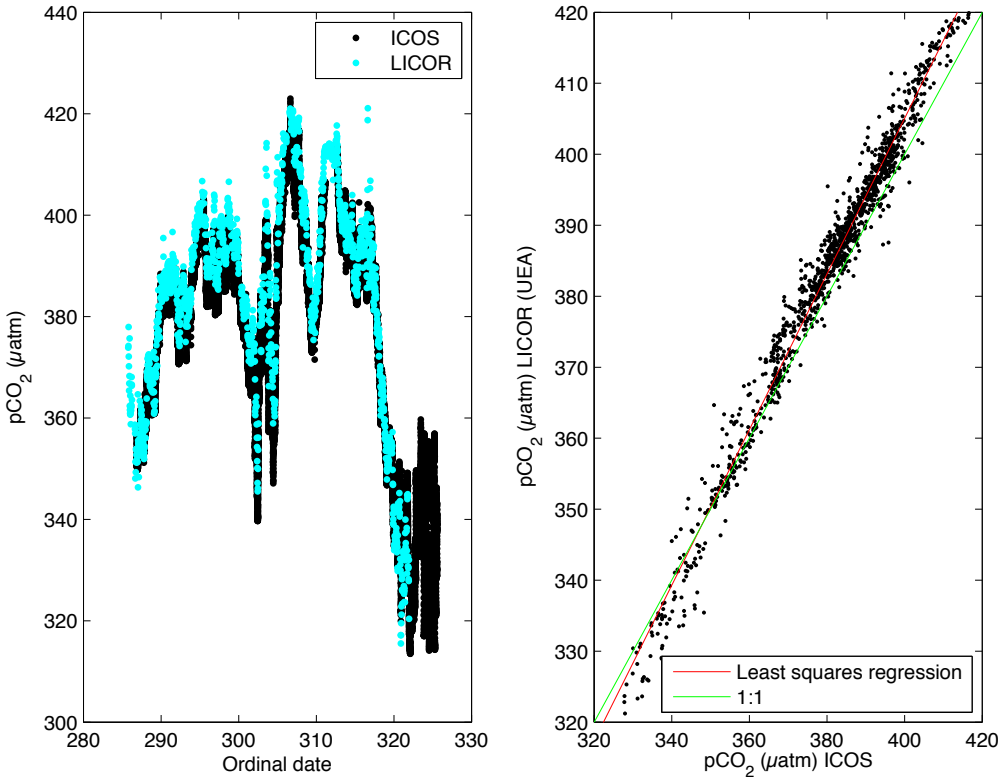

Figure 2. 35: (Left panel): Inter-comparison study between pCO_2 measured by the ICOS (black) and the LI-COR (PML) (cyan) instruments during the AMT22 cruise. (Right panel): Relationship between pCO_2 ICOS and pCO_2 LI-COR (PML) datasets (Pearson's correlation: r = 0.989, p=<0.001) during AMT22. The lines of perfect agreement (green) and least squares regression (red) are shown.

Chapter 3: Surface water distribution of nitrous oxide in the northwestern European shelf seas.

3. 1: Introduction

This chapter describes the surface distribution and ocean-atmospheric flux of N_2O in the Northwestern European shelf seas (D366 OA cruise). Dry mole fractions of N_2O were measured at sea, in both the atmosphere and from surface waters using ICOS spectrometry (N_2O/CO 23d *Los Gatos Research*) and used to calculate surface water concentration, saturation and ocean-atmospheric fluxes of N_2O during the cruise. Surface saturations were also calculated for CH_4 and CO, along with the partial pressure of CO_2, and used to establish any empirical relationships between the climatically relevant gases in surface waters.

3.1. 1: Objectives

The objectives of this chapter are:

- To quantify the mean surface concentration, saturation and air-sea flux of N_2O in the summer of June and July 2011 in the NW European shelf seas.
- To identify whether the NW European Shelf seas acted as a N_2O source or sink.
- To identify the locations where surface waters were under and supersaturated.
- To use the high resolution data to understand the processes influencing the distribution of surface N_2O at both large scales across the NW European shelf seas, and within smaller localised regions.

3.1. 2: Aims

N_2O is the third most important long-lived greenhouse gas after CO_2 and CH_4, with approximately one quarter of global emissions arising from the open ocean, coastal zones, as well as rivers and estuaries. This chapter aims to identify whether the NW European shelf sea regions acted as a source or sink in the summer of 2011. This is the first high-resolution surface N_2O study in the NW

European shelf seas and therefore this chapter aims to identify key influential processes on the surface distribution of N_2O in shelf sea environments by examining the relationship between this trace gas, meteorological parameters and the other gases measured in the surface waters.

3. 2: Methods

3.2. 1: Underway datasets

Section 2. 3 describes how the sea surface concentration, saturation and ocean-atmosphere flux values were measured and calculated, respectively. Underway data, including sea surface temperature (SST), sea surface salinity (SSS) and surface chl-a were used to interpret the N_2O surface data for the D366 OA cruise. On the D366 OA cruise the temperature of the water was measured in degrees Celsius using a thermosalinograph hull sensor. Surface salinity measurements also were made by thermosalinograph, and computed using the UNESCO 1983 algorithm (Fofonoff and Millard Jr, 1983). The units for salinity are dimensionless. Surface water chl-a concentration measurements, per unit volume of the water body (μg chl-a L^{-1}), were made using a through-flow fluorometer plumbed into the non-toxic seawater supply. The manufacturer's calibration was applied to calibrate the dataset. Absolute wind speed, used to calculate the air-sea fluxes, was measured in the atmosphere (m s^{-1}) using an in-situ anemometer and corrected to 10 m height above sea level (Large and Pond, 1981). The data was corrected for both the ship's heading and speed.

3.2. 2: Correlations between surface nitrous oxide and other measured parameters

The surface ocean N_2O data collected during the D366 was of high resolution (47330 samples along a cruise track of 4730 nautical miles), providing the unique opportunity to identify relationships between surface N_2O and other parameters and gases also measured at high-resolution during the cruise. To identify relationships between these parameters, Spearman's correlations were completed between surface ocean N_2O concentration (nmol L^{-1}) and saturation

(%), with surface chl-a concentration (µg l^{-1}), SST (°C), SSS, surface CH_4 and CO concentration (nmol l^{-1}) and saturation (%) and the surface pCO_2 (µatm) over the entire D366 dataset for each parameter. Spearman's correlation is a non-parametric measure of the relationship between two parameters. The results are found in section 3.3.3 1.

To identify localised relationships a programme was written using Matlab R2013b, and used to identify where strong positive and negative correlations occurred between the sea surface saturation values for N_2O and SST, SSS and chl-a concentration, and the surface saturations (CH_4 and CO) and surface partial pressure (CO_2) for other climatically active gases. The aim of the programme was to use Spearman's correlation analysis as a tool to provide insight into processes occurring in the European shelf seas that influence the surface distribution of N_2O. The programme identified correlations between surface N_2O saturation and the other parameters, selecting only the significant relationships (p-value <=0.05). From the selected data, the correlation coefficients (r-values) were plotted on distribution maps (Figures 3. 7 to 3. 12), highlighting regions in the surface waters of the Northwest European shelf seas with strong positive or negative correlations.

Experimentation with the programme examined the influence of: 1) how often a correlation was run (e.g. in time steps of every 5 minutes in ordinal date along the cruise track), and 2) the length of time the correlation was run for (e.g. for 5 hours), on the maps produced. The aim was to understand which combination of these factors could identify regions where strong relationships occurred between surface N_2O and the other parameters. Results indicated that:

- Running the programme with time steps that were too short produced too many points on the maps, causing the later correlation coefficients to overlap the ones plotted earlier making visual assessment of the maps produced difficult.

- If time steps were greater than ten minutes, gaps formed between points on the maps. The aim was to produce maps with as many points as possible to detect where correlations occurred.
- Running the correlation for short durations, for example every hour, produced maps showing localised regions where correlations occurred, making it difficult to identify key areas and relationships within the shelf sea.
- When the correlation was run over longer periods of time, larger regions with strong correlations between variables could be identified, however if the correlation was run for more than twelve hours, many correlations decreased in strength.

In conclusion, a combination of running the programme every ten minutes for twelve hours was selected as optimum. The correlation distribution maps can be found in section 3.3.3 2.

3. 3: Results

3.3. 1 D366 nitrous oxide data description

3.3.1. 1 Nitrous oxide concentration, saturation and ocean to atmosphere flux

The majority of the surface waters were supersaturated for N_2O with respect to the atmospheric value, with a mean saturation of 102 ± 2 % (97 to 110 %) (Figure 3. 1), a mean concentration of 9 ± 0 nmol L^{-1} (Figure 3. 2) and a mean ocean-atmosphere flux of 997 ± 1250 nmol m^{-2} d^{-1} (Figure 3. 3). The surface saturation is similar to those previously reported in the North Sea between 100 to 104 % (Law and Owens, 1990a, Bange et al., 1996b). According to Uher (2006) the total areal extent of the North Sea and the Irish Sea combined 8.7 x 10^5 km^2. Using this surface area the ocean to atmosphere flux of N_2O for these regions are calculated as 1.3 x 10^7 kg N_2O yr^{-1}. This is greater than the estimate from the North Sea of 9.5 x 10^7 kg N_2O yr^{-1} (Law and Owens, 1990a), but this difference can be attributed to the larger surface area.

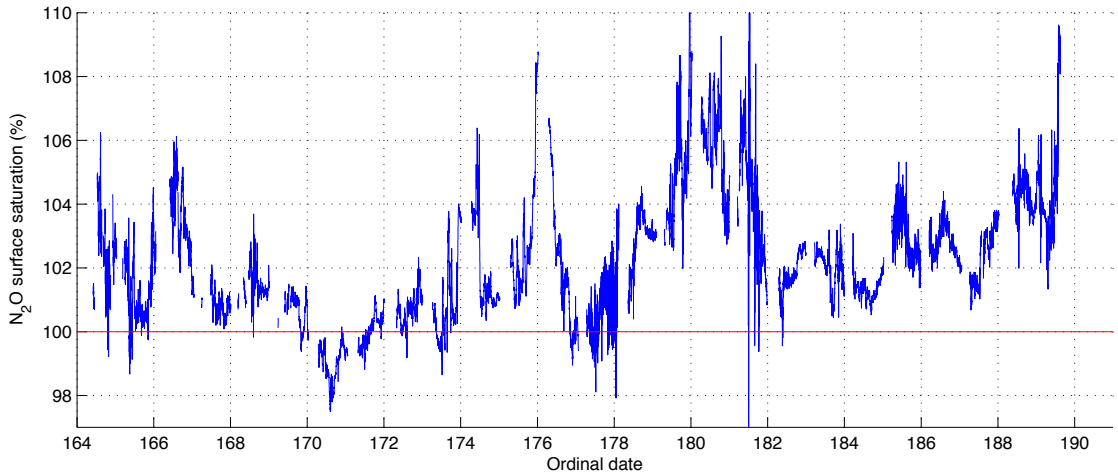

Figure 3. 1: Sea surface saturation for N_2O with respect to the atmospheric value along the D366 cruise track. The mean sea surface saturation measured along the cruise track was slightly supersaturated at 102 ± 2 %. The red line shows 100% saturation. Atmospheric values used in the saturation were measured on the ship and discussed in section 2.6.2. Details of how surface saturation for N_2O was calculated are found in section 2.3.2.

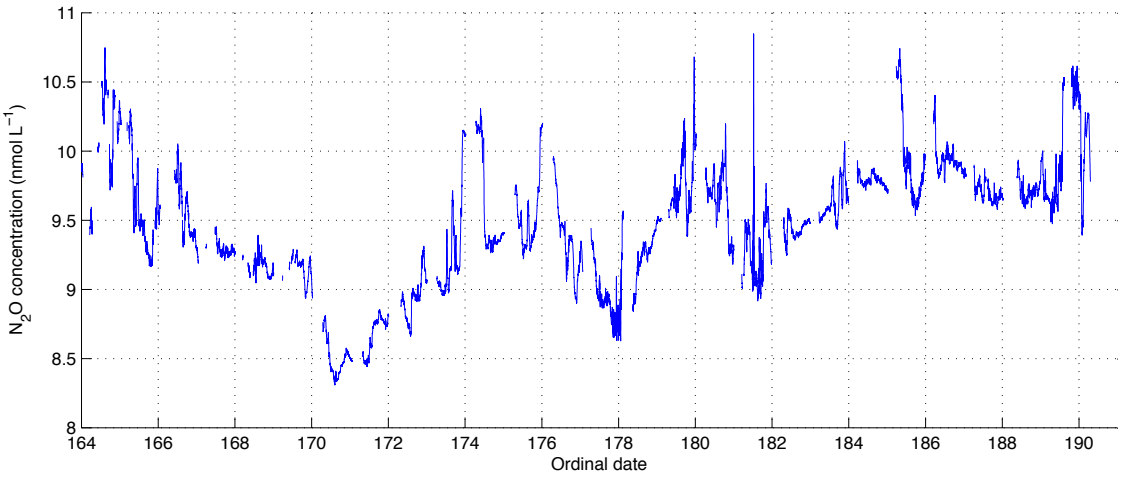

Figure 3. 2: Sea surface concentration of N_2O measured along the D366 cruise track. The mean sea surface concentration measured along the cruise track was 9 ± 0 nmol L^{-1}. Details of how surface concentration for N_2O was calculated are found in section 2.3.2.

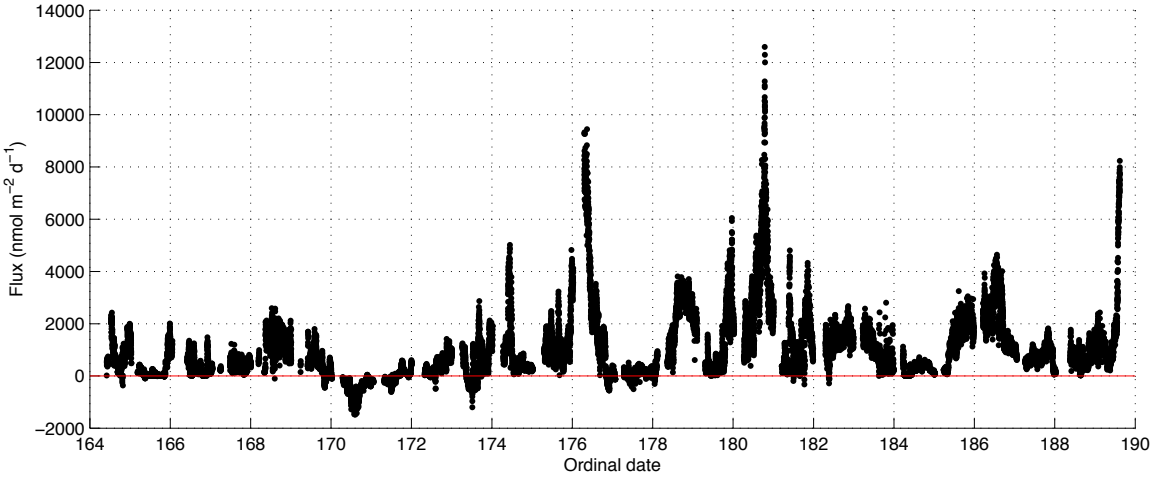

Figure 3. 3: The ocean-atmosphere flux of N_2O calculated along the OA D366 shelf seas cruise track. The surface water was a slight source of N_2O to the atmosphere at 997 ± 1250 nmol m^{-2} d^{-1}. Details of how the ocean to atmosphere flux is calculated are found in section 2.3.4.

3.3.1. 2: The distribution of surface water nitrous oxide saturation.

Figure 3. 4 shows the distribution of N_2O saturation in the NW European Shelf sea surface waters for June/July 2011. The most supersaturated regions in the NW European shelf sea surface waters, reaching supersaturations of >104%, were located:

1. Ordinal date 164.4 - 164.8, off the east coast of Ireland (Irish Sea).
2. Ordinal date 165.8 - 167.2 and 173.9-174.5, off SW Cornwall.
3. Ordinal date 175.6 - 176.6, in the English Channel.
4. Ordinal date 178 - 182, in the central North Sea and into and around the Skagerrak.
5. Ordinal date 185.7 - 186, south of the Shetlands.
6. Ordinal date 186.2 - 187, in the NE Atlantic and the northern Scottish Shelf.
7. Ordinal date 189.55 - 189.61, in the Northern Irish/ Malin Sea

(Refer to Figure 3. 1 for ordinal dates and Figure 3. 4 for a distribution map).

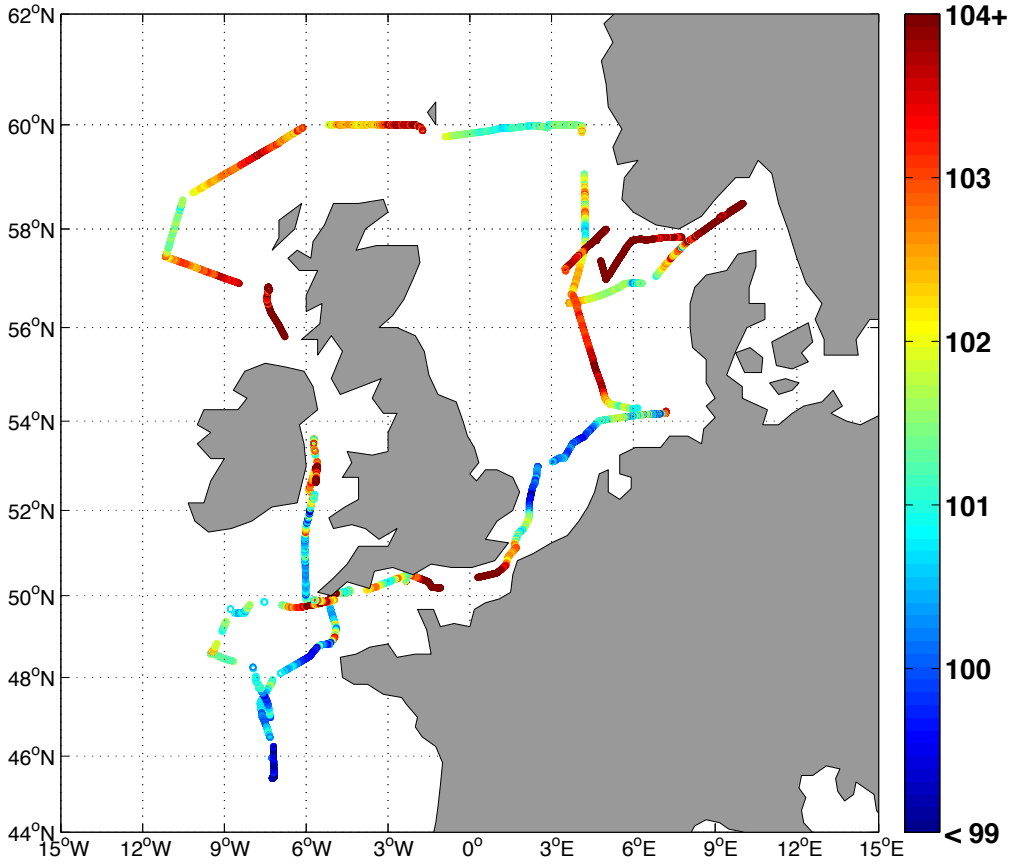

Figure 3. 4: Surface water saturation (%) for N_2O with respect to the atmospheric value in the NW European shelf sea.

The undersaturated regions, (undersaturated to 92.6 %) (Figure 3. 5), were located:

1. Ordinal date 164.80 - 165.50, four small, localised regions off the east coast of Ireland (Irish Sea) (Figure 3. 5, black and blue, reaching undersaturation of 98.6 %).
2. Ordinal date 181.50 - 181.51, one region in the Skagerrak (Figure 3. 5, yellow, reaching undersaturated of 92.6 %).
3. Ordinal date 176.80 - 178.00, two larger regions in the Bay of Biscay (Figure 3. 5, (1) red and magenta, reaching an undersaturation of 97.4 % and (2) cyan and green at an undersaturation of 97.8 %).
4. Ordinal date 176.80 - 178.00, regions in the southern North Sea (Figure 3. 5, cyan and green, reaching undersaturation of 97.8 %).

(Refer to Figure 3. 5 for ordinal day locations and Figure 3. 4 for a distribution map.) The largest regions of undersaturation were found in the Celtic Sea and the Bay of Biscay, moving out into the open ocean.

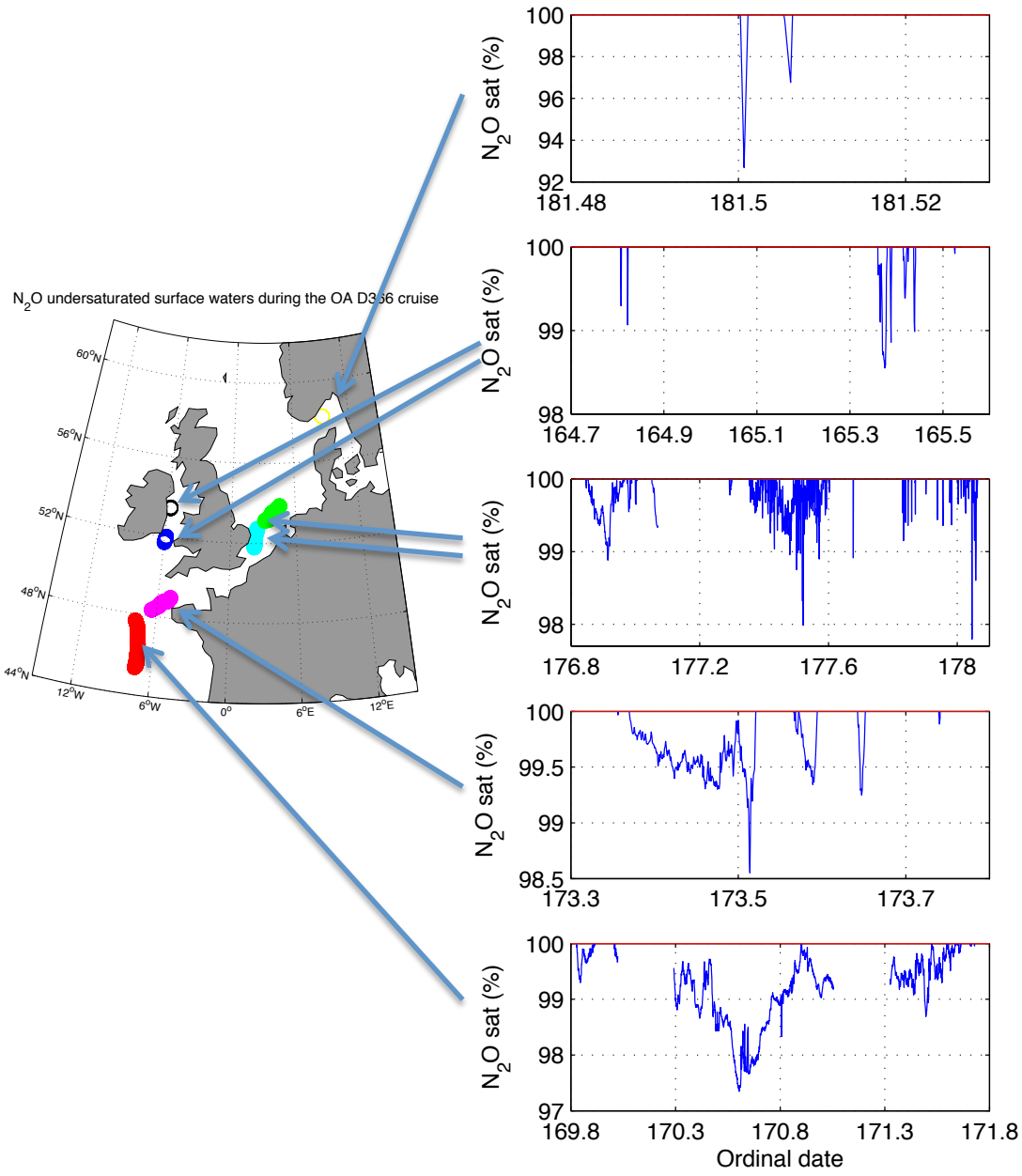

Figure 3. 5: Locations where surface water undersaturation (%) for N_2O occurred in the NW European shelf sea. Note: figures exclude saturations exceeding 100 %.

3.3. 2: Measured underway parameters

On the D366, the mean surface saturation of CH_4 observed on the D366 was 118 ± 21 (102 to 318 %) (Figure 2. 18), surface concentration was 3 ± 0 nmol L^{-1} (2.6 to 8.4 nmol L^{-1}) (Figure 2. 19), pCO_2 was 343 ± 31 µatm (240 to 330 µatm) (Figure 2. 31), surface saturation of CO was 2342 ± 908 (950 to 7500 %) (Figure 2. 25), and surface concentration was 3 ± 0 nmol L^{-1} (1.2 to 8.0 nmol L^{-1}) (Figure 2. 26).

The surface distribution maps for SST, SSS and surface chl-a concentration are found in Figures 3. 6 - 3. 8. During D366 the surface SST ranged between 10 and 18 °C (Figure 3. 6), SSS between 26 and 36 (Figure 3. 7), and surface chl-a concentration 0.1 and 18.0 µg L^{-1} (Figure 3. 8). The water column was stratified/partially mixed during the majority of D366, with the English Channel, the southern North Sea and parts of the Irish Sea fully mixed (Figure 3. 9).

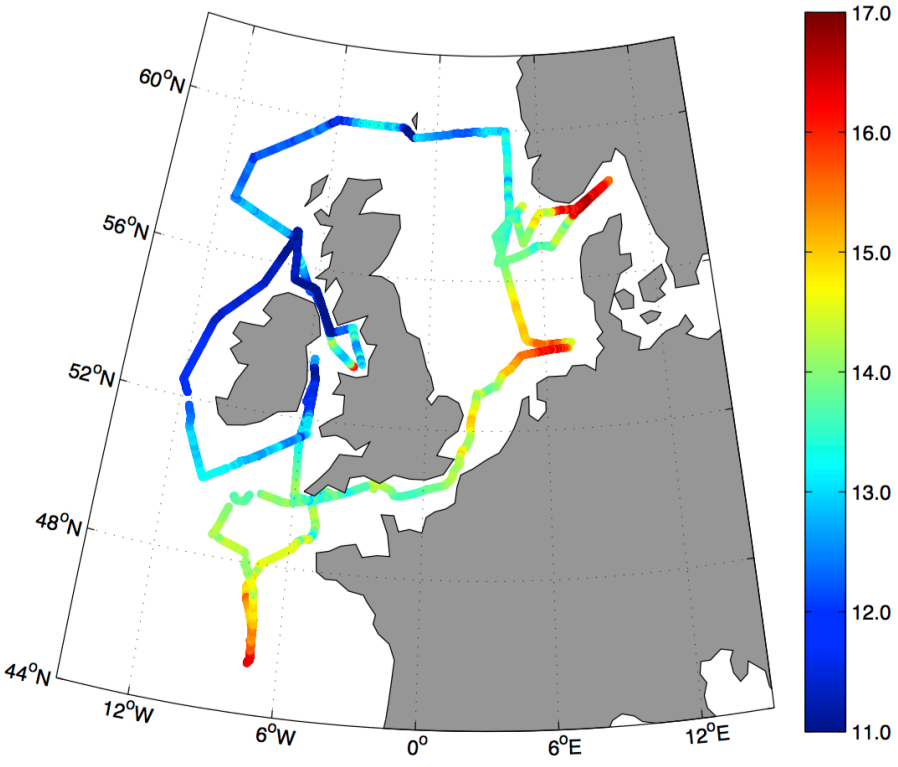

Figure 3. 6: Sea surface temperature distribution (°C) during D366.

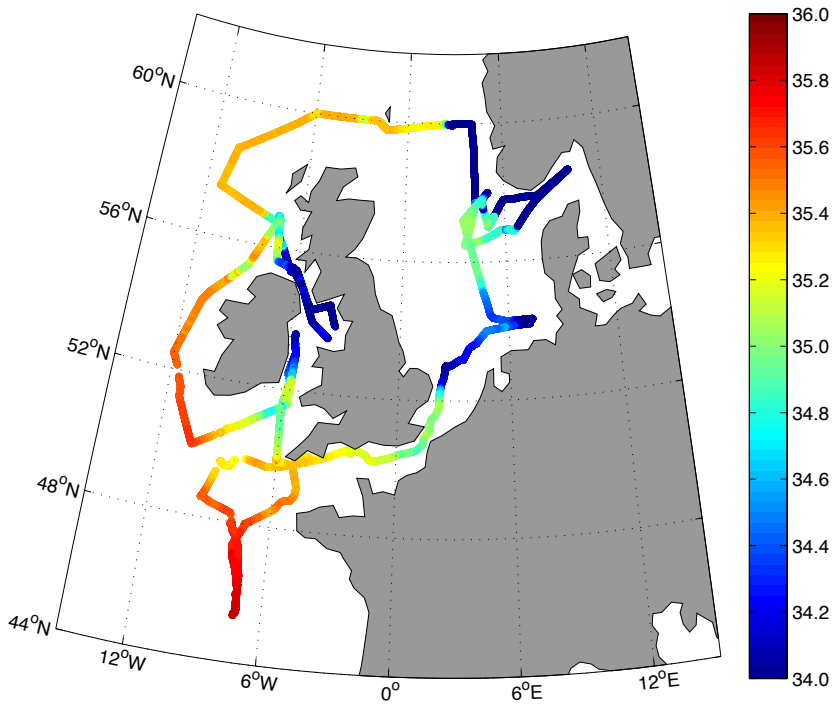

Figure 3. 7: Sea surface salinity distribution during D366.

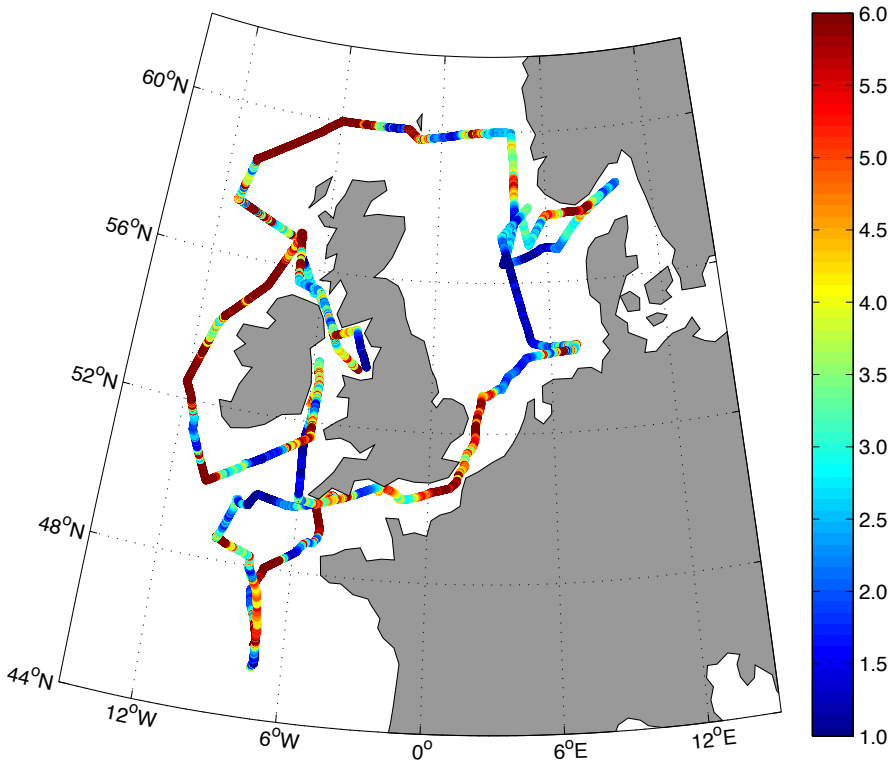

Figure 3. 8: Sea surface distribution of chl-a concentration (µg L^{-1}) during D366.

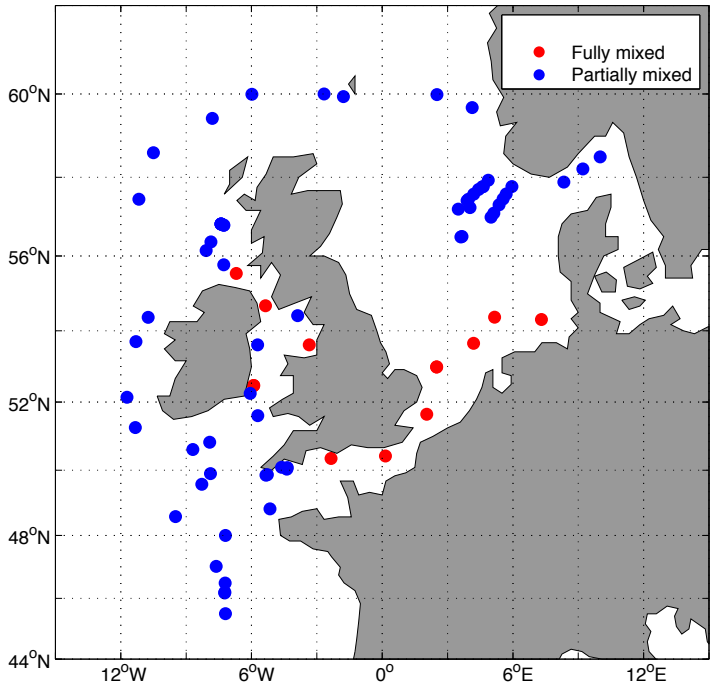

Figure 3. 9: The CTD stations around the NW European shelf seas that were fully mixed (red) and partially mixed (blue) during the OA D366 cruise. Mixed layer depth calculated based on a density criteria of 0.05 kg m^{-3} (Hickman et al., 2012).

3.3. 3: Correlations between surface nitrous oxide and other measured parameters

3.3.3 1: Correlations between parameters for the whole NW European shelf sea

Pearson's correlations were completed between surface ocean N_2O concentration (nmol L^{-1}) and saturation (%), with surface chl-a concentration (µg l^{-1}), SST (°C), SSS, surface CH_4 and CO concentration (nmol l^{-1}) and saturation (%) and the surface pCO_2 (µatm) over the entire D366 dataset for each parameter. The only strong correlation found at this level across the entire NW European shelf seas sampled was a negative correlation between the surface concentration of N_2O and SST (r=-0.87, p= 0.05) (Figure 3. 10, Table 3. 1).

Table 3. 1: Spearman's correlations over the entire NW European shelf seas sampled, between the surface ocean N_2O concentration (nmol L^{-1}) and saturation (%), with surface chl-a concentration (µg L^{-1}), SST (°C), SSS, windspeed (m s^{-1}), surface CH_4 and CO concentration (nmol L^{-1}) and saturation (%) and the surface pCO_2 (µatm).

Surface parameter 1	Surface parameter 2	Correlation coefficient (r-value)	p-value	Figure
N_2O saturation	SST	-0.36	0.05	-
N_2O concentration	SST	-0.87	0.05	Figure 3. 6
N_2O saturation	SSS	-0.46	0.05	-
N_2O concentration	SSS	-0.32	0.05	-
N_2O saturation	Windspeed	-0.21	0.05	
N_2O concentration	Windspeed	-0.16	0.05	
N_2O saturation	Chl-a concentration	0.13	0.05	-
N_2O concentration	Chl-a concentration	0.22	0.05	-
N_2O saturation	CH_4 saturation	0.31	0.05	-
N_2O concentration	CH_4 concentration	0.13	0.05	-
N_2O saturation	CO saturation	+0.14	0.05	-
N_2O concentration	CO concentration	-0.42	0.05	-
N_2O saturation	pCO_2	-0.11	0.05	-
N_2O concentration	pCO_2	-0.34	0.05	-

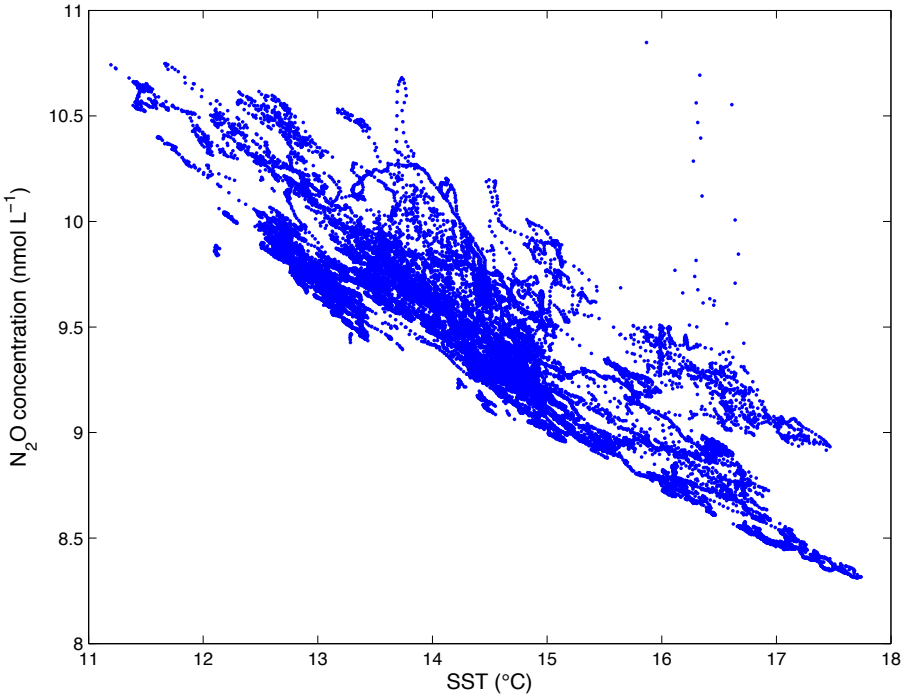

Figure 3. 10: Nitrous oxide and SST over the entire NW European shelf sea region sampled.

3.3.3 2: Correlation distribution maps.

To gain an understanding of the influence of the same parameters on the surface distribution of N_2O, within smaller regions of the NW European shelf seas, a correlation program (described in section 3.2.3) was used. The distribution maps below show the r-values from correlations run every ten minutes for twelve-hour durations, between the sea surface saturation for N_2O and SST (Figure 3. 11), SSS (Figure 3. 12), surface chl-a concentration (Figure 3. 13), sea surface saturation for CH_4 (Figure 3. 14) and CO (Figure 3. 15) and the surface partial pressure of CO_2 (Figure 3. 16). Spearman's correlations are used as an exploratory technique to create distribution maps that identify regions where strong positive and negative correlations occurred between surface N_2O and different parameters along the cruise track. The initial stages of the cruise from Liverpool Bay and around Ireland had no calculations for surface saturation because the atmospheric measurements had not yet commenced.

Scatter plots were used to visualise the data in regions of the shelf where strong correlations were identified (appendix figures 3.A 1 to 3.A 24). The programme identified two types of changes between the surface saturation of N_2O and the other parameters tested:

1. A correlation, where both surface saturation for N_2O and another parameter measured shifted gradually from high to low or vice versa simultaneously.
2. A region where a rapid transition between high and low surface saturation for N_2O occurred simultaneously to a rapid transition with one or more of the other parameters.

Figure 3. 7 displays relationships in different regions of the NW European shelf seas between surface saturation for N_2O and SST. The most pronounced relationship is found in the eastern English Channel, where there is a strong negative correlation between these two parameters. Figure 3. 9 shows predominantly positive correlations between surface N_2O and chl-a concentration over small regions of the NW European shelf sea. There were

various positive and negative correlations over relatively large areas between surface N_2O and CO saturation, where as, the distribution maps did not display many regions with strong positive or negative correlations between surface saturation for N_2O and CH_4, CO_2 and SSS. Regions with strong high and low correlations between the parameters and the interpretation of these interacts are discussed in more detail in section 3.3.4.

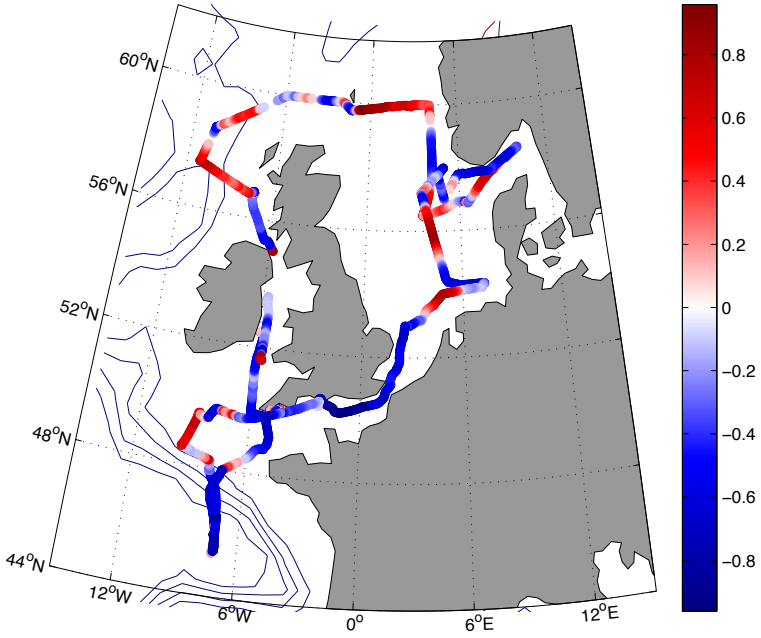

Figure 3. 11: The distribution of the strength of both positive and negative correlations (displayed by the correlation coefficients (r-values)) between the sea surface saturation for N_2O and SST. All values plotted were significant to a p-value of <0.05. The colour bar shows the correlation coefficient (r) value.

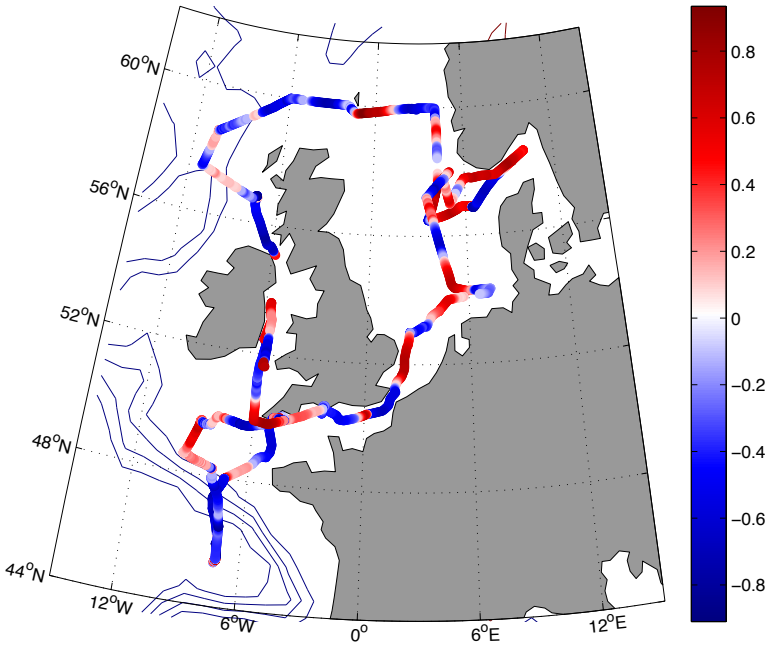

Figure 3. 12: The distribution of the strength of both positive and negative correlations (displayed by the correlation coefficients (r-values)) between the sea surface saturation for N_2O and SSS. All values plotted were significant to a p-value of <0.05. The colour bar shows the correlation coefficient (r) value.

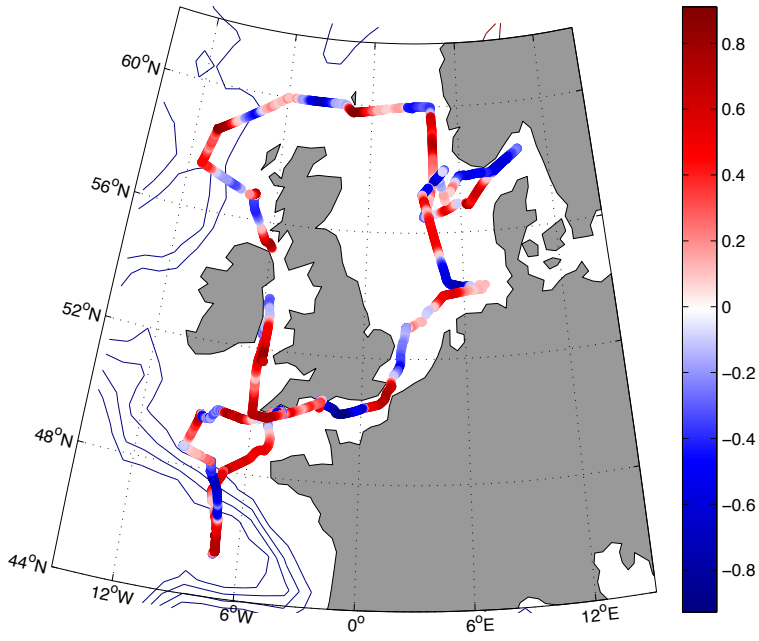

Figure 3. 13: The distribution of the strength of both positive and negative correlations (displayed by the correlation coefficients (r-values)) between the sea surface saturation for N_2O and surface chl-a concentration. All values plotted were significant to a p-value of <0.05.

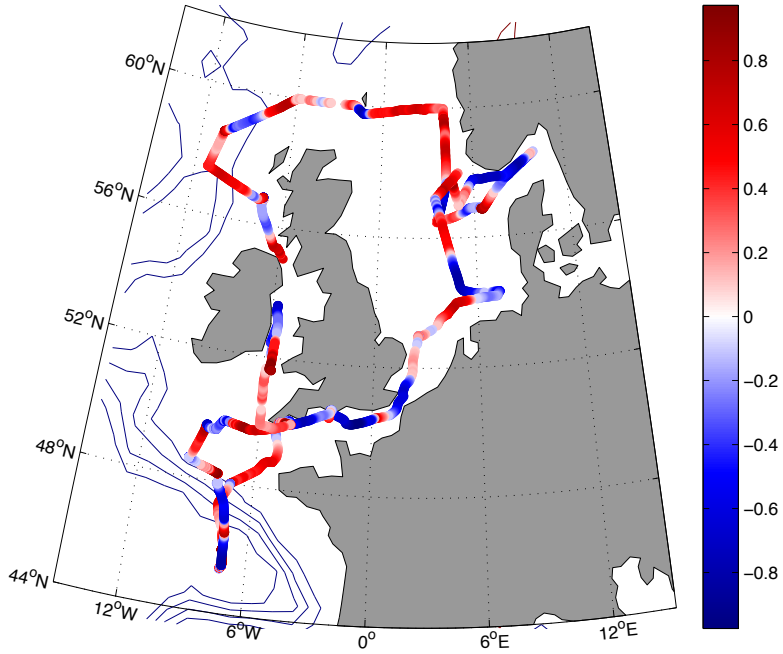

Figure 3. 14: The distribution of the strength of both positive and negative correlations (displayed by the correlation coefficients (r-values)) between the sea surface saturation for N_2O and CH_4. All values plotted were significant to a p-value of <0.05.

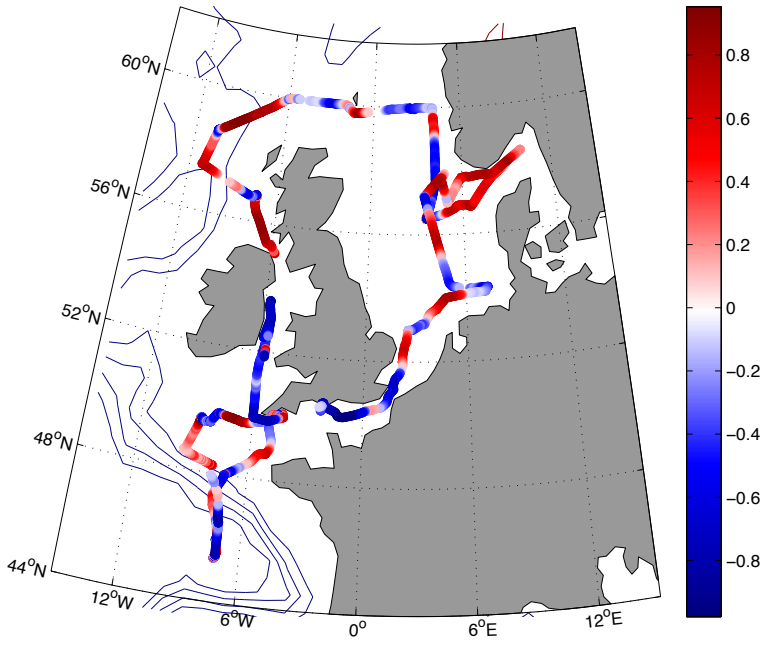

Figure 3. 15: The distribution of the strength of both positive and negative correlations (displayed by the correlation coefficients (r-values)) between the sea surface saturation for N_2O and CO. All values plotted were significant to a p-value of <0.05.

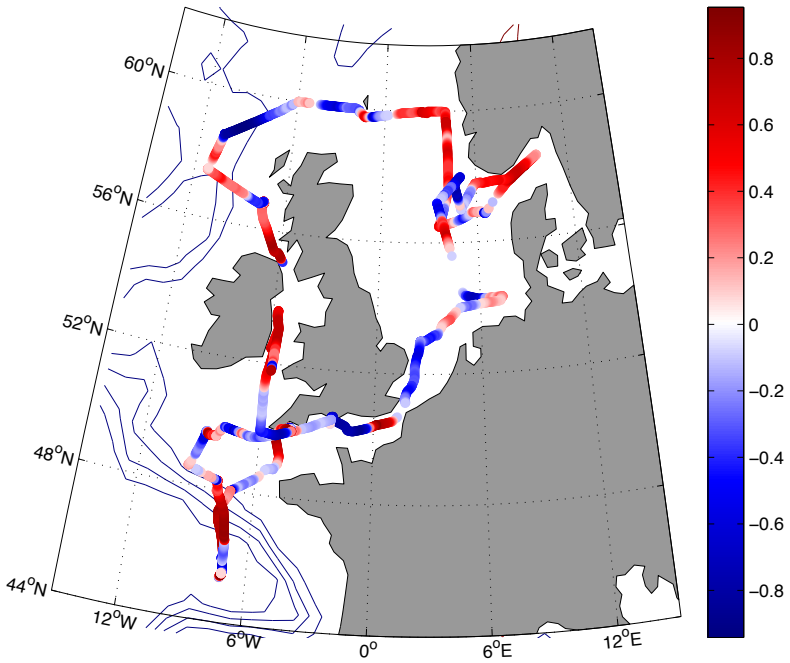

Figure 3. 16: The distribution of the strength of both positive and negative correlations (displayed by the correlation coefficients (r-values)) between the sea surface saturation for N_2O and the surface partial pressure of CO_2. All values plotted were significant to a p-value of <0.05.

3.3. 4: Ventilation time of nitrous oxide in the NW European shelf seas

The ventilation time (the length of time N_2O remains in the water column before venting out to the atmosphere) of N_2O was calculated in the NW European shelf seas during the period of the D366 cruise (Equation 3. 1) (Figure 3. 17). The equilibration time of N_2O was estimated as approximately two weeks, with the assumptions of a uniform mixed layer depth throughout the NW European shelf sea of 26.29 m (mean mixed layer depth calculated during the D366), a consistent windspeed of 9.19 m s^{-1} (mean windspeed observed during the D366), and an uniform SST of 14.22 °C (mean SST recorded during D366). The ventilation time increased at warmer SST's because the solubility of N_2O decreased, and also also at higher wind speeds, and decreased with the depth of the mixed layer.

Equilibration time (s) = mixed layer depth (m)/ piston velocity (m s^{-1}).

Equation 3. 1

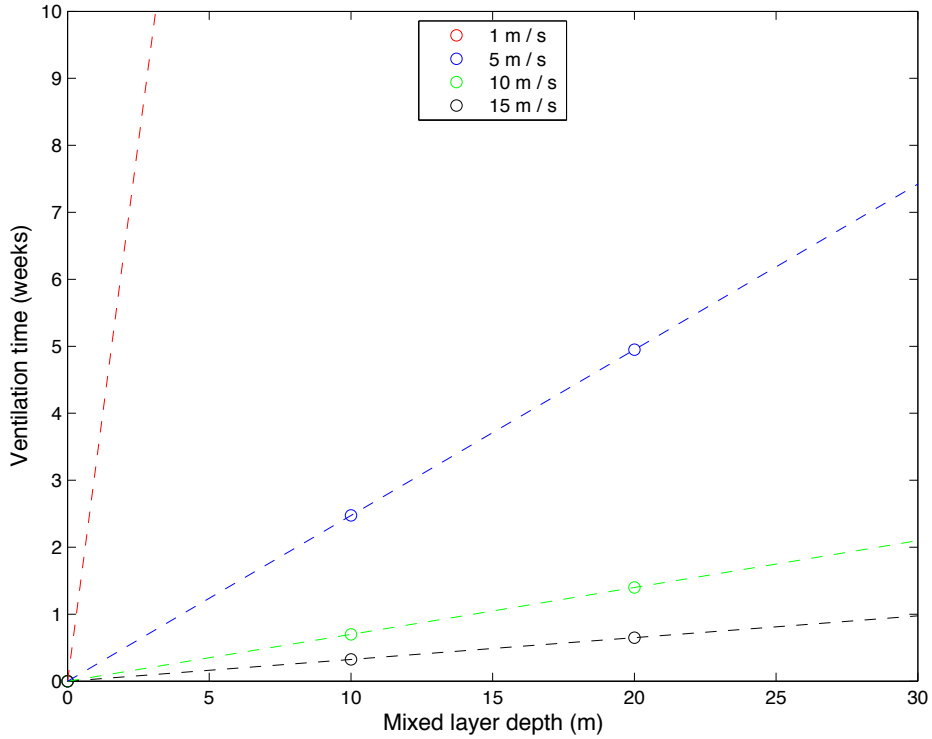

Figure 3. 17: The ventilation time of N_2O at a SST of 14.22 °C, at different mixed layer depths and wind speeds. On the D366 the mean mixed layer depth was calculated as 26.29 m, mean SST was measured at 14.22 °C and mean wind speed was 9.19 m s^{-1}. The ventilation time for N_2O using these mean values was approximately two weeks.

The ventilation time calculated gives an indication of how long N_2O would remain in the water column in this environment before venting out to the atmosphere. However, the estimate is limited by it's assumptions, for example areas of the NW European shelf seas that have a fully mixed water column would be expected to have a greater ventilation time then that calculated.

3. 4: Biogeochemical and physical processes influencing the surface N_2O saturation.

The regions shown in Figure 3. 4 that were highly saturated in N_2O were investigated in more detail (see section 3.4 1) to understand the processes leading to/causing this.

3.4 1: Regions of freshwater influence (ROFI's): The Skagerrak, Norwegian Trench and NE North Sea.

In this thesis the region consisting of the Skagerrak, the Norwegian Trench and the NE North Sea described below, will be referred to as the Skagerrak region.

3.4.1 1 Hydrography: The Skagerrak, Norwegian Trench and NE North Sea.

The Skagerrak is a dynamic transitional region between the Baltic Sea and the North Sea. The area has a complex hydrography, consisting of an anticlockwise circulation that mixes six water masses, the Baltic Water, southern North Sea water, central North Sea water, Kattegat Water, Jutland Current Water, and NE Atlantic Water (Figure 3. 18) (Svansson, 1975, in Skov and Dunrinck 2000). The sea surface waters in the Skagerrak are of low salinity, between 28 to 31 (Figure 3. 19), in comparison to many other regions of the NW European shelf seas. This is due to high inputs of low saline Baltic waters, southern North Sea waters (particularly from the German Bight), and from large rivers within the Skagerrak region (Gustafsson and Stigebrandt, 1996). Circulation and stratification in the Skagerrak are highly influenced by vast quantities of freshwater that enter the region. Low density waters contribute to buoyancy inputs creating strong horizontal gradients of salinity, driving the circulation. Stratification occurs as the low density waters over-lie more saline waters, preventing mixing of the water column. The strong stratification influences biological production (Gustafsson and Stigebrandt, 1996).

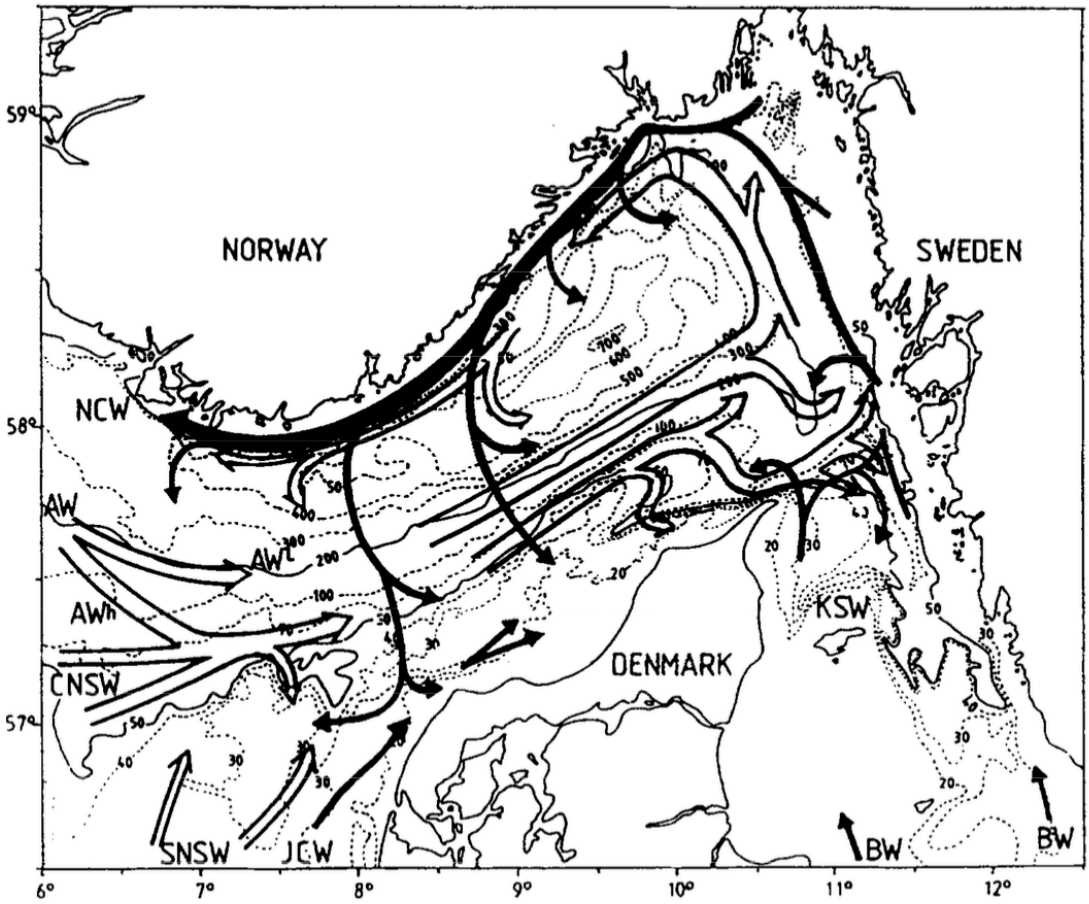

Figure 3. 18: The circulation in the Skagerrak region, with the six interacting water masses: BW= Baltic water, SNSW= South North Sea water, CNSW= Central North Sea water, KSW=Kattegat Water, JCW= Jutland Current Water, AW= Atlantic Water. From Svendsen et al., (1996).

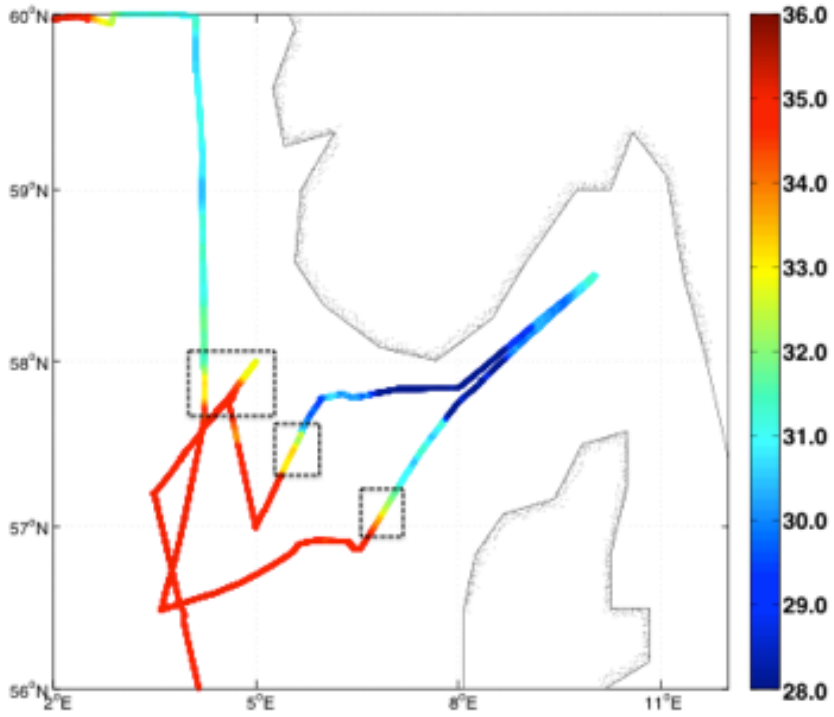

Figure 3. 19: The SSS distribution in the Skagerrak region on the D366 cruise. The dashed boxes indicate transitional regions where vertical mixing occurs between more and less saline waters.

The main inflow into the Skagerrak is from the west, along the Danish Coast, via the Jutland Current (Figure 3. 18), which originates from the southern and central North Sea. This inflow is of a higher salinity, at ~35, than that found in the Skagerrak (Figure 3. 19) due to high North Sea influence. However, as a consequence of its origin, this water also has a high nitrate concentration believed to be due to large rivers spilling into the German Bight (Lee, 1980). The main outflow from the Skagerrak is from the Norwegian Coastal Current (NCC), which flows from Baltic waters and moves along the Norwegian coast in a westerly direction (Figure 3. 18). The NCC is a density driven current primarily fed by vast quantities of brackish water from the Baltic, but also from fresher waters from the coast. The NCC flows over deep and dense water within the Norwegian Trench, which lies adjacent to the coast. These conditions result in low frictional stress from the seabed and therefore minimal vertical mixing when winds are low. The water column therefore remains stratified, containing the low salinity NCC waters, along the Norwegian Coast (Simpson and Sharples, 2012). The stratified NCC surface waters are 2 to 3 °C warmer than waters

located around the mouth of the Skagerrak (Figure 3. 20). Freshwater that accumulates along the Norwegian Coast recirculates in the Skagerrak (Gustafsson and Stigebrandt, 1996). A strong surface front is located at the boundary between the Baltic outflow and the North Sea water. High density seawater, from the NE Atlantic and the northern North Sea, enters the Skagerrak northwest of Jutland. A cyclonic circulation is created from this inflow, entering along the Danish coast, and the outflow, leaving along the Norwegian coast (Rodhe, 1996). Large gyres are usually found in the Skagerrak (Eisma and Kalf, 1987). During the cruise, the chl-a concentration measured in surface waters was found to be the greatest in areas adjacent to the coast, moving towards the mouth of the Skagerrak (5 to 7 µg/L^{-1}) (Figure 3. 21). This could be due to riverine inputs of nutrients stimulating production. The Norwegian Trench has a depth exceeding 700m and connects the Skagerrak to the Northern North Sea and North Atlantic Ocean (Lee, 1980).

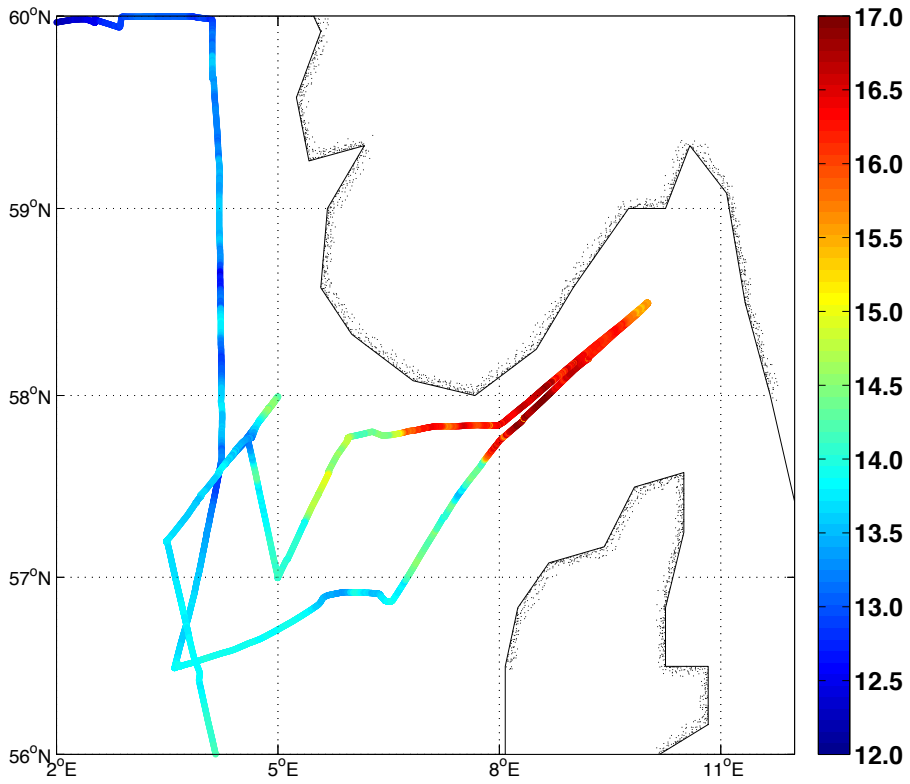

Figure 3. 20: The SST distribution (°C) in the Skagerrak region on D366.

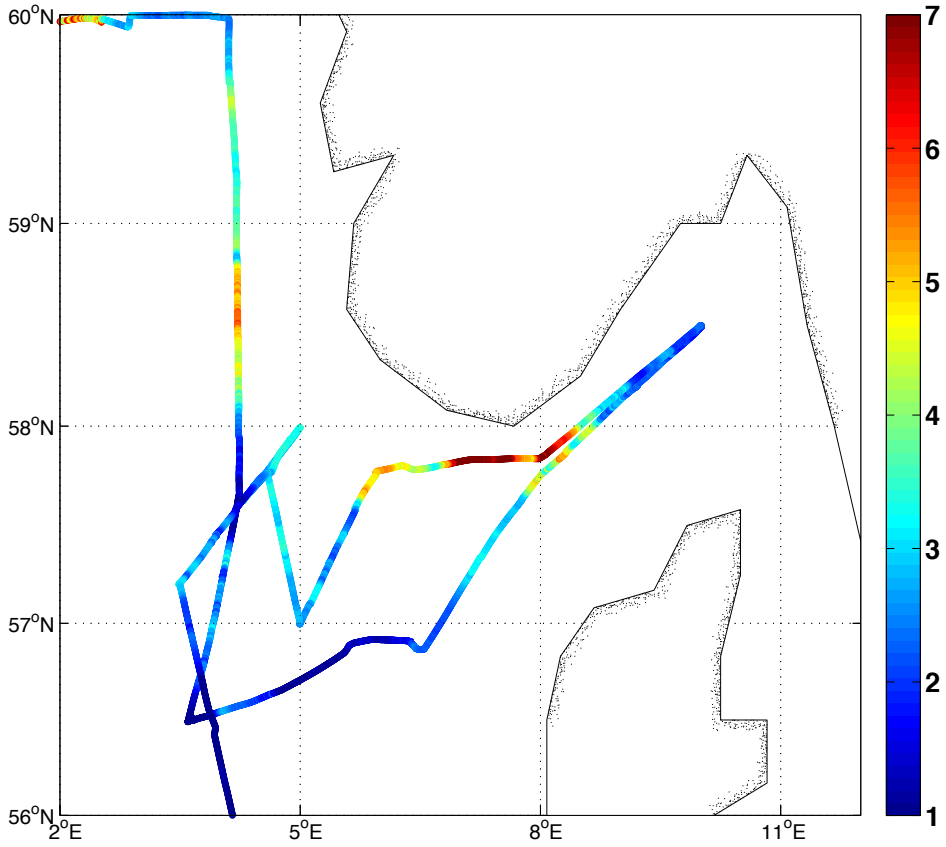

Figure 3. 21: The distribution of surface chl-a concentration (µg l^{-1}) in the Skagerrak region on D366.

3.4.1 2: Results: The Skagerrak, Norwegian Trench and NE North Sea.

Surface waters throughout this region were supersaturated in N_2O with respect to the atmospheric value (101 to 107 %) (Figure 3. 22). The regions with the greatest surface supersaturations (>106 %), were located between 57 to 58 °N, 4 to 6 °E and 58.5 °N, 9.5 °E. The lowest surface supersaturations (<103 %) were located to the furthest south and west of the region (Figure 3. 22). Positive correlations were found between surface N_2O saturation and surface chl-a in the Norwegian Trench (red region in Figure 3. 23) and cyan region (Figure 3. 23) in the Skagerrak ($r=0.75$ $p\leq0.05$ $n=793$; $r=0.57$ $p\leq0.05$ $n=116$) (Table 2. 3; Figures 3.A 2 and 3.A 3). A negative correlation was identified in the yellow region (Figure 3. 23) between surface saturation for N_2O and surface salinity ($r=-0.95$ $p\leq0.05$ $n=260$) (Table 3. 2; Figure 3.A 1).

In the green region of the NCC (Figure 3. 23), the surface saturation for N_2O increased in an easterly direction into the Skagerrak (Figure 3. 22). Two different water types were identified. The first water type, located to the more western and central parts of the region, had lower surface saturation for N_2O (102.5 to 104.8 %), lower salinity (24.5 to 28), higher SST (16.0 to 16.6 °C) (Figure 3. 24), higher supersaturation for CH_4 (165 to 215 %), lower partial pressure of CO_2 (77 to 88 %) (Figure 3. 25) and higher surface chl-a concentration (5 to 9 µg l^{-1}) (Figure 3. 26). The second water type was located further east. This region displayed surface waters with higher supersaturation for N_2O (103 to 107.5 %), higher salinity (29.5 to 31.5), lower SST (15.3 to 15.6 °C) (Figure 3. 24), higher partial pressure of CO_2 (94 to 98 %), lower supersaturation for CH_4 (120 to 135 %) (Figure 3. 25) and lower chl-a concentration (1 to 2.5 µg l^{-1}) (Figure 3. 26).

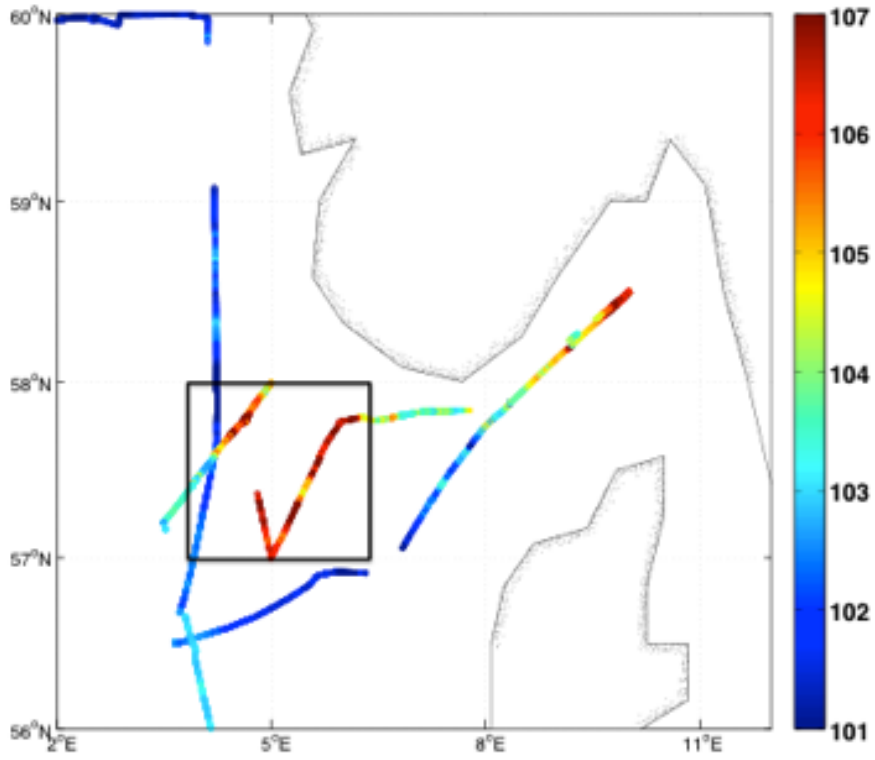

Figure 3. 22: The surface water distribution of saturation for N_2O (%) in the Skagerrak region. The black box indicates the location of a dying coccolithophorid bloom.

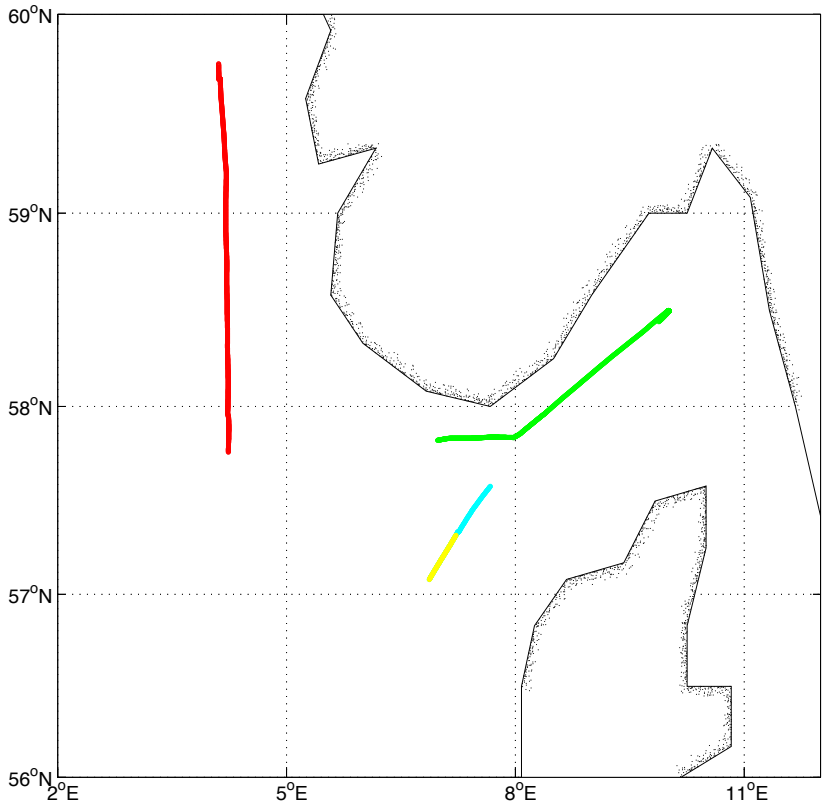

Figure 3. 23: The locations in which strong correlations, or rapid shifts, were found between sea surface saturation of N_2O and SST, SSS, surface chl-a concentration, saturation for CH_4 and the surface partial pressure of CO_2 (µatm) in the Skagerrak region (refer to Table 3. 2 for more details).

Table 3. 2: The coloured regions, located in Figure 3. 23, where strong correlations, or rapid transitional zones, were found between sea surface N_2O saturation and SST, SSS, chl-a concentration, saturation for CH_4 and the surface partial pressure of CO_2 during D366. The correlation coefficient (r) and the p values for the correlations are shown below. N/A: a correlation coefficient only occurs with correlations not where there is a transitional zone. The parameters tested had a non-normal distribution and therefore Spearman's correlations were used.

Surface N_2O saturation and surface parameter	Location on map	Correlation or rapid transitional zone	Correlation coefficient (r)	p value	n=	Figure (including Appendix figures)
SSS	Green	Transitional zone	N/A	N/A	N/A	Figure 3. 24
SSS	Yellow	Correlation	-0.95	≤0.05	260	Figure 3.A 1
SST	Green	Transitional zone	N/A	N/A	N/A	Figure 3. 24
Chl-a	Green	Transitional zone	N/A	N/A	N/A	Figure 3. 26
Chl-a	Red	Correlation	0.75	≤0.05	793	Figure 3.A 2
Chl-a	Cyan	Correlation	0.57	≤0.05	116	Figure 3.A 3
Partial pressure of CO_2	Green	Transitional zone	N/A	N/A	N/A	Figure 3. 25
CH_4 saturation	Green	Transitional zone	N/A	N/A	N/A	Figure 3. 25

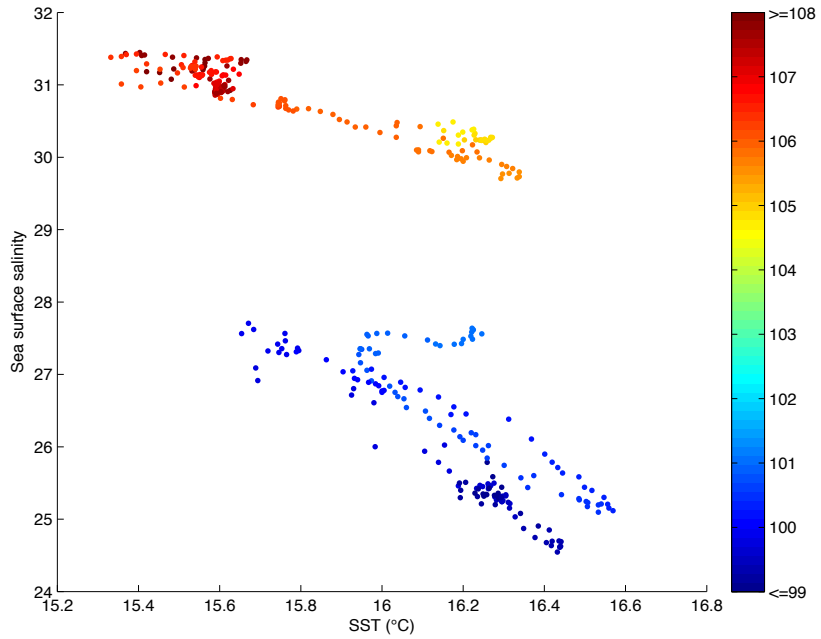

Figure 3. 24: Scatterplot showing the relationship between SST (°C), SSS and surface saturation for N_2O in the green region in Figure 3. 19. The colour bar displays the surface saturation of N_2O in respect to the atmospheric value (%).

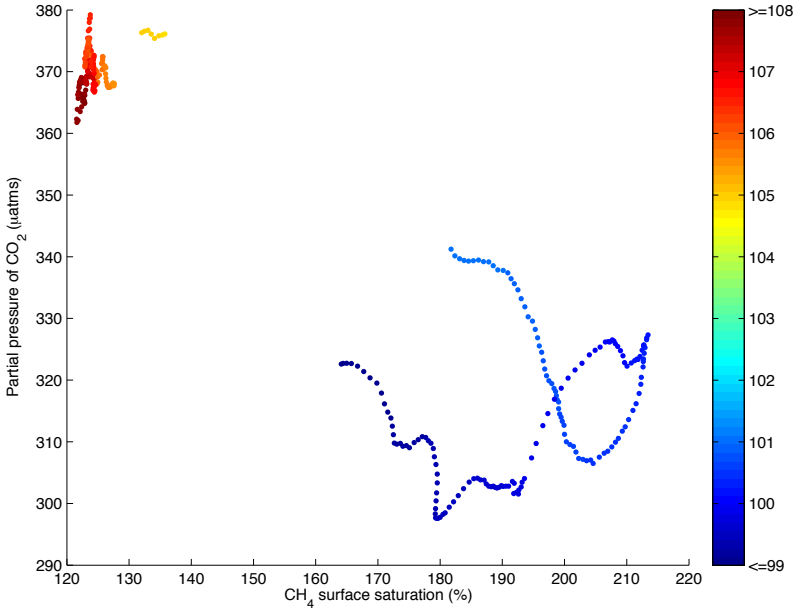

Figure 3. 25: Scatterplot showing the relationship between the surface saturation of CH_4 (%), the surface partial pressure of CO_2 (µatm) and surface saturation of N_2O in the green region shown in Figure 3. 19. The colour bar displays the surface saturation of N_2O in respect to the atmospheric value (%).

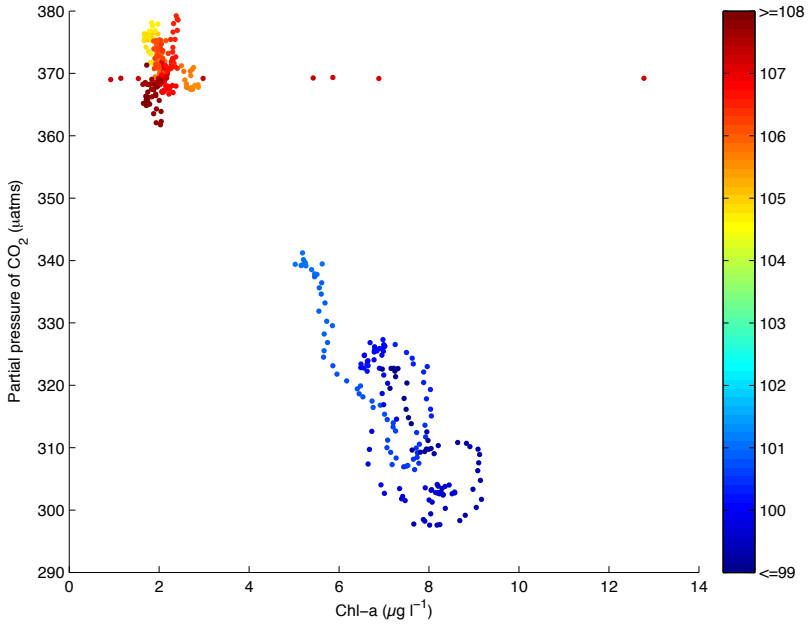

Figure 3. 26: Scatterplot showing the relationship between surface chl-a concentration (µg l^{-1}), the surface partial pressure of CO_2 (µatm) and the surface saturation of N_2O (%) in the green region shown in Figure 3. 19.

3.4.1 3: Discussion: The Skagerrak, Norwegian Trench and NE North Sea.

Along the Norwegian Trench (Figure 3. 23, red line) there was a positive correlation between surface N_2O supersaturation and chl-a ($r=0.75$ $p\leq0.05$) (Table 3. 2). It is postulated that an increase in surface chl-a leads to more organic matter reaching deeper waters where high yields of N_2O will result from the nitrification and denitrification pathways. As the organic matter sinks it is remineralised, releasing nitrogen in the form of NH_4^+. This is then oxidised to NO_2^- by Ammonia Oxidising Bacteria (AOB) and Ammonia Oxidising Archea (AOA). During this initial oxidation reaction, N_2O is released as a by-product. Nitrate produced during the nitrification pathway, is reduced within the anoxic marine sediments by denitrifying microorganisms to NO_2^- and N_2O, before being further reduced to N_2. N_2O produced at depth reaches the surface waters by entrainment. Chemical oxidants in seawater, including iron, manganese and organic compounds undergo redox reactions with NO_2^-, hydroxylamine and nitric oxide in the production of N_2O. It is currently uncertain whether the production of N_2O occurs solely by biotic enzymatic reactions or whether abiotic

N_2O production also acts as a significant pathway in aquatic environments (Zhu-Barker et al., 2015).

In the region located 57 to 58 °N, 4 to 6 °E (see black square on Figure 3. 22), surface waters were supersaturated in N_2O with respect to the atmospheric value at >106 %. The area was subject to a dying coccolithophorid bloom, with satellite images showing that this bloom was at its most intense two to three weeks before sampling (Krueger-Hadfield et al., 2014, Poulton et al., 2014). As a result, high quantities of organic material would have sunk to the deeper waters and sediments, producing N_2O through both the nitrification and denitrification pathways. The water column in this area was generally stratified, however, the convergence of the saline northern North Sea waters (salinity of ~35) and the fresher NCC (salinity of 28 to 31) created transitional zones (fronts), which can be observed in three locations in Figure 3. 19, indicated by the dashed boxes, where the salinity was around 33. In these transitional areas, vertical mixing reduces the horizontal transport of buoyancy, producing localised mixing of the water column (Linden and Simpson, 1988). It is postulated therefore that within these localised regions N_2O is mixed to the surface, enhancing the surface saturation in the surrounding regions.

In the green region in Figure 3. 23 of the NCC, two different water types were identified in the surface waters. The more westerly water type had low surface N_2O saturation, as well as low SSS (salinity of 24.5 to 28), high supersaturation for CH_4 (160 to 215 %) and elevated surface chl-a concentrations (Figures 3. 25 to 3. 26). This water type was most likely influenced by brackish and freshwater influxes from the Baltic Sea and rivers. Estuaries are usually supersaturated in CH_4 due to methanogenesis in the anoxic sediments and CH_4 seepage into the water column (Abril and Borges, 2005), as well as being nutrient rich due to run off of organic material from land, stimulating primary productivity. The SST in the surface waters was also higher than found outside this water mass (> 15.6 °C) (Figure 3. 20), which can occur as a consequence of stratification due to the freshened surface layer. In comparison, the surface waters found to the east had higher saturation for N_2O and the surface partial pressure for CO_2, higher SSS

and lower SST, chl-a concentration and saturation for CH_4 than the water located more westward (Figures 3. 24 to 3. 26). It is proposed that this is caused by mixing of deeper cold, saline water, rich in both N_2O and CO_2, and less supersaturated in CH_4 (due to microbial oxidation), from under the thermocline to the surface in this region. Higher CO_2 may also have resulted from the decrease in primary productivity, where less CO_2 would be taken up for photosynthesis.

3.4 2: Fully mixed water column: The southern North Sea

3.4.2 1: Hydrography: The southern North Sea

The southern North Sea, south of the Flamborough-Helgoland front (see shaded region Figure 3. 27) is predominantly shallow (10 - 30 m), with strong tidal mixing. As a result, the water column in this region is fully mixed (Figure 3. 27), except in regions of freshwater inputs. Primary production in the southern North Sea is influenced by wind, wave and tidal mixing processes, which affect nutrient and light availability through the re-suspension of sediments (Tett et al., 1993, McCandliss et al., 2002). Along with this, freshwater inputs from large rivers and estuaries influence the circulation (Tett et al., 1993). Further north (north of the shaded region, Figure 3. 27) the waters are deeper and seasonal stratification occurs, with spring and autumn blooms.

Saline Atlantic water, from the English Channel, passes through the Dover Strait in a northeast direction along the continental coast towards the German Bight and northwards towards the Skagerrak (Figure 3. 28). The flow is assisted by westerly winds (Lee, 1980) creating a gradient in salinity, from saline (SSS greater than 35) to fresher water (SSS around 33), from the English Channel outflow to the German Bight (Figure 3. 28). Currents within the southern North Sea are strong and produce re-suspension of sediments into the water column (Eisma and Kalf, 1987). A large gyre can be found in the German Bight (Eisma and Kalf, 1987). Waters adjacent to the continental coast are subject to large river water inputs (Artioli et al., 2012) (Figure 3. 29), lowering the salinity, producing SST changes (ranging from 14 to 16 °C during the D366) (Figures 3.

28 and 3. 30) and increasing the nutrient content of the water column. The nutrient enhancement from these inflows of river water stimulates primary production in various locations with suitable light conditions (Figure 3. 31). Stratification occurs within some areas of this region, as a consequence of the freshwater inputs from large rivers and estuaries, creating buoyancy driven flows (Simpson and Sharples, 2012). Waters sampled during the D366 cruise were well mixed, as the cruise track did not sample close enough to the coast where the water column was influenced by freshwater inputs (Figure 3. 28). Because of the location of the cruise track nutrient enhancement from rivers would also not be expected to be a control on primary production in the waters sampled.

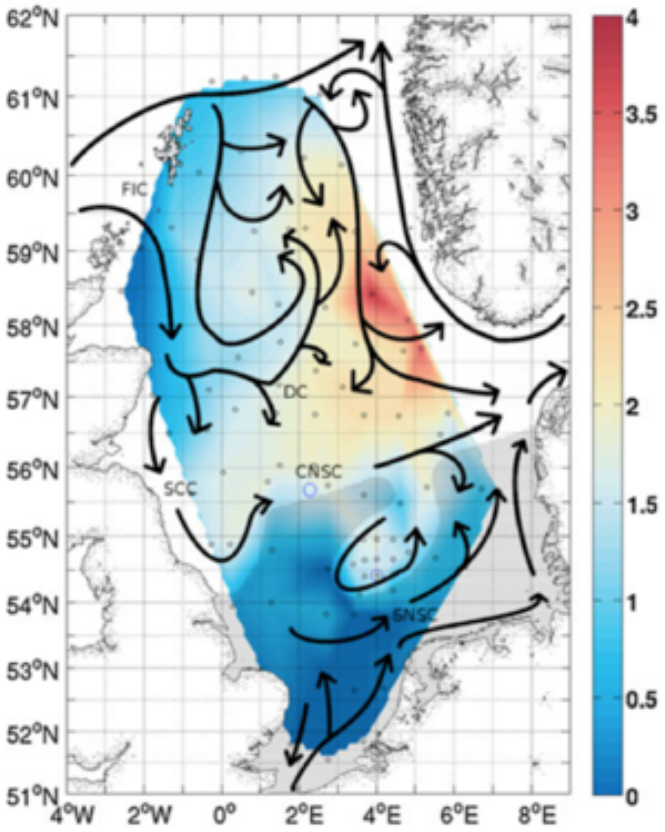

Figure 3. 27: Circulation of the North Sea from Queste et al (2013). The shaded region in the south indicates the region usually well mixed throughout the year. The northern North Sea north of this shaded region displays seasonal stratification in the summer months. The colour bar shows the density difference (kg m^{-3}) between the surface and bottom mixed layers. DC: Dooley Current, SCC: Scottish Coastal Current, CNSC: Central North Sea Current, SNSC: Southern North Sea Current.

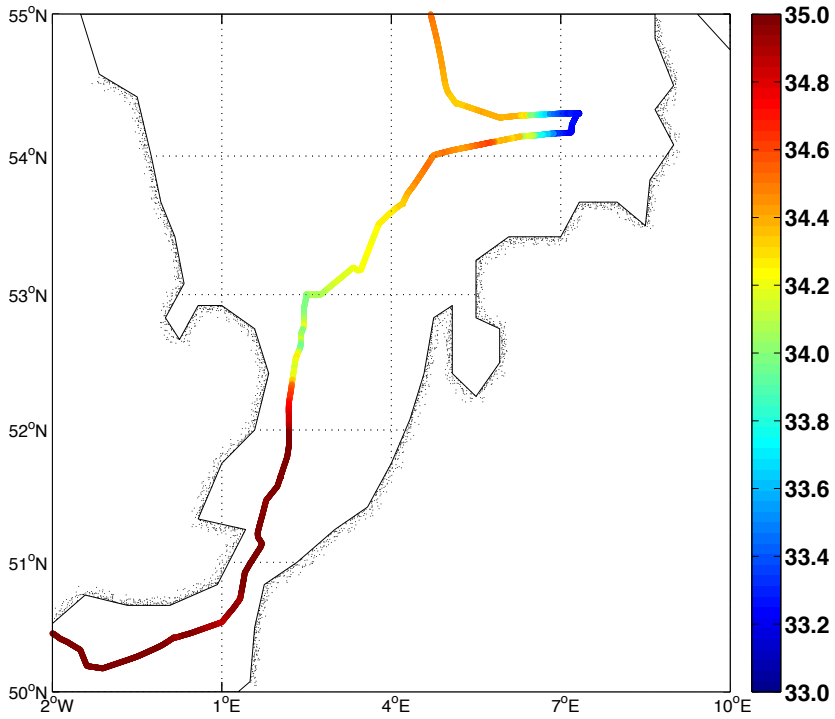

Figure 3. 28: The SSS distribution in the southern North Sea during the OA D366 cruise.

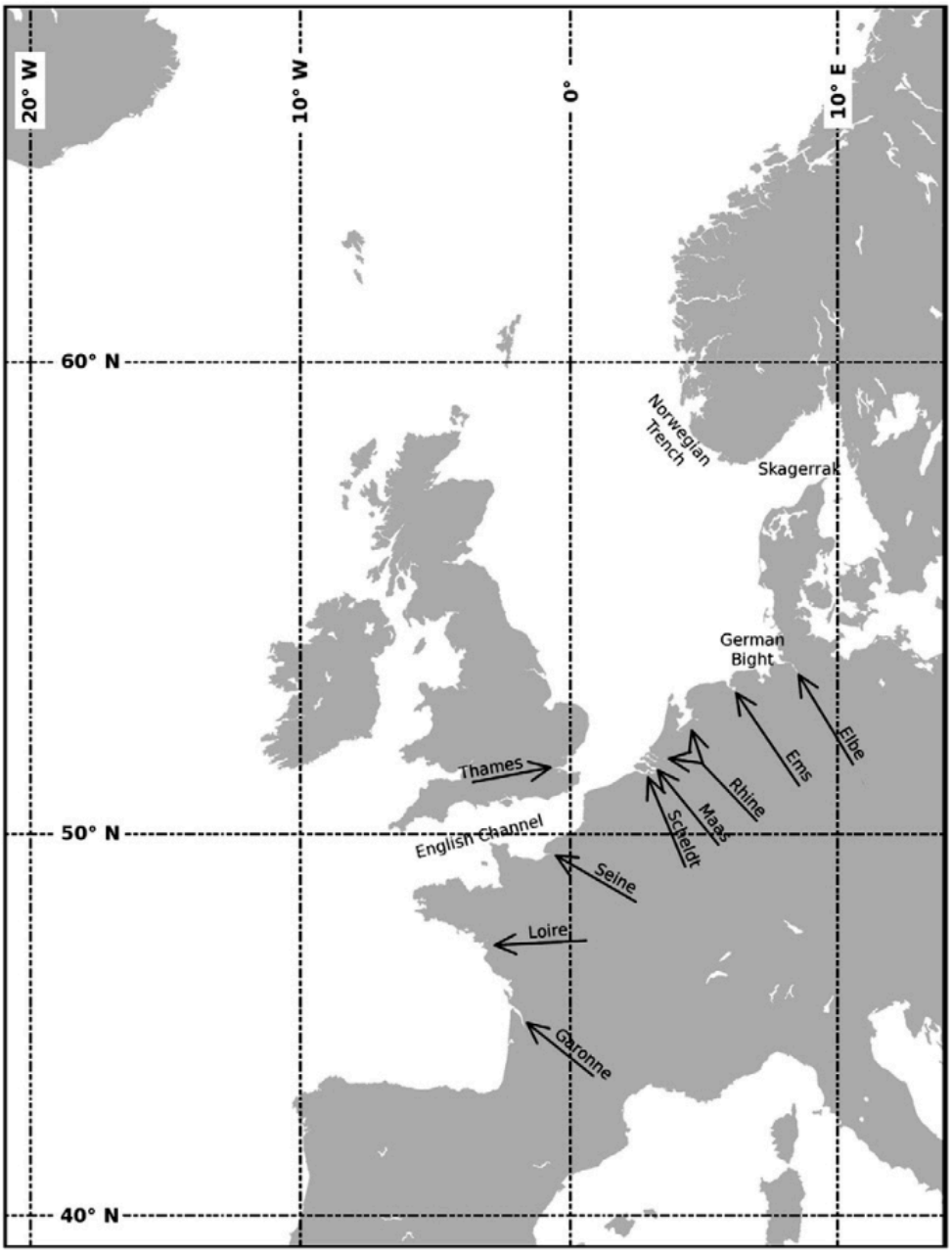

Figure 3. 29: The large river inputs into the southern North Sea. From Artioli et al., (2012).

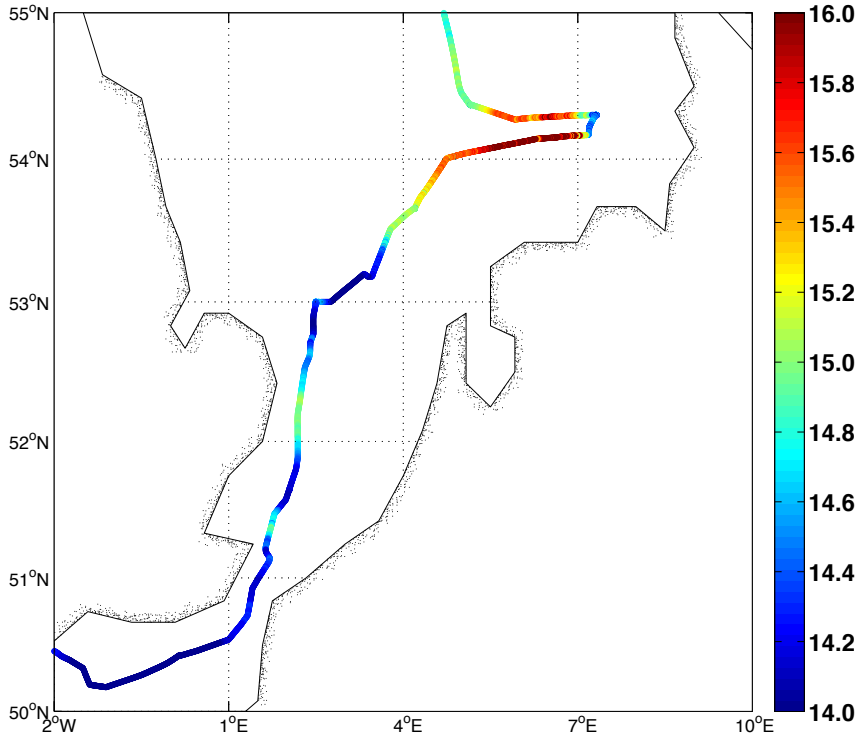

Figure 3. 30: The SST distribution (°C) in the southern North Sea during D366.

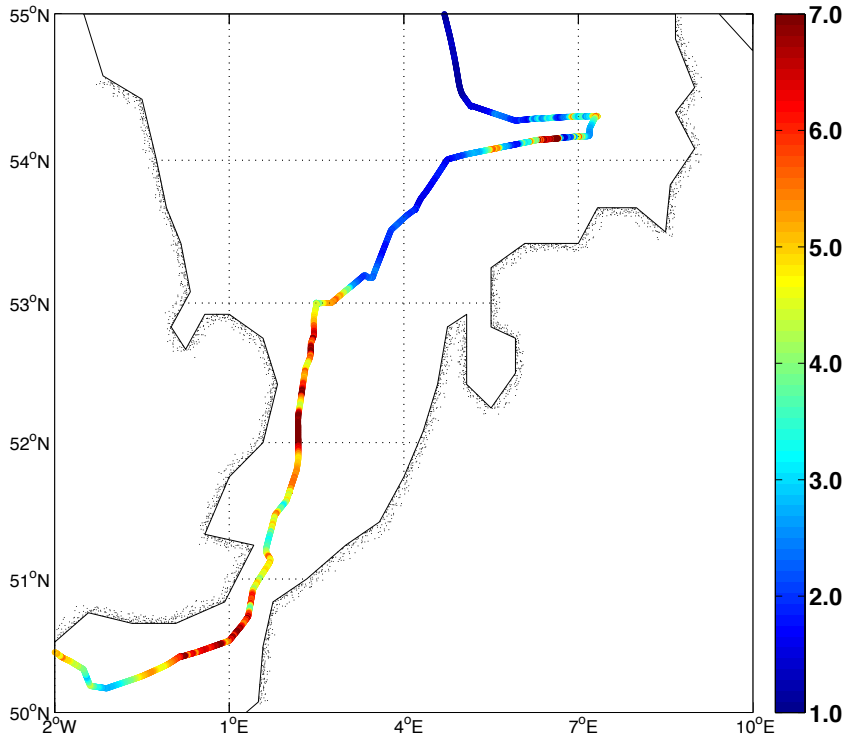

Figure 3. 31: The surface chl-a concentration distribution (µg l^{-1}) in the southern North Sea during D366.

3.4.2 2: Results: The southern North Sea

Between the latitudes of 51 to 52 °N, and along the majority of the cruise track, from 54 to 55 °N, surface waters were supersaturated in N_2O with respect to the atmospheric value (100.1 to 102.0 %), (Figure 3. 32). Surface waters undersaturated in N_2O were measured between the latitudes of 52 to 54 °N of the cruise track, adjacent to the continental coast (99.5 to 100 %), (Figure 3. 32). As the SST decreased in the blue and red regions of the German Bight in Figure 3. 33, the surface N_2O supersaturation was found to increase ($r=-0.71$ $p\leq0.05$ $n=1354$) (Figure 3. 32, Table 3. 3) (Figure 3.A 5). In the black region in Figure 3. 33 of the southern North Sea, the salinity increased simultaneously with the N_2O surface supersaturation ($r=0.84$ $p\leq0.05$ $n=289$) (Table 3. 3) (Figure 3.A 4). A positive correlation was found between surface supersaturation for N_2O and SST in the magenta region ($r=0.90$ $p\leq0.05$ $n=433$) (Figure 3. 33, Table 3. 3) (Figure 3.A 6), along with a negative correlation with surface chl-a concentration in the blue region ($r=-0.73$ $p\leq0.05$ $n=548$) (Figure 3. 33, Table 3. 3) (Figure 3.A 6).

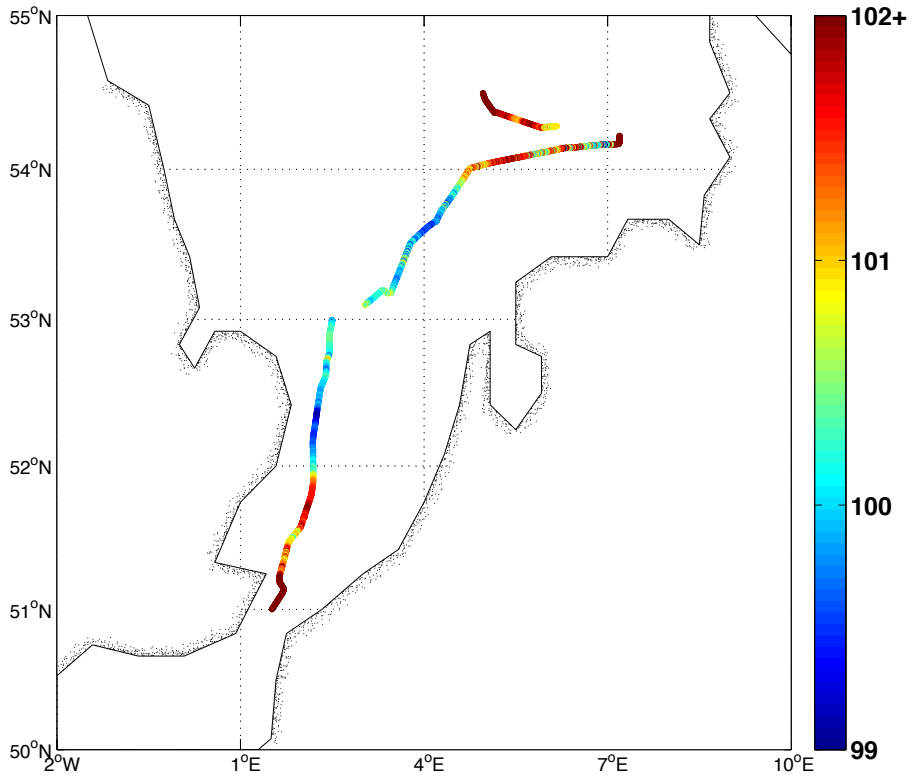

Figure 3. 32: The surface water distribution of N_2O saturation (%) with respect to the atmospheric value in the southern North Sea on D366.

Table 3. 3: The coloured regions (displayed in Figure 3. 33) where strong correlations were found between sea surface water saturation for N_2O and SST, SSS and surface chl-a concentration. The correlation coefficient (r) and the p values for the correlations are shown below. The parameters tested had a non-normal distribution and therefore Spearman's correlations were used.

Surface N_2O saturation and surface parameter	Location on map	Correlation coefficient (r)	p value	n=	Figure (including Appendix figures)
SSS	Black	0.84	≤0.05	289	Figure 3.A 4
SST	Blue and red	-0.71	≤0.05	1354	Figure 3.A 5
SST	Magenta	0.90	≤0.05	433	Figure 3.A 6
Chl-a concentration	Blue	-0.73	≤0.05	548	Figure 3.A 7

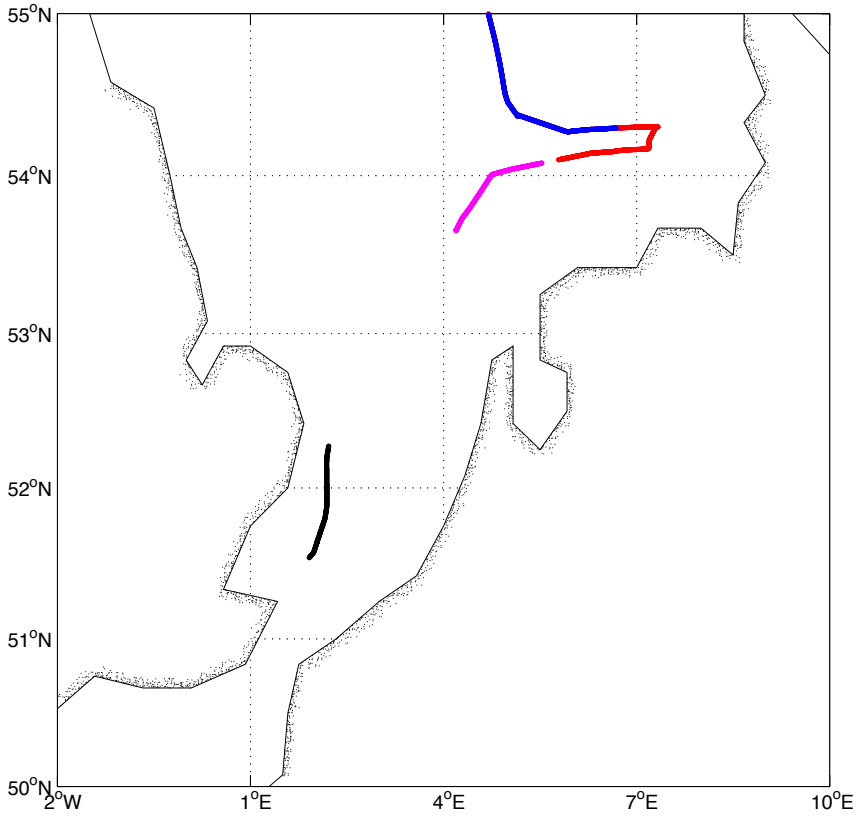

Figure 3. 33: The regions in which positive and negative correlations were found between sea surface saturation of N_2O and SST, SSS, and surface chl-a concentration (refer to Table 3. 3 for more details).

3.4.2 3: Discussion: The southern North Sea

The majority of the southern North Sea was slightly supersaturated at 100.1 - 102.0 %. This is consistent with the surface saturations estimated by Bange (1996b), including: 104 ± 1 % (central North Sea, September 1991), 101 ± 2 % (German Bight, September 1991) and 99 ± 1 % (German Bight, September 1992), but significantly lower than measured in the German Bight by Law and Owens (1990a) at 130 % (German Bight, July 1987). The southern North Sea is shallow and subjected to strong physical influences including high wind/wave activity, tidal currents and freshwater inputs, particularly in the German Bight. In the southern North Sea, high surface N_2O was found in different locations to high surface chl-a concentrations (Figures 3. 31 and 3. 32). This is because primary production is greater in periods of low turbulent energy, for example, when there are weak neap tides and low wind/wave activity but still a fully mixed water column (McCandliss et al., 2002), but not in high turbulent energy, found during spring tides and high wind/wave activity, as it causes the re-suspension of sediments affecting the light quality in surface waters, limiting photosynthesis (McCandliss et al., 2002). Nitrous oxide in contrast, is produced by nitrification in the water column and denitrification in anoxic sediments. High turbulent energy would therefore simultaneously re-suspend N_2O produced during partial denitrification in anoxic sediments and organic material that could then be nitrified in the water column, enhancing the surface water concentrations.

Surface waters slightly supersaturated for N_2O at around 100.1 – 102 % were found between the latitudes of 51 to 52 °N, and 54 to 55 °N (Figure 3. 32). The region located between the latitudes of 51 to 52 °N acts as a transitional pathway for surface N_2O between the higher eastern English Channel waters and the lower southern North Sea waters. Rapid variability was found in both surface N_2O and chl-a concentrations in the German Bight (54 to 55 °N). It is proposed that this is a consequence of the complex hydrography in this region that acts in a similar way to an estuary, with a transition from waters largely influenced by river inflows, such as the Elbe and the Ems, towards the saline North Sea waters (Figure 3. 29). As a consequence of this and strong tidal mixing, gradients in salinity, nutrients, and turbidity are created (Becker et al., 1983), along with

small-scale salinity fronts (Becker and Prahm-Rodewald, 1980, in Becker et al. 1983). The hydrography in this region is therefore suggested to be influencing the quantity of N_2O produced by nitrification, by influencing the re-suspension/distribution of organic material.

Undersaturation at around 99 % was found in the surface waters between the latitudes of 52 to 54 °N (Figure 3. 32) did not appear to be due to limited mixing of deep waters to the surface as proposed by Nevison et al., (1995) as the water column was fully mixed. The cause of this undersaturation is unknown, but could be attributed to a cooling effect, where the surface waters become more soluble as they cooled but have an uptake lag with the atmosphere of approximately two weeks (Figure 3. 17), producing undersaturation. With a fully mixed water column with a depth of ~30 m, the ventilation time for N_2O would be just over two weeks at a SST of 14.2 °C (Figure 3. 27)(assuming the mean windspeed during D366 of 9.19 m s^{-1}). The longest timescale over which any lag effects could be observed is likely to be about a week. If the SST reduced by 0.3 °C in a week, this would produce a reduction in surface N_2O saturation by 0.75 °C, and therefore appears to be a plausible explanation for the surface undersaturation observed.

3.4 3: Fully mixed water column regions: The English Channel

3.4.3 1: Hydrography: The English Channel

Waters in the English Channel flow in an easterly direction, bringing saline and cooler Atlantic waters through to the less saline, and slightly warmer southern North Sea (Lee, 1980) (Figures 3. 34 and 3. 35). The hydrography of the region is defined through depth and tidal mixing, with the eastern English Channel and eastern part of the southern North Sea remaining fully mixed throughout the year and the western English Channel displaying seasonal stratification in the summer (Figure 3. 9) (Lee, 1980). Surface chl-a concentration is enhanced in the eastern section of this region due to mixing of nutrients to the surface, stimulating primary production (Figure 3. 36).

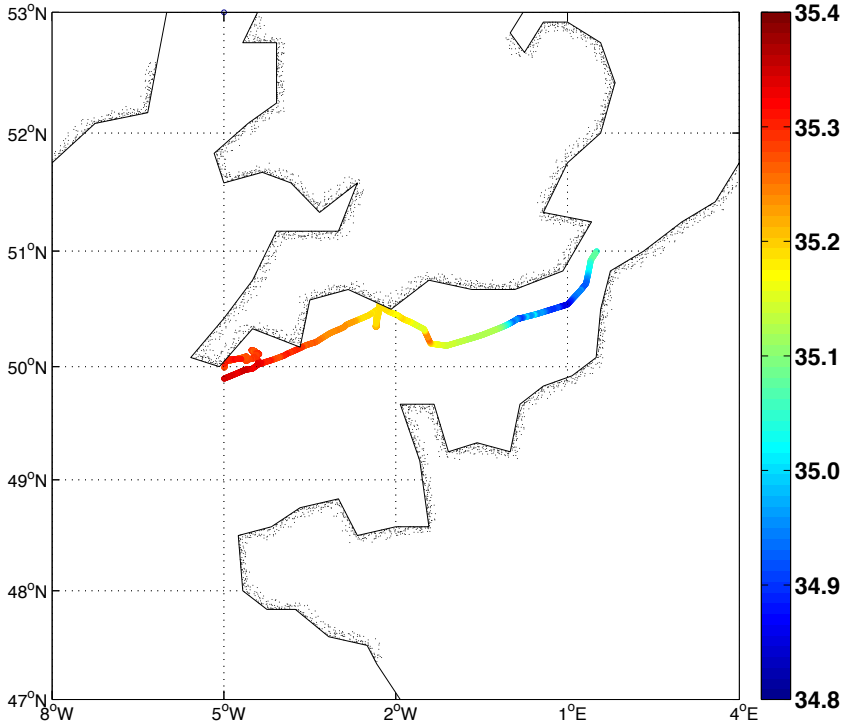

Figure 3. 34: The SSS distribution in the English Channel during D366.

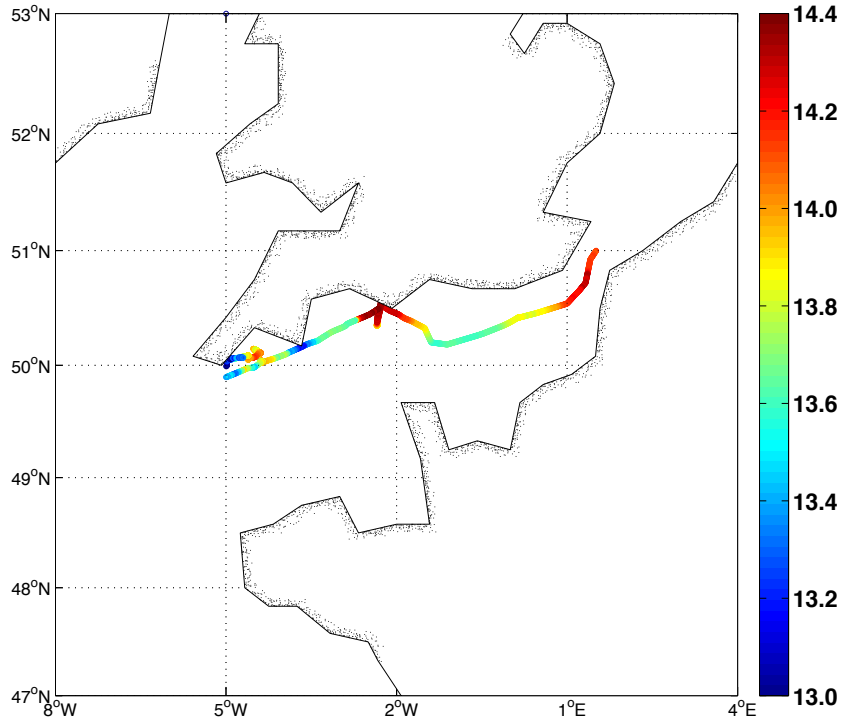

Figure 3. 35: The SST distribution (°C) in the English Channel during D366.

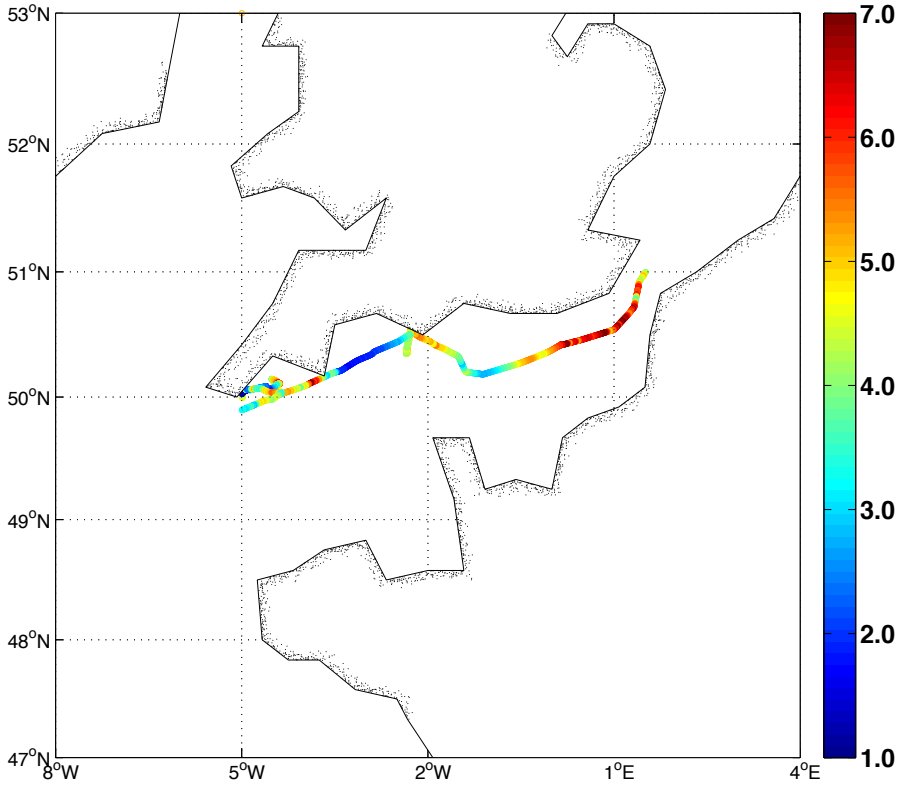

Figure 3. 36: The surface chl-a concentration distribution (µg l^{-1}) in the English Channel during D366.

3.4.3 2: Results: The English Channel

Throughout the English Channel surface waters were supersaturated for N_2O with respect to the atmospheric value (100 to 108 %). Surface N_2O supersaturation was highest along the cruise track between the longitudes of 1 °E – 2 W° (>103 %). The western region of the English Channel had less supersaturation (100 to 102.5 %) than the central and eastern regions (102.5 to 104 %), (Figure 3. 37).

The surface N_2O supersaturation estimated in the green, black and red regions (Figure 3. 37) was found to increase as the SST decreased ($r=-0.60$ $p\leq0.05$ $n=734$) (Table 3. 4). In the green region (Figure 3. 38), where N_2O was supersaturated to >104 %, there was a negative correlation with surface chl-a concentration ($r=-0.79$ $p\leq0.05$ $n=721$), and also with the surface supersaturation

for CO (r=-0.83 p≤0.05 n=721) (Table 3. 4). A negative correlation was also found in the red region (Figure 3. 38) between surface supersaturation for N_2O and SSS (r=-0.92 p≤0.05 n=202) (Table 3. 4).

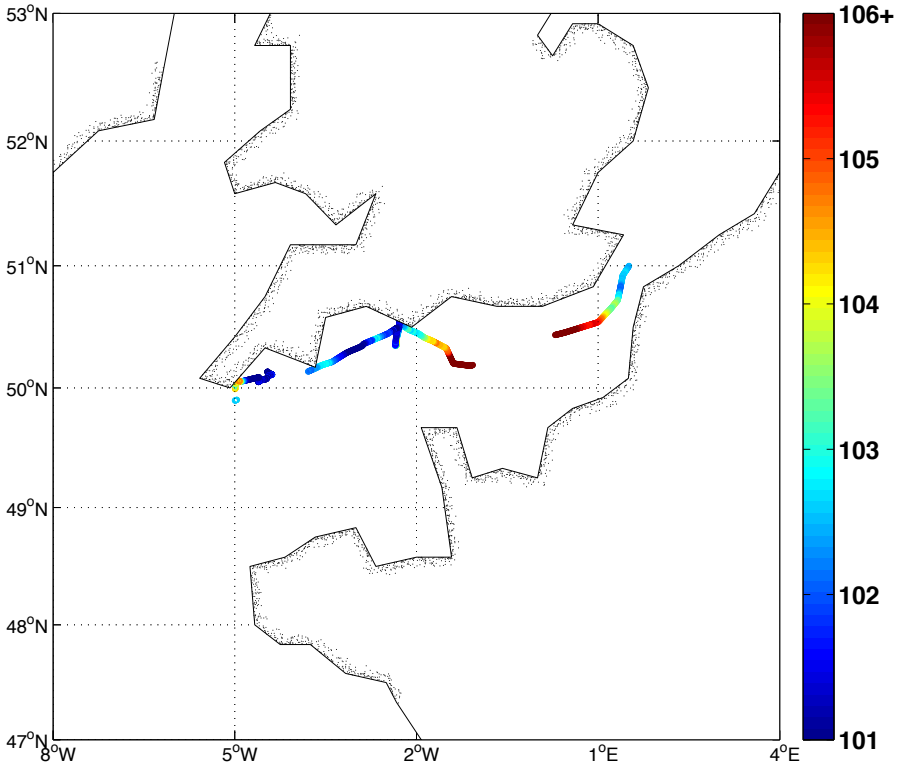

Figure 3. 37: The surface water distribution of saturation for N_2O (%) in the English Channel during the D366.

Table 3. 4: The coloured regions (Figure 3. 38) where strong correlations were found between sea surface saturation for N_2O and SST, SSS, surface chl-a concentration, and saturation for CO during D366. The correlation coefficient (r) and the p values for the correlations are shown below. The parameters tested had a non-normal distribution and therefore Spearman's correlations were used.

Surface N_2O saturation and surface parameter	Location on map	Correlation coefficient (r)	p value	n=	Figure (including Appendix figures)
SSS	Red	-0.92	≤0.05	202	Figure 3.A 8
SST	Green, black and red	-0.60	≤0.05	734	Figure 3.A 9
Chl-a	Green	-0.79	≤0.05	721	Figure 3.A 10
CO saturation	Green	-0.83	≤0.05	721	Figure 3.A 11

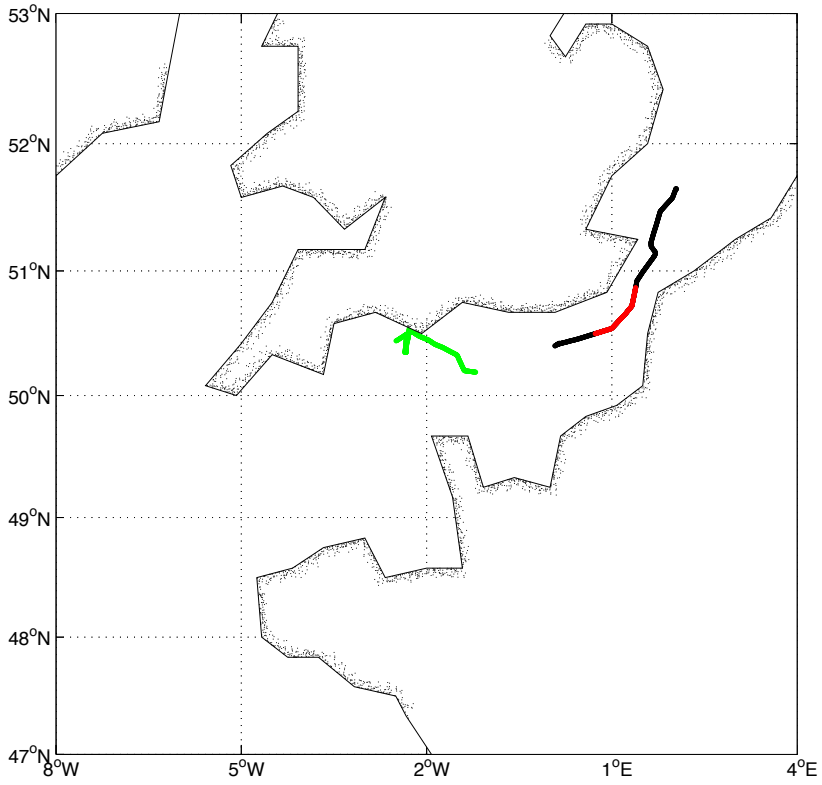

Figure 3. 38: The regions in which strong correlations were found between sea surface N_2O saturation and SST, SSS, chl-a concentration, CH_4 and CO surface saturation, and the partial pressure of CO_2 during the D366 cruise (refer to Table 3. 4 for more details).

3.4.3 3: Discussion: The English Channel

The surface waters of the English Channel were supersaturated for N_2O at 101 – 108 %. The highest sea surface supersaturations for N_2O were located between 2 °W and 1 °E (108 %), (Figure 3. 37). The surface saturation for N_2O was greater in the eastern side of the English Channel, where the water column was fully mixed, then in the west where it was seasonally stratified (Figures 3. 9 and 3. 37). There is a negative correlation between surface saturation for N_2O and SST ($r=-0.60$ $p\leq0.05$ $n=734$) (Figure 3. 38: green, black and red regions, Table 3. 4). This indicates a solubility effect where the cooler waters are influencing the amount of N_2O in the surface waters. The surface waters warm as they move from the central region of the English Channel (influenced by cool Atlantic waters) towards the southern North Sea (Figure 3. 35), and this is accompanied by a decrease in surface saturation for N_2O as the waters warm (Figure 3. 37). This is because the solubility of N_2O increases in cooler waters, therefore concentrations will be higher than in the warmer waters. However, the difference in the surface saturation of N_2O between the west and east side of the English Channel is 5 %, which could not be caused by the temperature difference of 0.6 °C and associated solubility change alone. Therefore the higher surface saturations of N_2O are suggested to be caused by a combination of solubility effects due to the gradient in SST, and also the vertical mixing of N_2O, produced at depth and in the marine sediments during the nitrification and denitrification pathways, to surface waters in the regions where there is a fully mixed water column. The latter appears to be the dominant process.

3.4 4: Tidal front regions

3.4.4 1: Hydrography: Tidal front regions

Tidal fronts are transitional regions between fully mixed and seasonally stratified waters. Tidal fronts have strong temperature and pressure gradients and are sites of enhanced primary productivity due to lifting of nutrients contained below the stratified waters to the surface at the frontal location stimulating plankton growth (Simpson and Sharples, 2012). Figure 3. 39 displays the modelled locations of the tidal fronts in the NW European shelf seas

(Holt and Umlauf, 2008). In addition, Figure 3. 40 displays the Aqua MODIS monthly composite for surface chl-a concentration in June 2011, showing the locations where tidal front mixing stimulated phytoplankton blooms (black circles indicate the location of the fronts).

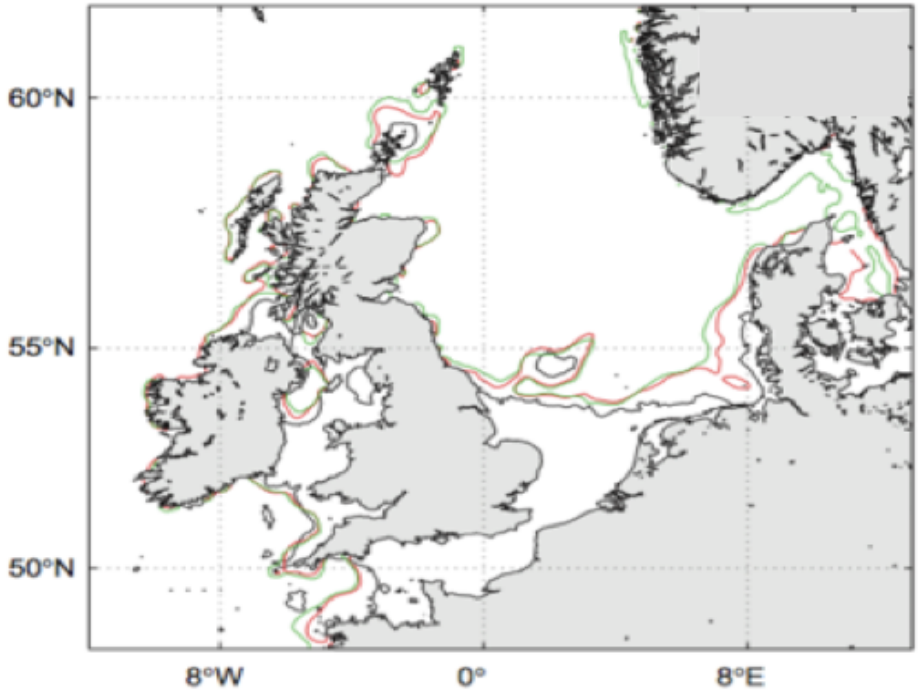

Figure 3. 39: The modelled locations of tidal fronts in the NW European shelf seas. The black line represents the mean frontal positions estimated from ICES data, and the red and green lines are from model outputs Exp 4 and Exp 5. The map is from Holt and Umlauf (2008).

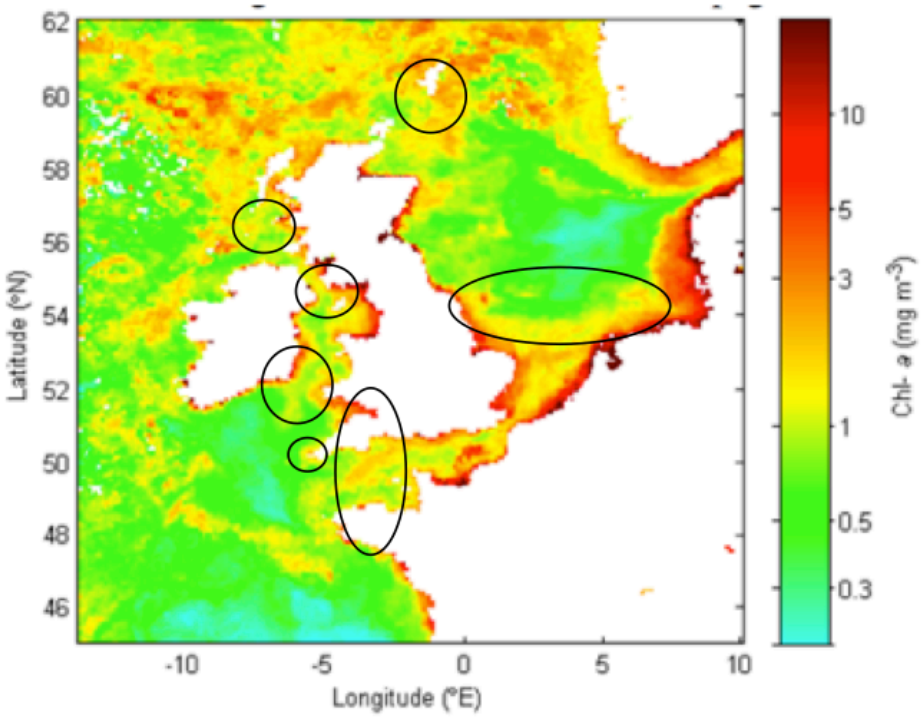

Figure 3. 40: The Aqua MODIS monthly composite satellite image of surface water chl-a concentration across the study area in June 2011. The black circles indicate the location of tidal fronts. From Tyrrell and Achterberg (2014).

The Irish Sea is located 52 to 55 °N and 3 to 6 °W, between Ireland and Great Britain. The Irish Sea forms a long channel system, approximately 300km in length, connected to Atlantic waters at either end. There is a large catchment area (43,000 km^2) in comparison to the area of sea (47,000 km^2), resulting in a large quantity of freshwater runoff. The circulation of this semi-enclosed shelf sea is driven by wind, density and the interaction of two tidal waves (Dabrowski et al., 2012). The depth of the Irish Sea is generally shallow, with the exception of a deeper channel to the north, running west of the Isle of Man into the North Channel; west of Galloway depths reach around 275m. The waters are generally well mixed, except within: 1) deeper waters where tidal streams are weak, for example southwest of the Isle of Man where a localised anti-clockwise circulation occurs, and 2) within shallow coastal areas such as the north-west of England. In these areas a summer thermocline develops (Lee, 1980). Saline Atlantic water flows northwards, through the Irish Sea, reduced in salinity by the coastal freshwater inputs. Salinity gradients occur decreasing both south to

north and centrally towards the sides of the sea. The fast flow rate through the region has been approximated as 0.5 km per day, resulting in complete renewal of seawater within a year (Lee, 1980). Aside from the general northwards flow, there is also a southerly counter-flow close to the Irish coast of the North Channel (Lee, 1980). The water column is mixed in some regions of the Irish Sea and seasonally stratified in others (Figure 3. 9). Frontal transitional zones between the fully mixed and summer stratified regions, manifesting either in the surface waters and/or reaching down to the sea-bed, influence local mixing of the water column and primary productivity. These fronts are located within the Irish Sea, as well as between St. George's Channel and the Celtic Sea (Loder and Wright, 1985; Howarth, 2005) and in the Malin Sea (Malin Head front) (Simpson et al., 1979) (Figures 3. 39 and 3. 40).

In the region surrounding the Shetland Islands, a tidal front is located between the Fair Isle and the Southwest of the Shetlands, identified by predictable chl-a fronts (Miller et al., 2014) (Figures 3. 39 and 3. 40). The fronts that occur in this region are created by the strong tidal currents, which act to create the well defined fronts that separate the fully mixed and stratified waters (Inall et al., 2009).

The North Sea can be divided into two separate biogeographical regions, the northern North Sea and the southern North Sea, due to vast differences in their hydrography (Rees et al., 2007). The northern North Sea is between 100-140 m in depth and influenced predominantly by Atlantic water inflow, whereas the southern North Sea is much shallower, at 10 to 30 m depth and is exposed to a weak inflow from the English Channel and freshwater inputs from the continent and UK. In the wintertime the entire North Sea is fully mixed. However in the spring and summer months, seasonal stratification occurs in the northern North Sea, while the southern North Sea remains fully mixed. At the boundary between the fully mixed and stratified water masses frontal zones occur, such as the Flamborough-Helgoland front. The northern North Sea is influenced by the southern North Sea due to the northerly flowing circulation bringing the nutrient rich, fresher water from the south towards the Skagerrak (Figures 3. 27).

3.4.4 2: Results: Tidal front regions

During the D366 OA cruise, all five known tidal frontal regions had surface water supersaturation greater than 103.5 % for N_2O with respect to the atmospheric value. They were located: 1) south of the Shetland Islands (~105 %), 2) Malin Head (~109.5 %), 3) St George's Bank (~106 %), 4) the English Channel/ SW coast of England (106.5 %), and 5) Flamborough-Helgoland frontal zone in the North Sea at approximately 55 °N (103 %), (Figure 3. 41).

Four out of five of these tidal front regions displayed rapid changes in surface water supersaturation for N_2O simultaneously with other parameters. The surface water supersaturation for N_2O increased from a partially mixed water column to a fully mixed water column in the Malin Sea, (Figure 3. 42: black line; Figures 3. 43 and 3. 44), in the Shetlands, (Figure 3. 42: red line) (Figures 3.A 13 and 3.A 15), around St Georges Bank (Irish Sea)(Figure 3. 42: magenta line) (Figure 3.A 16), and off the SW coast of England, (Figure 3. 42: cyan line) (Figure 3.A 19). This transition occurred simultaneously to a rapid drop in SST when moving from the partially mixed to a fully mixed water column in the Malin Sea (Figure 3. 42: black line; Figure 3. 45), and near the Shetlands (Figure 3. 42: red line) (Figure 3.A 13). The change occurred parallel to an increase in surface water chl-a concentration from a partially to fully mixed in the Malin Sea, (Figure 3. 42: black line; Figure 3. 46), the Shetlands (Figure 3. 42: red line) (Figure 3.A 15) and at St George's Bank (Figure 3. 42: magenta line) (Figure 3.A 16). Off the SW coast of England, (Figure 3. 42: cyan line), there was a simultaneous rapid transition of supersaturation for CO in surface waters, from high in a partially mixed water column and low where full mixing occurred (Figure 3.A 19). Surface waters were found to have high CO where N_2O saturation was low.

Correlations were identified between the following parameters: at the Flamborough-Helgoland frontal zone (Figure 3. 42: blue line) the surface supersaturation for N_2O and SSS were found to increase together ($r=0.91$ $p\leq0.05$ $n=216$) (Figure 3.A 12). Off the SW coast of England, (Figure 3. 42: cyan line) a negative correlation was found between surface saturation for N_2O and SST ($r=-0.78$ $p\leq0.05$ $n=1153$) (Figure 3.A 14) and a positive correlation with chl-a

(r=0.71 p≤0.05 n=1153). A negative correlation between surface supersaturation for N_2O and undersaturation for CO was also found off St Georges Bank (Figure 3. 42: green line) (r=-0.68 p≤0.05 n=721) (Figure 3.A 18).

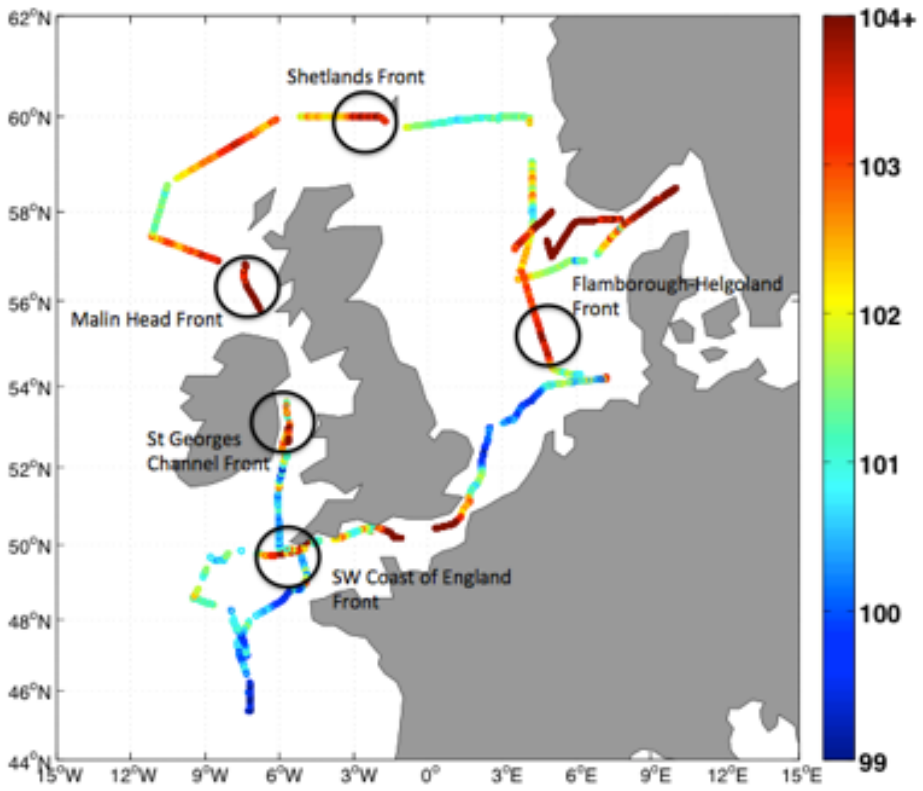

Figure 3. 41: The surface water distribution of saturation for N_2O (%) with respect to the atmospheric value in the NW European shelf seas during D366. The black circles highlight the locations where tidal frontal zones occur and the surface waters were supersaturated for N_2O.

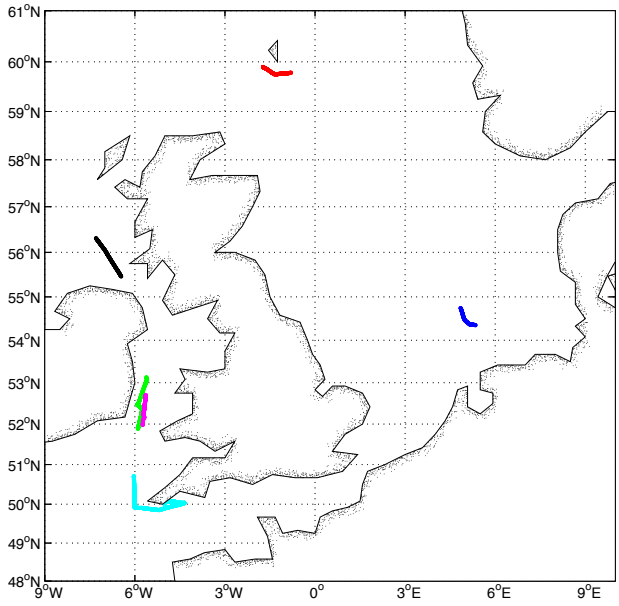

Figure 3. 42: The regions in which either rapid transitions in SST, SSS and surface chl-a concentration occurred simultaneously with changes in surface N_2O saturation, or strong correlations between the sea surface parameters (Table 3. 5).

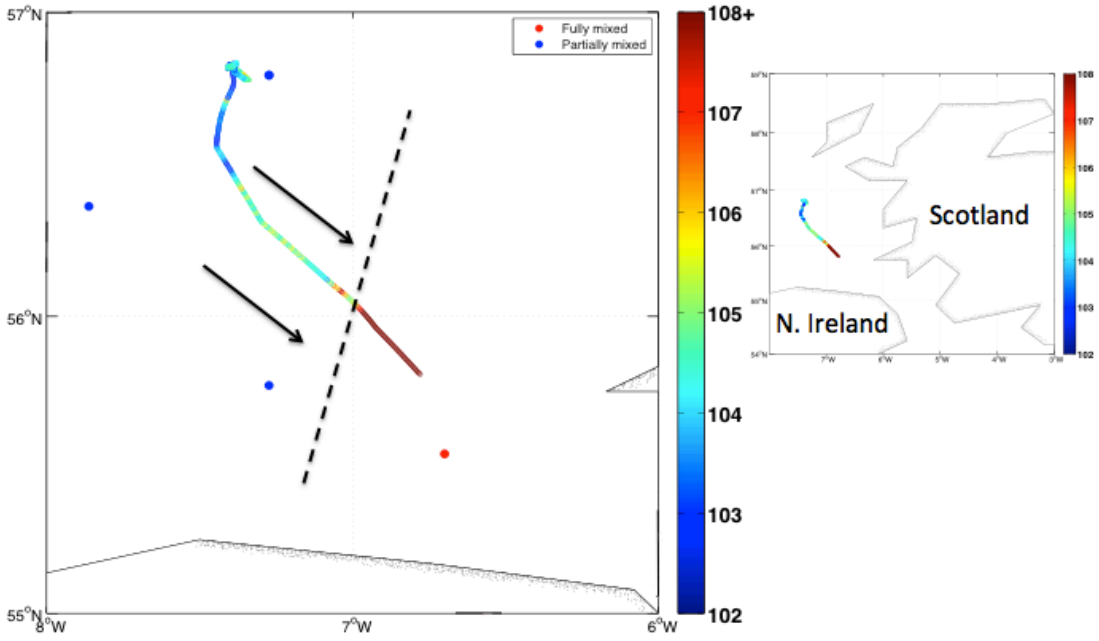

Figure 3. 43: The sea surface supersaturation for N_2O (%) calculated in the Malin Sea. The blue and red dots display CTD stations where the mixed layer depth was calculated. The blue dots indicate locations where the water column is partially mixed and the red dots fully mixed. The dashed line suggests the approximate location where the water column makes a transition from partially to fully mixed conditions, reflected as an increase in surface supersaturation for N_2O. The black arrows indicate the direction the ship was moving in. The CTD stations are not on the cruise track due to the CTD stations being sampled on the outbound journey and the ICOS measurements being made in the returning journey.

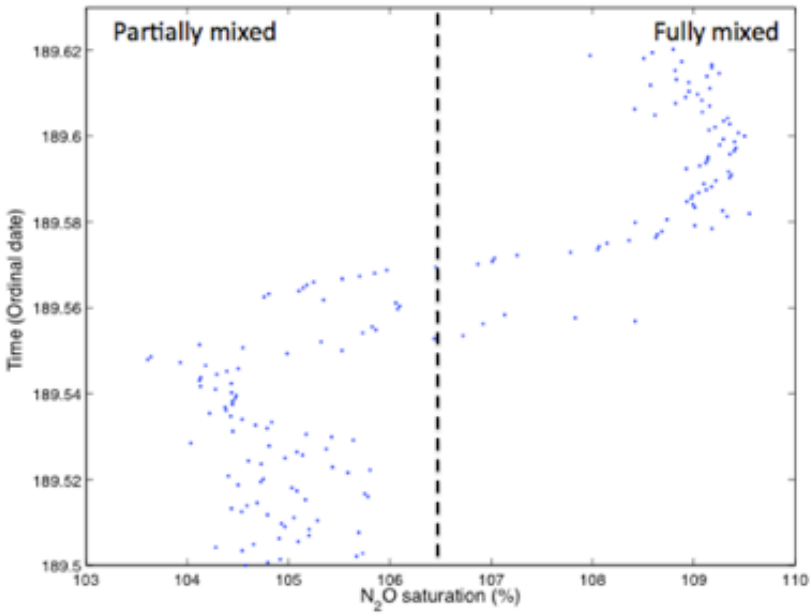

Figure 3. 44: The transition from lower to higher saturation for N_2O in surface waters as the ship crossed from a partially mixed water column to a fully mixed one in the Malin Sea (black region; Table 3. 5).

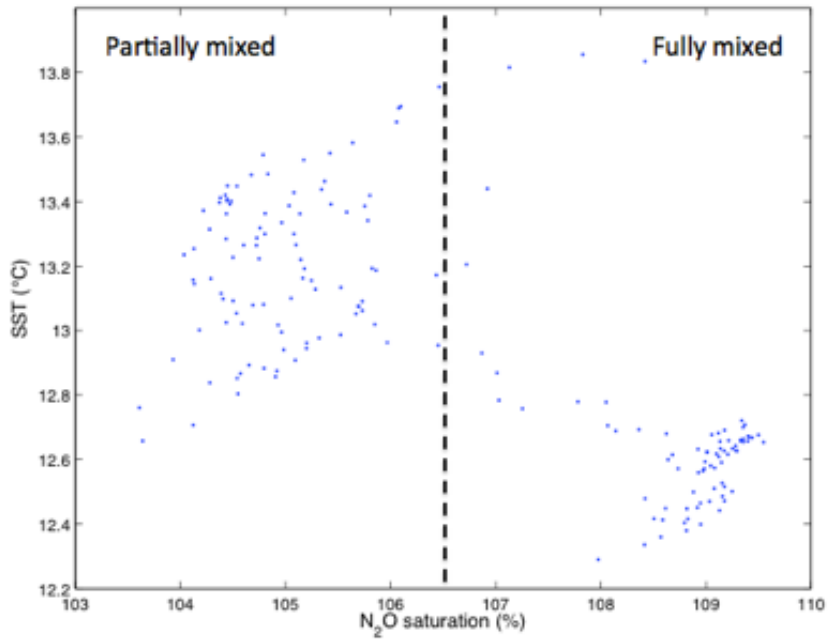

Figure 3. 45: The transition of surface waters from lower to higher saturation for N_2O and higher to lower SST, as the ship crossed from a partially mixed water column to a fully mixed one in the Malin Sea (black region; Table 3. 5).

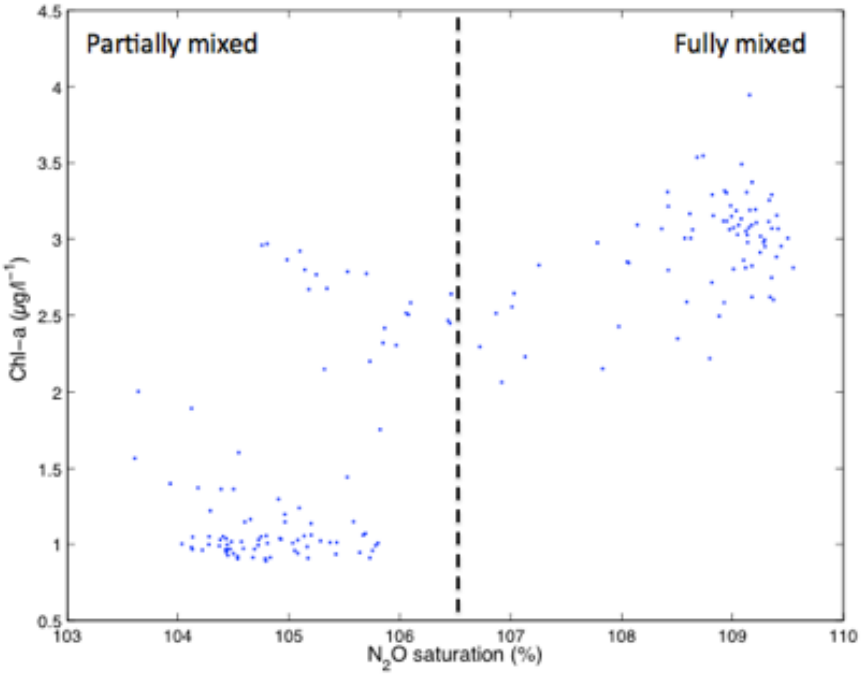

Figure 3. 46: The transition of surface waters from lower to higher saturation for N_2O and concentration of chl-a, as the ship crossed from a partially mixed water column to a fully mixed one in the Malin Sea (black region; Table 3. 5).

Table 3. 5: The coloured regions (Figure 3. 42) where strong correlations/rapid transitional regions were found between sea surface saturation for N_2O and SST, SSS, surface chl-a concentration and CO saturation during D366. The correlation coefficient (r) and the p values for the correlations are shown. The parameters tested had a non-normal distribution and therefore Spearman's correlations were used. N/A: a correlation coefficient only occurs with correlations not where there is a transitional zone.

Surface N_2O saturation and surface parameter	Location on map	Correlation or rapid transitional region	Correlation coefficient (r)	p value	n=	Figure (including Appendix figures)
SSS	Blue	Correlation	0.91	≤0.05	216	Figure 3.A 12
SST	Red	Transitional region	N/A	N/A	N/A	Figure 3.A 13
SST	Black	Transitional region	N/A	N/A	N/A	Figure 3. 45
SST	Cyan	Correlation	-0.78	≤0.05	1153	Figure 3.A 14
Chl-a	Red	Transitional region	N/A	N/A	N/A	Figure 3.A 15
Chl-a	Black	Transitional region	N/A	N/A		Figure 3. 46
Chl-a	Magenta	Transitional region	N/A	N/A	N/A	Figure 3.A 16
Chl-a	Cyan	Correlation	0.71	≤0.05	1153	Figure 3.A 17
CO saturation	Green	Correlation	-0.68	≤0.05	721	Figure 3.A 18
CO saturation	Cyan	Transitional region	N/A	N/A	N/A	Figure 3.A 19

3.4.4 3: Discussion: Tidal front regions

These high-resolution surface measurements provide us with the discrimination to observe the changes in surface N_2O that occur at tidal fronts that lower resolution methods are unable to detect. Surface saturations of N_2O of up to 110 % were observed overlying tidal front regions, increasing from stratified waters to a fully mixed water column. This is believed to be the first time this has been reported and provides evidence of N_2O production on the shelf.

Comparing the high-resolution N_2O measurements with the other high-resolution parameters recorded (e.g. SST, SSS, surface chl-a concentration, surface CH_4 and CO saturation and pCO_2) provided insight into the processes that occurred at tidal front regions that may be important in influencing the high surface N_2O saturations observed. For example, SST was found to decrease as the water column changed from stratified to fully mixed (Figure 3. 45) and surface chl-a concentration increased (Figure 3. 46). Within frontal zones, reduced mixing within the seasonally stratified region will mean the surface waters are both warmer and have lower nutrient concentrations due to limited mixing of cooler, deeper and nutrient rich waters from below the thermocline, as well as being subjected to surface warming from the sun. At the tidal front, the transitional zone between the seasonally stratified and fully mixed water column, cold, deep and nutrient rich waters, saturated for N_2O, are lifted from below the thermocline to the surface. The resulting increase in organic matter in the surface waters, as a consequence of mixing, enhances primary production. An increase in primary production would lead to more organic matter entering the water column, which would undergo ammonification, then nitrification and denitrification in marine sediments, producing N_2O.

In the tidal front region located off the SW coast of England, rapid transitions were observed from high surface saturation of CO in the partially mixed regions to lower saturation of CO in fully mixed zones (Figure 3.A 19). A negative correlation between the surface N_2O and CO saturation at St Georges Bank (Figure 3. 42: green line) ($r=-0.68$ $p\leq0.05$ $n=721$) (Figure 3.A 18) further reinforces this relationship. It is proposed that increased vertical mixing at tidal

fronts that acts to enhance surface N_2O also reduces CO, because it is produced in the surface waters from the photolysis of chromophoric dissolved organic matter (CDOM) and therefore mixing would dilute the surface concentration. The relationships described above did not occur at the Flamborough-Helgoland tidal front zone, perhaps because other processes dominated in this region.

3.4 5: Shelf Break Front Regions

3.4.5 1: Shelf break fronts

Along continental shelves internal waves are generated, creating vertical mixing, as the barotropic tide travels across the steep topography. The internal waves create areas of intense surface and bottom mixing in the shelf break region. Biological consequences of the internal tide include an increase in primary productivity, due to an increased flux of nutrients from below the thermocline (Druon et al., 2001). There are two locations in the study region where the cruise track approached and crossed the shelf edge/break: 1) The NE Atlantic/ NW Scotland, and 2) The Celtic Sea/Bay of Biscay.

3.4.5 2: Hydrography: NE Atlantic/West coast of Scotland

The important features of the circulation off the Scottish shelf consist of the Scottish Coastal Current (SCC), which flows close to the shore in a northerly direction, carrying a mixture of Irish Sea and Clyde waters freshened with outflows from western Scotland (Figures 3. 47 and 3. 48). Moving towards the outer limits of the shelf the seawater is of Atlantic origin with a salinity greater than 35 (Figure 3. 48). Along the continental slope the European Slope Current (ESC) flows in a northerly direction towards the north of the Shetland Islands (Inall et al., 2009) (Figure 3. 47). The bathymetry can be seen in figure 3. 46, showing the shelf sea floor down to approximately 150 – 170 m, the shelf edge and the drop off into the open ocean. The SST in this region ranged from 10-13 °C, with the cooler waters leaving the Irish/Malin Sea and the warmer waters

moving towards the NE Atlantic (Figure 3. 50). Surface water chl-a concentrations ranged from 1 to 4.5 μg l^{-1} throughout this region, with the lowest chl-a concentrations located around the northern Irish Sea and Malin Sea and the highest found north of 58.5 °N, along the shelf edge band (Figure 3. 51).

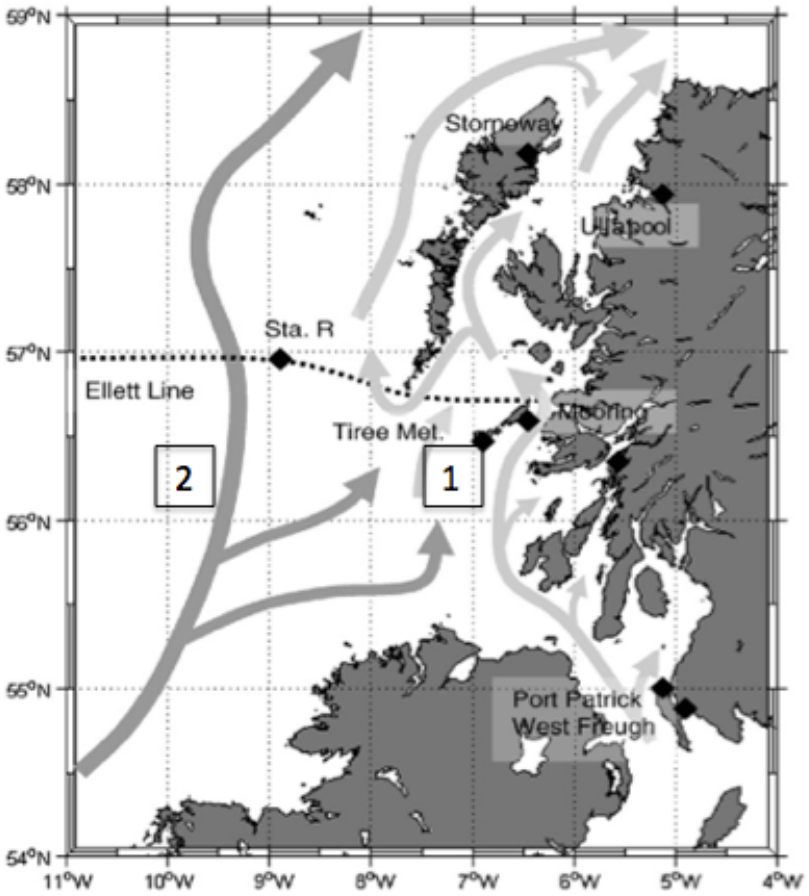

Figure 3. 47: The circulation off the west coast of Scotland. From Inall et al., (2009). 1) The Scottish Coastal Current (SCC), and 2) the European Slope Current (ESC).

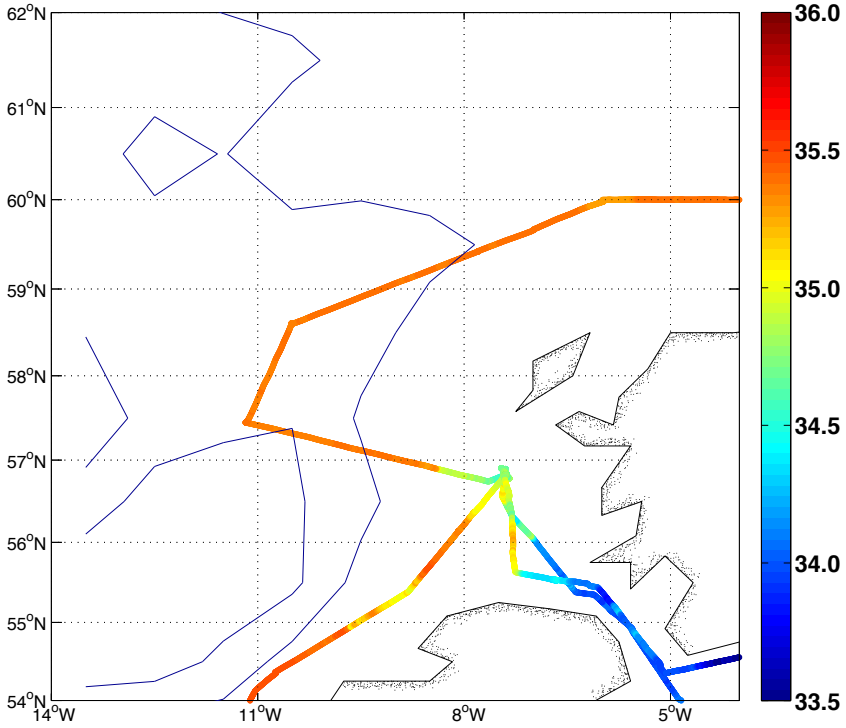

Figure 3. 48: The SSS distribution off the west coast of Scotland during the D366 cruise. The lines indicate the location of the shelf edge. The contour elevations are at 1000 m intervals.

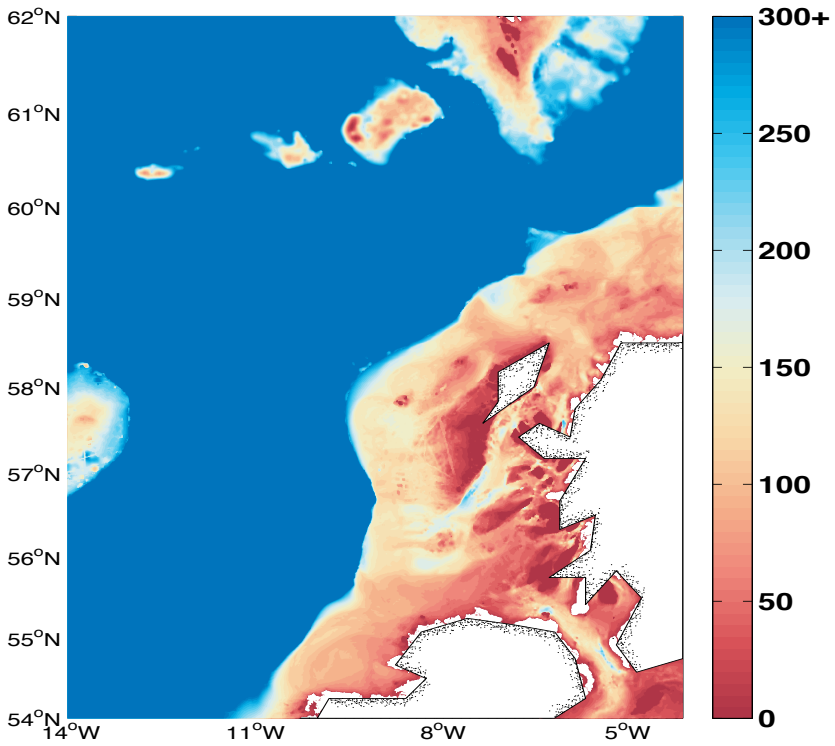

Figure 3. 49: The bathymetry (m) off the west coast of Scotland. Data from General Bathymetric Chart of the Oceans (GEBCO, 2014).

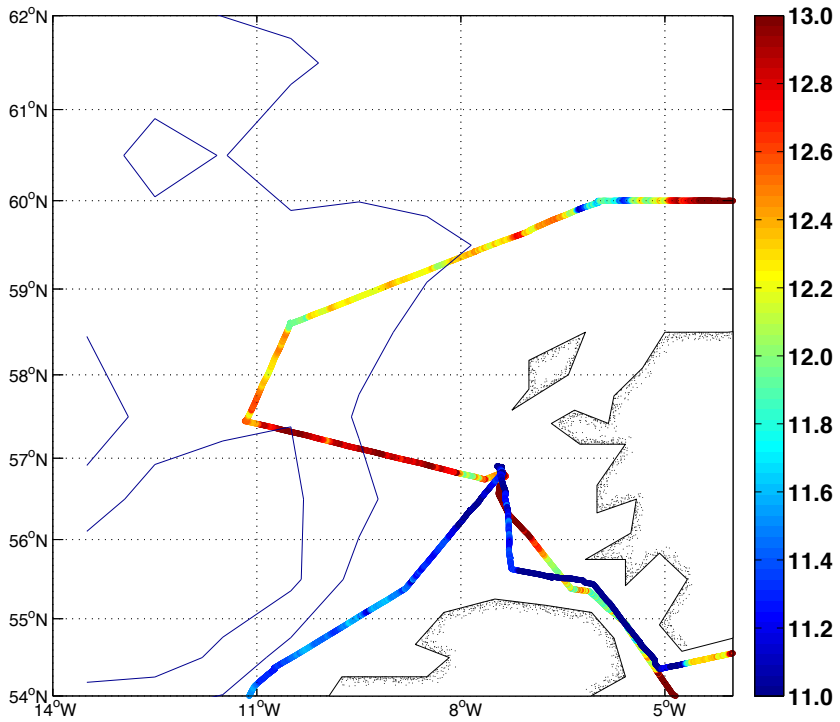

Figure 3. 50: The SST (°C) distribution off the west coast of Scotland during D366. The lines indicate the location of the shelf edge. The contour elevations are at 1000 m intervals.

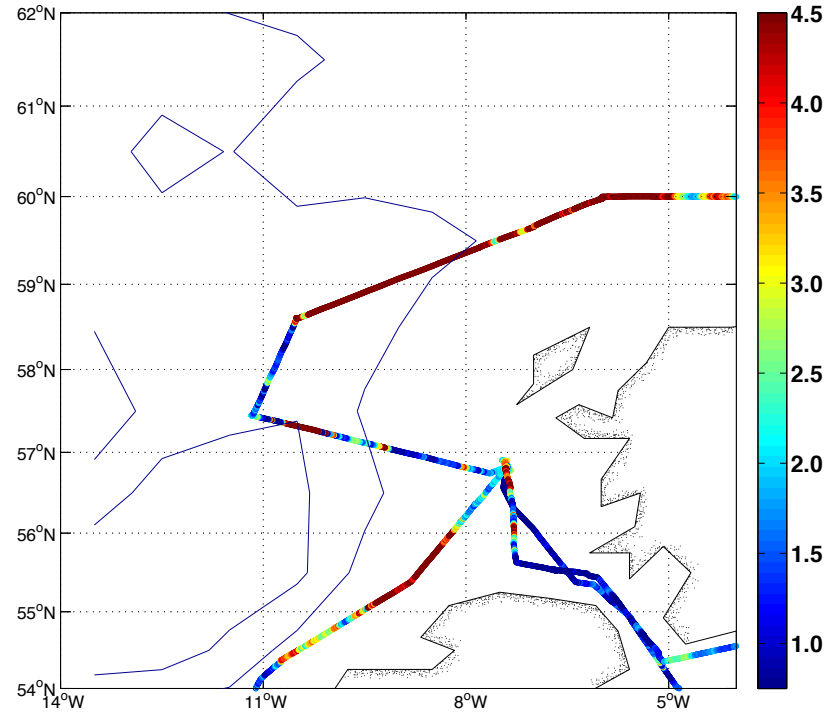

Figure 3. 51: The surface chl-a concentration distribution (µg l^{-1}) off the west coast of Scotland during D366. The lines indicate the location of the shelf edge. The contour elevations are at 1000 m intervals.

3.4.5 3: Results: NE Atlantic/west coast of Scotland

The sea surface waters found off the west coast of Scotland and into the NE Atlantic Ocean were supersaturated for N_2O with respect to the atmospheric value (101 to 104 %), (Figure 3. 52). Excluding the Malin shelf region (discussed earlier section 3.3.4.4), the highest surface supersaturations were located 56 to 56.5 °N, 8.5 to 9 °W and 59.2 to 59.8 °N, 7.5 to 8.5 °W (>103.5 %). The lowest surface supersaturations were found 57.5 to 58.5 °N, 10.5 to 11 °W (101 – 101.5 %)(Figure 3. 52). Strong positive correlations were found between the surface saturation for N_2O and both surface chl-a concentration and saturation for CO (r=0.88 p≤0.05 n=1065; r=0.91 p≤0.05 n=577) (Figure 3. 53: green and black lines, Table 3. 6; Figures 3.A 20 and 3.A 21), and a negative correlation with the partial pressure of CO_2 (r=-0.94 p≤0.05 n=577) (Figure 3. 53: black line, Table 3. 6, Figure 3.A 22).

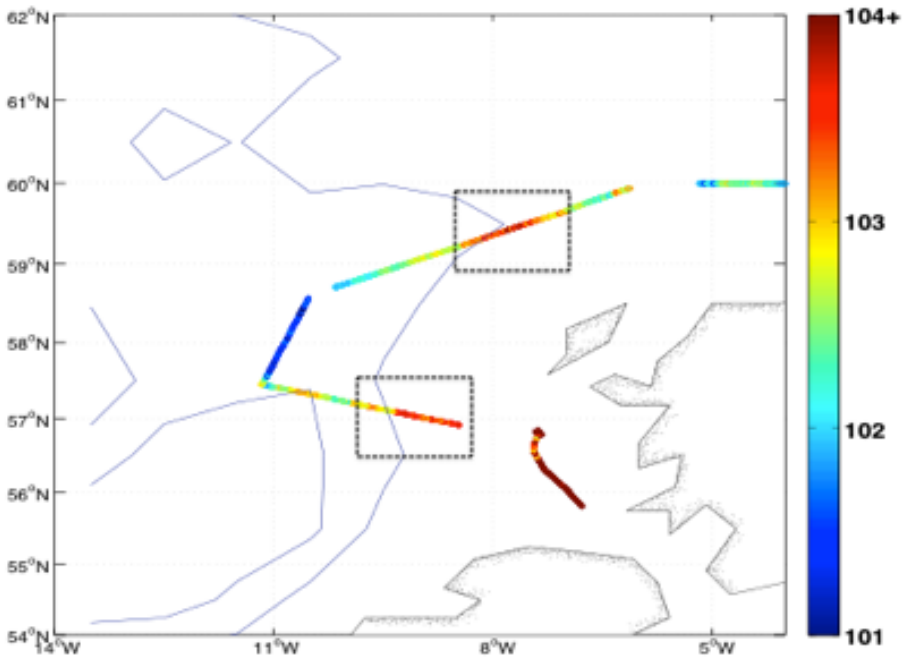

Figure 3. 52: The surface water distribution of N_2O saturation (%) with respect to the atmospheric value off the west coast of Scotland during the D366 OA research cruise. The dashed boxes indicate high surface N_2O assumed to be a result of mixing from internal waves. The lines indicate the location of the shelf edge. The contour elevations are at 1000 m intervals.

Table 3. 6: The coloured regions (found in Figure 3. 53), with strong correlations between sea surface N_2O saturation and sea surface chl-a concentration, the partial pressure of CO_2 and CO saturation during D366. The correlation coefficient (r) and the p values for the correlations are shown. The parameters tested had a non-normal distribution and therefore Spearman's correlations were used.

Surface N_2O saturation and surface parameter	Location on map	Correlation coefficient (r)	p value	n=	Figure (including Appendix figures)
Chl-a	Green	0.88	≤0.05	1065	Figure 3.A 20
CO saturation	Black	0.91	≤0.05	577	Figures 3.A 21
pCO_2	Black	-0.94	≤0.05	577	Figures 3.A 22

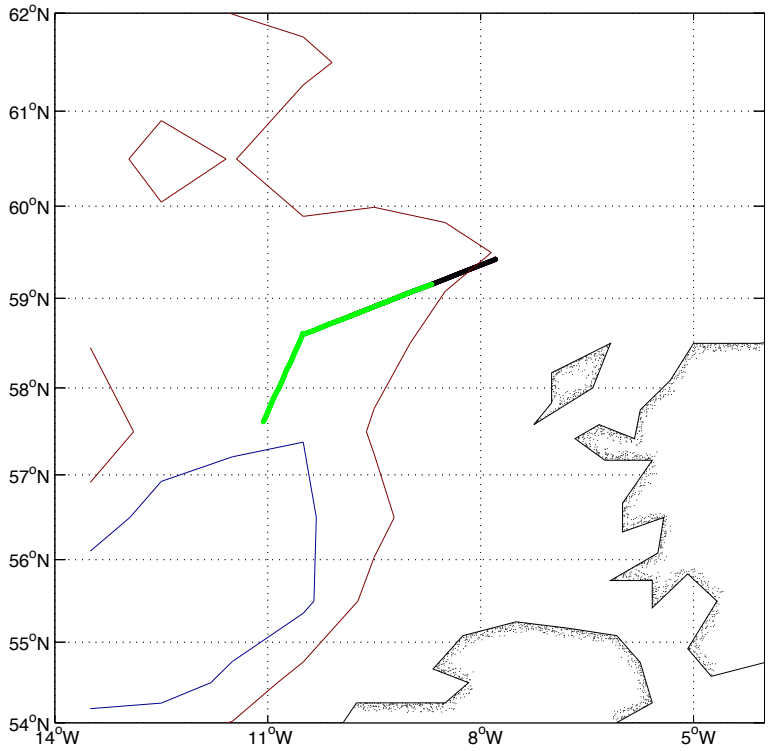

Figure 3. 53: The regions in which strong correlations were found between sea surface N_2O saturation and sea surface chl-a concentration, the partial pressure of CO_2 and CO saturation during the D366 OA research cruise (Table 3. 6). The lines indicate the location of the shelf edge. The contour elevations are at 1000 m intervals.

3.4.5 4: Hydrography: Celtic Sea and Bay of Biscay

The Celtic Sea is bordered by southern Ireland, southwest Wales, Cornwall and Brittany. The water flow is eastwards from NE Atlantic waters through the English Channel (Pingree, 1980). The Celtic Sea displays seasonal stratification, with the thermocline initiating south of Ireland and penetrating the English Channel within a month. Strong tidal mixing around Lands End, the Bristol Channel, the Channel Isles and the eastern English Channel prevents stratification. Shelf sea frontal zones are created along the continental shelf edge, where the deep sea meets the coastal ocean. Shelf break fronts occur at the edge of continental shelves, whereas vertical mixing occurs at the shelf break (Holligan, 1981). The bathymetry is shown in Figure 3. 54, displaying the shelf seabed at approximately 150 -170 m, and the shelf edge dropping off to the open ocean.

In this region the SST increased during the cruise from approximately 13.5 ° C in the northern Celtic Sea in a southerly direction to approximately 16° C in the Bay of Biscay (Figure 3. 55). The SSS also increased in this direction from a fresher salinity of 35.5 in the northern Celtic Sea to 36.0 in the Bay of Biscay, as the waters became less influenced by freshwater outflows (Figure 3. 56). During the summer months high concentrations of chlorophyll occur in surface and subsurface waters along the continental shelf break as a consequence of the mixing of oceanic and shelf waters, consequently lifting nutrient-rich waters to the surface and enhancing primary production (Holligan, 1981). This can be observed from the D366 underway surface chl-a data (Figure 3. 57). This band identifies the regions where the oceanic and shelf sea waters merge.

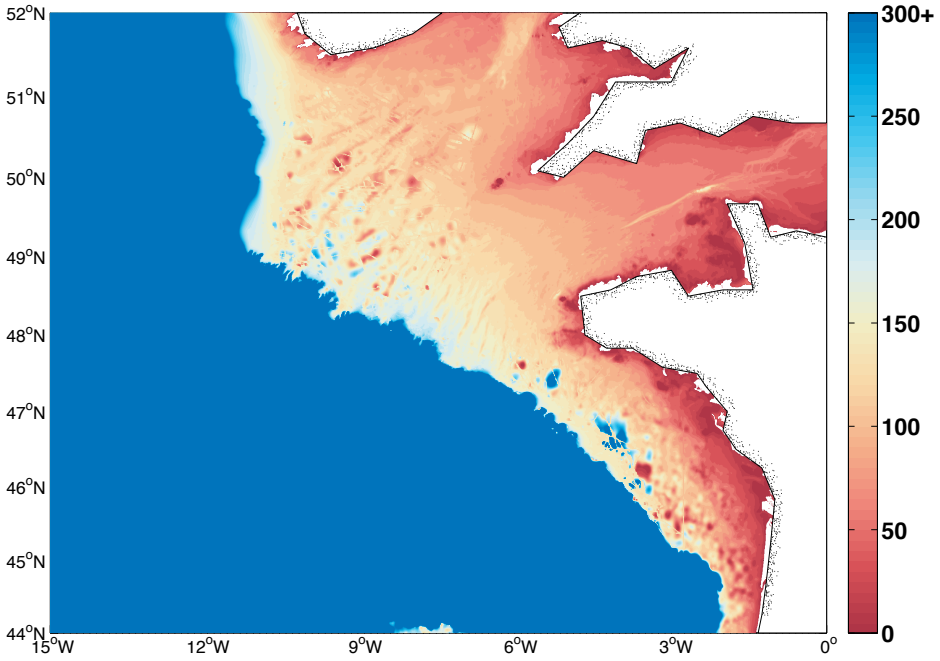

Figure 3. 54: The bathymetry around the Celtic Sea and the Bay of Biscay (m) (GEBCO, 2014).

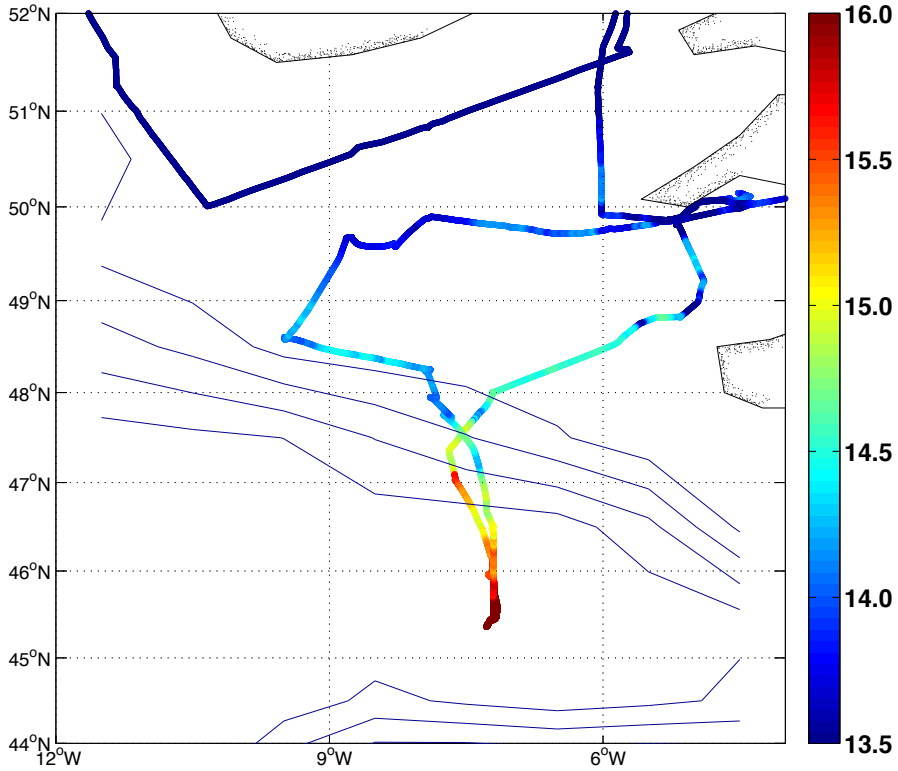

Figure 3. 55: The SST distribution (°C) within the Celtic Sea and Bay of Biscay during D366. The lines indicate the location of the shelf edge. The contour elevations are at 1000 m intervals.

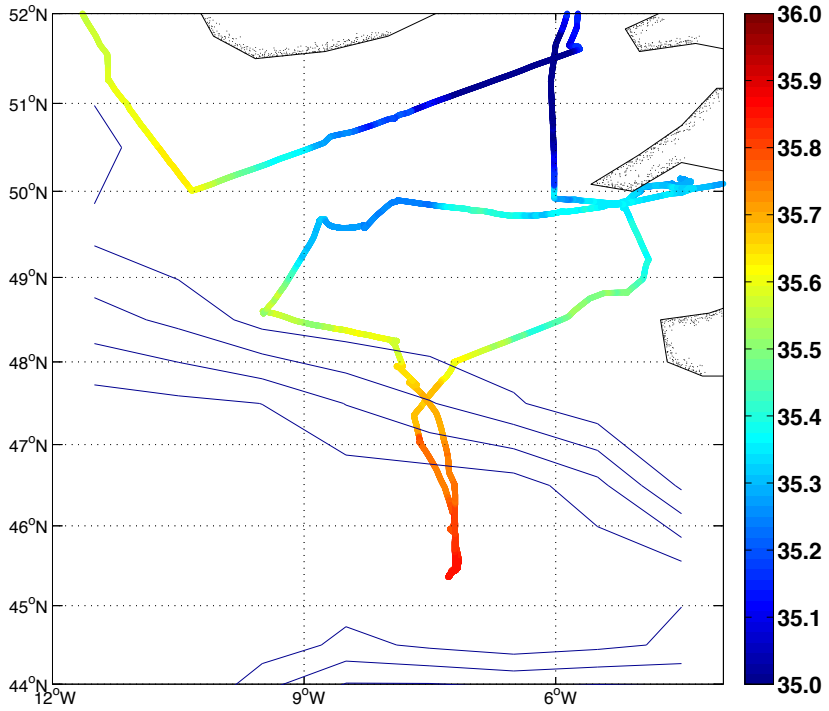

Figure 3. 56: The SSS distribution in the Celtic Sea and Bay of Biscay during D366. The lines indicate the location of the shelf edge. The contour elevations are at 1000 m intervals.

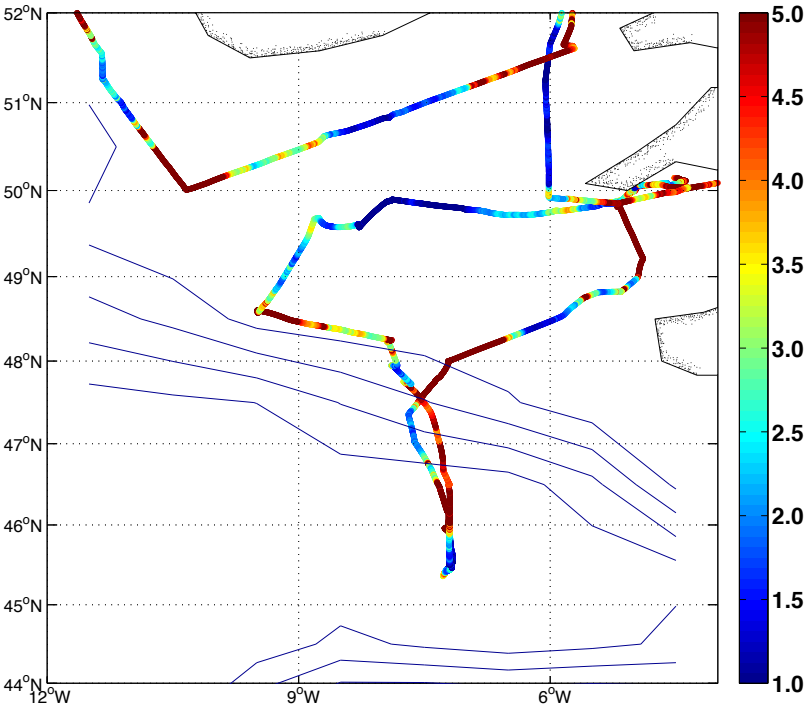

Figure 3. 57: The surface chl-a concentration distribution (µg l^{-1}) in the Celtic Sea and Bay of Biscay during D366. The lines indicate the location of the shelf edge. The contour elevations are at 1000 m intervals.

3.4.5 5: Results: Celtic Sea and Bay of Biscay

In the Celtic Sea and Bay of Biscay region (excluding the tidal front region discussed earlier off the SW coast of England section 3.3.4.4), the surface waters ranged in saturation from undersaturated at 99.0 % to slightly supersaturated at 102.5 % (Figure 3. 58). Saturation decreased from the shelf out into the open waters of the Bay of Biscay. The decrease in surface saturation for N_2O off the shelf had a negative correlation with SST, which increased off the shelf ($r=-0.84$ $p\leq0.05$ $n=4753$) (red region: Figure 3. 59; Table 3. 7). Three localised regions on the continental shelf had higher surface N_2O than the surrounding regions at 102.0 – 102.5 % (Figure 3. 58: dashed boxes). In the red region (Figure 3. 59), a negative correlation was found between surface water saturation for N_2O and SSS ($r=-0.84$ $p\leq0.05$ $n=4753$) (Figures 3.A 23 and 3.A 24).

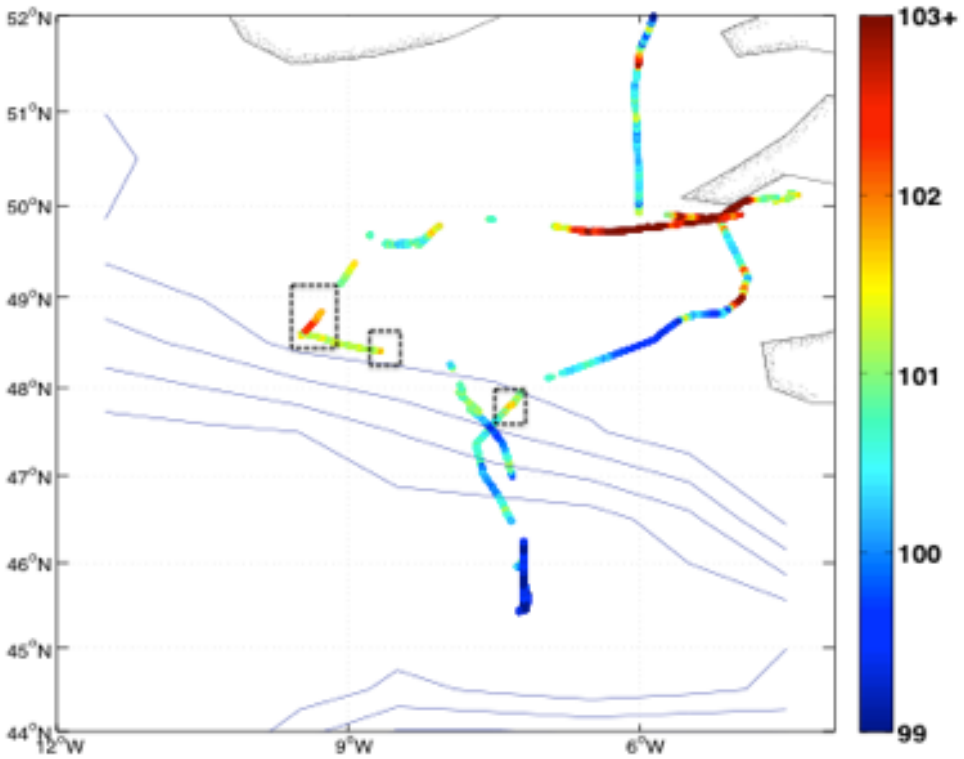

Figure 3. 58: The surface water saturation for N_2O (%) in the Celtic Sea and the Bay of Biscay. The lines indicate the location of the shelf edge. The dashed boxes indicate high surface N_2O assumed to be a result of mixing from internal waves. The lines indicate the location of the shelf edge. The contour elevations are at 1000 m intervals.

Table 3. 7: The coloured region (Figure 3. 59) where strong correlations were found between sea surface N_2O saturation and SST and SSS during D366. The correlation coefficient (r) and the p values for the correlations are shown. The parameters tested had a non-normal distribution and therefore Spearman's correlations were used.

Surface N_2O saturation and surface parameter	Location on map	Correlation coefficient (r)	p value	n=	Figure (including Appendix figures)
SSS	Red	-0.84	≤0.05	4753	Figure 3.A 23
SST	Red	-0.84	≤0.05	4753	Figure 3.A 23

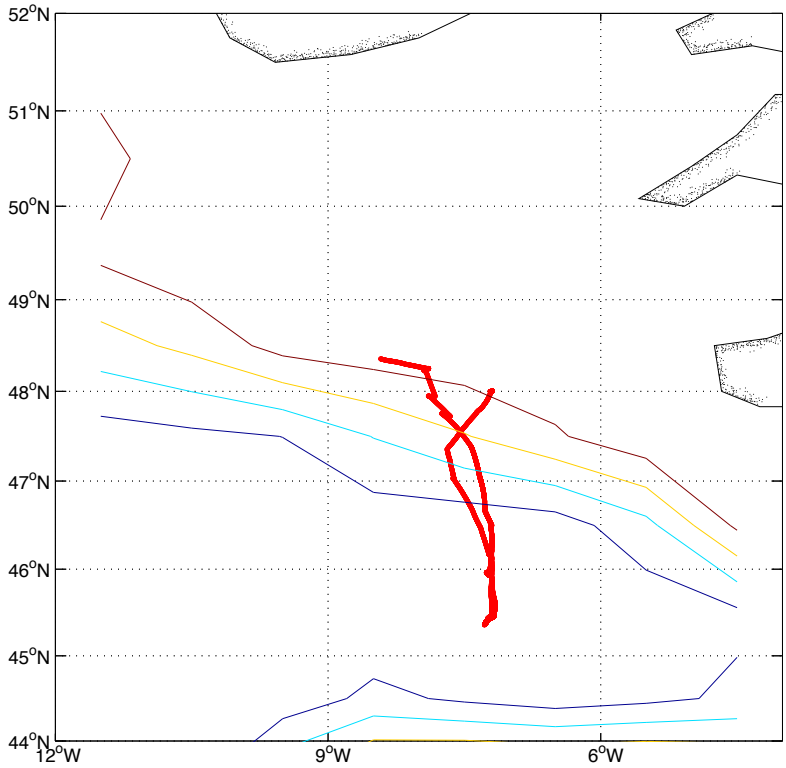

Figure 3. 59: The region within the Celtic Sea where strong correlations were established between sea surface saturation for N_2O and SST and SSS during D366 (Table 3. 7). The lines indicate the location of the shelf edge. The lines indicate the location of the shelf edge. The contour elevations are at 1000 m intervals.

3.4.5 6: Discussion: shelf frontal regions

Significant quantities of energy arise from internal tidal motions on the shelf edge. This energy mixes the pycnocline within stratified waters near the continental edge (Pingree and Mardell, 1985). Most of the energy from internal tides on the Celtic Sea edge dissipates within 50 to 75 km of the tide, producing intensive internal mixing in close proximity of the shelf edge (Green et al., 2008). During the D366, surface water saturation for N_2O was slightly enhanced in three locations along the shelf edge in the Celtic Sea (Figure 3. 58) and in two along the shelf edge region off NW Scotland (Figure 3. 52) suggesting that mixing induced by internal waves brought N_2O produced at depth by nitrification and denitrification to the surface waters.

Higher surface N_2O supersaturations were found on the shelf edge located off the west of Scotland (103 to 103.7 %) (Figure 3. 52), than along the Celtic Sea shelf edge (101 to 102.5 %), (Figure 3. 58). Differences in the surface saturation for N_2O found between these locations could be produced by the strength of mixing occurring at each site, or by the content in subsurface waters. The strength of mixing could be influenced by numerous factors including the time of day, spring and neap tides, where spring tides produce stronger mixing, than neap tides (Sharples et al., 2007).

Regions displaying enhanced surface chl-a concentrations, within the shelf edge proximity, are often indicative of regions where vertical mixing occurs, as they tend to arise where nutrient-rich waters have been mixed to the surface. However, primary production does not always occur directly at the site of mixing because of the requirement of adequate light conditions, which maybe disturbed where mixing occurs. A strong positive correlation between surface water supersaturation for N_2O and chl-a concentration was found along the shelf edge band in the NE Atlantic, off West Scotland ($r=0.88$ $p=\leq 0.05$ $n=1065$) (Table 3.6, Figure 3. 53: green line). It is proposed that in regions where higher surface chl-a concentrations are found, an increase sinking organic matter takes place. As this organic matter reaches the euphotic zone or deeper waters, N_2O is produced during the nitrification pathway. As NO_3^- reaches the marine sediments, it is

respired anaerobically to NO_2^- and then N_2O, before it is further reduced to N_2 during the denitrification pathway. Nitrous oxide that is produced is vertically mixed to the surface.

3. 5: Conclusion

Globally the surface waters of the ocean are slightly supersaturated with N_2O, at ~103.5% (Nevison et al., 1995). Therefore the ocean acts as a net source of N_2O to the atmosphere. Shelf sea regions have been proposed to account for a negligible fraction of global N_2O subsurface production (Freing et al., 2012). This study has shown Freing et al (2012) to be incorrect. Although, surface waters of the NW European shelf sea during D366, were only slightly supersaturated for N_2O, with a mean saturation of 102.19 ± 1.99 % (97 to 110 %), the total global surface area of shelf seas produces a significant source of N_2O to the atmosphere. Bange (2006) estimate this contribution as up to 26 % of global oceanic N_2O emissions. The major contribution of N_2O production in coastal areas, not influenced by upwelling, has been suggested to arise from nitrogen-rich river plumes and estuaries (Bange, 2006, Barnes and Upstill-Goddard, 2011). Although estuarine systems are a far greater source of N_2O than the shelf seas, with surface saturations around 467 % (Bange, 2006), this study shows N_2O production does occur in shelf sea environments and due to the greater surface area of shelf seas in comparison to rivers and estuaries this will also produce a significant source.

There is a strong relationship right across the NW European shelf seas between the surface water N_2O concentration and SST, where cooler waters associate to higher N_2O concentrations. This is due to the solubility of N_2O in water, with more N_2O dissolving into cooler waters than warmer waters. Surface saturation for N_2O and SST also show a very strong relationship in the surface waters of the eastern English Channel, where cooler Atlantic waters associated with higher N_2O saturations than the warmer southern North Sea waters.

Positive relationships between surface N_2O and chl-a were found in some areas of the NW European shelf sea. This could be due to higher surface concentrations of chl-a increasing the quantity of organic material sinking into the water column, and therefore more nitrification occurring in the euphotic zone, or at depth. During the initial step of nitrification NH_4^+ is oxidised to NO_2^- and N_2O is given off as a by-product, which then reaches the surface waters by entrainment. If the nitrification rate increases, more NO_3^- is likely to reach the marine sediments where it is respired under anoxic conditions by denitrifying organisms, producing a further source of N_2O. High surface N_2O was measured in an area within the western mouth of the Skagerrak where there was a dying Coccolithophorid bloom, reinforcing this idea.

On the shelf, various physical processes producing enhanced vertical mixing from below the thermocline, associated with high surface N_2O. They include:

1. Tidal front regions: where seasonally stratified and fully mixed water columns meet.
2. Shelf break front regions: as the barotropic tide passes over the continental shelf, the change in topography causes the tide to move upwards, pushing the thermocline up and creating internal waves.
3. Regions with a fully mixed water column, which may re-suspend organic material from the seafloor into the water column and biogenic gases, such as N_2O.
4. Freshwater-seawater transitional zones: in regions with a high freshwater influx, such as in the Skagerrak, transitional zones between fresher and more saline seawater, produce localised vertical mixing.

Vertical mixing of the water column stimulates primary production in the local area by mixing organic matter from below the thermocline into the euphotic zone. As mentioned above, an increase in phytoplankton can result in more organic material reaching deeper waters where it is then oxidised by nitrifiers during nitrification, and the resulting nitrate is reduced during denitrification in the marine sediments, producing N_2O.

Some vertically mixed regions with high surface N_2O did not have high surface chl-a concentrations, such as in the English Channel, indicating another source. This source could be either:
1) Partial denitrification in the anoxic sediments, with the N_2O produced being mixed to the surface before complete denitrification can take place,
2) The re-suspension of organic material from the seafloor that is then nitrified in the water column.
3) Due to SST and solubility effects as previously discussed.

Undersaturation in surface waters was identified in a few areas including the Bay of Biscay and the southern North Sea. Nevison et al. (1995) proposed that undersaturation in surface waters occurs as a result of summertime stratification reducing mixing between the deeper waters and the surface waters. However, the southern North Sea region was fully mixed in the locations where the surface waters were undersaturated. Therefore another driver, such as a localised cooling effect must be influencing these waters, where lower SSTs increase the solubility of the surface waters but the lag with the atmosphere leads to undersaturation.

Nitrous oxide is produced at high quantities in riverine and estuarine environments (Barnes and Upstill-Goddard, 2011). However the regions sampled within the outflows of large rivers and estuaries during the D366 did not display higher supersaturations than the surrounding regions. The residence time for N_2O during the D366 cruise was estimated at approximately two weeks at the mean wind speed of 9.19 m s^{-1}, SST of 15 °C, and mixed layer depth of 26.29 m. This is consistent with Najjar (1992), who reported a ventilation time for N_2O of three weeks. This indicates that N_2O produced in rivers and estuaries ventilates to the atmosphere before reaching the shelf seas. De Wilde and de Bie (2000) also found this, reporting that nearly all the N_2O produced in the regions of the Schelde Estuary that they sampled were lost to the atmosphere, rather than transported into the open sea.

Chapter 4: Surface water distribution of methane in the northwestern European shelf seas.

4. 1: Introduction

This chapter describes the surface ocean concentration and saturation distribution, as well as the ocean-atmospheric flux, of CH_4 in the NW European shelf seas (D366 OA cruise).

4.1 1: Aims and objectives

CH_4 is the second most important long-lived greenhouse gas after CO_2 (not including water vapour), with between 1 to 4 % of the global atmospheric source arising from the ocean. This chapter aims to identify whether the NW European shelf sea regions acted as a source or sink in the summer of 2011. This is the first high-resolution surface CH_4 dataset for the NW European shelf seas. This chapter aims to identify key influential processes on the surface distribution of CH_4 in shelf sea environments by examining the relationship between this trace gas, meteorological parameters, such as sea surface temperature (SST), salinity (SSS), windspeed, chlorophyll-a concentration (chl-a) and other trace gases measured in the surface waters (i.e. CO_2 and CO).

Specifically, the objectives of this chapter are:

- To quantify the mean surface concentration, saturation and air-sea flux of CH_4 in June and July 2011 in the NW European shelf seas.
- To identify whether the NW European shelf seas acted as a CH_4 source or sink.
- To identify the locations where surface waters were under and supersaturated for CH_4.
- To use the high resolution data to understand the processes influencing the distribution of surface CH_4 at large scales across the NW European shelf seas, and within smaller localised regions.

Chapter 4: Surface water distribution of methane in the northwestern European shelf seas.

4. 2: Methods

The surface water and atmospheric measurements used to calculate concentration, saturation and ocean-atmospheric fluxes were measured in dry mole fractions in the field, using ICOS spectrometry (CO_2/CH_4 *Los Gatos Research* analyser). Section 2. 3 describes how the sea surface concentration, saturation and ocean- atmosphere flux values were calculated for surface CH_4, and the atmospheric and surface water measurements are discussed in section 2.9.2.

Spearmans's correlations over the entire NW European shelf sea, along with a correlation programme able to identify smaller scale relationships were used as tools to detect relationships between surface water CH_4 concentration (nmol L^{-1}) and saturation (%) and surface chl-a concentration (µg L^{-1}), SST (°C), SSS, windspeed (m s^{-1}), surface CH_4 and CO concentration (nmol L^{-1}) and saturation (%) and the surface pCO_2 (µatm) in the NW European shelf seas (described in section 3.2.2). As explained in the methods chapter the ICOS instruments measured surface CO_2 and CO simultaneously to N_2O and CH_4. These datasets are used throughout this chapter with the aim to gain insight into fundamental processes across the European shelf seas that influence the surface distribution of CH_4. The results are found in section 4.3.3.

4. 3: Results

4.3. 1: D366 CH_4 data description

The surface waters measured in the NW European shelf sea during the D366 cruise, were supersaturated for CH_4 with respect to the atmospheric value, with a mean supersaturation of 118.38 ± 21.67 (100 – 315 %)% (Figure 4. 1), a mean concentration of 3.05 ± 0.64 nmol L^{-1} (2.6 – 8.4 nmol L^{-1}) (Figure 4. 2), and a mean ocean-atmosphere flux of 2.32 x 10^3 ± 3.69 x 10^3 nmol m^{-2} d^{-1} (0 – 3.7 x 10^3 nmol m^{-2} d^{-1})(Figure 4. 3). Various regions had surface waters supersaturated for CH_4 reaching saturations up to 315 %. These will be discussed in more detail in section 4. 4. The mean surface saturation calculated fits well with those previously reported in the North Sea at mean saturations of 113 to 338 % (Conrad and Seiler, 1988, Scranton and McShane, 1991, Bange et al., 1994,

Rehder et al., 1998, Upstill-Goddard et al., 2000). The mean ocean to atmosphere flux calculated at 2.32 x 10^3 nmol m^{-2} d^{-1} is consistent with that calculated by Bange (1994) in the southern North Sea at 2.17 x 10^3 nmol m^{-2} d^{-1}.

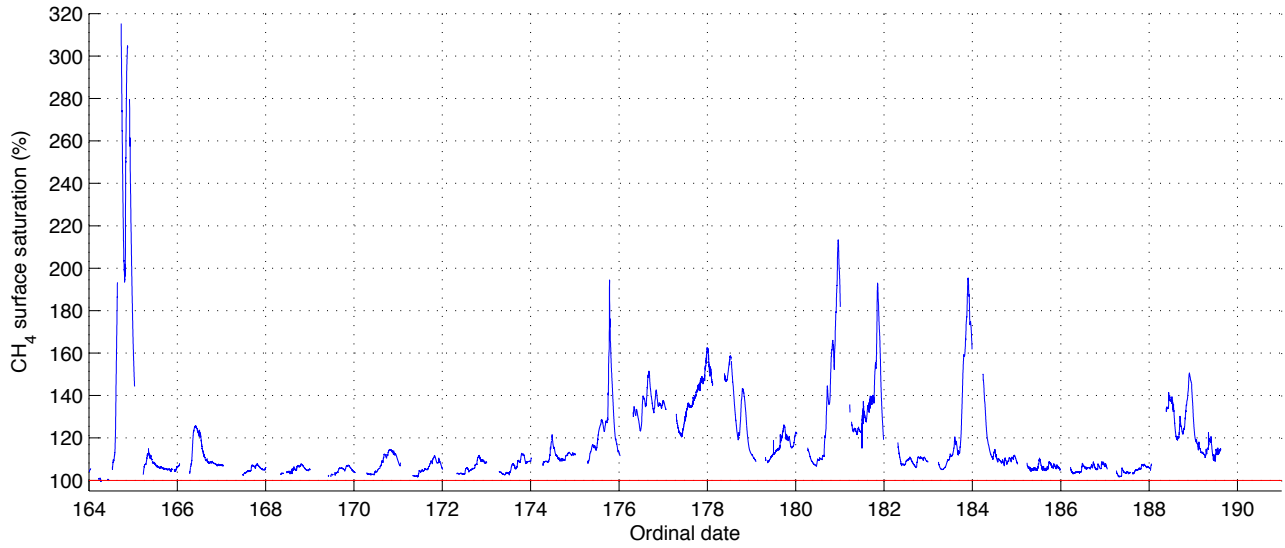

Figure 4. 1: The sea surface saturation for CH_4 along the D366 cruise track. The mean sea surface saturation was supersaturated in respect to the atmospheric equilibrium concentration at 118.38 ± 21.67 %. The red line shows 100 % saturation. Details of how surface saturation for CH_4 was calculated are found in section 2.3.2.

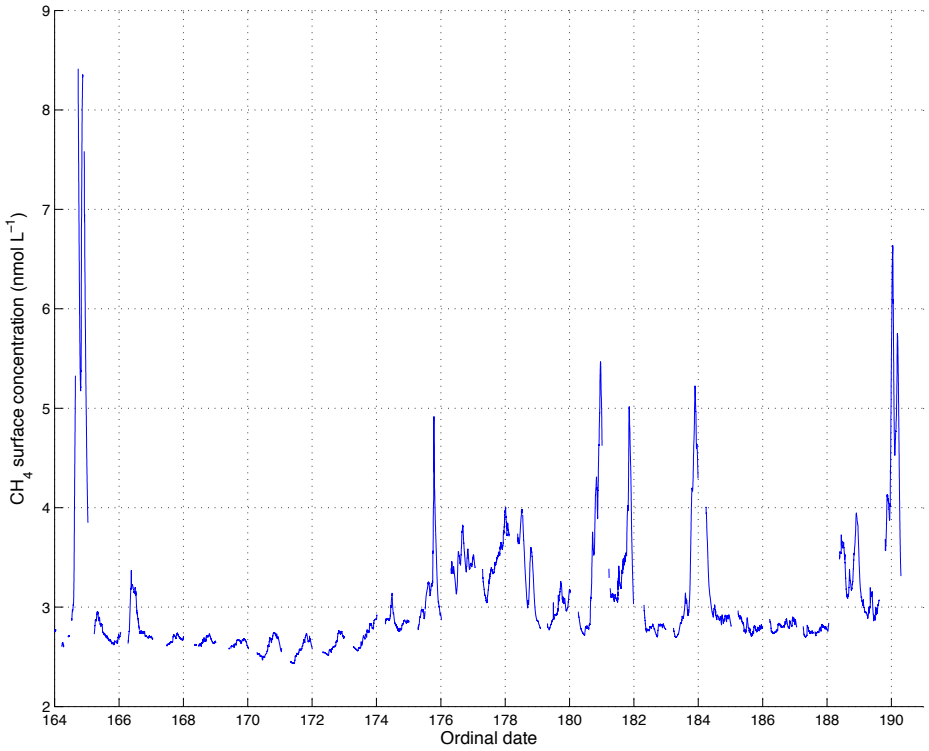

Figure 4. 2: The sea surface concentration of CH_4 along the D366 cruise track. The mean sea surface concentration was 3.05 ± 0.64 nmol L^{-1}. Details of how the surface concentration for CH_4 was calculated are found in section 2.3.2.

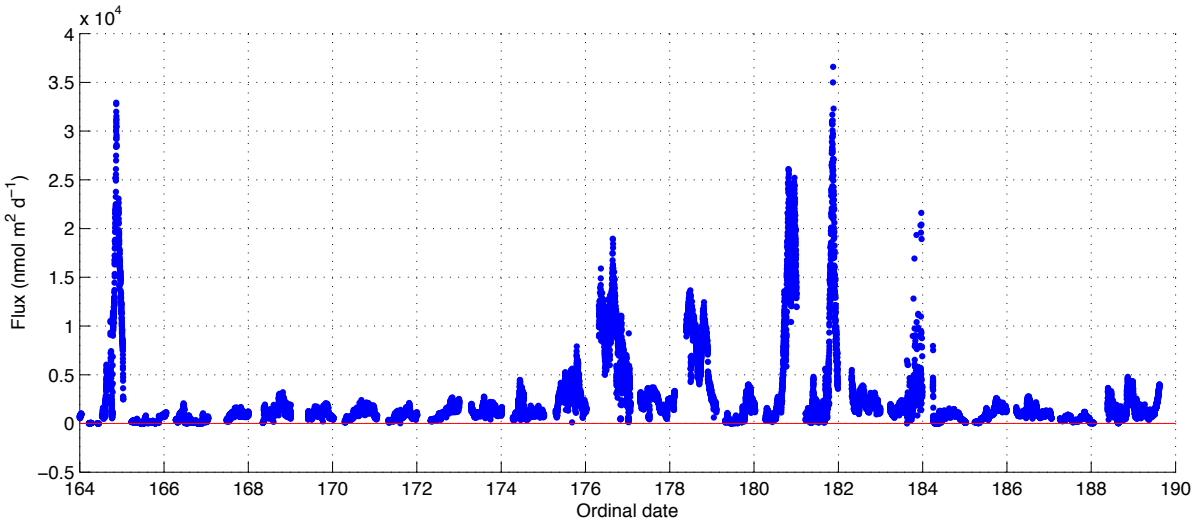

Figure 4. 3: The ocean-atmosphere flux of CH_4 calculated along the D366 cruise track. The mean ocean-atmosphere flux of CH_4 was 2.32 x 10^3 ± 3.69 x 10^3 nmol m^{-2} d^{-1}, making the shelf seas a source to the atmosphere. Details of how the ocean to atmosphere flux is calculated are found in section 2.3.4.

4.3. 2: Surface water CH_4 saturation distribution.

Sea surface waters in the NW European shelf sea with the highest surface saturation for CH_4 (exceeding 130 %), were found predominantly in the central and eastern English Channel, the southern and central North Sea, the Skagerrak and along the Norwegian Trench (Figure 4. 4), with the highest saturations, reaching 315 %, found in the SW Irish Sea. These regions will be discussed in section 4. 4.

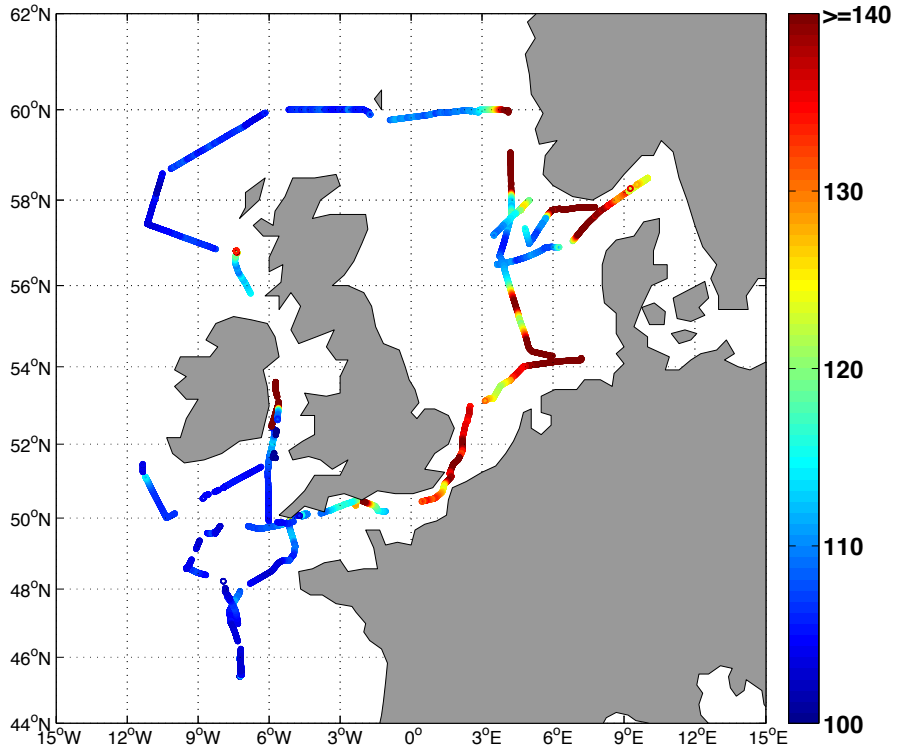

Figure 4. 4: The D366 cruise track displaying the surface water saturation of CH_4 (%), with respect to the atmospheric value.

4.3. 3: Correlations between surface CH_4 and other measured parameters

4.3.3 1: Correlations between parameters for the whole NW European shelf sea

Spearman's correlations were determined between surface ocean CH_4 concentration (nmol L^{-1}) and saturation (%), with surface chl-a concentration (µg L^{-1}), SST (°C), SSS, surface N_2O and CO concentration (nmol L^{-1}) and saturation (%) and the surface pCO_2 (µatm) over the entire D366 dataset. Over such a large hydrographically diverse area mostly only weak correlations were found between the tested variables (Table 4. 1). The strongest relationships

were found between surface CH_4 saturation and concentration and SSS with correlation coefficients of -0.72 and -0.69 (Table 4. 1). The influence of three freshwater outflows in the SW Irish Sea, the Skagerrak and in the Norwegian Trench on the surface CH_4 can be observed in Figure 4. 5. The freshwater end-members from each outflow are of different CH_4 saturations, with the outflow into the SW Irish Sea greatly exceeding the others at approximately 315 % saturation. The correlations between the surface CH_4 saturation and concentration and windspeed over the entire area of the NW European shelf seas sampled are weak negative correlations at r= -0.27 and -0.33 (Table 4.1). This indicates that the ocean to atmosphere exchange of CH_4 plays only a small role in influencing the surface distribution at this scale. The hydrological diversity of the NW European shelf seas is the most probable explanation for the weak correlations found between surface CH_4 and other parameters across the entire region. Correlations tested over smaller regions are used to understand the localised relationship between CH_4 distribution and the other parameters (Section 4.4).

Table 4. 1: Spearman's correlations over the entire NW European shelf seas sampled, between the surface ocean CH_4 concentration (nmol L^{-1}) and saturation (%), with surface chl-a concentration (µg L^{-1}), SST (°C), SSS, windspeed (m s^{-1}), surface CO concentration (nmol L^{-1}) and saturation (%) and the surface pCO_2 (µatm).

Surface parameter 1	Surface parameter 2	Correlation coefficient (r-value)	p-value	Figure
CH_4 saturation	SST	0.22	≤0.05	-
CH_4 concentration	SST	0.17	≤0.05	-
CH_4 saturation	SSS	-0.69	≤0.05	Figure 4. 5
CH_4 concentration	SSS	-0.72	≤0.05	-
CH_4 saturation	Windspeed	-0.27	≤0.05	
CH_4 concentration	Windspeed	-0.33	≤0.05	
CH_4 saturation	Chl-a concentration	0.03	≤0.05	-
CH_4 concentration	Chl-a concentration	0.04	≤0.05	-
CH_4 saturation	CO saturation	0.12	≤0.05	-
CH_4 concentration	CO concentration	-0.04	≤0.05	-
CH_4 saturation	pCO_2	0.29	≤0.05	-
CH_4 concentration	pCO_2	0.29	≤0.05	-

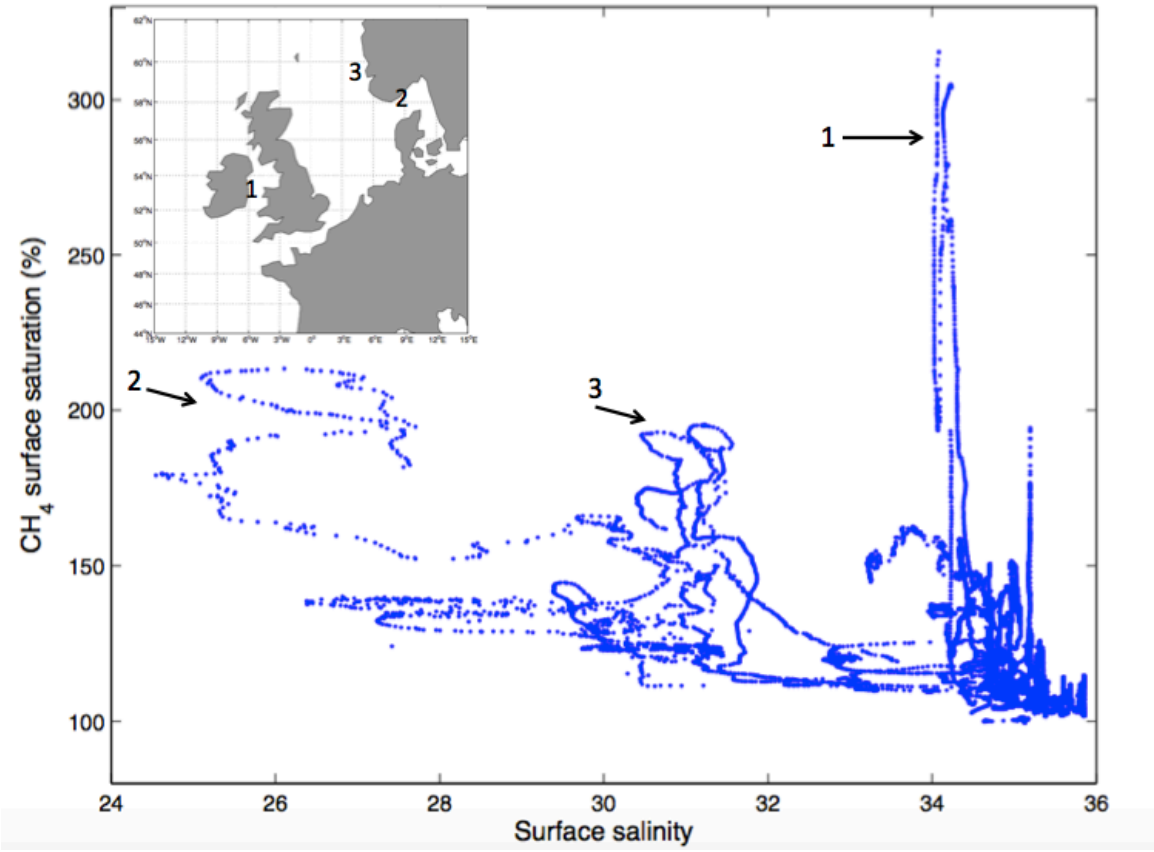

Figure 4. 5: The relationship between surface salinity and surface saturation for CH_4 across the NW European shelf seas during D366. The small map shows the location of the freshwater end-members of 1, 2 and 3. 1: SW Irish Sea in close proximity to Dublin Bay; 2: the Skagerrak, and 3: the Norwegian Trench.

4.3.3 2: Correlation distribution maps

Figure 4. 6 shows that SST and surface CH_4 saturation generally showed weak relationships with each other, but small bands where stronger positive and negative relationships can be seen, for example in the Celtic Sea. In contrast, SSS displayed strong negative correlations in a few larger regions, for example, off the east coast of Ireland and within the Skagerrak and northern North Sea (Figure 4. 7), highlighting a relationship between SSS and surface CH_4 saturation. The surface concentration of chl-a predominantly displayed weak positive correlations with surface CH_4 saturation throughout the NW European shelf seas. However, in a few areas, such as the Norwegian Trench, these positive correlations were much stronger (Figure 4. 8). Generally weak positive and negative relationships between surface CH_4 and CO_2 were found, but adjacent to the west coast of Norway, in the Norwegian Trench, there was a strong positive

correlation between these parameters (Figure 4. 9). Surface saturation for CO and CH_4 were found to correlate both positively and negatively with one another. Some of these interactions, such as in the southern North Sea and in the Skagerrak, were strong (Figure 4. 10). More explanation about these correlations is provided in section 4.4 under the discussion sections for each region in which they occurred (e.g. Section 4.4.1.2 for the Skagerrak).

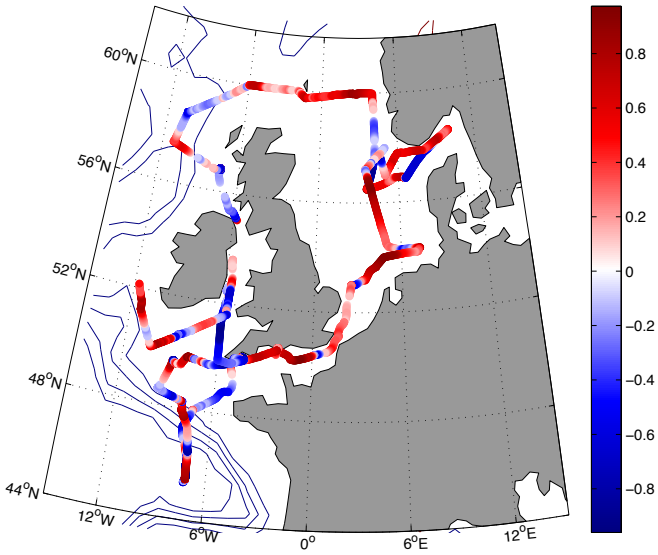

Figure 4. 6: The distribution of the strength of positive and negative correlations (displayed by the correlation coefficients (r- values)) between the sea surface saturation of CH_4 and SST. All values plotted were significant to a p-value of ≤0.05.

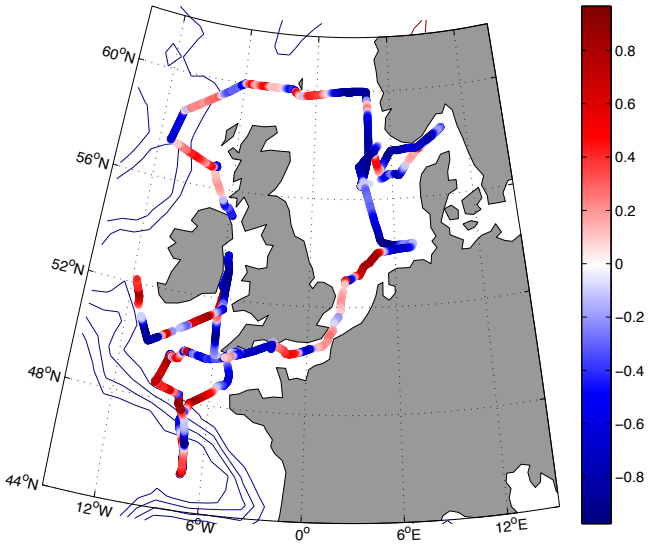

Figure 4. 7: The distribution of the strength of positive and negative correlations (displayed by the correlation coefficients (r- values)) between the sea surface saturation of CH_4 and SSS. All values plotted were significant to a p-value of ≤0.05.

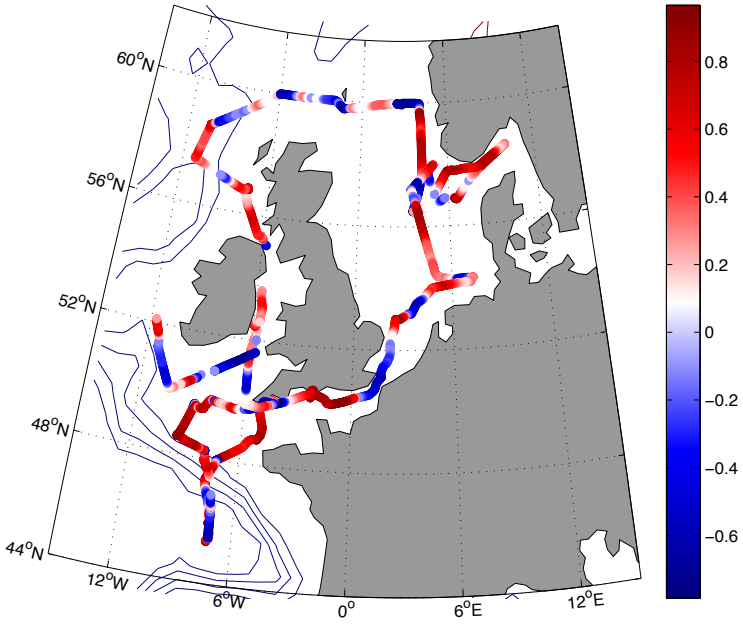

Figure 4. 8: The distribution of the strength of positive and negative correlations (displayed by the correlation coefficients (r- values)) between the sea surface saturation of CH_4 and surface chl-a concentration. All values plotted were significant to a p-value of ≤0.05.

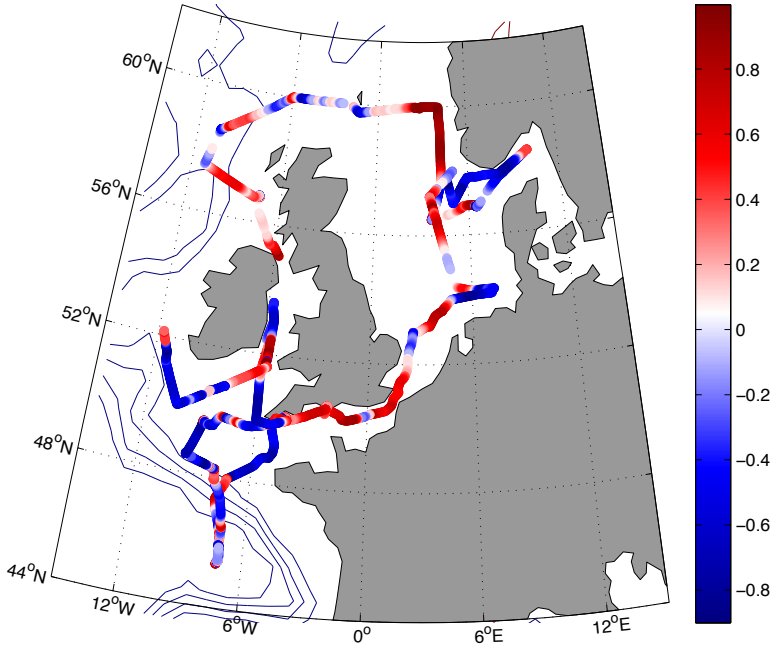

Figure 4. 9: The distribution of the strength of positive and negative correlations (displayed by the correlation coefficients (r- values)) between the sea surface saturation of CH_4 and partial pressure of CO_2. All values plotted were significant to a p-value of ≤0.05.

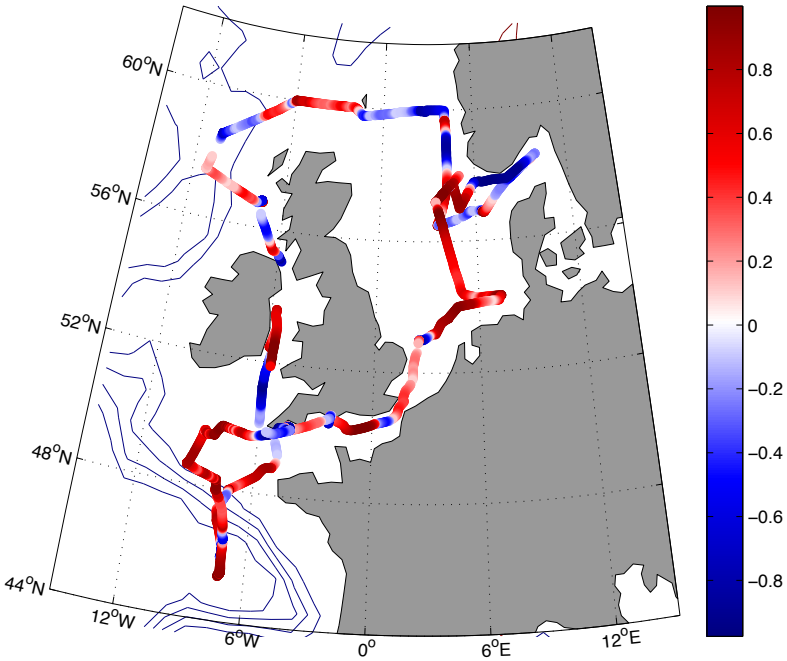

Figure 4. 10: The distribution of the strength of positive and negative correlations (displayed by the correlation coefficients (r- values)) between the sea surface saturation of CH_4 and CO. All values plotted were significant to a p-value of ≤0.05.

4.3. 4: Ventilation time of methane in the NW European shelf seas

The ventilation time for CH_4 (the length of time CH_4 remains in the water column before venting out to the atmosphere) calculated in the NW European shelf seas was very similar to that of N_2O, estimated as approximately two weeks. The method of calculating the ventilation time and assumption are discussed in section 3.34 (Equation 3.1).

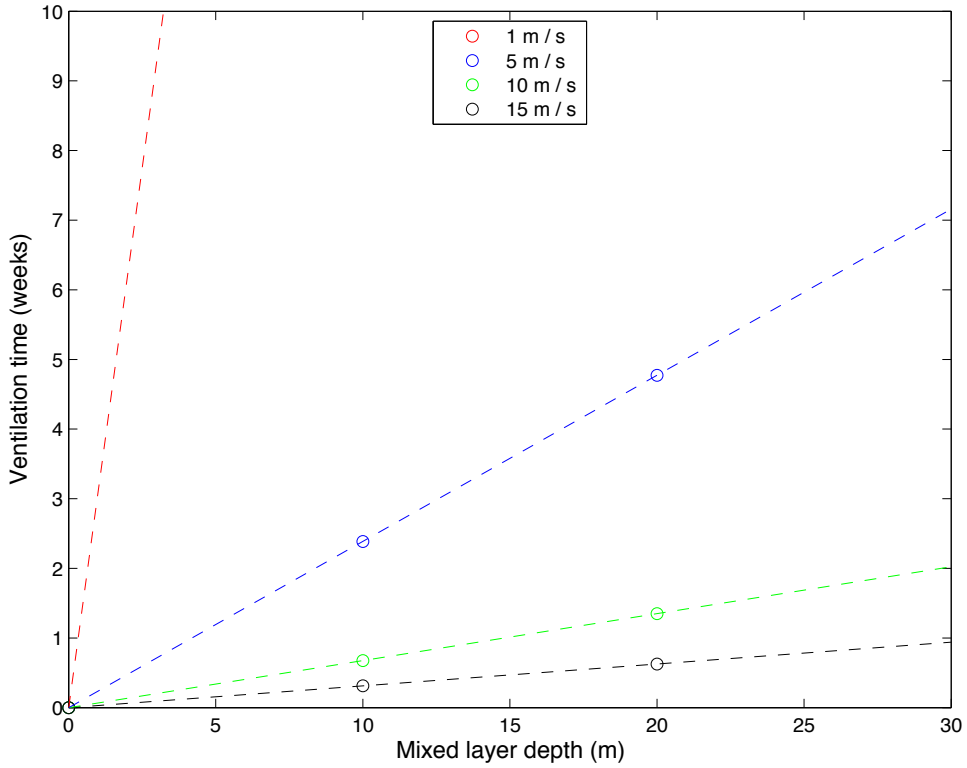

Figure 4. 11: The ventilation time of CH_4 at a SST of 14.22 °C, at different mixed layer depths and wind speeds. On the D366 the mean mixed layer depth was calculated as 26.29 m, mean SST was measured at 14.22 °C and mean wind speed was 9.19 m s^{-1}. The ventilation time for CH_4 using these mean values was approximately two weeks.

4. 4: Biogeochemical and physical processes influencing the surface CH_4 saturation.

This section investigates the regions where the surface waters were found to be most supersaturated for CH_4 to understand the influential processes and parameters. For a description of the hydrography for each region refer to section 3. 4.

4.4. 1: The Skagerrak, Norwegian Trench and NE North Sea.

4.4.1. 1: Results: The Skagerrak, Norwegian Trench and NE North Sea.

Surface saturation for CH_4 in the Skagerrak, Norwegian Trench and NE North Sea was between 102 - 215 %, with the highest supersaturations in the southern part of the Norwegian Trench and in the mouth (west) of the Skagerrak in the range of 160 – 215 % (Figure 4. 12). The lowest supersaturations, between 102 – 118 %, were located in the NE North Sea (Figure 4. 12). Throughout this region there was a strong inverse relationship between SSS and surface saturation for CH_4, where high salinities occurred simultaneously to low supersaturations and vise versa (Figure 4. 13). There was a lag response, of approximately thirty minutes, of the surface saturation of CH_4 to any changes observed in the SSS data. This lag effect could be due to the slow equilibration time of CH_4 in the equilibrator used. Two regions within the Skagerrak and surrounding regions displayed strong negative correlations between the parameters ($r=-0.88$, $p\leq0.05$ $n=721$: red region of Figure 4. 14; $r=-0.98$, $p\leq0.05$ $n=217$: magenta region of Figure 4. 14; Table 4. 2). These two locations were within the mouth of the Skagerrak (Figure 4. 15 and appendix Figure 4.A. 1).

Positive correlations were identified between surface chl-a concentration and surface saturation for CH_4 within two locations around the mouth of the Skagerrak ($r=0.64$ $p\leq0.05$ $n=557$, blue region, Figures 4. 16 and 4.A. 3; $r=0.60$ $p\leq0.05$ $n=117$, red region: Figures 4. 16 and 4.A. 4, Table 4. 2), as well as within a large area in the southern Norwegian Trench ($r=0.79$ $p\leq0.05$ 721, green region,

Figures 4. 16 and 4.A. 5). Increases in the surface concentration of chl-a were also found to slightly preceed the increase in surface saturation for CH_4 by around thirty minutes (Figure 4. 17).

Moving from the southern to the northern end of the Norwegian Trench there was a gradient of decreasing surface chl-a concentration and surface saturation for CH_4 and CO_2 (Figure 4. 18). In this region there was a positive correlation between surface CO_2 and CH_4 saturation ($r=0.93$ $p\leq0.05$ $n=1153$) (Figure 4.A. 2, Table 4. 2; Figure 4. 14: green). As the ship moved out of the Norwegian Trench and into the northern North Sea (indicated by the dashed grey lines in Figure 4. 18) the surface concentration of chl-a increased again, but both surface CH_4 and CO_2 remained lower than in the Norwegian Trench.

Contrasting relationships arose between the surface saturation for CH_4 and CO in two different areas within this region. In the NE North Sea (cyan region: Figure 4. 16) there was a positive relationship between these two parameters ($r=0.98$, $p=\leq0.05$ $n=1585$, Table 4. 2, Figure 4.A. 6), whereas in the southern part of the Norwegian Trench (black and green: Figure 4. 15) a negative correlation was identified ($r=-0.99$, $p=\leq0.05$ $n=289$, Table 4. 2, Figure 4.A. 7).

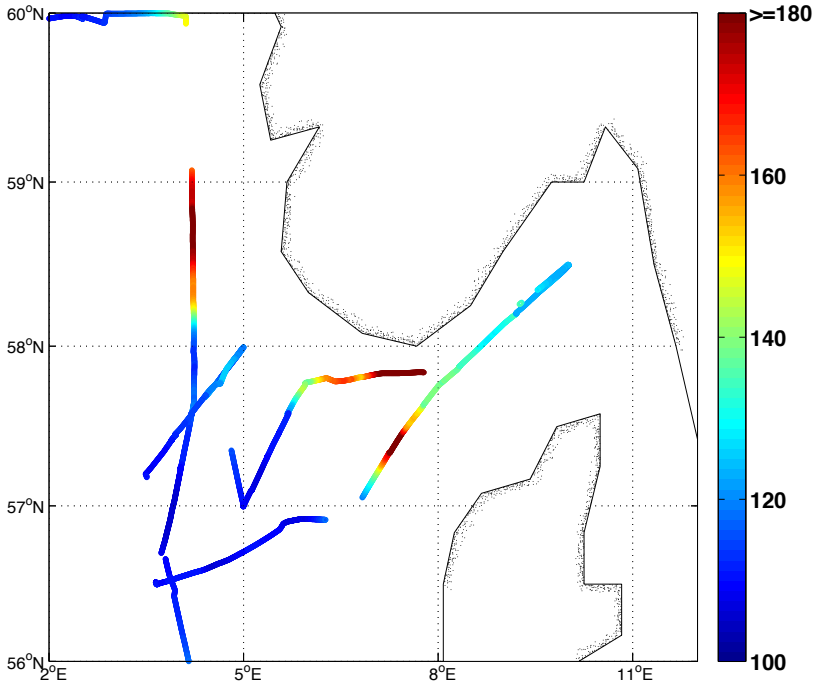

Figure 4. 12: The distribution of surface water saturation of CH_4 (%) with respect to the atmospheric value in the NE North Sea, Skagerrak and Norwegian Trench.

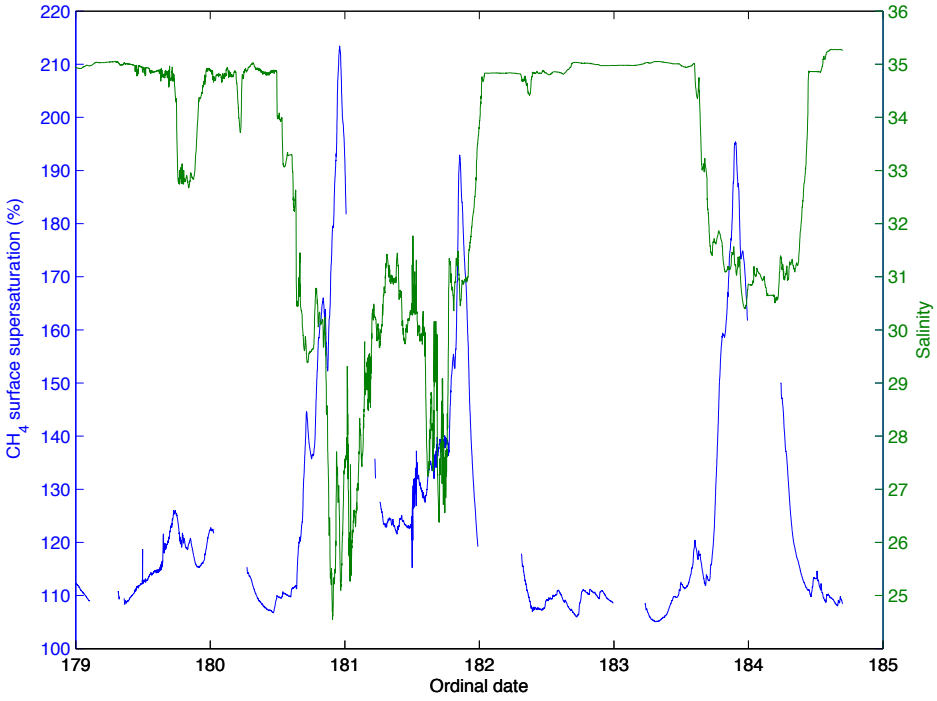

Figure 4. 13: The inverse relationship between SSS and surface saturation of CH_4 over time in the NE North Sea, Skagerrak and Norwegian Trench (location displayed by the blue, red, green and magenta regions in Figure 4. 14).

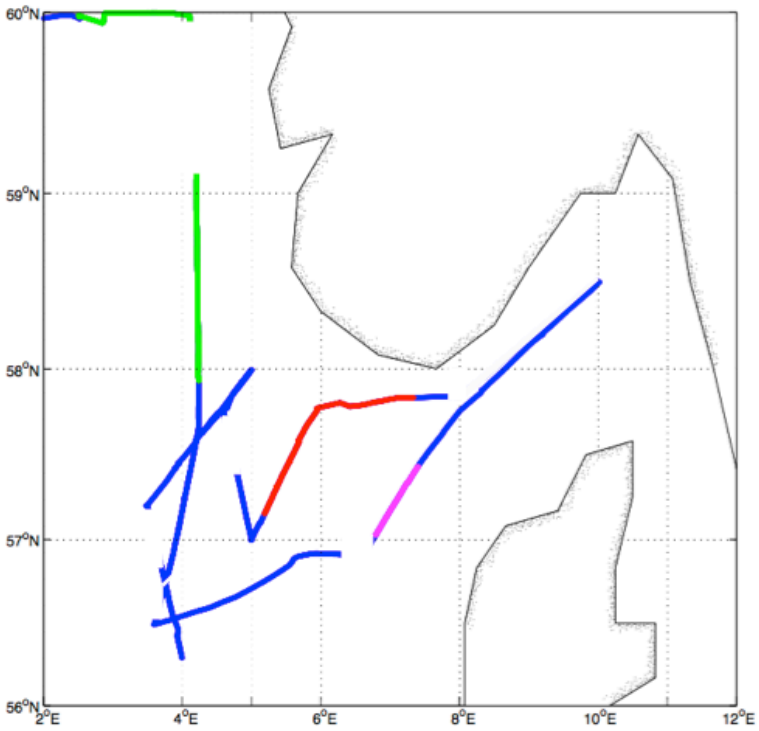

Figure 4. 14: The regions in which correlations were found between SSS, surface chl-a concentration and surface saturation of CO_2 and CH_4. The majority of the blue, red and magenta regions displayed an inverse relationship between SSS and CH_4 saturation. Within both the red and magenta regions strong negative correlations were found between SSS and saturation of CH_4 and within the green region, a strong positive correlation was found between surface CO_2 and CH_4 saturation (refer to Table 4. 2 for more details).

Table 4. 2: Relationships between surface saturation of CH_4 and other parameters in the NE North Sea, Skagerrak and Norwegian Trench (refer to Figures 4. 14 and 4. 16 for locations of the correlations). The parameters tested had a non-normal distribution and therefore Spearman's correlations were used.

Surface CH_4 saturation and surface parameter	Location on map	Correlation coefficient (r)	p value	n=	Figure (including Appendix figures)
SSS	Red (Figure 4. 14)	-0.88	≤0.05	721	Figure 4. 15
SSS	Magenta (Figure 4. 14)	-0.98	≤0.05	217	Figure 4.A. 1
CO_2 saturation	Green (Figure 4. 14)	0.93	≤0.05	1153	Figure 4.A. 2
Chl-a concentration	Blue (Figure 4. 16)	0.64	≤0.05	557	Figure 4.A. 3
Chl-a concentration	Red (Figure 4. 16)	0.60	≤0.05	117	Figure 4.A. 4
Chl-a concentration	Green (Figure 4. 16)	0.79	≤0.05	721	Figure 4.A. 5
CO saturation	Cyan (Figure 4. 16)	0.98	≤0.05	1585	Figure 4.A. 6
CO saturation	Black and green (Figure 4. 16)	-0.99	≤0.05	289	Figure 4.A. 7

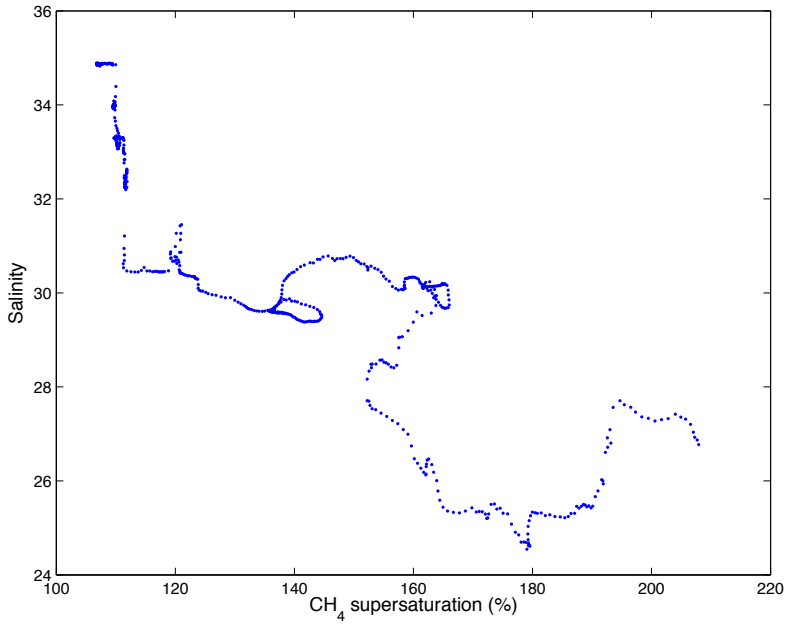

Figure 4. 15: Sea surface salinity and surface saturation of CH_4 in the red region of the Skagerrak (Figure 4. 14; r=-0.88, p≤0.05).

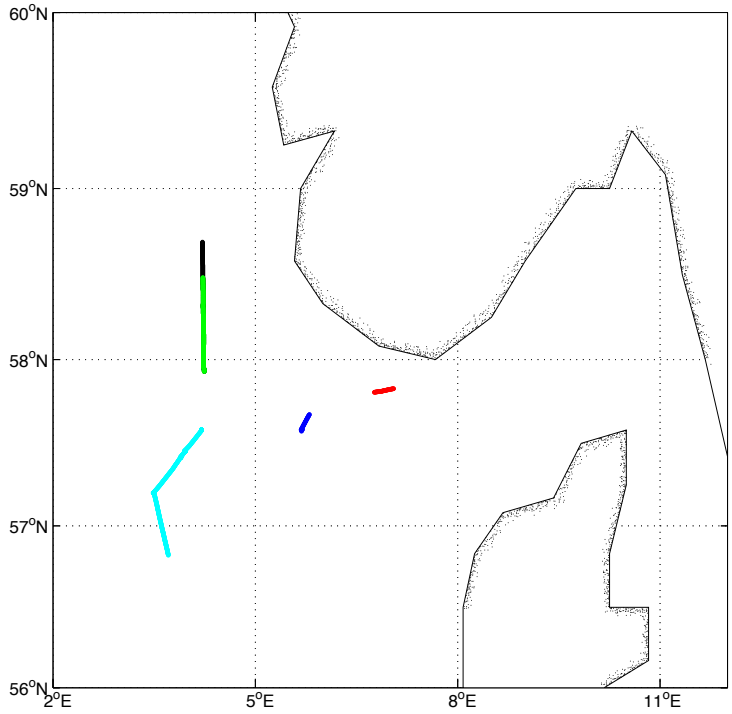

Figure 4. 16: The locations where positive and negative correlations were located between sea surface saturation of CH_4 and surface chl-a concentration and saturation of CO in the Skagerrak, Norwegian Trench and NE North Sea (refer to Table 4. 2 for details).

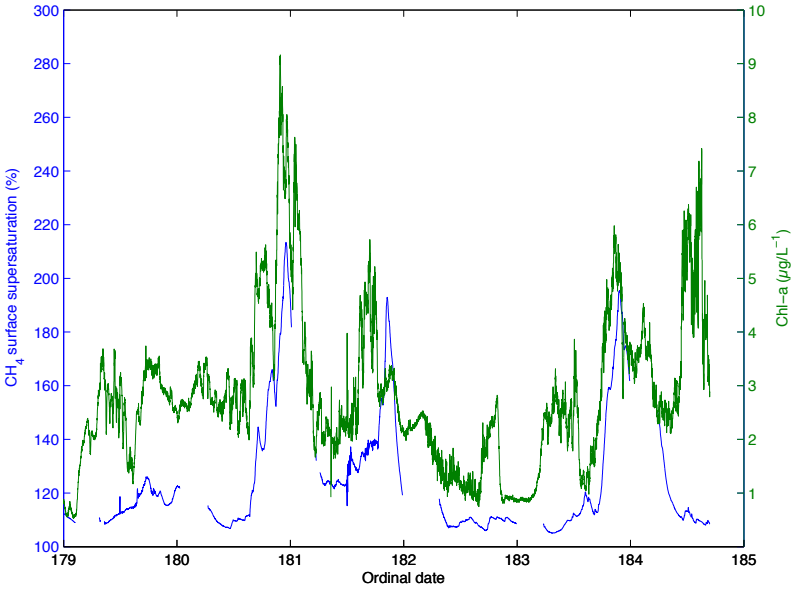

Figure 4. 17: The relationship between surface saturation of CH_4 and the surface concentration of chl-a, over time, in the Skagerrak throughout the blue, red, green and magenta regions on map (refer to Figure 4. 14 for location).

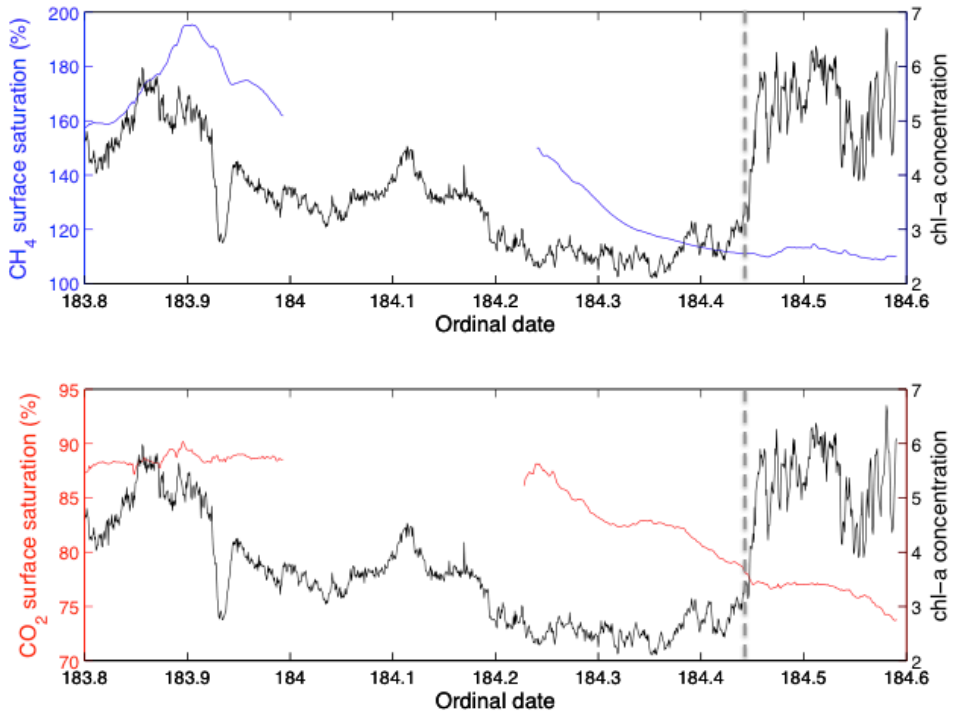

Figure 4. 18: (Top panel): Surface saturation of CH_4 and surface chl-a concentration from south to north along part of the Norwegian Trench (green line in Figure 4. 14). (Bottom panel): Surface saturation of CO_2 and surface chl-a concentration from the south to north along part of the Norwegian Trench (green line in Figure 4. 14). The dashed grey lines indicate the transition out of the Norwegian Trench into the northern North Sea.

4.4.1. 2 Discussion: The Skagerrak, Norwegian Trench and NE North Sea.

In the Skagerrak and surrounding region the predominant control on the surface supersaturation of CH_4 appears to be the input of freshwater from rivers, fjords, or the brackish inputs from the Baltic Sea. This is evident from the strong inverse relationship found between surface CH_4 and SSS. The fresher waters had a higher surface saturation for CH_4 ~130 %, indicating that rivers, fjords and/or the Baltic waters highly influenced the surface water CH_4 concentration in the Skagerrak region. Summertime CH_4 in the Baltic Sea had a mean saturation of 395 ± 8 % (July, 1992) (Bange et al., 1994). The residence time of water parcels from the Baltic to the Skagerrak have been estimated at 27 to 55 days (Stigebrandt, 1983). With a ventilation time for CH_4 of approximately 2 weeks, most of the CH_4 in the waters of Baltic origin would be expected to be lost to the atmosphere. This therefore indicates that freshwater inputs from rivers and fjords appear to be the dominant source of CH_4 in these waters. Organic material transported from rivers, fjords and the Baltic Sea may undergo methanogenesis in surface waters providing an additional source of CH_4.

Two areas within the mouth (west) of the Skagerrak, and a large area in the southern Norwegian Trench, had high concentrations of chl-a in surface waters that positively correlated with the surface supersaturation for CH_4, suggesting a link between these variables. Research has suggested that the presence of CH_4 in surface oxic waters may be due to production within small anoxic micro-niches found in decaying organic particles, faecal pellets, as well as in zooplankton intestines (Lamontagne et al., 1973, Karl and Tilbrook, 1994). More recently, research has highlighted different pathways that allow phytoplankton to utilise phosphorus and nitrogen stores in the ocean, releasing CH_4 in the process (Karl et al., 2008, Damm et al., 2010). Phytoplankton have been shown to actively release various compounds, such as methylated substrates, including methylphosphonate (Mpn) and dimethylsulfoniopropionate (DMSP). Both these substrates can be used by bacteria during methylotrophic methanogenesis for energy supply in aerobic systems. Within phosphate-limited waters CH_4 has been shown to be released as a by-product during the bacterial decomposition of Mpn (Karl et al., 2008). Alternatively, in nitrate-limited waters, where phosphate

is widely available, bacteria have displayed an ability to compete for phosphate, using DMSP as a carbon source, producing CH_4 during the process (Damm et al., 2010). A south to north gradient of reducing surface CH_4 saturation and chl-a concentration was found adjacent to the east coast of Norway in the Norwegian Trench. The gradient may have arisen as the nutrient-rich and CH_4 saturated freshwater/brackish freshwater inputs are diluted with the surrounding seawater, reducing both primary production and surface saturation for CH_4. This gradient indicates that the association between CH_4 saturation and chl-a concentration in surface waters is a consequence of freshwater/brackish water inputs into this region that are nutrient rich, and therefore stimulate primary production, and that are supersaturated for CH_4 due to methanogenesis in the anoxic sediments of rivers and estuaries.

The positive relationship found between surface saturation for CH_4 and CO in the NE North Sea (cyan region, Figure 4. 16), which occurred between approximately 2am and 2pm, may indicate a diurnal effect whereby coloured dissolved organic matter (CDOM) was undergoing increasing rates of photochemical degradation as the sunlight increased throughout the day, releasing CO (Wilson et al., 1970, Conrad et al., 1982). CDOM is found naturally in aquatic environments primarily as a result of tannins released from decaying detritus (originating from land into rivers and estuaries). Methane in surface waters simultaneously increased into the daytime, as the ship moved closer to freshwater inputs, which were more saturated than the open waters in this region. Podgrajsek et al. (2014) reported a duirnal cycle of CH_4 with high night time and low day fluxes in a Swedish lake. The durinal cycling was attributed to convective mixing at night time, bringing CH_4-rich water from the bottom of the lake to the surface and triggering bubble release from the sediment. No duirnal cycle could be found in the D366 CH_4 dataset, most probably due to the vast distances travelled within 24-hours on the ship, passing through biogeographically diverse regions with a high influence of river inputs, which may have masked any diurnal effects. Similarly, the negative correlation found between these same two parameters in the southern Norwegian Trench (black and green regions, Figure 4. 16), which took place betwwen 4.45pm and 10.30pm, can also be explained by the diurnal cycling of

CO. The production of CO decreases towards midnight as the sun went down and photolysis stopped. Simultaneous to this, surface CH_4 saturation increased as the ship moved closer to the freshwater outflow supersaturated for CH_4 in the Norwegian Trench (labelled 3 in Figure 4. 5).

4.4. 2 Central and southern North Sea

4.4.2. 1 Results: Central and southern North Sea

In the central and southern North Sea, the surface saturation for CH_4 ranged between 120 - 252 % (Figure 4. 19). The highest supersaturations, exceeding 150 % saturation, were found within the German Bight and adjacent to the Thames Estuary, at 51.50 °N, 0.58 °E (Figure 4. 19). The lowest supersaturations, reaching a minimum of 115 %, were located in two regions north of the Bight, around 55.00 °N and 56.00 °N in the central North Sea, and one area south-west of the German Bight at ~53.40 °N (Figure 4. 19).

Off the SE coast of England there were three increases in surface CH_4, shown in Figures 4. 19 and 4. 20 as A, B and C. Within, and north of the German Bight , a strong inverse relationship was found between SSS and surface CH_4 saturation, with frequent and rapid simulataneous increases and decreases in both parameters along the cruise track (Figure 4. 21).

A positive correlation was found in the blue and green regions (Figure 4. 22) of the central and southern North Sea, where increases in SST occurred simultaneously to increases in surface saturation for CH_4 over this large region ($r=0.79$ $p\leq0.05$ $n=692$) (Figures 4.A. 8 and 4. 22, Table 4. 3). Further positive correlations were identified between surface saturation for CH_4 and CO in the green region ($r=0.86$, $p\leq0.05$ $n=577$) and for CO_2 in the magenta region ($r=0.71$, $p\leq0.05$ $n=404$) (Figures 4.A. 9, 4.A. 10 and 4. 22, Table 4. 3).

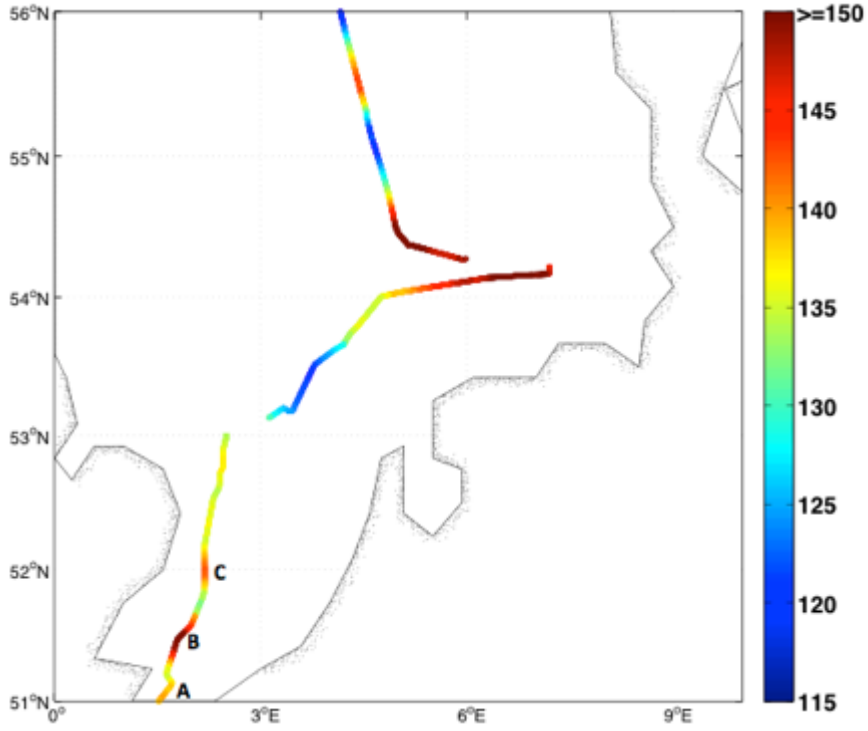

Figure 4. 19: The surface water distribution of saturation of CH_4 (%), with respect to the atmospheric value in the southern and central North Sea.

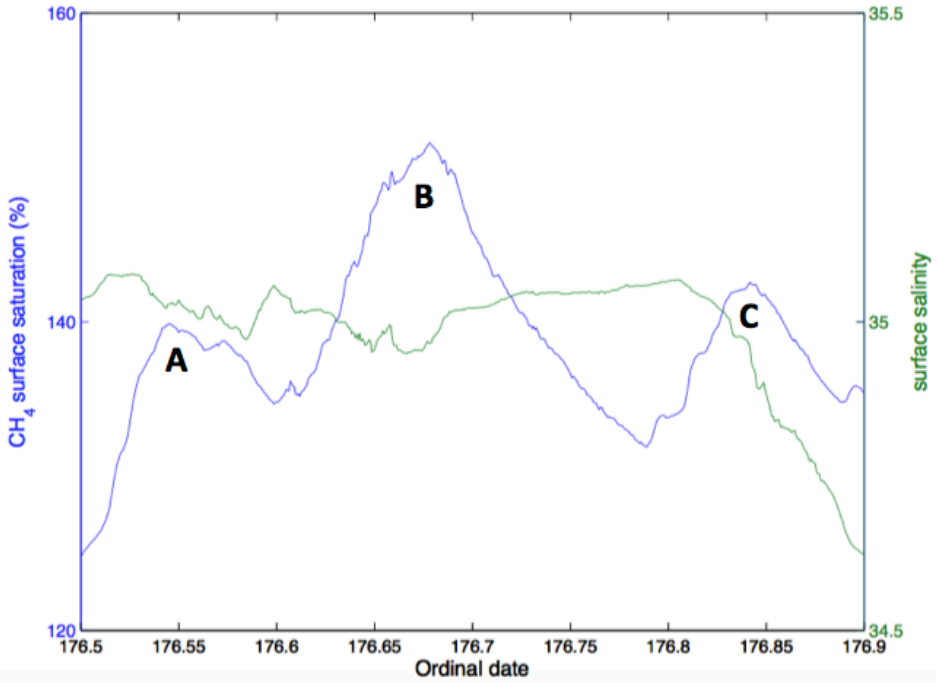

Figure 4. 20: Surface CH_4 saturation (blue) at locations A, B and C on Figure 4. 19 and surface salinity (green).

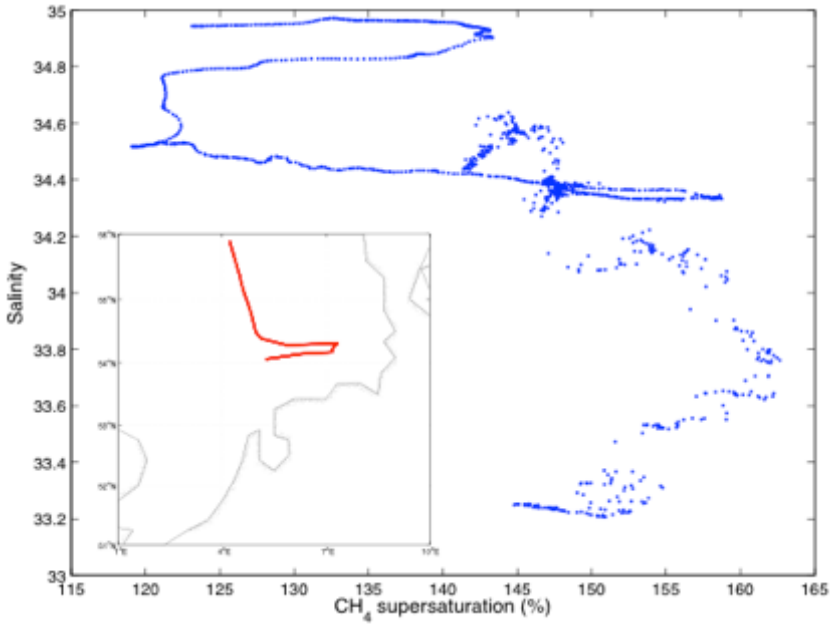

Figure 4. 21: (Large): the relationship between SSS and surface saturation of CH_4 within, and north of, the German Bight. (Small): a map showing the location of these measurements.

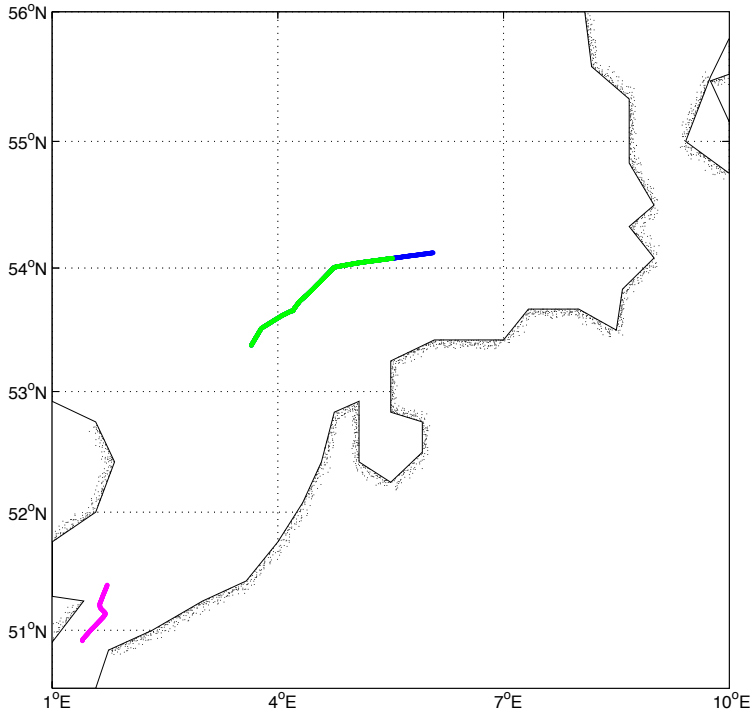

Figure 4. 22: The locations where positive correlations were found between sea surface saturation of CH_4 and SST, and surface saturation of CO and CO_2 in the central and southern North Sea (refer to Table 4. 3 for more details).

Table 4. 3: The relationship between surface saturation of CH_4 and other parameters in the southern and central North Sea.

Surface CH_4 saturation and surface parameter	Location on map	Correlation coefficient (r)	p value	n=	Figure (including Appendix figures)
SSS	A, B, C (Figure 4. 20)	-----	-----	-----	Figure 4. 20
SSS	Red (Figure 4. 22)	-----	-----	-----	Figure 4. 21
SST	Blue and green (Figure 4. 23)	0.79	≤0.05	692	Figure 4.A. 8
CO saturation	Green (Figure 4. 23)	0.86	≤0.05	577	Figure 4.A. 9
CO_2 saturation	Magenta (Figure 4. 23)	0.71	≤0.05	404	Figure 4.A. 10

4.4.2. 2 Discussion: Central and southern North Sea

The saturation for CH_4 in the central and southern North Sea ranged between 116 and 163 %. This is inline with the mean surface saturation of 126 ± 8 % (September 1991), in the German Bight reported by Bange (1994), Conrad and Seiler (1988) of 140 % in the southern North Sea (November 1980), Scranton and McShane (1991) of 113 % (95 – 130 %) in the Southern Bight (March 1989) and Rehder et al (1998) of 120 to 332 % in the central North Sea (May 1994). This region is influenced by freshwater influxes from large rivers and also inputs from extensive tidal mudflats in the Wadden Sea. Grunwald et al., (2009) found mudflats as an important source of anaerobically produced CH_4, which is released to the water column from the sediments. In tidal flat sediments Archaea produce CH_4 (Wilms et al., 2006), which then enters the water column by diffusion and advection (Hovland et al., 1993). Methane concentrations between 200 – 500 nmol L^{-1} have been measured in the Wadden Sea (Grunwald et al., 2007). Methanogenic archaea have also been reported in the oxic water column attached to photoautotrophs, which may supply methanogenic substrates as well as enable growth within anaerobic environments (Grossart et al., 2011).

Methane consumption at oxic-anoxic interfaces, attributed to micro-aerobic CH_4 oxidation at nanomolar concentrations of O_2, may act as an important control on the concentration of CH_4 found in these environments (Blees et al., 2014).

Along the SE coast of England, the surface saturation for CH_4 increased to 140 - >150 % on three occasions (Figures 4. 21 and 4. 20). Each location was adjacent to a river or estuary outflow, including Pegwell Bay, the Thames, Stour and Orwell estuaries. However, no relationship was found between SSS and surface saturation for CH_4 at any of the three locations (Figure 4. 20).

An inverse relationship between SSS and surface CH_4 was observed within and slightly north of the German Bight, where surface waters, highly influenced by freshwater influxes, were found to be the most supersaturated for CH_4, and the waters less influenced having a higher salinity and lower saturation for CH_4. This was apparent through the frequent and rapid changes in SSS observed and the simultanous inverse reponse observed in the surface CH_4 dataset (Figure 4. 21). Decreasing SSS was observed moving southwards into the German Bight towards the continental coast. This gradient was likely to have been created by freshwater inputs from large rivers, such as the River Weser, (Figure 4. 23) into the more southern regions, which may have been supersaturated for CH_4 in comparison to North Sea waters. Evidence for the relationship between CH_4 saturation and river inputs in this region arises from Grunwald et al. (2009), who observed a gradient in surface CH_4 within the River Weser. Surface concentrations of the low salinity end member were reported to reach 1860 nM (supersaturation of 7.90×10^4 %), reducing to 400 nM in close proximity to the river and outwards to approximately 50 nM in the central North Sea (Figure 4. 23). The resolution of the Grunwald et al. (2009) surface CH_4 measurements was every minute, which is sufficient to identify this gradient of surface CH_4 from the rivers to the sea. Further evidence arises from Scranton and McShane (1991) who reported high CH_4 concentrations in the Rhine between 50 and 150 nM. In addition, the Elbe, although to a much lesser extent than the Weser and Rhine, has also been shown to contribute to the high CH_4 found in the surface waters of the southern North Sea. There are currently no estimations for saturation for

this river, but the concentration at the low salinity end member of the river was measured at 80 nM (Rehder et al., 1998). The evidence therefore indicates that within the southern North Sea freshwater outflows are the dominant influence on surface CH_4 distribution.

In riverine systems, methanogenesis occurs in the anoxic sediments producing bubbles of CH_4 that will either, 1) escape the seabed and dissolve into the water column, or 2) be directly transported from the seabed to the atmosphere, leaving little trace in the water (Leifer and Patro, 2002). Characteristics of the bubbles, such as bubble size and release intensity, as well as the properties of the environment, including sediment qualities and temperature, play an influential role in the determining the transportation method (Leifer and Patro, 2002). If seepage is slow CH_4 diffuses into the water column, with only a fraction of the CH_4 reaching the surface (except in shallow seeps). At high rates of CH_4 seepage little diffusion into the water column occurs (Leifer and Patro, 2002).

In estuaries methanogenesis is influenced by the availability of dissolved sulphate (SO_4^{2-}), and the associated sulphate reducing bacteria (SRB) that outcompete methanogens (Capone and Kiene, 1988). As a result, CH_4 production decreases dramatically in a seaward direction (Abril and Borges, 2005). Due to the influence of large rivers in the German Bight and surrounding regions, and the probable inputs of CH_4, the predominant control on surface CH_4 saturation was SSS, with inverse relationships between the two parameters apparent (Figure 4. 21).

Both the surface saturation for CH_4 and CO increased into the German Bight, where the freshwater inputs were high. This could be attributed to rivers transporting more detritus into the area, meaning higher quantities of CDOM in surface waters, and the diurnal cycling of CO. As the intensity of the sun increased throughout the day and the photolysis of the CDOM increased, more CO was produced. Simultaneously, as explained previously surface waters in the German Bight were more saturated in CH_4 than surrounding regions due to the large freshwater influxes of waters supersaturated in CH_4, and therefore surface

CH_4 also increased. Alternatively, the CO could have been produced in the rivers and transported into the sea.

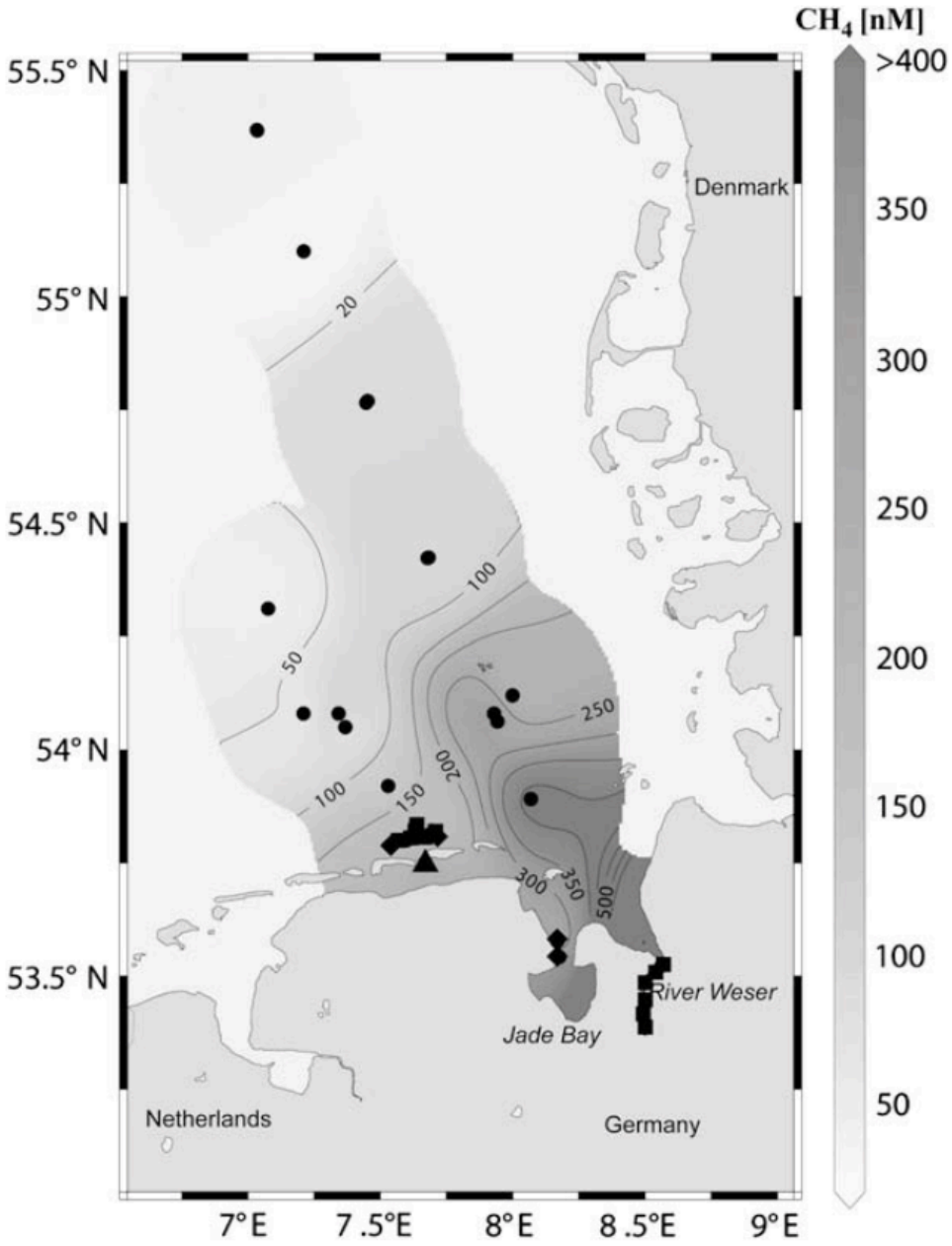

Figure 4. 23: CH_4 concentration (nM) measured in the German Bight, River Weser and the surrounding region. Squares: show data from cruise HE188 (May, 2003); circles display data from HE238 (September, 2005), and triangles: time-series data (October-November, 2005). From Grunwald et al., (2009). Contours are displayed for 50 – 400 nM CH_4.

4.4. 3 Southern Irish Sea

4.4.3. 1 Results: Southern Irish Sea

In this region, the majority of surface waters south of 52.50 °N were found to be saturated to supersaturated for CH_4, at 100 – 110 %. The surface waters with the highest supersaturation for CH_4 (up to 320 %) were located mostly north of 52.50 °N (Figure 4. 24). Within the northern section of this area, an inverse relationship was found between SSS and surface saturation of CH_4, with the exception of a small area, where this relationship broke down (Figure 4. 25; Figure 4. 26: green section). This was the most northern point during this section of the cruise. In the red and the blue regions, shown in Figure 4. 27, positive correlations were found between SST and surface saturation for CH_4 ($r = 0.61$, $p \leq 0.05$, $n = 1009$) and CO and CH_4 surface saturation ($r = 0.98$, $p \leq 0.05$, $n = 433$; Table 4. 4; Figures 4.A. 11 and 4.A. 12).

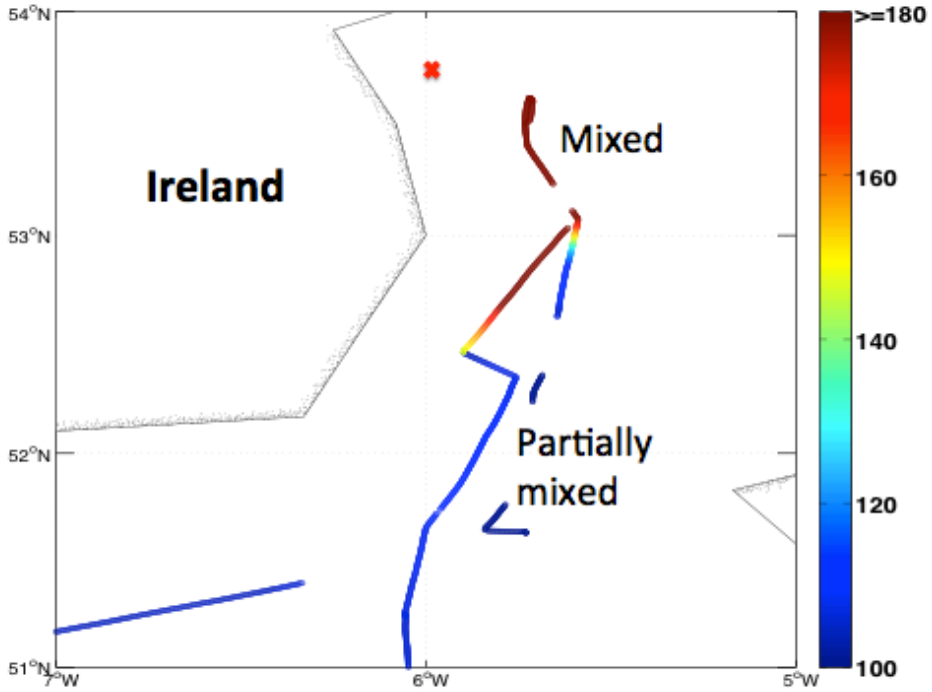

Figure 4. 24: The surface water distribution of saturation of CH_4 (%), with respect to the atmospheric value in the SW Irish Sea. The red cross indicates the approximate location of Dublin Bay.

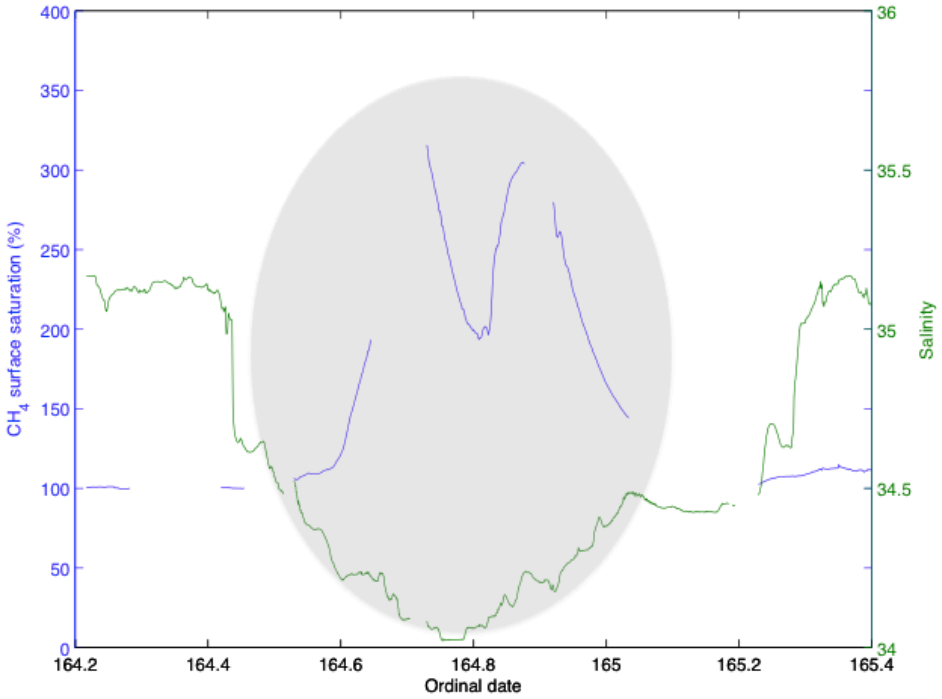

Figure 4. 25: Sea surface salinity and surface CH_4 saturation in the Irish Sea. The shaded area shows the inverse relationship found between SSS and surface CH_4 (which breaks down in the middle-at the most northern point) found in the green region (Figure 4. 26) of the SW Irish Sea.

Table 4. 4: Relationships between surface saturation of CH_4 and other measured parameters in the SW Irish Sea. Refer to Figures 4. 26 and 4. 27 for the locations.

Surface CH_4 saturation and surface parameter	**Location on map**	**Correlation coefficient (r)**	**p value**	**n=**	**Figure (including Appendix figures)**
SSS	Green (Figure 4. 26)	------	------	----	Figure 4. 25
SST	Red (Figure 4. 27)	0.61	≤0.05	433	Figure 4.A. 11
CO saturation	Blue (Figure 4. 27)	0.98	≤0.05	1009	Figure 4.A. 12

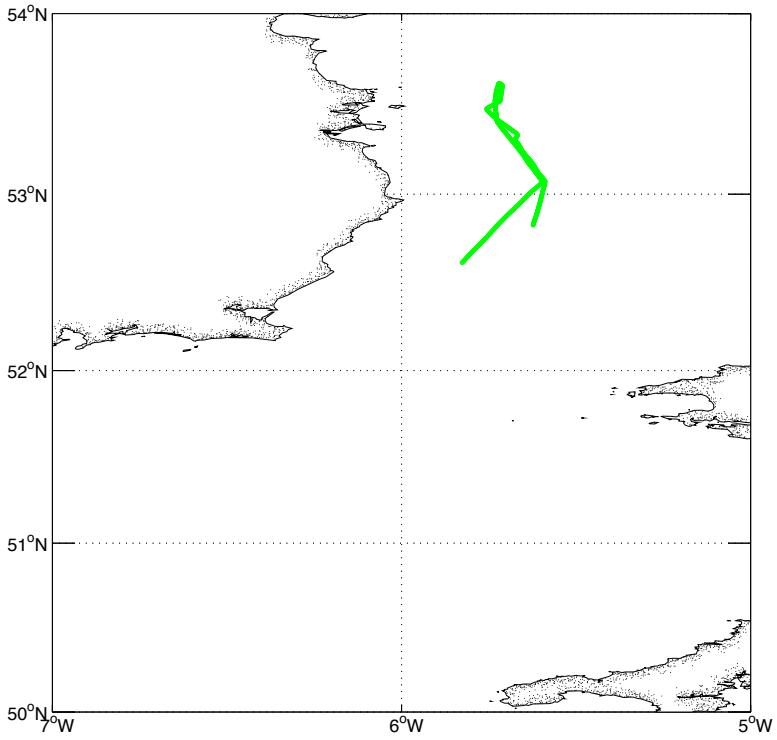

Figure 4. 26: The green line shows the location of the inverse relationship found between SSS and surface saturation of CH_4 (shaded area in Figure 4. 25).

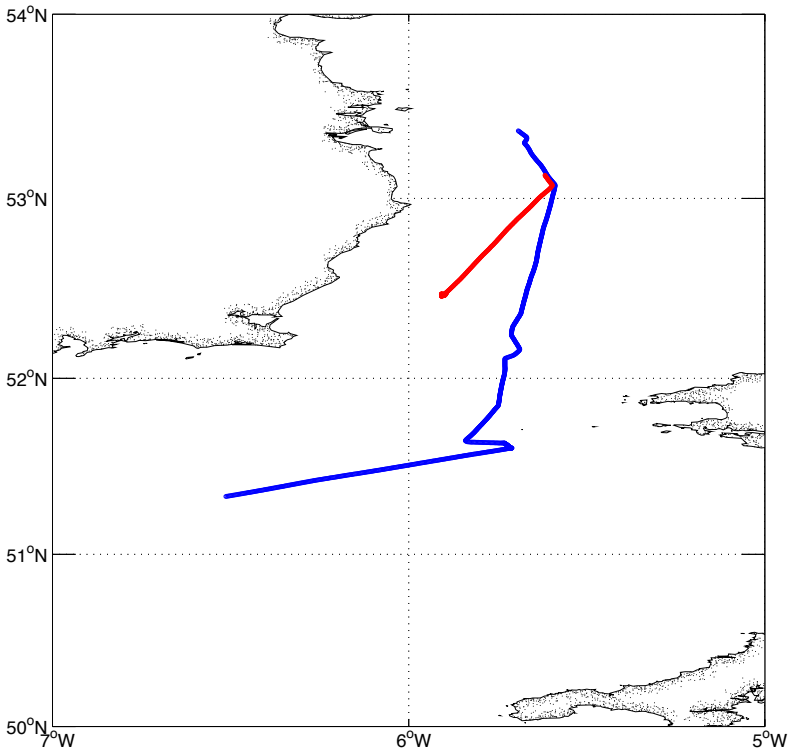

Figure 4. 27: The locations where positive correlations were identified between surface saturations of CH_4, CO and SST in the Irish Sea (Table 4. 4).

4.4.3. 2 Discussion: Southern Irish Sea

In the surface waters of the Irish Sea, the highest saturation for CH_4 was found in the region south of Dublin Bay, reaching supersaturations of up to 315 % (Dublin Bay: indicated by red cross: Figure 4. 24; 53.35 ° N and 6.30 ° W). The inflow of freshwater to Dublin Bay is from rivers. The fresher waters, presumably supersaturated for CH_4, from Dublin Bay mixed with the sea surface waters closest to this location, consistent with the inverse relationship between SSS and surface CH_4 saturation in that region (green region: Figure 4. 26). The water column furthest from the mouth of Dublin Bay was fully mixed. If CH_4 were produced by methanogenesis in the sediments of this region, it would have provided an additional source as it was mixed to the surface. In the blue region (Figure 4. 27) there was a positive correlation between surface CH_4 and CO, which could be due to the diurnal cycling of CO and increases surface CH_4 saturation produced by freshwater inputs from the Dublin Bay.

4.4. 4 English Channel

4.4.4. 1 Results: English Channel

Surface waters in the English Channel were supersaturated for CH_4 (105 to >140 %)(Figure 4. 28). A general trend of increasing surface saturation for CH_4 (from 105 to 135 %) and decreasing salinity (from 35.50 to 34.00) was apparent, moving from the west to the east of the English Channel into the North Sea (Figure 4. 29). The highest surface saturation for CH_4 was found between 2.00 to 2.50 ° W off the south coast near Weymouth/ Portland Bill, exceeding 140 % (Figure 4. 28). During this period the ship sailed very close to the coast for approximately six hours. A strong positive correlation was found between surface water CH_4 and CO saturation in the red region (Figure 4. 30) ($r=0.99$, $p=\leq 0.05$, $n=763$; Table 4. 5; Figure 4.A. 13).

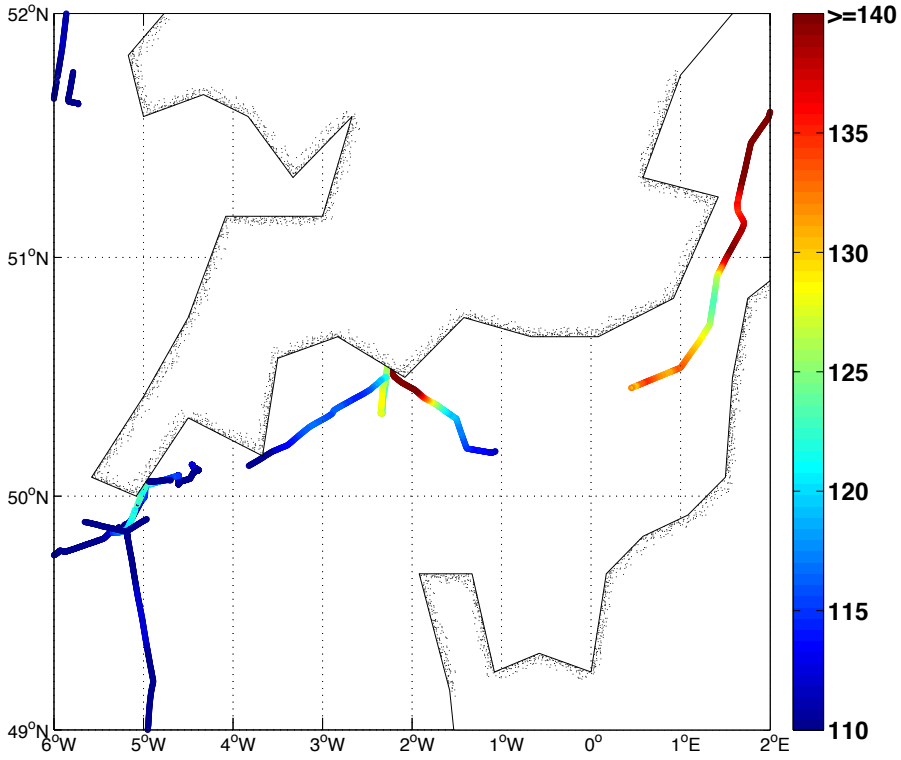

Figure 4. 28: The surface water saturation distribution of CH_4 (%), with respect to the atmospheric value in the English Channel.

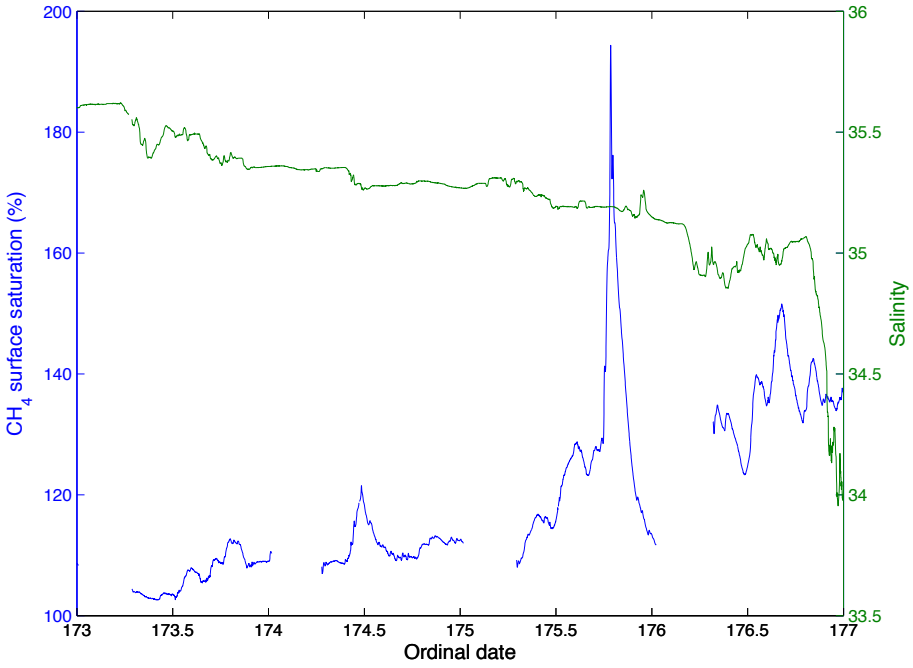

Figure 4. 29: The relationship between SSS and surface saturation of CH_4 along the English Channel (west to east).

Table 4. 5: The relationship between surface CH_4 and CO saturation in the English Channel (refer to Figure 4. 32 for location).

CH_4 saturation and parameter	**Location on map**	**Correlation coefficient (r)**	**p value**	**n=**	**Figure (including Appendix figures)**
CO saturation	Red	0.99	≤0.05	763	Figure 4.A. 13

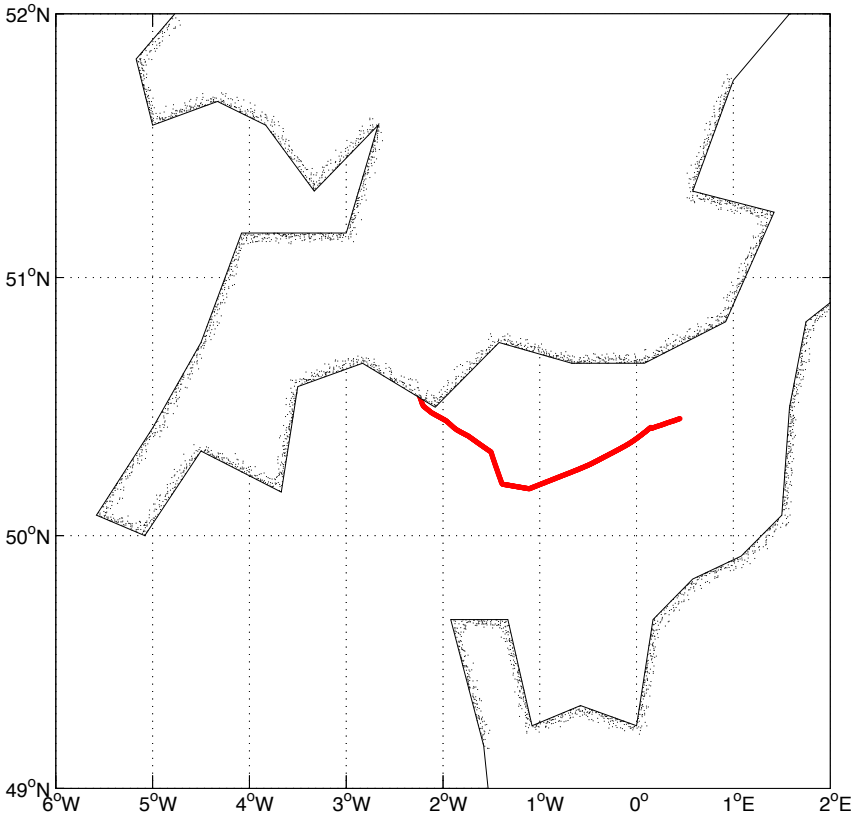

Figure 4. 30: The location where a positive correlation was found between surface CH_4 and CO saturation (Table 4. 5).

4.4.4. 2 Discussion: English Channel

The salinity in the English Channel decreased from the more saline Atlantic waters to the slightly fresher waters found on the east side of the Channel, due to higher freshwater influxes from rivers and estuaries entering the system. As the freshwater from many rivers and estuaries is more saturated for CH_4 due to methanogenesis in sediments than seawater, this could explain this gradual increase in surface saturation from the west to the east side of the Channel. In addition to this, the water column becomes fully mixed in the east side of the English Channel. A fully mixed water column could mix CH_4 produced in the sediments of the shelf seas throughout the water column, increasing the saturation. The surface waters found most saturated for CH_4 were located adjacent to the coast off Portland Bill/Weymouth, and can be assumed to be influenced by freshwater, supersaturated for CH_4, from land due to the ship's close proximity.

There was a strong positive correlation between surface saturation for CH_4 and CO from approximately 2.5 ° W across to 0.5 ° E along the cruise track, which took place from approximately 7.30 am till 8.00 pm. As discussed earlier, this relationship is most probably due to the simultaneous photochemical degradation of CDOM, releasing CO, which increased throughout the day, with an increase in the surface CH_4 in the east of the English Channel, due to an increase in freshwater inputs supersturated for CH_4 and a fully mixed water column.

4. 5: Conclusions

The distribution of surface CH_4 found in the NW European shelf seas environment is a consequence of the sources and sinks for this trace gas. The predominant source of CH_4 in the marine environment is methanogenesis, which occurs in anoxic environments, although the production of CH_4 within oxic environments (the methane paradox) has also been described (Lamontagne et al., 1973, Scranton and McShane, 1991, Bange et al., 1994, Bange et al., 1996b, Upstill-Goddard et al., 2000, Bange, 2006, Karl et al., 2008, Grunwald et al., 2009, Damm et al., 2010). The main sinks for CH_4 are microbial oxidation, which can

occur both in oxic and anoxic environments, as well as loss to the atmosphere through air-sea exchange. Within the NW European shelf seas the marine sources were greater than the sinks, resulting in all surface waters being supersaturated for CH_4, with an average saturation of 118.38 ± 21.67 %, producing an ocean-atmosphere flux of 2315.40 ± 3691.30 nmol m^{-2} d^{-1}. The mean surface saturation calculated for CH_4 during the D366 is within the measurement uncertainties of that calculated by Bange (2006) for the European shelf sea at 224 ± 142 %, which included regions not sampled during the D366, such as the Mediterranean Sea.

Saturation for CH_4 in the NW European shelf seas generally increased towards the coast. Surface waters with the highest supersaturations were estimated between 120 to 315 %, and located within the Skagerrak and Norwegian Trench, the German Bight, the SE North Sea, the English Channel and the SW Irish Sea. These regions were subject to freshwater and/or brackish inflows from rivers, estuaries and the Baltic Sea. Most of these areas displayed an inverse relationship between SSS and saturation for CH_4, with fresher waters associating with higher saturations for CH_4, supporting the link between the two parameters. Rehder et al. (1998), Upstill-Goddard et al. (2000), Bange (2006) and Grunwald et al. (2009) also reported freshwater inputs into the marine environment to act as a source of CH_4. The relationship between SSS and surface CH_4 saturation can clearly be observed in three locations during the D366 cruise, in the Skagerrak, in the Norwegian Trench and in the Irish Sea in close proximity of Dublin Bay (Figure 4. 5). Different freshwater end-members had varying saturations for CH_4, with surface waters around Dublin Bay region greatly exceeding the others at 315 %. These differences reflect the amount of CH_4 produced within each freshwater/brackish water system. High non-linear relationships between SSS and CH_4 concentrations were also identified by Upstill-Goddard et al. (2000) in the southern North Sea. Methane is produced in organically enriched coastal, estuarine and riverine systems by methanogenesis, with saturations of up to 7.0 x 10^4 % measured in river systems (low salinity end member in the Weser river) (Grunwald et al., 2009) and 2.2 x 10^4 % in estuaries (Tyne estuary) (Upstill-Goddard et al., 2000), respectively. Methane has a fast

equilibration time with the atmosphere (estimated at approximately two weeks during the D366 cruise). Regardless of this, the high production of CH_4 within rivers and estuaries, results in supersaturation of CH_4 in surface waters of the shelf seas surrounding these environments. Gradients from fresher surface waters, with a high saturation for CH_4, to more saline waters, with lower saturation for CH_4, were found from the surface waters influenced by outflows of rivers and estuaries out into the open shelf seas. Methane production in estuaries decreases in a gradient from fresher to more saline water (Abril and Borges, 2005), due the availability of dissolved sulphate (SO_4^{2-}), and the presence of sulphate reducing bacteria (SRB) that outcompete methanogens (Capone and Kiene, 1988).

High surface saturations for CH_4 (110 to 210 %) were found between the ordinal dates of 175.0 and 184.5. This is the region from the eastern English Channel up to the Norwegian Trench. The region from the eastern English Channel to the central North Sea had a fully mixed water column (Figure 3. 9). This may have influenced surface waters by mixing CH_4 produced in anoxic sediments by methanogenesis to the surface.

In close proximity of freshwater inputs, detritus in the water column is enhanced due to land runoff. As the detritus decays, tannins are released producing coloured dissolved organic matter (CDOM). CO is released from the CDOM by photolysis (Wilson et al., 1970, Conrad et al., 1982). On several occasions during the D366, positive correlations were identified between between the surface saturation for CH_4 and CO. The correlations were found to occur from early morning throughout the day and are believed to be linked to the duirnal cycling of CO, with the photolysis of CDOM increasing as the sunlight increases in intensity towards the afternoon maximum. In regions where the ship was moving towards freshwater inflows, the surface saturation for CH_4 was also found to increase creating the relationship between these two parameters.

In the Skagerrak region and the Norwegian Trench, positive correlations were identified between surface saturation for CH_4 and surface chl-a concentration. The relationship between these two parameters could either be assigned to:

1) Methane being produced in oxic surface waters where phytoplankton are abundant, within small anoxic microenvironments where methanogenesis can occur (Lamontagne et al., 1973, Karl and Tilbrook, 1994).

2) Methane being produced by bacteria for energy in aerobic systems in nutrient-limited surface waters (Karl et al., 2008, Damm et al., 2010).

3) The association between high surface CH_4 and surface chl-a concentration may be due to the fresh/brackish water inputs in this region that are high in nutrients, stimulating primary production, but also supersaturated for CH_4. This is the most likely explanation in the regions described as the associations occurred in close proximity to freshwater outflows.

Chapter 5: Surface nitrous oxide and methane in the Atlantic Ocean

5. 1: Introduction

This chapter discusses surface CH_4 and N_2O measurements across the Atlantic Ocean from Southampton, UK, to Punta Arenas, Chile, in September and October 2012, on the Atlantic Meridional Transect cruise 22 (AMT22). The processes influencing the surface concentration and saturation state of both trace gases are explored. This chapter also compares the dataset to an additional four-high resolution surface ocean N_2O datasets collected on the AMT programme (Bale, 1996, Rhee et al., 2009, Grefe, 2013, Zubkov, 2013).

5.1. 1: Aims

This chapter aims to quantify the surface concentration, saturation and ocean to atmosphere flux of CH_4 and N_2O in the boreal autumn and austral spring seasons of 2012. The chapter describes the fundamental processes affecting the surface N_2O and CH_4 in the Atlantic Ocean, including the influence of seasons on the surface saturation and ocean to atmosphere fluxes of these trace gases. The chapter compares five high-resolution surface water N_2O datasets collected over an eighteen-year period, from 1996 to 2013, during the AMT programme to determine whether a change in the source-sink characteristic of surface N_2O has occurred during this time period.

5.1. 2: Objectives

The specific objectives of this chapter are:

- To quantify the mean surface concentration and saturation of CH_4 and N_2O in the Atlantic Ocean in the boreal autumn and austral spring of 2012.
- To identify whether the Atlantic Ocean acted as a CH_4 and N_2O source or sink during this period.
- To identify whether the surface saturation and the ocean to atmosphere flux of CH_4 and N_2O varies seasonally.

- To describe the processes influencing the surface concentration and saturation of CH_4 and N_2O along the AMT transect.
- To determine whether a temporal change in surface concentration and saturation has taken place over the eighteen years that high-resolution surface N_2O measurements have been made along the AMT transect in the Atlantic Ocean.

5.1. 3 Hydrography of the AMT transect

A detailed oceanographic review of the AMT transect region is available by Aiken et al., (2000), but details important to this project are summarised below.

5.1.3. 1: Topography

The AMT program samples from waters overlying many regions of the Atlantic Ocean including: the UK continental margin, the Porcupine and Iberian Plain, the Canary Basin, the Cape Verde plateau, the Brazil Basin, the Argentine Basin and the South American continental margin (Aiken et al., 2000). Most of these regions have depths greater than 3000 m, with the exception of the UK continental margin and the South American shelf. From the north of the Atlantic Ocean (Iceland) to the south (Tristan da Cunha and Bouvet Island), the Mid-Atlantic Ridge divides the ocean into two elongated depressions (the Eastern and Western Atlantic troughs), reaching depths of 5000 m (Aiken et al., 2000).

5.1.3. 2: Circulation

The major circulation features relevant to the AMT cruise tracks are shown in Figure 5. 1. The Gulf Stream (GS) enters the NE Atlantic in the form of two currents, the North Atlantic Current (NAC) and the Azores Current (AC). The AC is derived from the north subtropical Atlantic gyre (NAG), which is bordered by the Portugal Current (PC), the Canary Current (CC) and the North Equatorial Current (NEC). The equatorial surface currents consist of: 1) the NEC flowing in a westward direction across the Atlantic, north of 10 °N; 2) the North Equatorial Counter Current (NECC), which is seasonal and most powerful during boreal autumn and almost non-existent during February, flowing in an easterly direction between 3 and 9 °N to depths of 100 m; and 3) the South Equatorial

Current (SEC), which flows in a westward direction from 3 to 15 °S. The south Atlantic subtropical gyre (SAG) is bordered by the SEC, the Brazil Current (BC), the South Atlantic Current (SAC) and the Benguela Current (BenC) (Aiken et al., 2000). The Brazil-Malvinas Confluence Zone (BMCZ) is a region where the warm and saline Brazil Current (BC), which flows in a pole-ward direction parallel with the Brazilian Coast, converges with the cold, fresher Falklands Current (FC) (Malvinas Current), which travels towards the equator along the western edge of the Argentine Basin. The BMCZ is characterised by complex circulation patterns and high energy (Gordon, 1981).

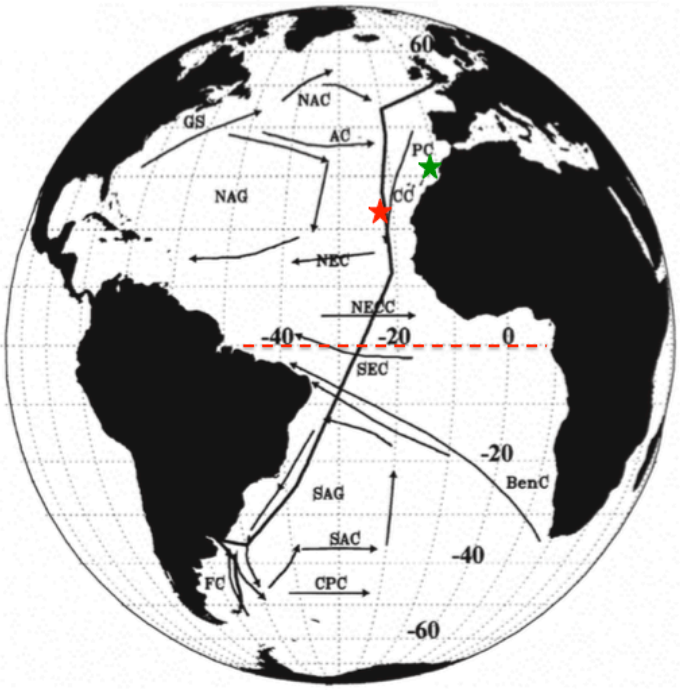

Figure 5. 1: The major circulation patterns in the Atlantic Ocean that influence the AMT cruise track. The black line shows the AMT-2 cruise track. The abbreviations are as follows: Gulf Stream (GS), North Atlantic Current (NAC), Azores Current (AC), Portugal Current (PC), Canary Current (CC), North Equatorial Current (NEC), South Equatorial Current (SEC), the Brazil Current (BC), the South Atlantic Current (SAC) and the Benguela Current (BenC) and the North Equatorial Counter Current (NECC). The red dashed line indicates the equatorial upwelling, the red star the Guinea Dome upwelling region and the green star the western African Upwelling system. Adapted from Aiken et al., (2000) and Tomczak and Godfrey (1994).

5.1.3. 3: Physical structures in the Atlantic Ocean

Different physical structures exist in the Atlantic Ocean, including oligotrophic subtropical gyres (NAG and SAG), eutrophic upwelling regions, and convergence zones of high variability (e.g. BMCZ). These structures influence productivity in the water column and also potentially the surface concentration and saturation of N_2O and CH_4. Three important regions of upwelling are described below (Figure 5. 1).

1. The equatorial upwelling is the result of the Coriolis force, which drives the currents north and south of the equator to deflect in opposite directions. This produces a zone of divergence where deep nutrient-rich waters replace the surface waters (Mann and Lazier, 2006).
2. The Guinea Dome upwelling region, found between 10 and 15 °N, 22 °W in the Atlantic Ocean, occurs as the NECC approaches the African coast, on the eastern boundary, and the water splits both left and right, eventually joining the NEC and SEC. During this process, a cyclonic gyre is generated enclosing the ascending water masses. Sea surface water in the Guinea Dome is similar physically, chemically and biologically to that in the equatorial upwelling region and supports a rich phytoplankton bloom downstream of the upwelling region (Blackburn, 1981).
3. Upwelling off western Africa occurs between 20 and 25 °N throughout the year. South of 20 °N, upwelling is strong throughout winter and spring, and north of 25 °N in summer and autumn (Van Camp et al., 1991).

In addition to the upwelling systems described, other important physical features include the NECC, which transports productive water from the Amazon plume outflow in an easterly direction, between 3 and 9 °N, across the Atlantic Ocean (Muller-Karger et al., 1988), and the inter-tropical convergence zone (ITCZ). The ITCZ is a narrow zone near the equator where the northern and southern trade winds converge, producing low atmospheric pressure and elevated rainfall.

5.1.3. 4: Physical-biological structures in boreal autumn/austral spring

During boreal autumn in the northern extremes of the Atlantic Ocean (north of 40 °N), the water column is partially or deeply mixed after the autumn breakdown of stratification. The water column in the southern extreme (south of 40 °S) is partially mixed or stratified, as warming in the spring heats the surface waters. The water column north and south of the subtropical gyres is stable, has good nutrient availability and moderate light levels. As a result of these conditions, the surface ocean phytoplankton biomass is greatest in these regions of the AMT transect. Moving from the temperate to subtropical waters in the NH, autumn-time stratification occurs, with a subsurface florescence maximum in the thermocline at around 40 to 50 m. In September the austral spring phytoplankton bloom is more productive than the boreal autumn bloom. The tropical Atlantic Ocean has a permanently stratified water column with a deep-mixed layer, reaching depths of over 100 m (Aiken et al., 2000). Low macronutrient concentrations (<0.2 μM) are found throughout the subtropical and tropical regions of the AMT transects.

The AMT passes through seven biogeographical provinces (NADR, CNRY, NAST, NATR, WTRA, SATL, SSTC), defined by Longhurst (1998), on the basis of satellite imagery (CZCS), supported by other measurements including light, near surface hydrography, nutrient distribution and plankton ecology (Figure 1 .6). Many AMT studies have used these provinces to help analyse their datasets e.g. Forster et al. (2009), Hill et al. (2011) and Brotas et al. (2013). Forster found N_2O depth profiles to be amenable to analysis on the basis of Longhurst provinces, showing common features within the biogeographical regions. Methane profiles did not show this pattern (Forster et al., 2009).

5. 2: Methods

5.2. 1: Comparison of AMT N_2O datasets

5.2.2. 1: Data sources and distribution measurements of all four gases (N_2O, CO, CH_4 and CO_2) occurring. For more

All the AMT cruises that are compared in this chapter left the UK in the boreal autumn (September/October) and arrived into South America in austral spring (October/November). The high-resolution measurements were made using different instrumentation, including detection by Electron Capture Detection (ECD) and Integrated Cavity Output Spectrometry (ICOS). Table 5. 1 displays the details regarding each research cruise in the collection of the datasets. Three types of equilibrator were used during the five AMT cruises. During AMT7 the Weiss-type equilibrator (Butler et al., 1988, Weiss et al., 1992) had a significantly greater headspace at 21 L , than the showerhead equilibrator used during AMT3, at 1 L (Bale, 1996) and the percolating packed glass bed equilibrator (Cooper et al., 1998) used during AMT20, 22 and 23, at ~0.2 L (Grefe and Kaiser, 2013; Tarran, 2012; Zubkov, 2013). The water flow rate through the equilibrator was also faster at 24 – 30 L min^{-1}, compared to 0.75 L min^{-1} (AMT3) and 1.8 L min^{-1} (AMT20, 22 and 23) .

Table 5. 1: Measurement characteristics for each research cruise.

Cruise	Date	Ship	Discrete (CTD)/ continuous (underway)	Instrument for N_2O detection	Sampling depth	Type of equilibrator	Standards	Atmospheric data	Publication
AMT3	26.09.96 - 25.10.96	RRS JCR	Continuous	Shimadzu ECD	6 m	Showerhead-type equilibrator (NH) and phase contactor (LiquiCell) (SH)	Working standards (307.80 and 362.20 nmol mol^{-1}) cross-calibrated against NOAA/CMDL reference gas	Not measured.	Bale (1996)
AMT7	14.09.98 – 25.10.98	RRS JCR	Continuous	(Automated) Hewlett-Packard gas chromatograph (HP 5890) with ECD.	6 m	Weiss-type equilibrator	Standards: (277.70±0.40 and 349.60±0.20 nmol mol^{-1}), cross-calibrated against SIO-1993 standard scale.	Hourly through sampling inlet at foremast of ship.	Rhee et al., (2009)
AMT20	12.10.10 – 25.11.10	RRS JC	Continuous	ICOS N_2O/CO analyser (Los Gatos Research, model N_2O/CO-23d) connected to a 1.7 L glass bed equilibrator.	5 m	1.7 L percolating packed glass bed Weiss-type equilibrator	Dried air as a working reference. N_2O content was 323.70 nmol mol^{-1}, calibrated against IMECC/NOAA standards.	Every 8 hours from the ship's bow. Mean value taken of the final 5 minutes of a 20-minute run.	Grefe and Kaiser (2013)
AMT22	10.10.12 – 24.11.12	RRS JC	Continuous	As AMT20	5 m	As AMT20	Three certified reference standards (298.07, 325.47, 344.07 nmol mol^{-1}, calibrated against IMECC/NOAA standards.	Every 4 hours from the Monkey Island. Mean value taken from final 5 minutes of a 10-minute run.	Tarran (2012)
AMT23	07.10.13 – 08.11.13	RRS JCR	Continuous	As AMT20	6 m	As AMT20	As above with reference standards of 300, 320, and 340 nmol mol^{-1}.	Air measured every 12 hours, (Monkey Island) Mean value from final 5 minutes of a 20-minute run.	Zubkov (2013)

*** ECD for Electron Capture Detector; *ICOS for Integrated Cavity Output Spectrometry;**

***JCR for James Clark Ross; *JC for James Cook**

5.2.2. 2: Cruise tracks

During the eighteen years of measurements, two main cruise tracks can be distinguished between the UK and South America (Figure 5. 2). The first, including AMT3 and 7, sampled the West African Upwelling system (WAU) and along the east coast of South America, measuring within the western part of the South Atlantic Subtropical Gyre (SAG). The second cruise track during AMT20, 22, and 23, sampled further west in the NH and east in the SH into the North Atlantic Subtropical Gyre (NAG) and the SAG, with a more central route down the Atlantic Ocean. AMT23 did not travel as far west in the northern hemisphere as AMT20 and AMT22 (Figure 5. 2).

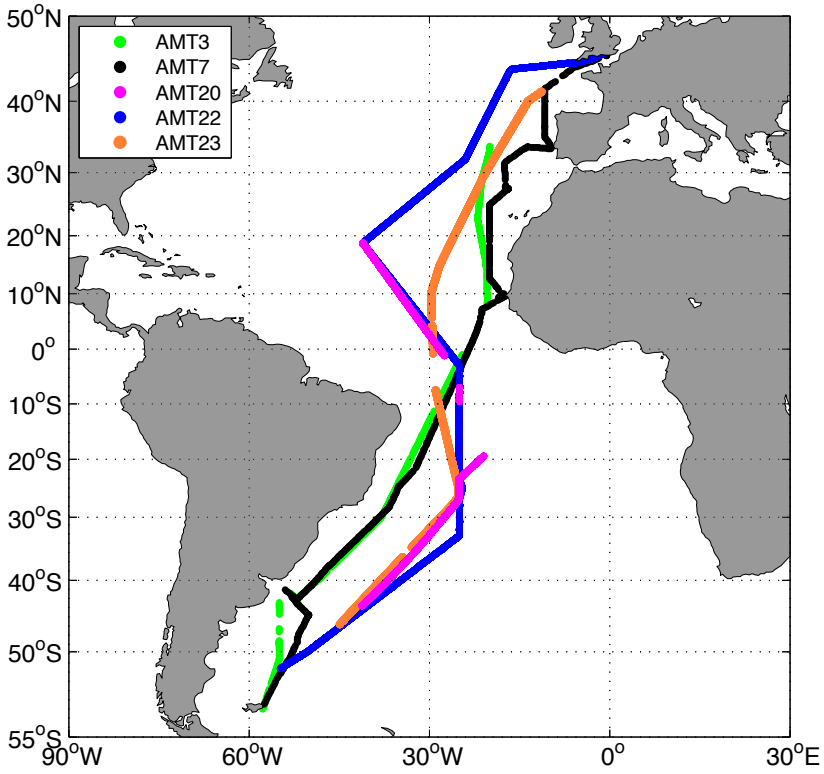

Figure 5. 2: The cruise tracks for the five surface N_2O AMT datasets.

5.2.2. 3: Atmospheric concentrations

Atmospheric measurements for N_2O were not made during AMT3. To ensure that the N_2O saturations estimated for each dataset were comparable, the monthly mean atmospheric value for the year of each cruise was used with one value for the NH, as taken from Mace Head (AGAGE, 1994-03 -2014-03), and one for the SH as taken from Cape Grim (AGAGE, 1993-08 -2014-03).

5.2.2. 4: Surface water concentration and saturation measurements

The authors of each dataset calculated surface water concentrations from their measurements. The datasets were corrected for temperature effects on the solubility of N_2O, and for the effects of water vapour (Weiss and Price, 1980). The surface seawater concentration (Csw), was calculated by multiplying the dry mole fraction of N_2O (x') with the solubility coefficient F (mol kg^{-1} atm^{-1}) (as a function of equilibrator temperature and salinity) (Weiss and Price, 1980), and pressure (atms) (P) (assumed to be equal to atmospheric pressure) (Equation 5. 1). Surface saturation estimates (s) were calculated from the sea surface water concentration (Csw) and the atmospheric equilibrium concentration (x' atmos * F (Tin,S) * P) (Equation 5. 2). The equilibrium value was calculated from the dry mole fraction of N_2O in the atmosphere, F (as a function of SST and salinity) and atmospheric pressure. Saturation calculations were based on gravitational concentration units (nmol kg^{-1}).

$$Csw = x' * F\ (Tequil, S) * P$$

Equation 5. 1

$$\mathrm{s} = \left(\frac{Csw}{(x'atmos * F(Tin, S) * P)}\right) * 100$$

Equation 5. 2

5.2.2. 5: Selection of regions

All five datasets were binned into three latitudinal regions, with each containing as many of the datasets as possible. The regions were located at 30 – 40 °N, 10 °N – 10 °S and 10 – 30 °S. The three regions deliberately avoided the highly variable Brazil-Malvinas Confluence Zone (BMCZ) with the associated eddies and frontal activity, as well as the WAU. This is because high regional variability makes it difficult to get accurate mean concentration and saturation values for comparison. The region at 30 – 40 °N fell within the NAST (E) Longhurst province, 10 °N – 10 °S in the WTRA and SATL provinces, and 10 – 30 °S in the SATL province.

For the temperate to subtropical North Atlantic region (30 – 40 °N), the measurements were made in the boreal autumn. During this season, surface waters at this latitude are subject to seasonal cooling and stratification of the water column (Aiken et al., 2000), limiting mixing from deeper waters to the surface. The different cruise tracks varied in longitude from the European and African coast (AMT7) to the NAG, with AMT22 sampling furthest west into the NAG. The water column in the tropical region (10 °N – 10 °S) is permanently stratified, with a low nutrient availability in surface waters (Aiken et al., 2000). Two main cruise tracks occurred in this region. The first, consisting of AMT3 and 7, travelled from West African coastal waters in a southwest direction. The second route, taken during AMT20, 22 and 23 followed a more central route across the Atlantic, with AMT23 crossing the equator further west than the others. For the temperate to subtropical South Atlantic region (10 - 30 °S), measurements were made in the austral spring. Surface waters at this latitude during spring are subject to surface warming, are well mixed from winter and have a productive spring phytoplankton bloom in September (Aiken et al., 2000). The different cruise tracks varied in longitude from 25 – 35 °W in this region.

5. 3 Results

5.3. 1: Surface methane across the AMT22 transect

The mean surface saturation for CH_4 calculated across the AMT22 transect was 107 ± 5 % (Figure 5. 3: top), mean surface concentration was 2 ± 0 nmol L^{-1} (Figure 5. 3: middle), and the mean ocean to atmospheric flux was 3.57 x 10^2 ± 3.28 x 10^2 nmol m^2 d^{-1} (Figure 5. 3: bottom), making the Atlantic Ocean an atmospheric source of CH_4. Sea surface temperature, salinity and windspeed are shown along the AMT22 transect in Figure 5. 4. The surface saturation along the transect ranged from 100 to 135 %, with the highest saturations located between the latitudes of 4 to 8 °N, and the second highest 23 to 27 °N (Figures 5. 3 and 5. 5). Neither of the areas with elevated surface CH_4 were found to be regions of upwelling (Figures 5. 6 and 5. 7). The region located between 4 and 8 °N had a lower salinity than the surrounding latitudes, (Figure 5. 4: top). This is most likely to be due to high rainfall or humidity verses evaporation issues (discussed further in section 5.4.1). The region located between 23 and 27 °N was the section of the cruise track that was furthest west into the NAG (Figure 5. 5 and 5. 7). A strong negative relationship was found between the surface concentration of CH_4 and SST across the AMT22 cruise ($r=-0.74$, $p=<0.05$, Spearman's correlation), which broke down at SST's greater than 28 °C (Figure 5. 8). During the AMT22, significantly higher surface saturations and ocean to atmosphere fluxes for CH_4 were observed in the northern hemisphere (NH) (15 to 41 °N), at 107 ± 4 % and 4.26 x 10^2 ± 3.53 x 10^2 nmol m^2 d^{-1}, than in the southern hemisphere (SH) (15 to 41 °S), at 105 ± 3 % and 2.67 x 10^2 ± 3.18 x 10^2 nmol m^2 d^{-1} (two-sample t-test, n=17122, h=1, p=0) (Figure 5. 9 and 5. 10). Forster et al (2009) also found higher fluxes of CH_4 in the NH than in the SH during AMT13 (during the same seasons), but these were an order of a magnitude larger than those of AMT22, at 6.23 x 10^3 nmol m^2 d^{-1} and 4.40 x 10^3 nmol m^2 d^{-1}.

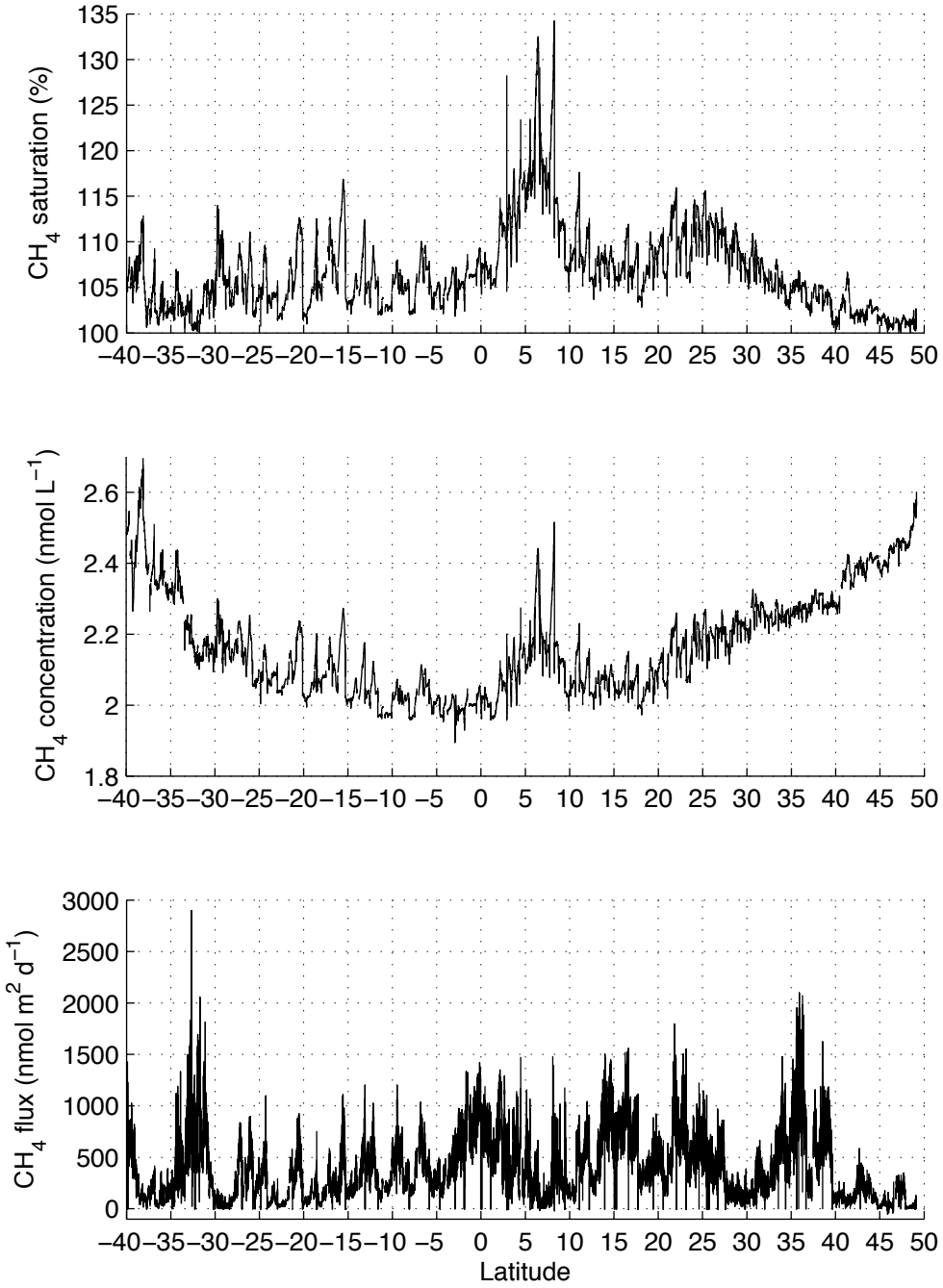

Figure 5. 3: (Top) The sea surface saturation of CH_4 along the AMT22 cruise track. Positive numbers indicate the NH and negative numbers the southern hemisphere. The mean sea surface saturation was supersaturated in respect to the atmospheric equilibrium concentration at 107 ± 5 %. (Middle) The sea surface concentration of CH_4 along the AMT22 cruise track. The mean sea surface concentration was 2 ± 0 nmol L^{-1}. (Bottom) The ocean to atmosphere flux of CH_4 along the AMT22 transect. The mean flux was 3.57 x 10^2 ± 3.28 x 10^2 nmol m^2 d^{-1}.

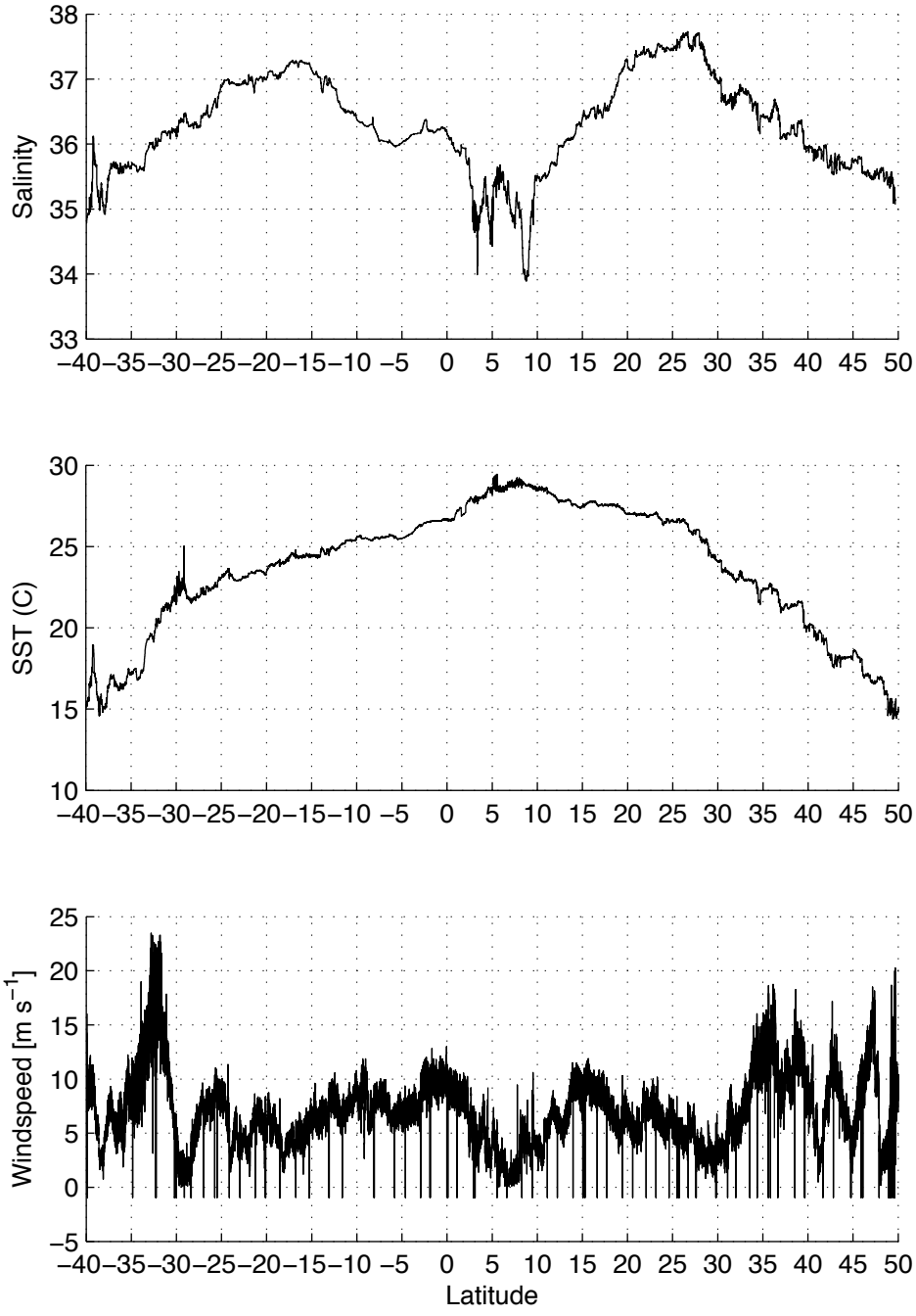

Figure 5. 4: (Top) Sea surface salinity along the AMT22 transect. (Middle) Sea surface temperature (°C) during AMT22. (Bottom) Windspeed during AMT22 (m s^{-1}).

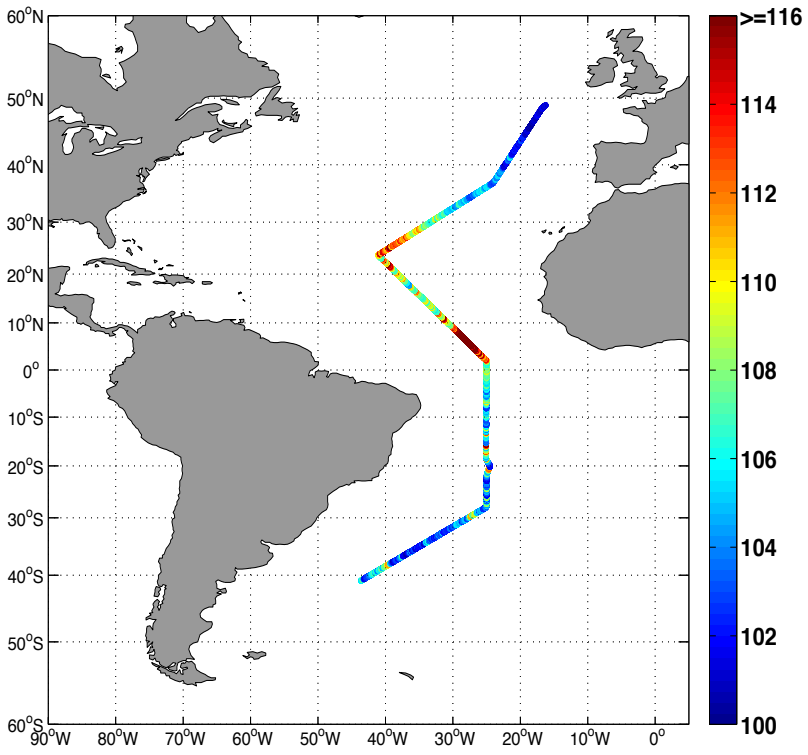

Figure 5. 5: The sea surface saturation map for CH_4, in respect to the atmospheric equilibrium value, along the AMT22 transect (September-October, 2012). The colour bar shows the sea surface saturation for CH_4 (%).

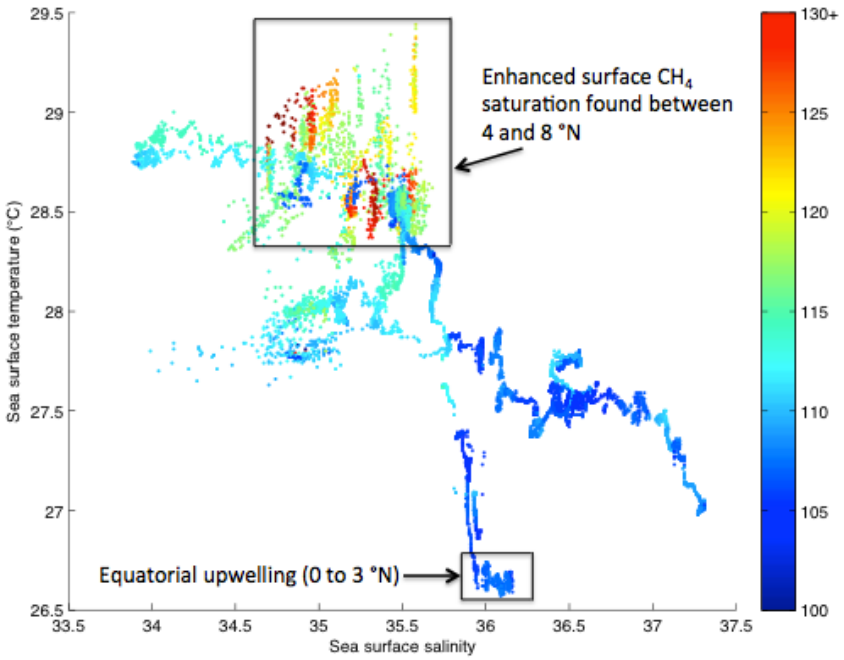

Figure 5. 6: Sea surface temperature and salinity plot, with surface CH_4 saturation (between the latitudes of 0 to 20 °N) during the AMT22 cruise. The colour bar shows surface saturation of CH_4 (%).

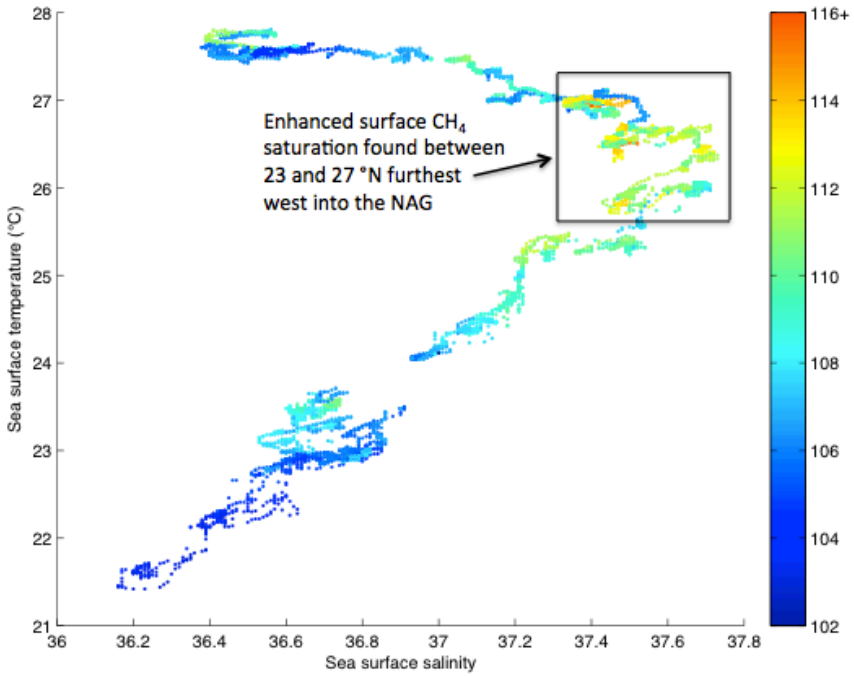

Figure 5. 7: Sea surface temperature and salinity plot, with surface CH_4 saturation (between the latitudes of 15 to 35 °N) during the AMT22 cruise. The colour bar shows surface saturation of CH_4 (%).

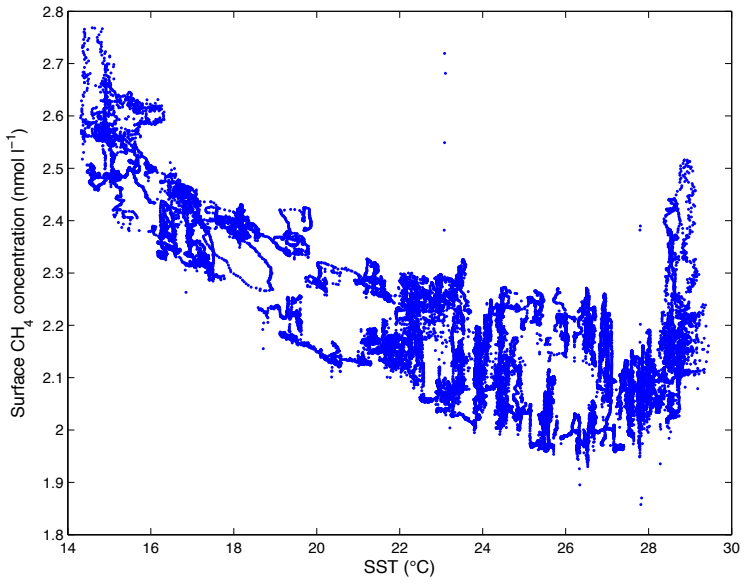

Figure 5. 8: Sea surface temperature and surface CH_4 concentration across the AMT22 cruise track.

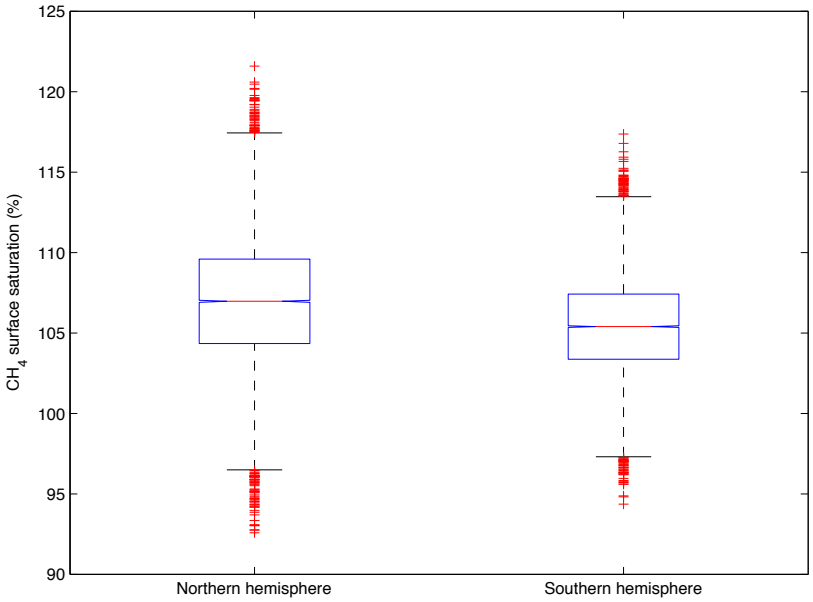

Figure 5. 9: The mean surface saturation for CH_4 (%) calculated in the northern hemisphere (15 to 41 °N) at 107 ± 3 %, and southern hemisphere (15 to 41 °S) at 105 ± 3 % was found to be significantly different from one another during the AMT22 cruise (unpaired t-test, p=0.05, n=17122). The mean is shown by the red and blue line in the centre of the box. The box indicates the 25th percentile and the black lines the 75th percentile. The red crosses are outliers larger than the 75th percentile.

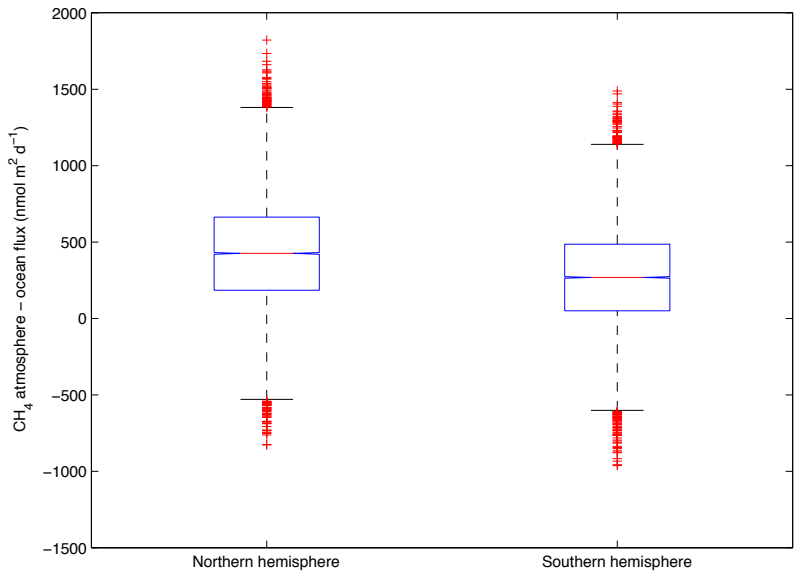

Figure 5. 10: The mean flux of CH_4 from the ocean to the atmosphere calculated in the northern hemisphere (15 to 41 °N), at 426 ± 353 nmol m^2 d^{-1}, and in the southern hemisphere (15 to 41 °S) at 267 ± 318 nmol m^2 d^{-1} was found to be significantly different from one another during the AMT22 cruise (unpaired t-test, p=0.05, n=17122). The mean is shown by the red and blue line in the centre of the box. The box indicates the 25th percentile and the black lines the 75th percentile. The red crosses are outliers larger than the 75th percentile.

5.3. 2: Comparison of AMT N_2O surface water datasets

5.3.2. 1: Atmospheric measurements

The difference between the measured and monthly mean atmospheric values (Mace Head/Cape Grim) can be found in Figure 5. 11. A mean difference of 1 nmol mol^{-1} was found between the mean measured values and mean values used, which corresponds to a 0.30 % change in surface saturation. Disagreements between the Mace Head and Cape Grim monthly mean values and the measurements may have arisen as a consequence of latitudinal gradients in the atmospheric concentration of N_2O. Additionally, measurements may have been made from different air masses that had been influenced by various natural and anthropogenic sources, such as ventilation and thermal outgassing of the oceans, emissions from soils on land and fertiliser use, leading to values higher or lower then the Mace Head and Cape Grim values.

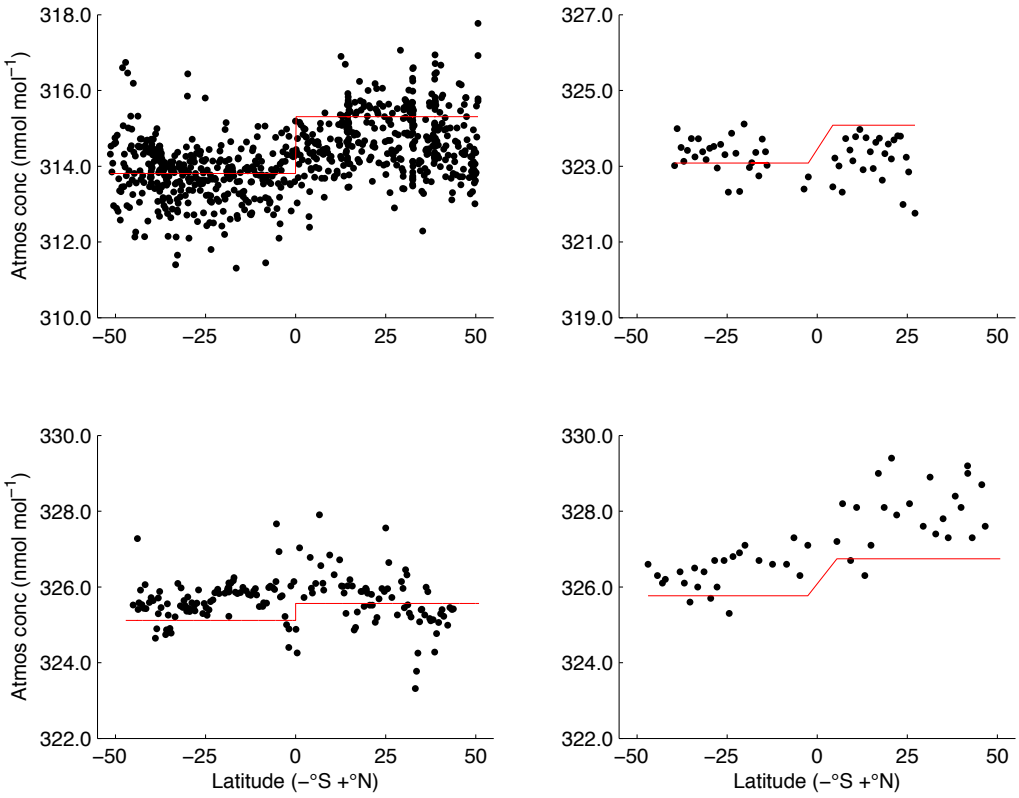

Figure 5. 11: Measured atmospheric values on (top left) AMT7, (top right) AMT20, (bottom left) AMT22, and (bottom right) AMT23. The red lines show the mean Mace Head (NH) and Cape Grim (SH) atmospheric values for the relevant months used in the comparison.

5.3.2. 2: Surface water distribution of nitrous oxide concentration and saturation

During the AMT22 transect, the mean surface concentration of N_2O was 7 ± 1 nmol kg^{-1} (Figure 5. 12: top). Surface waters were generally slightly undersaturated in N_2O with respect to the atmospheric value, with a mean saturation of 98 ± 2 % (Figure 5. 12: bottom), estimated using the monthly mean Mace Head and Cape Grim atmospheric values. The surface measurements were found to be more undersaturated when using the direct atmospheric measurements observed on the cruise. Regions with surface waters undersaturated for N_2O were found in all the AMT datasets examined (AMT3, 7, 20 and 23). This was a small region for AMT7 located between 45 and 50 °N. The more recent datasets, AMT20 and 23, also displayed a mean state of undersaturation across the AMT transect. AMT3 had surface waters undersaturated for N_2O between 20 and 35 °N.

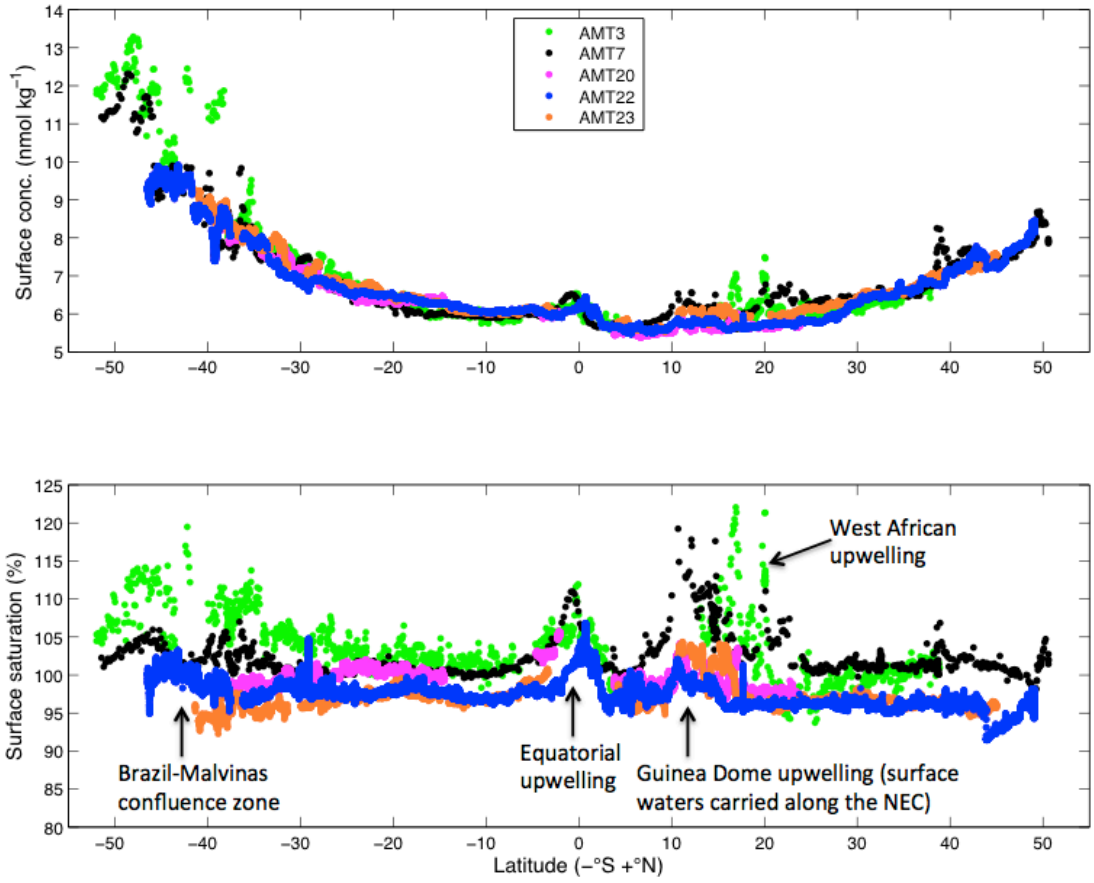

Figure 5. 12: (Top) surface concentration of N_2O (nmol kg^{-1}), and (bottom) estimated surface saturation for N_2O during all cruises with latitude, using Mace Head and Cape Grim monthly mean atmospheric values.

Source regions, with surface saturations of up to 107 %, were found between 3 °N and 2 °S (Figure 5. 12), identified as the equatorial upwelling region due to the high SSS and low SST in this region (Figure 5. 13); between the latitudes of 9 and 16 °N (which was not a region of upwelling) (Figures 5. 12 and 5. 13), and within the Brazil-Malvinas Confluence Zone (BMCZ) (36 - 50 °S) in the southwest Atlantic Ocean (Figure 5. 12). The WAU, located at 15 – 25 °N on the AMT3 and AMT7 cruise tracks acted as an additional source of N_2O to surface waters, with surface supersaturations reaching ~120 % (Figure 5. 12).

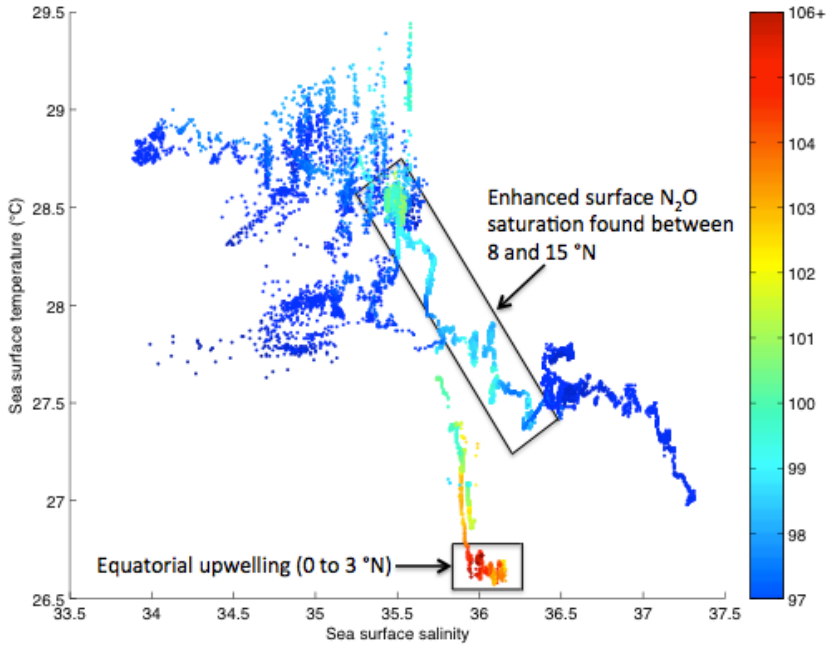

Figure 5. 13: Sea surface temperature and salinity plot, with surface N_2O saturation (between the latitudes of 0 and 20 °N) during the AMT22 cruise. The colour bar displays surface saturation for N_2O (%).

During AMT22, the northern hemisphere (NH) (15 - 45 °N) had a significantly lower mean surface concentration and saturation (Figure 5. 14 and 5.15), at 6 ± 0 nmol kg^{-1} and 96 ± 0 % than the southern hemisphere (SH) (15 - 45 °S), at 8 ± 1 nmol kg^{-1} and 98 ± 1 % (unpaired t-test, p=0.05, n=16980) (Figure 5. 12). The NH was a significantly greater N_2O oceanic sink (mean flux of -963 ± 804 nmol m^2 d^{-1}) than the SH (mean flux of -375 ± 697 nmol m^2 d^{-1}) (unpaired t-test, p=0.05, n=16980) during AMT22 (Figure 5. 16). Grefe (2013) reported the northern (24 – 11 °N) and southern hemispheres (14 – 39 °S) to act as smaller

N_2O sinks at -140 nmol m^2 d^{-1} and -160 nmol m^2 d^{-1} during AMT20; whereas Forster et al. (2009) observed these regions to act as sources of N_2O at 510 nmol m^2 d^{-1} (NH) and 330 nmol m^2 d^{-1} (SH). A hemispheric difference in surface concentration and saturation, with lower N_2O in surface waters in the NH than in the SH, was also found during AMT3 and 20, with AMT23 only showing this trend in surface concentration. Both surface concentration and saturation for N_2O during AMT7 were higher in the NH due to sampling within the West African Upwelling (WAU) system (Figure 5. 2). Variability in the surface concentration, saturation and flux calculations for N_2O was much greater in the SH than in the NH during AMT22 (Figure 5. 14, 5. 15 and 5. 16). It is unclear what causes this, but it could be related to seasonal differences between the two hemispheres.

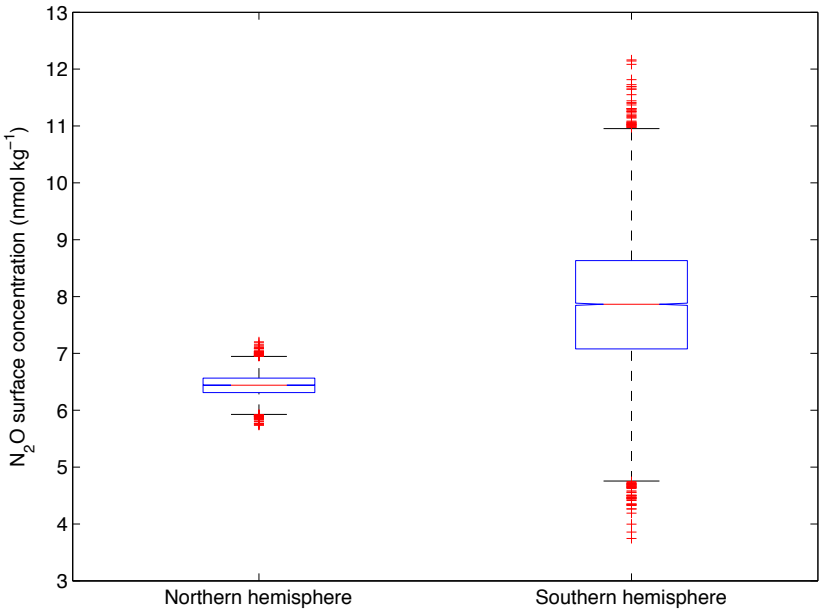

Figure 5. 14: The mean surface concentration for N_2O (nmol kg^{-1}) calculated in the northern hemisphere (15 to 45 °N) at 6 ± 0 nmol kg^{-1}, was significantly lower than that in the southern hemisphere (15 to 45 °S) at 8 ± 1 nmol kg^{-1}, during the AMT22 cruise (unpaired t-test, p=0.05, n=16980). The mean is shown by the red and blue line in the centre of the box. The box indicates the 25th percentile and the black lines the 75th percentile. The red crosses are outliers larger than the 75th percentile.

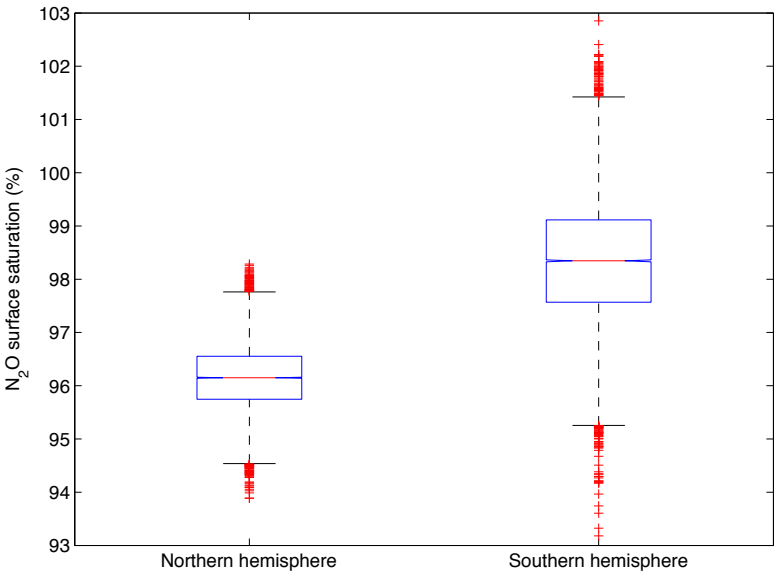

Figure 5. 15: The mean surface saturation for N_2O (%) calculated in the northern hemisphere (15 to 45 °N) at 96 ± 1 %, and southern hemisphere (15 to 45 °S) at 98 ± 1 % was found to be significantly different from one another during the AMT22 cruise (unpaired t-test, p=0.05, n=16980). The mean is shown by the red and blue line in the centre of the box. The box indicates the 25th percentile and the black lines the 75th percentile. The red crosses are outliers larger than the 75th percentile.

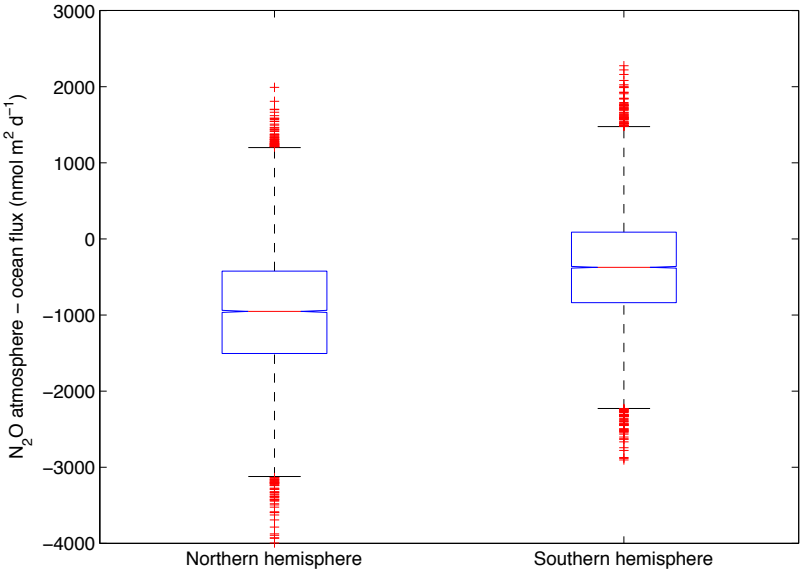

Figure 5. 16: The mean flux of N_2O from the atmosphere into the ocean calculated in the northern hemisphere (15 to 45 °N), at -963 ± 804 nmol m^2 d^{-1}, and southern hemisphere (15 to 45 °S) at -375± 697 nmol m^2 d^{-1}, was found to be significantly different from one another during the AMT22 cruise (unpaired t-test, p=0.05, n=16980). The mean is shown by the red and blue line in the centre of the box. The box indicates the 25th percentile and the black lines the 75th percentile. The red crosses are outliers larger than the 75th percentile.

5.3.2. 3: Comparing regions

In the region located between 30 and 40 °N, observations of the surface concentration of N_2O increased from 6.47 ± 0.22 nmol kg^{-1} to 6.70 ± 0.21 nmol kg^{-1} from 1996 to 2013. However, this is not a significant change. There was however a significant decrease in surface saturation for N_2O in this region over the eighteen-year period from slightly supersaturated to slightly undersaturated surface waters. AMT7 had the highest mean saturation for N_2O at 101.59 ± 1.08 % saturation, and AMT22 the lowest at 96.06 ± 0.47 % (Figure 5. 17). Both the AMT3 and 23 cruises took place at similar longitudes in this region. AMT23 had a mean surface concentration of 6.70 ± 0.21 nmol kg^{-1}, which was 0.23 nmol kg^{-1} greater than AMT3 at 6.47± 0.22 nmol kg^{-1}, but a surface saturation that was around 4 % lower (AMT3: 100.44 ± 1.30 %, AMT23: 96.57 ± 0.51 %)(Figure 5. 17). AMT20 did not have data in this region as measurements began at 23 °N.

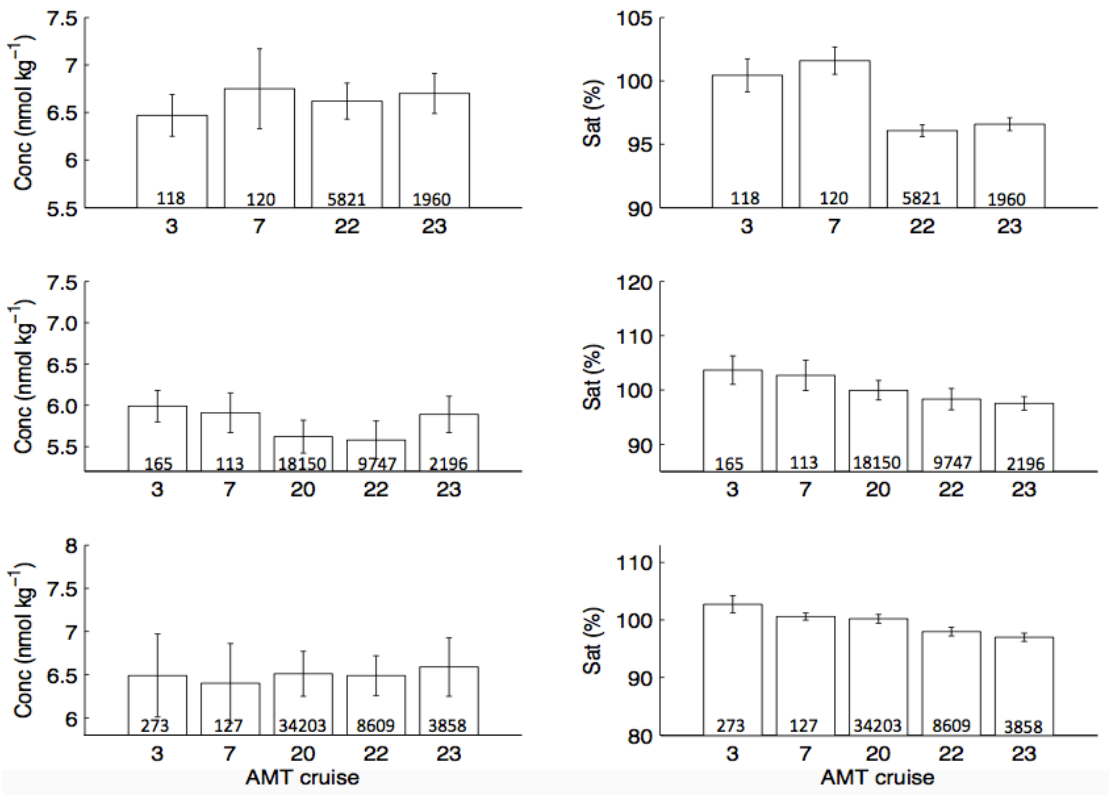

Figure 5. 17: (Left column) Mean surface water concentration (nmol kg^{-1}), and (right column) the mean surface saturation for N_2O for the regions 30 - 40 °N (top), 10 °N - 10 °S (middle) and 10 – 30 °S (bottom), for each cruise where data was available. The error bars display the standard deviation of the data. The numbers in each column indicate the sample size (n).

Within the region located at 10 °N – 10 °S, there was no detectable change in the surface concentration of N_2O over the eighteen-year study period. The surface saturation of N_2O displayed a slight decrease from the slightly supersaturated surface waters of AMT3 and 7 (103.66 ± 2.64 and 102.70 ± 2.80), to the slightly undersaturated surface waters of AMT20, 22 and 23 (99.94 ± 1.80, 98.30 ± 1,97 and 97.54 ± 1.25, but this was not significant (Figure 5. 17).

In the southern region (10 – 30 °S), there was once again no detectable change in the surface concentration of N_2O over the eighteen-year period. The surface saturation for N_2O decreased significantly over the 18 years, from slightly supersaturated at 102.72 ± 1.51 % (AMT3) to slightly undersaturated at 97.01 ± 0.75 % (AMT23) (Figure 5. 17). It was difficult to detect a change in surface water concentration in all three regions because the variation within each dataset exceeded the change between the datasets over time.

5.3.2. 4: The sensitivity of the surface saturation calculation

The sensitivity of the surface saturation calculation to changes in SST, SSS, the surface concentration/atmospheric equilibrium value, and the atmospheric mixing ratio for N_2O were examined. The AMT22 mean salinity at 36 was used for all calculations unless otherwise specified. Calculations were made at two SSTs (lowest and highest SST's measured on AMT22), to test the effect of temperature on the calculations. An increase of 1 °C in SST increased the surface saturation by between 2.00 % (at 29 °C) and 3.08 % (at 17 °C), whereas a 1 unit increase in salinity raised the surface saturation by 0.50 % (at 22°C and a salinity of 34 and 37). An increase in seawater concentration of 0.10 nmol kg^{-1} increased the surface saturation by between 1.21 % (at 17 °C) and 1.72 % (at 29 °C), similar inverse effects were observed by changing the equilibrium concentration. An increase in the atmospheric mixing ratio of 1.00 nmol mol^{-1} decreased the surface saturation by 0.30 %.

5. 4: Discussion

5.4. 1: Surface methane across the AMT22 transect

Surface waters across the entire Atlantic Ocean were supersaturated for CH_4 during the AMT22 cruise. The mean surface concentration of CH_4 measured during the AMT22 was 2 ± 0 nmol L^{-1}, which is within the range measured by Rhee et al. (2009), between 1.8 to 5.0 nmol kg^{-1}, with the highest concentrations closest to the coast. The mean surface water CH_4 saturation value of 107 ± 4 % during AMT22 is consistent with other surface saturations reported in the Atlantic Ocean, although seasonal and inter-annual variability in the surface saturation for CH_4 observed appears to be relatively high, for example comparing AMT12 and AMT13 (Forster et al., 2009). Conrad and Seiler (1988) reported surface saturations between 105 to 130 % in the Atlantic Ocean, Forster (2009) measured 116 to 156 % in the mixed layer during the boreal autumn/austral spring on AMT13. During AMT7, in the same seasons, Rhee et al. (2009) reported lower surface saturations at 99.97 to 101.20 %. Off central California and within the oligotrophic waters in the central North Pacific Ocean, saturations of 105 -175 % were reported (Tilbrook and Karl, 1995).

Surface CH_4 concentration across the Atlantic Ocean displayed a strong inverse relationship with SST, with the warmer surface waters associating with lower surface CH_4 concentrations than the cooler surface waters at higher latitudes. This is due to the solubility of CH_4 changing with temperature, with CH_4 more soluble in cooler surface waters, than in warmer waters. This relationship may also be attributed to higher production in the colder waters, and consequently more CH_4 being produced. The relationship between surface CH_4 concentration and SST broke down at temperatures exceeding 28 °C in the tropics, due to the high surface concentrations of CH_4 found between the latitudes of 4 and 8 °N, which were clearly influenced by a parameter other than SST. Figure 5. 8 showed that this is not a region of upwelling, as the SST is not reduced and the SSS increased in this location. Therefore another parameter is responsible for the breakdown off this relationship. Surface saturations of CH_4 between 4 and 8 °N reached 135 %. This region displayed a reduction in SSS (Figure 5. 4: top).

The surface waters between these latitudes may have been influenced by Amazon outflows, flowing along the NECC in an eastward direction. Discharge from the Amazon river has been found to travel along the NECC towards Africa between the months of June and January each year (Muller-Karger et al., 1988). If this were a direct influence, with waters highly supersaturated for CH_4 reaching the regions sampled, then this would require CH_4 to have a very long residence time in the surface waters. The main sinks for CH_4 in the ocean are air-sea exchange and microbial consumption. Ward et al. (1987) and Jones (1991) estimated the turnover time of microbial consumption of CH_4 in the ocean as averaging at around 65 years. Tilbrook and Karl (1995) used this average turnover time to calculate a consumption rate of CH_4 of 0.01 μmol m^{-2} d^{-1} and concluded that this rate was negligible in comparison to the loss of CH_4 associated with air-sea exchange. The dominant sink for CH_4 in the open ocean is therefore the ocean to atmosphere flux of this trace gas. Alternatively, the high surface CH_4 saturations observed between the latitudes of 4 to 8 °N may have arisen as an indirect influence of the Amazon outflow. As the band of highly productive waters travels from the Amazon outflow and along the NECC, it stimulates primary production across the Atlantic Ocean (Figure 5. 18). An enhancement of particles in the influenced surface waters may produce an increase in the sinking particle-associated CH_4 source (Tilbrook and Karl, 1995). The region located 4 to 8 °N is also influenced by the ITCZ, which could also explain the decrease in surface salinity in this region, due to high rainfall. Changes to the vertical structure of the mixed layer in this region may result from a combination of high rainfall, causing the mixed layer to re-stratify, along with high humidity verses evaporation rates, which may induce convective mixing. With increased turbulence, biological activity is stimulated in the mixed layer, increasing the production of particulate material in the water column, creating anoxic microhabitats for CH_4-producing bacteria (Tilbrook and Karl, 1995).

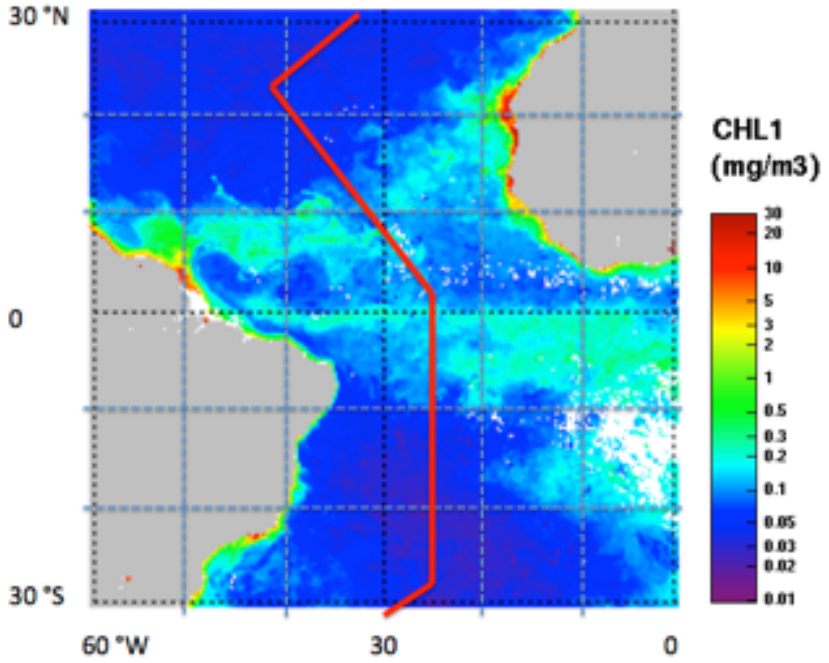

Figure 5. 18: A MERIS/MODIS/SeaWiFS merged CHL1-/OC3V5/ GlobColour 8-day Level 3 product[25] run from the 26/10/2012 to 03/11/2012. The product displays the average sea surface concentration of chl-a in the Atlantic Ocean between the latitudes of 30 °N and 30 °S during this time period. The colour bar displays the sea surface concentration of chl-a in mg/m^3. The red line shows the AMT22 cruise track.

The second highest surface CH_4 saturations found along the AMT22 cruise track, reaching 116 %, were found in the NAG between the latitudes of 20 to 28 °N (Figure 5. 3 and 5. 5). In the boreal autumn, surface waters in the NAG are stratified and therefore subject to limited vertical mixing, indicating that in-situ production of CH_4 must be occurring the in surface waters to produce the supersaturations observed. In the oligotrophic subtropical North Pacific the source of CH_4 in the surface mixed layer was also suggested to arise predominantly from in-situ production, with some inputs from diffusion of CH_4 from the bottom of the mixed layer (estimated as 8 %) (Tilbrook and Karl, 1995). Tilbrook and Karl (1995) suggested that a sinking particle-associated CH_4 source was important in the surface waters, but were unclear of the production source,

[25] **MERIS/MODIS/SeaWiFS product obtained from www.hermes.acri.fri**

as the production of CH_4 did not occur within the particles themselves. Various production sources have been proposed to explain this surface water 'CH_4 paradox', as methanogenesis is a process that occurs under anoxic conditions, yet appears to occur in the oxic, euphotic water layer of the ocean (Conrad and Seiler, 1988). To explain this phenomenon it has been proposed that methanogenesis may take place in small anoxic micro-niches found within decaying organic particles, faecal pellets, as well as in fish and zooplankton intestines (Lamontagne et al., 1973, Karl and Tilbrook, 1994, Van der Maarel et al., 1999). A more plausible explanation maybe linked to the very low surface concentrations of macro-nutrients in the subtropical and tropical Atlantic Ocean (Aiken et al., 2000). Recent studies have found that various actively released methylated substrates by phytoplankton, including methylphosphonate (Mpn) and dimethylsulfoniopropionate (DMSP) are used for energy supply in aerobic systems. Methylated substrates have been found to act as precursors for CH_4. Under low nitrate conditions bacteria have displayed the ability to use DMSP as a carbon source to compete for phosphate, producing CH_4 in the process (Damm et al., 2010). Similarly, under low phosphate conditions the decomposition of Mpn, under aerobic conditions, also releases CH_4 as a by-product (Karl et al., 2008). These two pathways could explain the surface supersaturation for CH_4 found across the subtropical Atlantic Ocean during the AMT22. The higher surface concentrations of CH_4 found in the NAG in comparison to the SAG maybe linked to potentially bio-limiting concentrations of dissolved inorganic phosphate reported in the NAG (Moore et al., 2009), indicating that the Mpn decomposition pathway (Karl et al., 2008) may act as an important source of CH_4 in this location. Additionally in the NAG, the stratified water column in the subtropical NH, in comparison to the vertically well-mixed subtropical SH, may act to reduce the removal of CH_4 from the surface waters by limiting advection and vertical mixing, therefore allowing CH_4 concentrations to build up in a stratified season. Surface saturation and the ocean to atmospheric flux of CH_4 were significantly greater in the NH than in the SH of the Atlantic Ocean during AMT22. This difference is due to the two large regions (2 to 10 °N and 20 to 28 °N), where the highest surface CH_4 saturations were located being in the NH. Differences in the

availability of nutrients, such as nitrogen and phosphate, between the NAG and SAG may explain the concentration difference of CH_4 in surface waters.

5.4. 2: Surface nitrous oxide in the Atlantic Ocean

The implications of using land-based atmospheric datasets were investigated by comparing 'real time' AMT22 atmospheric N_2O measurements to land-based N_2O measurements from Izaña atmospheric centre (selected as it had hourly measurements) over a five-day period from 15th to 18th October 2012 (Figure 5. 19). The real time measurements were generally lower and more variable than the land based measurements. The lower measurements of N_2O from the ship in comparison to the land measurements may be due to there being less influence of N_2O sources arising from agriculture and fertiliser use. The higher variability observed within the ship-based measurement dataset may be due to the different air-masses encountered along the cruise track, which had been subjected to different sources of N_2O.

Figure 5. 19: (Green dots) land-based N_2O measurements from Izana[26] atmospheric centre, (black line) 'real time' atmospheric measurements during AMT22.

[26] **Data source: World Data Centre for Greenhouse Gases, Izaña N_2O– AEMET (continuous) hourly, 2012-01-01 -2012-12-31.**

The main source regions in the Atlantic Ocean were located within the WAU (15 – 22 °N), 9 - 16 °N, in the EU region (3 °N - 2 °S) and within the BMCZ (35 -52 °S) (Figure 5. 12), as a consequence of N_2O-rich water, being upwelled or vertically mixed from depth to the surface (Pierotti and Rasmussen, 1980, Cline et al., 1987, Law and Owens, 1990b, Oudot et al., 2002, Nevison et al., 2004, Forster et al., 2009, Rhee et al., 2009). Nitrification is thought to be to be the dominant source of N_2O upwelled from depth (Yoshinari, 1976, Walter et al., 2006, Forster et al., 2009). The N_2O-rich water measured between 9-16 °N may have been transported from the Guinea Dome upwelling region, located between 10-15 °N, 22 °W. At the equator there is a zone of divergence where deep nutrient-rich water replaces the surface waters (Mann and Lazier, 2006), accompanied by a large source of N_2O. In the BMCZ, the interaction between the pole-ward moving, warm, Brazil Current (BC) and the fresh, cold, counter-flowing, Falklands Current (FC) a region of intensive mixing, created by a complex pattern of eddies (Brandini et al., 2000, Garcia et al., 2004). With strong mixing, deeper water supersaturated for N_2O, most probably due to sub-surface nitrification, is mixed to the surface (Figure 5. 12).

Figure 5. 17 shows that the surface saturation for N_2O decreased over the eighteen-year study period, in all three of the regions investigated. This could suggest that during the time period of this study, the surface ocean shifted from a slight atmospheric source to a slight atmospheric sink for N_2O. However, a shift from an atmospheric source to sink seems unlikely as the surface ocean is highly influenced by the atmospheric concentration of N_2O, which has been increasing over time. A more plausible explanation is that the surface waters in the subtropical gyres are undersaturated for N_2O, and those closer to the coast are slightly supersaturated, and always have been. This implies that there is a spatial influence on the datasets leading to these results. The datasets show that the highest surface saturations in the regions investigated, at 101.59 % in the

---

http://ds.data.jma.go.jp/gmd/wdcgg/pub/data/current/n2o/hourly/y2012/izo128n00.aemet.as.cn.n2o.nl.hr2012.dat. Last accessed: January 2016.

region 30 - 40 °N and 102.72 %, in the region 10 – 30 °S, were observed during AMT7 and AMT3, which were the cruise tracks closest to the coast. The lowest saturations observed in the region located between 30 and 40 °N, at 96.06 %, were found during AMT22, which was the cruise that sampled the furthest west into the NAG. In the region located 10 – 30 °S, the lowest surface saturations were found during AMT22 (97.98 %) and 23 (97.01 %), which both sampled the SAG further east from the coast than AMT3 and 7. It was therefore difficult to determine whether a change in the surface concentration and saturation had occurred over the eighteen-year period. This is because any possible changes over time were masked by the spatial influences in these regions, with surface waters closer to the coast, subjected to coastal influences such as enhanced inputs of organic material, having higher surface N_2O concentrations and saturations. In contrast, surface waters further west and east into the NAG and SAG had generally slightly lower surface concentrations of N_2O, and were undersaturated during boreal autumn and austral spring (Figure 5. 2).

The subtropical gyres were undersaturated for N_2O at approximately 4 % for the NAG, and 2-3 % for the SAG. To understand the processes that may lead to undersaturation in the surface waters of these regions, a sensitivity analysis was completed. During AMT22, the deepest mixed layer depth observed in the NAG was 30 m. Using this mixed layer depth and the average windspeed measured between 30 and 40 °N on AMT22, of 9 m s^{-1}, the equilibration time for N_2O was estimated at around two and a half weeks (Figure 3. 17), therefore the longest timescale over which any temperature lag effects could be observed is likely to be about 1 week. In one week the SST in the NAG in autumn reduces at a maximum rate of ~0.5 °C per week (Lefèvre and Taylor, 2002). An instantaneous reduction by 0.5 °C would lead to approximate reduction in the saturation of N_2O of 1.50 %. It appears therefore that seasonal changes in SST have a potentially significant effect on the surface saturation of N_2O, and most likely act as an important contributor of the observed undersaturation in the Atlantic subtropical gyres.

However, seasonal cooling does not account for the 4 % undersaturation observed in the NAG, or the undersaturation of N_2O found in surface waters in the SAG in spring, which we would expect to be warming. Therefore, there may also be an additional microbial N_2O consumption pathway occurring in the surface waters of the Atlantic subtropical gyres, contributing to the undersaturation found in surface waters. For example, recently, N_2O fixation has been identified as a N_2O sink in the surface waters of the eastern subtropical South Pacific (Cornejo et al., 2015). Alternatively, Wyman et al. (2013) identified a sink within the well ventilated, oceanic surface waters of the north-eastern Arabian Sea, where the expression the NosZ gene was found, leading to the production of N_2O reductase and the terminal step in the denitrification pathway. They suggested within tropical and subtropical surface waters, nitrogen oxides may be reduced within O_2-depleted micro-zones associated with filamentous diazotrophic cyanobacteria. Possible N_2O consumption pathways will need to be explored in the open Atlantic Ocean to understand the surface undersaturation observed.

The saturation calculation displayed a high sensitivity to small differences in the surface concentration/equilibrium concentration of N_2O, and SST. Consequently, small spatial influences or inter-annual differences between the cruise tracks were amplified in the saturation calculation as a 1.21 -1.72 % saturation difference. Any inaccuracies in SST measurements would also influence this calculation. Because of the high sensitivity of the saturation calculation to these parameters, along with the spatial differences between the cruise tracks, I am unable to draw definite conclusions on any change in the source-sink characteristic of the Atlantic Ocean in these regions with the length of the current time series.

AMT3, 20, and 22 display a hemispheric difference in surface concentration and saturation for N_2O, with lower surface saturations for N_2O in the NH than the SH (Figure 5. 12). AMT23 shows this trend only in the surface concentration. The concentration difference can be attributed to differences in SST between the northern and southern hemispheres, with warmer surface temperatures in the

boreal autumn in the NH than in austral spring in the SH (Figure 5. 20). Nitrous oxide is less soluble in warm waters than in cold waters, leading to the lower surface concentrations observed in the NH. Seasonal changes in SST and the lag in equilibration with the atmosphere, as discussed above, can explain the lower surface saturations found in the NH than in the SH. Surface cooling during boreal autumn in the NH increases the solubility of N_2O, however, the equilibration time, results in the surface waters being undersaturated in respect to the atmospheric value. In addition, stratification of the water column in autumn (NH) limits entrainment of N_2O from deeper waters, and a potential microbial N_2O sink in the surface waters may cause further undersaturation. In contrast, in the SH during austral spring, surface waters are warming causing the solubility of N_2O to decrease and degassing of N_2O to occur. Degassing of N_2O during austral spring would be expected to lead to surface waters slightly supersaturated, or at equilibrium with the atmospheric. The undersaturation observed in the SAG may, as previously suggested, be due to an additional microbial N_2O consumption pathway in the surface waters.

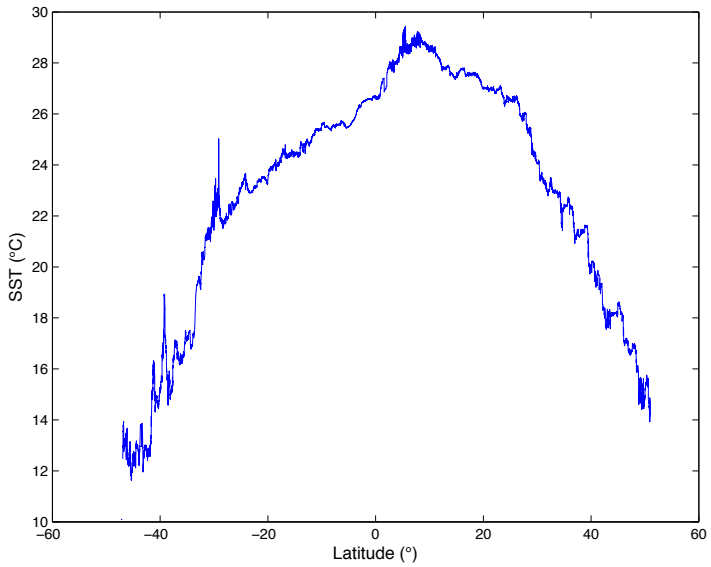

Figure 5. 20: Sea surface temperature with latitude, along the AMT22 transect. The northern hemisphere was warmer in boreal autumn than in the southern hemisphere in austral spring, at the same latitudes.

The findings from this study suggest that the concentration of N_2O in the surface ocean is increasing with, or just lagging behind the atmospheric concentration of N_2O. Certainty over this conclusion is difficult due to the large variation observed within each datasets, in comparison to the small surface concentration change over the eighteen years of the study. In addition to the variability, the spatial differences between the datasets, as discussed earlier, complicate this further by there being higher concentrations closer to the coast (earlier cruise tracks) and lower concentrations in the gyres (later cruise tracks). The similarity in location between the cruise tracks for AMT3 and 23 (within the 30-40 °N region), allowed temporal differences to be investigated over the eighteen-year period between these two datasets. The mean surface concentration for N_2O during AMT23 was 0.23 nmol kg^{-1} greater than that for AMT3, with AMT3 having a surface saturation for N_2O of 100.44 %, and AMT23 of 96.57 %. The surface water concentration increase over this time period is slightly less than expected if it were to have increased consistently with the atmospheric concentration. Over eighteen years the atmospheric increase in N_2O was approximately 13.5 nmol mol^{-1}, which, using the mean SST at 23.41 °C and SSS at 36.41 in this region for AMT3, calculates to an approximate 0.28 nmol kg^{-1} increase in seawater N_2O concentration to maintain 100 % saturation with the atmosphere.

The main challenges in determining the change in surface water concentration and saturation for N_2O in this study arose because of 1) spatial differences between the earlier and later cruises, where cruise tracks closer to the coast had higher N_2O concentrations and saturations than those in the subtropical gyres. 2) The variation between measurements within a dataset was often equal to or greater than the difference in seawater concentration change over the eighteen years of this study. 3) Changes in saturation over this time period were very small. With the sensitivity of the saturation calculation, small variations in parameters such as surface concentration between datasets, which may vary as a consequence of spatial influences, made definite conclusions in regards to changes in the source sink characteristic difficult.

To overcome these problems recommendations for the future programme of the AMT include:

1) To enable temporal changes in surface N_2O to be discriminated from spatial features, it is recommended that the AMT programme maintain a consistent cruise track in the future.
2) A longer time series is required to enable changes in surface water concentrations to be discriminated from any noise in the datasets.
3) The different authors of the datasets used in this study cross-calibrated to different primary standards, including NOAA/CMDL, SIO-1993 and IMECC. Differences in cross-calibrations may introduce error into the comparison, which is even more important when the differences over time in sea surface concentration are so small. Recommendations therefore are to standardise the method for the collection of N_2O surface water measurements on the AMT by using a single set of primary standards for cross-calibration of all working standards.

Chapter 6: Conclusions

6. 1: Measurements of surface nitrous oxide in the NW European shelf seas and the Atlantic Ocean.

6.1. 1: Nitrous oxide measurements in the NW European shelf seas.

In June and July 2011, during the D366 research cruise, sea surface waters in the NW European shelf seas were slightly supersaturated for N_2O with a mean saturation of 102 ± 2 %. Surface saturation ranged from 98 to 110 % depending on the location. These values compare well to previous measurements in this region (Table 1. 4), which mostly ranged between 99 and 104 %. The NW European shelf seas have a lower surface saturation than other shelf seas such as the shelf of the NW Black Sea at 112 %, the continental shelves of the Bering and Chukchi Seas at 113 %, and the East China Sea at 191 ± 74 % (Table 1. 4). The mean surface concentration of N_2O was measured at 9.47 ± 0.44 nmol L^{-1}, ranging from 8.3 to 10.6 nmol L^{-1}, respectively. This was consistent with the mean concentration measured by Rees and Brown (personal communication, 2014) on the D366 of 9.86 ± 0.95 nmol L^{-1}. A comparison between N_2O saturation and fluxes calculated in different regions show that both are the highest in estuaries, followed by shelf seas, with the lowest saturations and fluxes found in the open ocean (Table 6. 1).

Table 6. 1: Comparison of surface saturation and air- sea flux of N_2O and CH_4 between shelf seas, estuaries, rivers and the open ocean. The shelf and open ocean estimates for both N_2O and CH_4 are from the D366 and AMT22 cruises. The estuary estimates are from Barnes and Upstill-Goddard (2011) for N_2O and Upstill-Goddard et al. (2000) for CH_4.

N_2O	Shelf	Estuary	Open Ocean
Surface saturation (%)	102 ± 2 (97 – 110)	140 – 6500 (Humber) 140 – 2000 (Tees)	98 ± 2 (92 to 107)
Flux (nmol m^2 d^{-1})	9.97 x 10^2 (-1.50 x 10^3 to 1.22 x 10^4)	1.00 x 10^5 ± 1.94 x 10^4	-9.63 x 10^2 ± 8.04 x 10^2 (-5.00 x 10^3 to 2.00 x 10^3)
CH_4	**Shelf**	**Estuary**	**Open Ocean**
Surface saturation (%)	118 ± 22 (100 to 117)	6000 – 21000 (Humber) 21800 (Tyne) (at the low salinity turbidity maximum	107 ± 5 (100 to 135)
Flux (nmol m^2 d^{-1})	2.32 x 10^3 ± 3.69 x 10^3 (0 to 3.35 x 10^4)	7.15 x 10^3 (based on the Humber)	3.57 x 10^2 ± 3.28 x 10^2 (0 to 2.90 x 10^3)

6.1. 2: Ocean to atmosphere flux estimates for nitrous oxide in the NW European shelf seas and Atlantic Ocean.

6.1.2. 1: Comparison of flux estimates of nitrous oxide between the NW European shelf seas and coastal/estuarine environments.

According to Uher (2006) the total areal extent of the North Sea, the Irish Sea and the Bay of Biscay is 1.14 x 10^6 km^2, therefore the source of N_2O from these regions, using the mean flux calculated during the D366 of 997.20 nmol m^{-2} d^{-1}, would be estimated as 1.8 x 10^{10} g N_2O yr^{-1}. In comparison to the yield of N_2O from UK and European (including the UK) river and estuarine regions, at ~1.9 ± 1.2 × 10^9 g N_2O yr^{-1} and
6.8 ± 1.3 × 10^9 g N_2O yr^{-1} (Barnes and Upstill-Goddard, 2011), the production of N_2O in the shelf seas is greater due to the larger surface area. These estimates therefore do not agree with previous studies e.g. Bange (2006), Barnes and Upstill-Goddard (2011) and Freing et al. (2012) that the major contribution in shelf seas comes from estuarine and riverine systems. However, with this

approach there is a potential for double counting, as it assumes that N_2O produced in estuaries is not advected into the shelf seas. This is not always the case, for example, Barnes and Owens (1999) reported a source of N_2O from the Humber estuary into the North Sea throughout the year.

6.1.2. 2: Flux estimates of nitrous oxide from global shelf seas.

The global ocean has a total area of approximately 361 x 10^6 km^2, with shelf seas accounting for around 9 % of that area (Simpson and Sharples, 2012). Global shelf seas therefore have an approximate global area of 32.49 million km^2. With a summertime flux of 997.20 nmol m^2 d^{-1}, and with the assumption that shelf sea production of N_2O is globally similar, a summertime atmospheric flux of N_2O of 5.21 x 10^{11} g N_2O yr^{-1} would be produced. This approach is however limited by seasonal effects, where conditions in different seasons may lead to changes in the flux of N_2O to the atmosphere. It is also limited in the assumption that production is similar in all global shelf seas. Comparisons to other shelf seas that show regions such as the East China Sea produce much greater fluxes than the NW European shelf seas, estimated between 20900 ± 54800 nmol m^2 d^{-1} using the LM86 equations, and 36300 ± 95700 nmol m^2 d^{-1} using the W92 equation. This indicates the global flux of N_2O from shelf seas may be greater than calculated here, because the NW European shelf seas are at the lower end of N_2O production in comparison to other global shelf seas (Table 1. 4).

6.1.2. 3: Flux estimates of nitrous oxide from the Atlantic Ocean

The Atlantic Ocean covers an area of approximately 106.46 x 10^6 km^2 (www.oceanservice.noaa.gov). The flux during AMT22 was calculated as -963.48 nmol m^2 d^{-1}. With the assumption that the flux does not change throughout the year, or spatially, the Atlantic Ocean acts as an atmospheric sink for N_2O of -1.68 x 10^{12} g N_2O yr^{-1}. However, the results from this thesis indicate that the flux of N_2O does alter spatially in the Atlantic Ocean, with a change from a slight sink to source towards the coast (see section 5.4 2). Waters closer to the coast were found to have higher concentrations and saturations of N_2O, as they were subjected to coastal influences, such as enhanced inputs of organic mater,

leading to higher rates of nitrification in the water column. By comparing the AMT22 fluxes to other AMT cruises in the same season it is clear that there is variability in the fluxes reported, and that it is not realistic to assume that a flux calculated from a single cruise is adequate to represent the Atlantic Ocean based on a single cruise dataset. For example, during AMT20, Grefe and Kaiser (2014) found the northern and southern gyres (24 – 11 °N) and (14 – 39 °S) to act as sinks at -140 nmol m^2 d^{-1} and -160 nmol m^2 d^{-1}, and the equatorial region (11 °N – 5°S) to act as a slight atmospheric sink at 110 nmol m^2 d^{-1}. On average the Atlantic Ocean sampled acted as a slight sink at -63 nmol m^2 d^{-1} during AMT20. In contrast during AMT13, Forster et al. (2009) reported atmospheric fluxes of N_2O between 40 nmol and 710 nmol m^2 d^{-1} throughout all the provinces sampled, except the CNRY province, which had higher fluxes at 2730 to 4650 nmol m^2 d^{-1}.

6.1. 3: Nitrous oxide measurements in the Atlantic Ocean

In October and November 2012, during the AMT22 cruise, sea surface waters in the Atlantic Ocean had a mean surface concentration of 7 ± 1, and were slightly undersaturated for N_2O with a mean saturation of 98 ± 2 %. Surface saturation ranged from 92 to 107 %. These values compare well to N_2O measurements made on other AMT cruises (AMT3, 7, 20 and 23), which reported mean surface saturations between 99 and 104 % (Rhee et al. 2009; Grefe, 2013; Kaiser, 2015: personal communication; Law 2015: personal communication).

6. 2: Processes that influence the surface concentration and saturation of nitrous oxide.

6.2. 1: Processes that influence the surface concentration and saturation of nitrous oxide in NW European shelf seas.

6.2.1. 1: Sea surface temperature.

The surface concentration of N_2O displayed a strong relationship with SST along the entire NW European shelf seas that were sampled during the D366 cruise ($r=-0.87$, $p\leq0.05$, Spearman's correlation). This was generally much weaker between N_2O surface saturation and SST ($r=-0.36$, $p\leq0.05$), except in the eastern English Channel where a stronger negative relationship between these two parameters was apparent ($r=-0.60$ $p\leq0.05$). The solubility of N_2O changes with temperature. As water gets colder, N_2O becomes more soluble and therefore the seawater is able to take up more N_2O from the atmosphere than within warmer waters, leading to the higher surface concentration values. This shows that the main control on the surface water N_2O concentration during D366 is equilibration with the atmosphere as this process is much faster, at around 2.5 weeks, than N_2O destruction and production processes. Because of this, it is important to look at the N_2O deviation from saturation rather than the change in N_2O concentration. By looking at the saturation of N_2O in surface waters rather than the concentration, we are normalising the data and therefore removing this solubility effect. The magnitude of the temperature-solubility effect can be seen in Figure 6. 1, where the gradient for the line of best fit is much steeper for the relationship between SST and surface N_2O concentration, than for SST and the surface saturation of N_2O. This shows that the surface saturation of N_2O is far less dependent on SST, and therefore far less influenced by changes in SST.

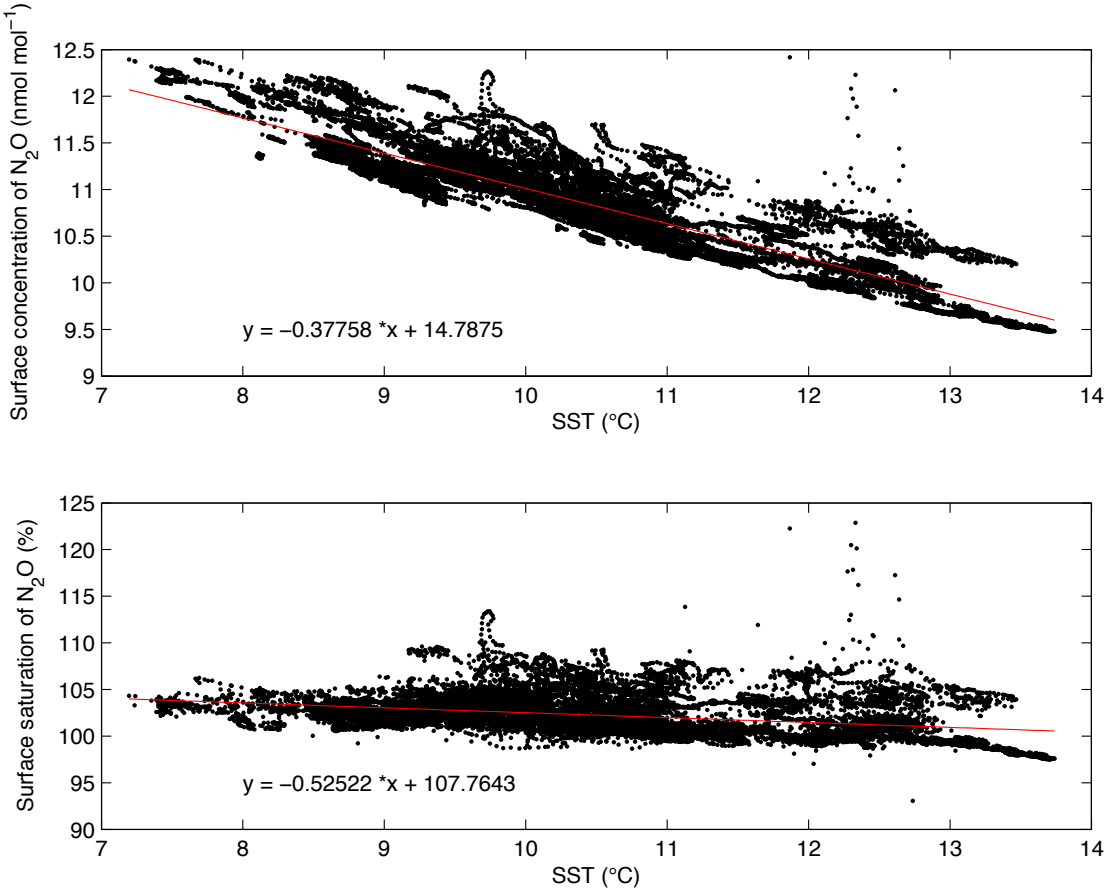

Figure 6. 1: (Top): the relationship between SST and the surface concentration of N_2O during D366. (Bottom): the relationship between SST and surface saturation of N_2O during D366.

6.2.1. 2: Sites where vertical mixing takes place.

Surface waters supersaturated in N_2O were found to occur at sites where vertical-mixing processes took place. Four types of vertical mixing processes were identified in the NW European shelf seas that associated with enhanced surface N_2O saturations:

1) Vertical mixing took place where the seasonally stratified and fully mixed water columns met at tidal fronts, for example in the Malin Sea, below the Shetlands, around St George's bank and off the SW coast of England (section 3.4.4 2).

2) At the shelf edge, enhanced vertical mixing occurred due to the formation of internal waves. Examples were found at shelf break front regions off the west coast of Scotland and in the Bay of Biscay (section 3.4 5).

3) Within regions where there were high freshwater inputs, density-driven vertical mixing took place as two water types with different salinities met, for example in the Skagerrak (section 3.4.1 3).
4) Areas where the water column was fully mixed, such as within the eastern side of the English Channel (section 3.4.3 3).

At sites where the water column is vertically mixed, such as the eastern Engliah Channel and southern North Sea, the nutrient supply to the euphotic zone is enhanced, stimulating primary production. As a result, many of the regions described above had high surface chl-a concentrations in the surface waters. An increase in phytoplankton leads to more organic material sinking to the deeper waters, where it is then oxidised. During the initial step of nitrification, NH_4^+ is oxidised to NO_2^- and N_2O is produced as a by-product. The final oxidised state of nitrogen during nitrification is NO_3^-, which is reduced in marine sediments during denitrification, also producing N_2O as an intermediate. Nitrous oxide produced by either pathway reaches the surface waters by vertical mixing.

6.2.1. 3: Surface chlorophyll-a concentration.

Positive relationships between the surface chl-a concentration and surface N_2O saturation were found in various regions not exposed to vertical mixing, such as within the Norwegian Trench and in the eastern mouth of the Skagerrak (meeting the North Sea). In these areas, estuaries, rivers and fjords appeared to play a significant role, presumably by increasing the nutrient supply to local waters. Nutrient enhancement would stimulate primary production in the euphotic zone, leading to more organic material sinking and therefore more nitrification and denitrification, resulting in the production of N_2O. With limited vertical mixing, euphotic nitrification may play an important role in the production of N_2O in these regions.

6.2. 2: Processes that influence the surface concentration and saturation of nitrous oxide in the Atlantic Ocean.

6.2.2. 1: Sea surface temperature.

In the surface waters of the Atlantic Ocean, N_2O was found to be lower in both concentration and saturation in the northern hemisphere (NH) than in the southern hemisphere (SH) (Figures 5. 14 and 5. 15). The surface concentration of N_2O was influenced by the seasonal SST differences between the hemispheres, with the NH being warmer in boreal autumn, and therefore N_2O being less soluble, than in the SH in austral spring. The lower saturation in the NH arose as a consequence of seasonal cooling in the boreal autumn, whereby the solubility of N_2O in the surface waters increased, but slower equilibration with the atmospheric concentration of N_2O caused slight undersaturation in the surface waters. In contrast, in the SH there was seasonal warming in spring and therefore the surface waters decreased in solubility, degassing N_2O in the process. The equilibration time for N_2O was estimated at approximately two and a half weeks (Figure 3. 17), therefore the longest timescale over which temperature lag effects could be observed would be expected to be around one week. In a single week the SST in the SAG can increase at a maximum rate of 0.6 ° C in a week (Lefèvre and Taylor, 2002). An instantaneous increase in SST of 0.6 ° C would lead to an increase in saturation of 1.8 %. During spring the water column is well ventilated from wintertime mixing. This may explain the slight undersaturation of N_2O found in the surface waters, rather then slight supersaturation.

6.2.2. 2: Upwelling and regions of intensified mixing.

In the Atlantic Ocean, regions of upwelling, such as the west African upwelling system and the equatorial upwelling system, as well as areas where intensified vertical mixing occurs such as in the Brazil-Malvinas confluence zone, enhanced the concentration and saturation of N_2O in surface waters. Within these locations, waters supersaturated in N_2O were mixed from depth to the surface.

6.2.2. 3: The atmospheric concentration of N_2O and air-sea exchange

The comparison of five high-resolution surface N_2O datasets, over a eighteen-year period of the AMT (section 5.5.4 2), suggested that the atmosphere plays an important temporal role in the regulation of the surface water concentration of N_2O in the open ocean. This was shown as a surface water concentration increase over an 18-year period, between the latitudes of 30 to 40 °N, similar to the atmospheric increase of N_2O at 13.5 nmol mol^{-1} during this time period. The surface waters of the ocean are therefore influenced by changes in the atmospheric concentration of N_2O over time by maintaining equilibrium via air-sea exchange.

6. 3: Comparing surface nitrous oxide in the NW European shelf seas and Atlantic Ocean environments.

6.3. 1: Comparison of the sources of surface nitrous oxide between shelf sea and open ocean environments.

The findings from this thesis indicate that the source strengths of N_2O differ between the NW European shelf seas and the open Atlantic Ocean environments, with the shelf sea environment acting as a stronger source of N_2O than the open ocean.

One key question is whether this high emission in the shelf seas is due to a nitrification source or a denitrification source. In order to compare different sources of data on production rates to try to answer this question, it is necessary to define a geographical area for which area and volume are known. Here the North Sea is selected (area 7.50 x 10^{11} m^2; volume 9.4 x 10^{13} m^3; http://www.mumm.ac.be/EN/NorthSea/facts.php). In the NW European shelf seas during cruise D366, an average per unit area flux of 997.20 nmol m^{-2} d^{-1} was observed. When scaled up to the area of the North Sea this gives a total flux of N_2O of 1.2 x 10^{10} g N_2O yr^{-1}.

Rates of nitrification measured in the North Sea vary over three orders of magnitude from 0.2 to 221 nmol N L^{-1} h^{-1} (Clark et al., 2008, Veuger et al., 2013).

The yield of N_2O produced from NH_4^+ oxidation also varies with the O_2 concentration in the water column (Goreau et al., 1980). Goreau et al. (1980) found the yield of production of N_2O during NH_4^+ oxidation ranged from 0.3 % at atmospheric O_2 concentrations, to 10 % at low oxygen concentrations. Using these upper and lower estimates, N_2O production from NH_4^+ oxidation within the volume of the North Sea at (http://www.mumm.ac.be/EN/NorthSea/facts.php), is estimated between of 1.09×10^{10} and 4.00×10^{14} g N_2O yr^{-1} (Clark et al., 2008, Veuger et al., 2013). The estimated flux of N_2O of 1.2×10^{10} g N_2O yr^{-1} from the areal extend of the North Sea during the D366 cruise fits into the very lower end of this range. As the North Sea is for the most part well oxygenated, the lower yield is more likely to be applicable, however to reconcile these numbers the nitrification rate must be at the lowest end of the literature values. This may be because of seasonal bias in sampling, or because the nitrification rate estimates used were obtained from incubations using ^{15}N and NH_4^+, and therefore possible incubation effects may have lead to the rates being higher than in-situ rates. Nonetheless it is possible to explain all of the N_2O emission by nitrification alone.

Seitzinger and Kroeze (1998) suggested that the yield of N_2O from denitrification is approximately 1 % of the nitrate consumed. Denitrification rates for the North Sea are highly variable, estimated between 0.9 to 255 mmol N m^{-2} yr^{-1} (Brion et al., 2004). Using these figures, a yield of N_2O from denitrification, calculated for the same areal extent as above for the North Sea, is estimated between 1.49×10^8 and 4.21×10^{10} g N_2O yr^{-1}. The estimated flux of N_2O of 1.2×10^{10} g N_2O yr^{-1} from the D366 cruise agrees well with this range. Therefore the production of N_2O from nitrification is estimated 100 to 1000 times greater than that produced by denitrification.

In the NW European shelf seas, N_2O production from both nitrification and denitrification could fully account for the flux of N_2O estimated during the D366 cruise. These calculations indicate that the marine N_2O budget is not closed, as there is still a large uncertainty over the rates of nitrification and denitrification, and associated production of N_2O, in the marine environment. However, many nitrification, denitrification and N_2O production rates are determined through

experiments in bottles, from which the reported rates are assumed to be the same as those within the natural environment. The unnatural conditions of the experiment may change the environment and therefore affect the rates of these processes. Further evidence from literature in this field indicates that nitrification may be the dominant source of N_2O. For example, globally, N_2O profiles show maxima in the oxic subsurface waters, with a strong correlation with O_2 concentration, which has been interpreted as evidence for nitrification (Yoshinari, 1976, Cohen and Gordon, 1978). In the North Sea, Law and Owens (1990a) supported this idea, reporting that most N_2O production occurred in the photic zone and suggested that this could be due to nitrification. They also found N_2O production in sediments by denitrification to be low.

In the open Atlantic Ocean, nitrification at depth appears to be the dominant pathway for N_2O (Yoshinari, 1976, Oudot et al., 2002, Nevison et al., 2003, Walter et al., 2006, Forster et al., 2009, Freing et al., 2009). Undersaturation for N_2O observed in the surface waters of the Atlantic Ocean suggests that euphotic nitrification is not an influential process in this environment. However studies have indicated that mixed layer nitrification undertaken by ammonia oxidising bacteria does occur in the ocean (Dore and Karl, 1996, Law and Ling, 2001, Morell et al., 2001, Wankel et al., 2007, Clark et al., 2008). Nitrification at depth occurs as organic particles sink and are remineralised. The production of N_2O by denitrification in the ocean's anoxic sediments, or in very deep low-oxygen environments, seems unlikely to influence the surface waters, with the exception of regions of upwelling, because it would remain at depth under the thermocline, due to slow vertical diffusive transport of water parcels.

6.3. 2: Comparing the saturation and ocean to atmosphere fluxes of nitrous oxide between the NW European shelf seas and Atlantic Ocean.

The mean saturation for N_2O in surface waters of the NW European shelf seas (D366) was significantly higher, at 102 ± 2 %, than that in the open ocean, at 97 ± 1 %, during the AMT22 cruise (unpaired t-test, p=0.05, n=47330) (Figure 6. 2). This difference can be attributed to different processes, as well as the close

proximity of coastal influences, such as estuaries and rivers, transporting organic matter into the water column and stimulating primary production. Particulate organic matter (POM) in the ocean, consisting of dead tissues, excreta, molts and aggregated dissolved organic matter (DOM), is decomposed by AOA and AOB during respiration. During the initial stages of remineralisation, nitrogen is released from the organic matter in the form of ammonium, which then under oxic conditions is oxidised to nitrite and then nitrate during the nitrification pathway. During the initial oxidation reaction from ammonium to nitrite, nitrous oxide is produced as a by-product. In anoxic marine sediments, the reduction of oxidised nitrogen compounds during the denitrification pathway produces a further source of N_2O. Shelf seas have a shallower water column than the open ocean and more incidences where vertical mixing could potentially lift organic matter and N_2O into the surface waters due to there being more substrate per surface area than in the open ocean, leading to higher surface saturations of N_2O in this environment. In the open ocean N_2O increases with depth, but limited mixing between deep and surface waters results in most of the N_2O remaining at depth, with only small amounts reaching the surface by entrainment. As a consequence of the higher surface saturations found in the shelf seas than in the Atlantic Ocean, a significance difference was also found in the ocean to atmosphere flux of N_2O (Figure 6. 3). During the D366, the NW European shelf seas were found to act as a slight atmospheric source of N_2O, at 997 ± 1250 nmol m^2 d^{-1}. In comparison, the Atlantic Ocean acted as a slight sink at -426 ± 554 nmol m^2 d^{-1} during AMT22 (unpaired t-test, p=0.05, n=47330) (Figure 6. 3). This conclusion is dependent on solubility measurements made in 1980 (Weiss and Price, 1980), which may require revisiting to ensure it's accuracy. Undersaturation of N_2O in surface waters is discussed in Section 6. 5.

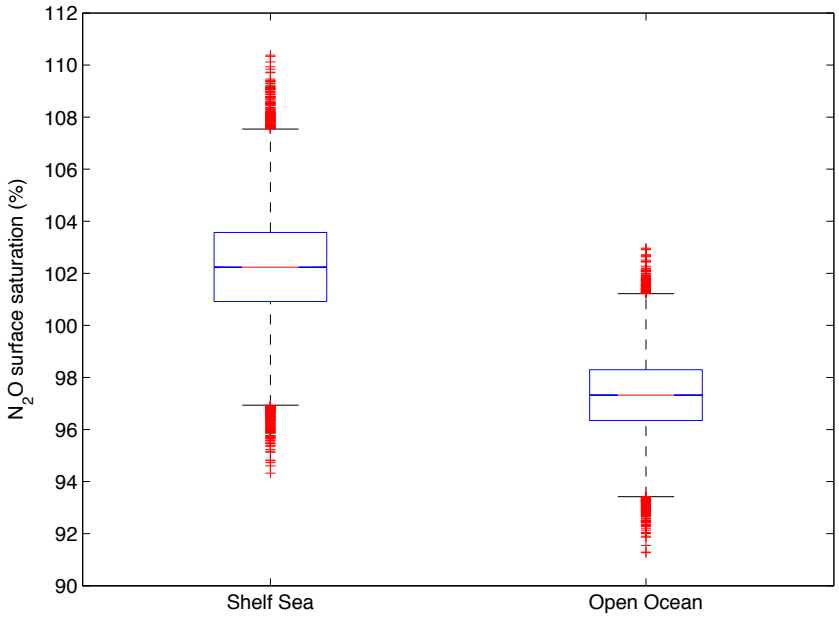

Figure 6. 2: The mean saturation of surface N_2O was found to be significantly higher in the NW European shelf seas (D366), at 102 ± 2 %, than in the open ocean (AMT22), at 97 ± 1 %, during the AMT22 cruise (unpaired t-test, p=0.05, n=47330). The mean is shown by the red and blue line in the centre of the box. The box indicates the 25th percentile and the black lines the 75th percentile. The red crosses are outliers larger than the 75th percentile.

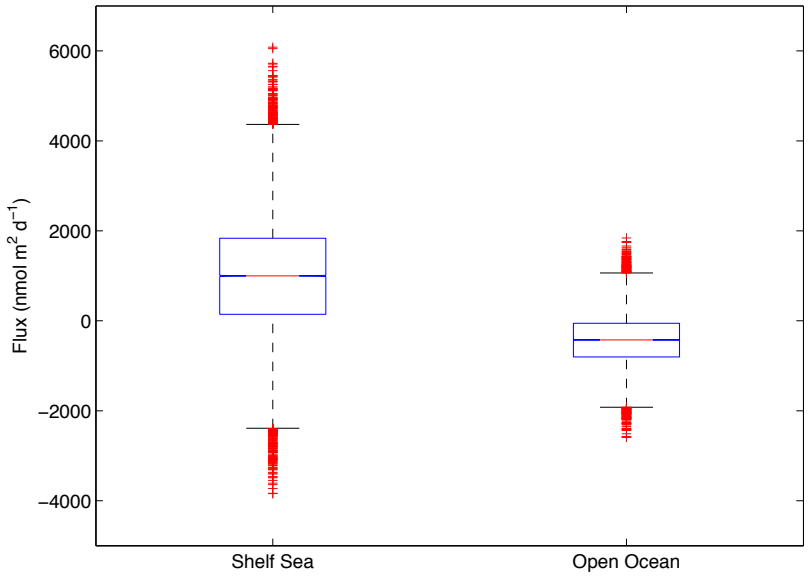

Figure 6. 3: The mean ocean to atmosphere flux of N_2O was found to be significantly different between the NW European shelf seas (D366), with an atmospheric source of 997 ± 1250 nmol m^2 d^{-1}, and the open ocean (AMT22), acting as a sink at -426 ± 554 nmol m^2 d^{-1} (unpaired t-test, p=0.05, n=47330). The mean is shown by the red and blue line in the centre of the box. The box indicates the 25th percentile and the black lines the 75th percentile. The red crosses are outliers larger than the 75th percentile.

6. 4: Change in the source–sink characteristic of surface nitrous oxide in the Atlantic Ocean over eighteen years.

It was difficult to determine whether a change in the source-sink characteristic of N_2O occurred between 1996 and 2013 in the Atlantic Ocean, due to spatial differences between the earlier (AMT3 and 7) and later (AMT20, 22 and 23) cruise tracks. The earlier cruise tracks generally sampled closer to the coast in two of the three compared regions than the later cruise tracks, which sampled further west and east into the NAG and SAG. The subtropical gyres were slightly undersaturated for N_2O in comparison to the surface waters closer to the coast, where the waters were slightly supersaturated. As a consequence of these spatial differences the earlier cruises sampled slightly higher N_2O surface concentrations.

6. 5: Undersaturation of nitrous oxide in surface waters of the Atlantic Ocean

All five of the surface N_2O AMT datasets examined displayed undersaturation in surface waters in regions (of varying sizes) across the AMT transect (Figure 5. 12). For the earlier cruises these regions were smaller at 20 to 40 °N (AMT3) and 45 to 50 ° N (AMT7), than found in the most recent datasets (AMT20, AMT22, and AMT23), where the surface waters were predominantly undersaturated in N_2O throughout the cruise. The more recent AMT cruises sampled further into the subtropical gyres than the earlier ones. The cause of undersaturation is unknown but maybe due to a N_2O consumption pathway occurring in surface waters. Possible pathways include N_2O fixation, where culture experiments found that certain cyanobacteria species have demonstrated the ability to fix N_2O into particulate organic matter, using it as an alternative substrate to N_2. In the oceans this biological mechanism has been described to act as an N_2O sink within both eutrophic and oligotrophic waters, with N_2O fixation taking place in subsurface waters and the oxygenated surface layer (Cornejo et al., 2015). Alternatively, denitrification within anoxic micro-zones in the surface waters of the ocean (Wyman et al., 2013) may also lead to surface undersaturation of N_2O. These pathways need to be investigated further.

6. 6: Measurements of surface methane in the NW European shelf seas and Atlantic Ocean.

6.6. 1: Surface methane measurements in the NW European shelf seas.

In June and July 2011, during the D366 research cruise, sea surface waters in the NW European shelf seas were supersaturated for CH_4 with respect to the atmospheric value. A mean surface concentration of 3 ± 1 nmol L^{-1} and a mean surface saturation of 118 ± 22 %, ranging from 100 to 315 %, were observed. The mean surface saturation value estimated for CH_4 is consistent with other estimates in this region, which ranged between 113 to 140 % (Table 1. 8). The surface saturations of CH_4 reported in the NW European shelf seas is lower than found in other shelf seas, including the Yellow Sea and East China sea at 134 % ± 22 (110 to 222) (Zhang et al., 2004), the NW Black Sea at 930 (173 – 10500) (Amouroux et al., 2002), and the East Siberian Arctic shelf at 800 – 2500 % (Shakhova and Semiletov, 2007) (Table 1. 8). A comparison of CH_4 saturation and fluxes calculated in different regions show that both are far higher in estuaries, than shelf seas and the open ocean, with the shelf seas exceeding the latter (Table 6. 1).

6.6. 2: Ocean to atmosphere flux estimates for methane

6.6.2. 1: Flux estimates for methane in the NW European shelf seas.

Using an areal extent of 1.14 x 10^6 km^2 (Uher, 2006) for the North Sea, the Irish Sea and the Bay of Biscay, and using the mean ocean to atmosphere flux of 2.32 x 10^3 ± 3.69 x 10^3 nmol m^{-2} d^{-1} calculated during the D366, the source of CH_4 from this region is calculated as 4.25 x 10^{10} g CH_4 yr^{-1}. The mean atmospheric flux of CH_4 estimated by Bange (2006) for D366 is in line with that estimated for European shelf regions at 2.67 x 10^3 nmol m^{-2} d^{-1}. Using the global areal extent of shelf seas (32.49 million km^2), with a summertime flux of 2.32 x 10^3 ± 3.69 x 10^3 nmol m^{-2} d^{-1}, and assuming that the production of CH_4 from all shelf seas globally is similar, a global summertime shelf sea atmospheric flux of CH_4 of 1.21

x 10^{12} g CH_4 yr^{-1} is estimated. The IPCC does not currently list shelf seas as a source of CH_4 to the atmosphere (Ciais et al., 2013). These calculations indicate that the global source of 1.2 Tg CH_4 yr^{-1} from shelf seas puts this in line with the source of CH_4 produced from permafrost at approximately 1 Tg CH_4 yr^{-1} (Ciais et al., 2013), which is currently in the IPCC report, indicating the shelf sea source of CH_4 should be listed. However, this estimation is biased, as the measurements were made in the summertime, and it therefore assumes fluxes will be consistent throughout the year, ignoring seasonal effects on CH_4 production. A further assumption that limits the approach, as discussed in section 6.1.2 2, is that the flux of CH_4 from the ocean to atmosphere is similar in all shelf seas. Fluxes of CH_4 estimated during two surveys in March and May 2001 in the Yellow Sea and East China seas were similar to the NW European shelf seas at 1.36 x 10^3 nmol m^{-2} d^{-1} and 2.30 x 10^3 nmol m^{-2} d^{-1} (Zhang et al., 2004). However, CH_4 flux estimates from the NW Black Sea were much higher at 2.60 x 10^4 nmol m^{-2} d^{-1}.

6.6.2. 2: Flux estimates for methane in the Atlantic Ocean

Using the approximate area of the Atlantic Ocean of 106.46 million km^2 (www.oceanservice.noaa.gov), along with an estimated flux of CH_4 of 4.26 x 10^2 nmol m^2 d^{-1}, the Atlantic Ocean acts as an atmospheric source of CH_4 of 7.44 x 10^{11} g CH_4 yr^{-1}. This estimation is made with the assumption that the flux of CH_4 does not change throughout the year, or spatially in the Atlantic Ocean. This approach is limited by this assumption, because Forster et al. (2009) showed that there were seasonal differences in CH_4 fluxes between AMT12 and 13, with AMT12 having a greater range of the fluxes estimated between 4.60 x 10^2 nmol m^2 d^{-1} and 9.70 x 10^3 nmol m^2 d^{-1} for AMT12 during boreal spring and austral autumn, and a smaller range found during AMT13 during boreal autumn and austral spring, at 1.21 x 10^3 nmol m^2 d^{-1} to 5.90 x 10^3 nmol m^2 d^{-1}. The AMT22 estimate is more inline with the lower end of the AMT12 CH_4 flux estimate, and an order of magnitude smaller than the AMT13 flux reported. Forster et al. (2009) also reported interstation flux variability showing that there is a large spatial variability in CH_4 fluxes as well as seasonal.

6.6. 3: Surface methane measurements in the Atlantic Ocean.

The mean surface saturation for CH_4 calculated across the AMT22 transect was 107 ± 5 %, concentration was 2 ± 0 nmol L^{-1}, and ocean to atmospheric flux was 357 ± 328 nmol m^2 d^{-1}, making the Atlantic Ocean an atmospheric source during October and November 2012. The range of surface water saturation values, between 100 to 135 %, observed during AMT22 were similar with the 105 to 130 % saturation reported by Conrad and Seiler (1988) in the surface Atlantic Ocean, higher than the 100 to 101 % surface saturation calculated by Rhee (2009) during AMT7, and significantly lower than the ranges reported during both AMT12 at 147 ± 17 to 198 ± 43 and AMT13 at 116 ± 3 to 156 ± 29. This shows that there is high inter-annual variation in the surface saturation of CH_4 in the Atlantic Ocean. In the NH, the AMT7 cruise track was further east than the AMT22, and did not sample the regions in the NAG that were found to have high surface supersaturations, explaining the lower measurements.

6. 7: Processes influencing the surface concentration and saturation for methane.

6.7. 1: The processes that influence surface methane in the NW European shelf seas.

6.7.1. 1: Sea surface salinity.

Surface CH_4 in the NW European shelf seas was highly influenced by freshwater inputs from estuarine and river systems. This was clear on many occasions where a strong inverse relationship and negative correlations were identified between surface CH_4 and SSS, where low SSS was an indicator of freshwater inputs. Studies have reported extremely high values exceeding 21,000 % of CH_4 in river and estuarine systems (Upstill-Goddard et al., 2000). The highest CH_4 concentrations tend to be found in close vicinity of the turbidity maximum and where the water-flow is slow. These values exceed any measurements made in rivers (Upstill-Goddard et al., 2000). In rivers and estuaries, methanogenesis takes place under anoxic conditions as the dominant source of CH_4. When

produced in sediments, ebullition occurs, where small bubbles of CH_4 gas form in the sediments and travel through the water column to the surface (Walter et al. 2007). Through this process CH_4 is transported into the water column. Rehder et al. (1998), Upstill-Goddard et al. (2000), Bange (2006) and Grunwald et al. (2009), reported freshwater inputs to act as a source of CH_4 to the marine environment. The data collected during the D366 cruise fit in with these findings, indicating that high quantities of CH_4 was produced in the freshwater environments surrounding the NW European shelf seas, and flowed out into the marine environment.

6.7.1. 2: Fully mixed water column.

The region extending from the eastern English Channel up to the Norwegian Trench had the highest surface saturations for CH_4 observed during the cruise. The water column is fully mixed between the eastern English Channel and the central North Sea all year round. In these regions, CH_4 produced in the sediments by methanogenesis may be vertically mixed throughout the water column, enhancing surface water concentrations.

6.7. 2: Processes influencing surface methane in the Atlantic Ocean.

6.7.2. 1: Sea surface temperature.

The surface concentration of CH_4 in the Atlantic Ocean displayed a strong negative relationship with SST. This is due to the changing solubility of CH_4 at different temperatures. Higher concentrations of CH_4 were found in colder waters, than in warmer waters, as the solubility of CH_4 is greater at cooler temperatures. As with N_2O, the main control on the surface water CH_4 concentration during D366 was equilibration with the atmosphere. Therefore again, looking at the saturation of CH_4 in surface waters rather than the concentration is important as it removes the solubility effect, allowing the influence of other parameters to be observed.

6.7.2. 2: Amazon outflow waters.

The highest supersaturations in CH_4 observed in the surface waters during the AMT22 were located between the latitudes of 2 to 10 °N. The NECC travels with an eastward flow between the approximate latitudes of 3 and 9 °N, to depths of 100 m. Discharge from the Amazon outflow has been found to travel along the NECC towards Africa between the months of June and January each year (Muller-Karger et al., 1988). The high supersaturation for CH_4 observed in surface waters between the latitudes of 2 to 10 °N may be due to:

1) Waters supersaturated for CH_4, originating from the Amazon river, could have influenced the surface waters sampled between 2 to 10 °N during the AMT22, by having a higher CH_4 content than the surrounding waters.

2) An enhancement of organic matter in surface waters, arising either from the Amazon outflow and travelling along these latitudes, or as a consequence of enhanced production in these waters, may create anoxic microenvironments where methanogenesis could take place.

6.7.2. 3: Stratification of the water column.

In the NAG the surface saturation for CH_4 was high compared to the surrounding locations. This could be due to the autumn-time stratification of the water column, which acted to reduce the removal of CH_4 produced in-situ from the surface waters by limiting vertical mixing and advection.

6. 8: Comparing surface methane in the NW European shelf seas and the Atlantic Ocean environments.

6.8. 1: Comparison of sources of surface methane between the NW European shelf seas and the Atlantic Ocean environments.

In the shelf sea environment, the dominant source of surface CH_4 arises from methanogenesis in anoxic sediments within estuarine environments, entering the water column by diffusion, and flowing into the shelf seas. This is not the

main source in the open ocean, because CH_4 released from ocean basins would undergo microbial oxidisation at depth, minimising the amount reaching the surface waters (Valentine et al., 2001). The dominant source of CH_4 in the open ocean therefore must be in-situ production, as the air-sea exchange of CH_4 would not lead to the supersaturations of CH_4 observed in surface waters during AMT22. In-situ production of CH_4 in the surface waters of the ocean, and may arise from:

1. Methanogenesis, which takes place within small anoxic micro-niches found within decaying organic particles, faecal pellets, as well as in fish and zooplankton intestines (Lamontagne et al., 1973, Karl and Tilbrook, 1994, Van der Maarel et al., 1999).
2. Methylotrophic methanogenesis, which occurs within nutrient-limited waters, such as within the oligotrophic subtropical gyres. Bacteria have been found to utilise methylated substrates released by phytoplankton, including methylphosphonate (Mpn) and dimethylsulfoniopropionate (DMSP) for energy in aerobic systems. These substances act as precursors for CH_4. Two pathways have currently been discovered. Firstly, under low nitrate conditions bacteria have displayed the ability to use DMSP as a carbon source to compete for phosphate, producing CH_4 in the process (Damm et al., 2010). Secondly, in phosphate-limited waters, bacteria can use Mpn as a sole source of phosphate for growth, with the decomposition of Mpn under aerobic conditions, releasing CH_4 as a by-product (Karl et al., 2008).

6.8. 2: Comparing the saturation and ocean to atmosphere fluxes of methane between the NW European shelf seas and the Atlantic Ocean.

The mean surface saturation and ocean to atmosphere flux of CH_4 was found to be significantly higher in the NW European shelf seas (D366), at 118 ± 22 % and 2315 ± 3691 nmol m^{-2} d^{-1}, than in the open Atlantic Ocean (AMT22), at 107 ± 5 % and 358 ± 308 nmol m^2 d^{-1} (unpaired t-test, p=0.05, n=47330) (Figures 6. 4 and 6. 5). The differences in the surface saturation and the atmospheric flux of CH_4 reflect the different yields of CH_4 produced by the dominant sources in each

environment. Shelf sea surface waters were predominantly influenced by methanogenesis that took place within anoxic sediments, which clearly produced a much greater source of CH_4 than in-situ production, as the main source in the surface waters of the Atlantic Ocean. The variability for both the surface saturation and ocean to atmosphere flux of CH_4 was much greater in the shelf sea environments than in the open ocean due to the extremely high sources of CH_4 arising from estuarine outflows of up to 315 %.

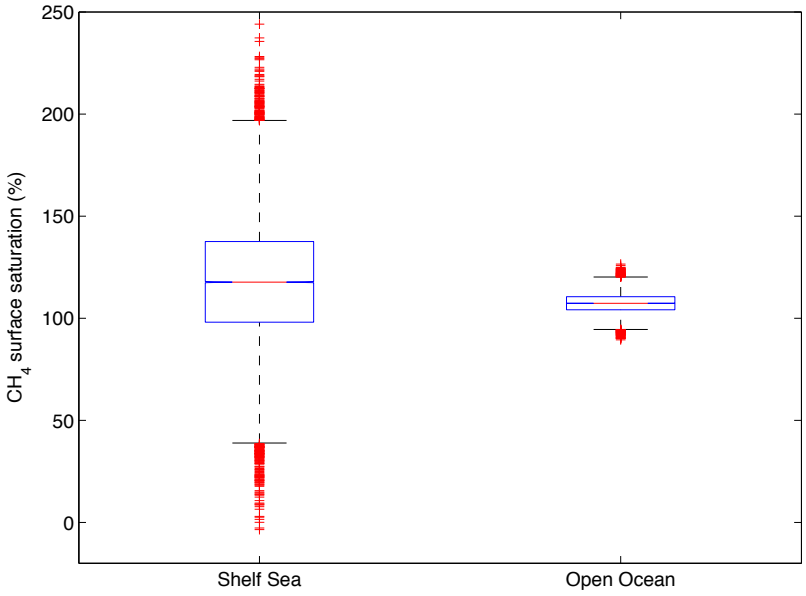

Figure 6. 4: The mean saturation for surface CH_4 was found to be significantly higher in the NW European shelf seas (D366), at 118 ± 22 %, than in the Atlantic Ocean (AMT22), at 107 ± 5 %, during the AMT22 cruise (unpaired t-test, p=0.05, n=47330). The mean is shown by the red and blue line in the centre of the box. The box indicates the 25th percentile and the black lines the 75th percentile. The red crosses are outliers larger than the 75th percentile.

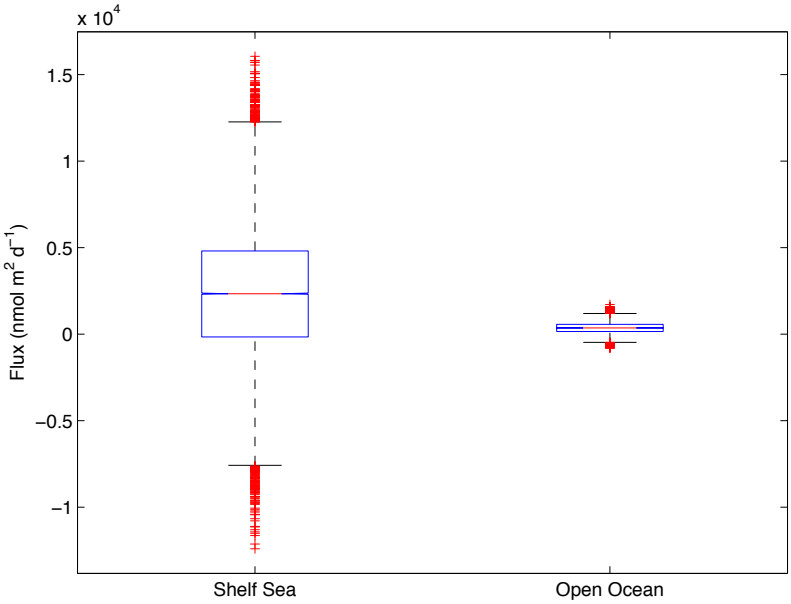

Figure 6. 5: The mean ocean to atmosphere flux for CH_4 was found to be significantly greater in the NW European shelf seas (D366), with an atmospheric source of 2315.40 ± 3691.30 nmol m^{-2} d^{-1}, than in the Atlantic Ocean (AMT22) at 357.55 ± 308.42 nmol m^2 d^{-1} (unpaired t-test, p=0.05, n=47330). The mean is shown by the red and blue line in the centre of the box. The box indicates the 25th percentile and the black lines the 75th percentile. The red crosses are outliers larger than the 75th percentile.

6. 9: Comparing nitrous oxide and methane within the NW European shelf seas and Atlantic Ocean.

6.9. 1: Why were the surface waters surrounding outflows of rivers and estuaries highly supersaturated in CH_4, but not in N_2O, when there is a high production of both gases in these environments?

Surface waters surrounding the outflows of rivers and estuaries were not highly supersaturated with N_2O, as they were for CH_4 during the D366 cruise. The residence time for both N_2O and CH_4 during the D366 cruise was similar, estimated at approximately two weeks (at the mean wind speed, SST and mixed layer depth during the D366) (sections 3.3. 4 and 4.3. 4), therefore not explaining this phenomenon. The difference between the two trace gases may be explained by the difference in their production rates within riverine and estuarine systems, leading to the higher surface saturation values of 6000 to 21,800 % reported in UK estuaries for CH_4 (Upstill-Goddard et al., 2000), and lower values of 140 to 6500 % described for N_2O (Barnes and Upstill-Goddard, 2011). Both CH_4 and

N_2O in surface waters ventilate at an exponential rate to the atmosphere. This means that most the most of these trace gases are lost from the surface waters within two weeks, but the remainder takes longer to ventilate. As higher quantities of CH_4 than N_2O are produced in estuaries and rivers, a higher concentration of this trace gas will be distributed from these environments into the surrounding shelf seas than N_2O. Additionally, enhanced organic material in the outflows of rivers and estuaries may lead to the production of anoxic micro-niches where methanogenesis and complete denitrification may occur, further enhancing surface CH_4 concentrations, whilst acting as an N_2O sink.

6.9. 2: Why were surface waters highly supersaturated at regions of upwelling in N_2O, but not for CH_4, when both trace gases are produced in high quantities at depth in the ocean?

During the AMT cruise the surface waters overlying regions of upwelling, such as the equatorial upwelling, were the most supersaturated for surface N_2O. In comparison, surface CH_4 was not enhanced in these regions. Typical depth profiles in these regions are shown by Forster et al. (2009). Both N_2O and CH_4 are produced at depth in the water column, N_2O by nitrification and denitrification, and CH_4 by methanogenesis. The nitrification pathway occurs under oxic conditions (Capone et al., 2008), so takes place at shallower depths in the water column than denitrification and methanogenesis. Denitrification and methanogenesis take place under anoxic conditions, or at very low oxygen concentrations, deep in the water column or within marine sediments (Levipan et al., 2007, Capone et al., 2008, Ferry and Lessner, 2008). Nitrous oxide produced by nitrification, and denitrification in OMZ's, is upwelled to the surface enhancing surface concentrations of N_2O. In comparison, any CH_4 produced at depth undergoes microbial oxidation as it is upwelled to the surface as methane oxidation rates are high in deep waters (Valentine et al., 2001) and transport to the ocean surface is relatively slow, drastically reducing or depleting the CH_4 source.

6. 10: Future work

1. Future work leading on from this thesis involves reducing the $\boldsymbol{\tau}$ (described in section 2. 4) for CH_4 and for CO for future cruises. Both CH_4 and CO had very slow equilibration times with the setup used for these cruises ($\boldsymbol{\tau} = 42$ minutes for CH_4 and 62 minutes for CO). When using the current setup, it was not possible to detect rapid changes in the surface waters of highly variable environments, such as within shelf seas, because the data was 'smoothed' out due to the slow equilibration times. Reducing the $\boldsymbol{\tau}$ for these gases would require testing different sized equilibrators to obtain the fastest equilibration time for all of the four gases measured. Smaller equilibrators are predicted to have a faster $\boldsymbol{\tau}$.
2. The two ICOS analysers and current setup offer the potential to collect simultaneous high-resolution measurements for N_2O, CH_4, CO_2 and CO. The following future step is therefore to automate the system, and set it up on a voluntary observation ship. This will ensure that high spatial and temporal coverage of the surface distribution of N_2O and CH_4, as well as CO_2 and CO, can be obtained. The aim of this would be to understand how the surface concentration and saturation distribution, along with the ocean to atmosphere fluxes of these trace gases, varies inter-annually, seasonally and spatially.
3. Taking this equipment on more AMT cruises will additionally extend the current time-series for surface N_2O so that potential decadal changes in surface concentration or the saturation state can start to be investigated.
4. There is currently a gap in our knowledge in understanding potential microbial consumption pathways for N_2O in the surface ocean. More work in this area is important to fully understand the biogeochemical cycling of N_2O in the ocean, and to gain insight into the causes of undersaturation in surface waters of the Atlantic Ocean.
5. During AMT22, high surface CH_4 was found in the NAG, but not in the SAG. It is important to establish what causes this difference by investigating differences in essential nutrients in each subtropical gyre, which bacterial species are abundant, and which pathways are taking place for CH_4 production to be confirmed.

6. A fundamental control on the production of N_2O and CH_4 in the marine environment is the concentration of oxygen (O_2). It is predicted that with the effects of climate change, alterations in ocean circulation and stratification may influence the O_2 concentration in the water column. In addition to this, an enhancement of nutrients from land, with increases in N_r run off into coastal systems, is predicted to cause an increase in organic matter respiration, further reducing O_2 levels. Methane hydrates stored within shallow ocean sediments and on the slopes of continental shelves are predicted to release large quantities of CH_4 in the future. This would lead to higher rates of microbial oxidation reducing O_2 levels in the ocean even more, as well as increasing ocean acidification. It is important to understand how these reductions in the O_2 concentration in the ocean may affect the production of N_2O and CH_4 in the future.
7. With the effects of climate change the ocean is warming. It is important to understand how warming of the ocean in the future might affect the saturation state of N_2O and CH_4. For example, warming may affect the surface concentration of each of these climatically relevant gases, as the solubility of N_2O and CH_4 changes, and how this may impact the flux of these climatically important gases to the atmosphere. In addition, it is important to understand how warming will affect the deep oceans ability to store N_2O, and how bacterial communities responsible for the production and consumption of these gases may alter in response to warmer waters.
8. Another important area for future research is to understand how ocean acidification will affect the source-sink characteristic of N_2O. Nitrification has been found to display a sensitivity to pH, and consequently this may lead to a reduction in nitrification rates in the coming few decades of 3 to 44 % (Beman et al., 2011). Inhibition of ammonium oxidation by low pH has been reported in the Atlantic and Pacific euphotic zone (Beman et al., 2011). However, other studies within shallow coastal systems and shelf seas have found contradictory results (Fulweiler et al., 2011), or that responses in nitrification rates to different pH treatments were location specific and that the response of N-regeneration to these treatments was

unclear (Clark et al., 2014). Further investigation to understand the response of nitrification to a more acidic ocean is clearly required.

9. Future recommendations for the AMT programme were made in section 5.4.2.

References

Abram, J. & Nedwell, D. 1978. Inhibition of methanogenesis by sulphate reducing bacteria competing for transferred hydrogen. *Archives of Microbiology,* 117**,** 89-92.

Abril, G. & Borges, A. 2005. Carbon dioxide and methane emissions from estuaries. *In:* Tremblay, A., Varfalvy, L., Roehm, C. & Garneau, M. (eds.) *Greenhouse Gas Emissions — Fluxes and Processes.* Berlin, Heidelberg: Springer

Agage 1993-08 -2014-03. N_2O (continuous,md_p) monthly Cape Grim. World Data Centre for Greenhouse Gases (WDCGG).

Agage 1994-03 -2014-03. N_2O (continuous,md_p) monthly Mace Head. World Data Centre for Greenhouse Gases (WDCGG).

Aiken, J., Rees, N., Hooker, S., Holligan, P., Bale, A., Robins, D., Moore, G., Harris, R. & Pilgrim, D. 2000. The Atlantic Meridional Transect: overview and synthesis of data. *Progress in Oceanography,* 45**,** 257-312.

Amouroux, D., Roberts, G., Rapsomanikis, S. & Andreae, M. O. 2002. Biogenic gas (CH_4, N_2O, DMS) emission to the atmosphere from near-shore and shelf waters of the north-western Black Sea. *Estuarine, Coastal and Shelf Science,* 54**,** 575-587.

Artioli, Y., Blackford, J. C., Butenschön, M., Holt, J. T., Wakelin, S. L., Thomas, H., Borges, A. V. & Allen, J. I. 2012. The carbonate system in the North Sea: Sensitivity and model validation. *Journal of Marine Systems,* 102–104**,** 1-13.

Bakwin, P. S., Tans, P. P. & Novelli, P. C. 1994. Carbon monoxide budget in the northern hemisphere. *Geophysical Research Letters,* 21.

Bale, A. J. 1996. AMT-3 cruise report. *Atlantic Meridional Transect (AMT).* Plymouth: Plymouth Marine Laboratory (PML).

Bange, H. W. 2004. Air-sea exchange of nitrous oxide and methane in the Arabian Sea: A simple model of the seasonal variability. *Indian Journal of Marine Sciences,* 33**,** 77 - 83.

Bange, H. W. 2006. Nitrous oxide and methane in European coastal waters. *Estuarine, Coastal and Shelf Science,* 70**,** 361-374.

Bange, H. W. & Andreae, M. O. 1999. Nitrous oxide in the deep waters of the world's oceans. *Global Biogeochemical Cycles,* 13**,** 1127-1135.

Bange, H. W., Bartell, U. H., Rapsomanikis, S. & Andreae, M. O. 1994. Methane in the Baltic and North Seas and a reassessment of the marine emissions of methane. *Global Biogeochemical Cycles* 8**,** 465-480.

Bange, H. W., Ramesh, R., Rapsomanikis, S. & Andreae, M. O. 1998. Methane in surface waters of the Arabian Sea. *Geophysical Research Letters,* 25**,** 3547-3550.

Bange, H. W., Rapsomanikis, S. & Andreae, M. O. 1996a. Nitrous oxide emissions from the Arabian Sea. *Geophysical Research Letters,* 23**,** 1944 - 8007.

Bange, H. W., Rapsomanikis, S. & Andreae, M. O. 1996b. Nitrous oxide in coastal waters. *Global Biogeochemical Cycles,* 10**,** 197-207.

Barnes, J. & Owens, N. J. P. 1999. Denitrification and Nitrous Oxide Concentrations in the Humber Estuary, UK, and Adjacent Coastal Zones. *Marine Pollution Bulletin,* 37**,** 247-260.

Barnes, J. & Upstill-Goddard, R. C. 2011. N_2O seasonal distributions and air-sea exchange in UK estuaries: Implications for the tropospheric N_2O source from European coastal waters. *Journal of Geophysical Research: Biogeosciences,* 116**,** G01006.

Becker, G. A., Fiúza, A. F. G. & James, I. D. 1983. Water mass analysis in the German Bight during Marsen, Phase I. *Journal of Geophysical Research: Oceans,* 88**,** 9865-9870.

Becker, M., Andersen, N., Fiedler, B., Fietzek, P., Körtzinger, A., Steinhoff, T. & Friedrichs, G. 2012. Using cavity ringdown spectroscopy for continuous monitoring of $\delta^{13}C(CO_2)$ and fCO_2 in the surface ocean. *Limnology Oceanography,* Methods 10 752–766.

Beman, J. M., Chow, C.-E., King, A. L., Feng, Y., Fuhrman, J. A., Andersson, A., Bates, N. R., Popp, B. N. & Hutchins, D. A. 2011. Global declines in oceanic nitrification rates as a consequence of ocean acidification. *Proceedings of the National Academy of Sciences,* 108**,** 208-213.

Blackburn, M. 1981. *Low latitude gyral regions,* New York, USA, Academic Press.

Blees, J., Niemann, H., Wenk, C. B., Zopfi, J., Schubert, C. J., Kirf, M. K., Veronesi, M. L., Hitz, C. & Lehmann, M. F. 2014. Micro-aerobic bacterial methane

oxidation in the chemocline and anoxic water column of deep south-Alpine Lake Lugano (Switzerland). *Limnology Oceanography,* 59**,** 311-324.

Boetius, A., Ravenschlag, K., Schubert, C. J., Rickert, D., Widdel, F., Gieseke, A., Amann, R., Jorgensen, B. B., Witte, U. & Pfannkuche, O. 2000. A marine microbial consortium apparently mediating anaerobic oxidation of methane. *Nature,* 407**,** 623-626.

Bousquet, P., Ringeval, B., Pison, I., Dlugokencky, E. J., Brunke, E.-G., Carouge, C., Chevallier, F., Fortems-Cheiney, A., Frankenberg, C., Hauglustaine, D. A., Krummel, P. B., Langenfelds, R. L., Ramonet, M., Schmidt, M., Steele, L. P., Szopa, S., Yver, C., Viovy, N. & Ciais, P. 2011. Source attribution of the changes in atmospheric methane for 2006 - 2008. *Atmospheric Chemistry and Physics,* 11**,** 3689 - 3700.

Brandini, F. P., Boltovskoy, D., Piola, A., Kocmur, S., Röttgers, R., P, C. A. & R., M. L. 2000. Multiannual trends in fronts and distribution of nutrients and chlorophyll in the southwestern Atlantic (30–62°S). *Deep-Sea Research Part I: Oceanographic Research Papers,* 47**,** 1015-1033.

Brion, N., Baeyens, W., De Galan, S., Elskens, M. & Laane, R. P. M. 2004. The North Sea: source or sink for nitrogen and phosphorus to the Atlantic Ocean? *Biogeochemistry,* 68**,** 277-296.

Brotas, V., Brewin, R. J. W., Sá, C., Brito, A. C., Silva, A., Mendes, C. R., Diniz, T., Kaufmann, M., Tarran, G., Groom, S. B., Platt, T. & Sathyendranath, S. 2013. Deriving phytoplankton size classes from satellite data: Validation along a trophic gradient in the eastern Atlantic Ocean. *Remote Sensing of Environment,* 134**,** 66-77.

Bussmann, I. & Suess, E. 1998. Groundwater seepage in Eckernforde Bay (western Baltic Sea): Effect on methane and salinity distribution of the water column. *Continental Shelf Research,* 18**,** 1795-1806.

Butler, J. H., Elkins, J. W., Brunson, C. M., Egan, K. B., Thompson, T. M., Conway, T. J. & Hall, B. D. 1988. Trace gases in and over the West Pacific and East Indian Oceans during the El Nino-Southern Oscillation event of 1987. *ERL ARL-16.* Air Resources Laboratory, Silver Spring, MD.

Capone, D. G., Bronk, D. A., Mulholland, M. R. & Carpenter, E. J. 2008. *Nitrogen in the marine environment (second edition),* Access online via Elsevier., Academic Press.

Capone, D. G. & Kiene, R. P. 1988. Comparison of microbial dynamics in marine and freshwater sediments: Contrasts in anaerobic carbon catabolism. *Limnology and Oceanography,* 33**,** 725-749.

Charpentier, J., Farías, L. & Pizarro, O. 2010. Nitrous oxide fluxes in the central and eastern South Pacific. *Global Biogeochemical Cycles,* 24**,** GB3011.

Ciais, P., Sabine, C., Bala, G., Bopp, L., Brovkin, V., Canadell, J., Chhabra, A., Defries, R., Galloway, J., Heimann, M., Jones, C., Le QuéRé, C., Myneni, R. B., Piao, S. & Thornton, P. 2013. Carbon and other biogeochemical cycles. *In:* Stocker, T. F., Qin, D., G-K., P., Tignor, M., Allen, S. K., Boschung, J., Nauels, A., Xia, Y., Bex, V. & Midgley, P. M. (eds.) *Climate change 2013: the physical science basis. Contribution of working group I to the fifth assessment report of the intergovernmental panel on climate change. .* Cambridge, United Kingdom and New York, NY, USA. : Cambridge University Press.

Cicerone, R. J. & Oremland, R. S. 1988. Biogeochemical aspects of atmospheric methane. *Global Biogeochemical Cycles,* 2**,** 299-327.

Clark, D. R., Brown, I. J., Rees, A. P., Somerfield, P. J. & Miller, P. I. 2014. The influence of ocean acidification on nitrogen regeneration and nitrous oxide production in the North-West European shelf sea. *Biogeosciences Discussions,* 11**,** 3113 - 3165.

Clark, D. R., Rees, A. P. & Joint, I. 2008. Ammonium regeneration and nitrification rates in the oligotrophic Atlantic Ocean: Implications for new production estimates. *Limnology and Oceanography,* 53**,** 52-62.

Cline, J. D., Wisegarver, D. P. & Kelly-Hansen, K. 1987. Nitrous oxide and vertical mixing in the equatorial Pacific during the 1982–1983 El Niño. *Deep Sea Research Part A. Oceanographic Research Papers,* 34**,** 857-873.

Codispoti, L. A. 2010. Interesting times for marine N_2O. *Science,* 327**,** 1339-1340.

Cohen, Y. & Gordon, L. I. 1978. Nitrous oxide in the oxygen minimum of the eastern tropical North Pacific: evidence for its consumption during denitrification and possible mechanisms for its production. *Deep-Sea Research,* 25**,** 509-524.

Conrad, R. & Seiler, W. 1988. Methane and hydrogen in seawater (Atlantic Ocean). *Deep-Sea Research Part A. Oceanographic Research Papers,* 35**,** 1903-1917.

Conrad, R., Seiler, W., Bunse, G. & Giehl, H. 1982. Carbon monoxide in seawater (Atlantic Ocean). *Journal of Geophysical Research: Oceans,* 87**,** 8839-8852.

Cooper, D. J., Watson, A. J. & Ling, R. D. 1998. Variation of pCO_2 along a North Atlantic shipping route (U.K. to the Caribbean): A year of automated observations. *Marine Chemistry,* 60**,** 147-164.

Cornejo, M., Murillo, A. A. & Farías, L. 2015. An unaccounted for N_2O sink in the surface water of the eastern subtropical South Pacific: Physical versus biological mechanisms. *Progress in Oceanography,* 137, Part A**,** 12-23.

Cubasch, U., Wuebbles, D., Chen, D., Facchini, M. C., Frame, D., Mahowald, N. & Winther, J.-G. 2013. Introduction. *In:* Stocker, T. F., Qin, D., Plattner, G.-K., Tignor, M., Allen, S. K., Boschung, J., Nauels, A., Xia, Y., Bex, V. & Midgley, P. M. (eds.) *Climate change 2013: The physical science basis. Contribution of working group I to the fifth assessment report of the intergovernmental panel on climate change. .* Cambridge, United Kingdom and New York, NY, USA.: Cambridge University Press.

Dabrowski, T., Hartnett, M. & Olbert, A. I. 2012. Determination of flushing characteristics of the Irish Sea: A spatial approach. *Computers & Geosciences,* 45**,** 250-260.

Damm, E., Helmke, E., Thoms, S., Schauer, U., Nöthig, E., Bakker, K. & Kiene, R. P. 2010. Methane production in aerobic oligotrophic surface water in the central Arctic Ocean. *Biogeosciences,* 7**,** 1099 - 1108.

De Wilde, H. P. J. & De Bie, M. J. M. 2000. Nitrous oxide in the Schelde estuary: production by nitrification and emission to the atmosphere. *Marine Chemistry,* 69**,** 203-216.

Desloover, J., Vlaeminck, S. E., Clauwaert, P., Verstraete, W. & Boon, N. 2012. Strategies to mitigate N_2O emissions from biological nitrogen removal systems. *Current Opinion in Biotechnology,* 23**,** 474-482.

Dlugokencky, E. J., Bruhwiler, L., White, J. W. C., Emmons, L. K., Novelli, P. C., Montzka, S. A., Masarie, K. A., Lang, P. M., Crotwell, A. M., Miller, J. B. &

Gatti, L. V. 2009. Observational constraints on recent increases in the atmospheric CH4 burden. *Geophysical Research Letters,* 36**,** L18803.

Dlugokencky, E. J., Myers, R. C., Lang, P. M., Masarie, K. A., Crotwell, A. M., Thoning, K. W., Hall, B. D., Elkins, J. W. & Steele, L. P. 2005. Conversion of NOAA atmospheric dry air CH_4 mole fractions to a gravimetrically prepared standard scale. *Journal of Geophysical Research: Atmospheres,* 110**,** D18306.

Dong, L. F., Nedwell, D. B., Colbeck, I. & Finch, J. 2005. Nitrous oxide emission from some English and Welsh rivers and estuaries. *Water, Air, and Soil Pollution: Focus,* 4**,** 127-134.

Dore, J. E. & Karl, D. M. 1996. Nitrification in the euphotic zone as a source for nitrite, nitrate, and nitrous oxide at Station ALOHA. *Limnology and Oceanography,* 41**,** 1619-1628.

Druon, J. N., Langlois, G. & Le FèVre, J. 2001. Simulating vertical mixing in a shelf-break region: addition of a shear instability model, accounting for the overall effect of internal tides, on top of a one-dimensional turbulence closure mixed layer model. *Continental Shelf Research,* 21**,** 423-454.

Duce, R. A., Laroche, J., Altieri, K., Arrigo, K. R., Baker, A. R., Capone, D. G., Cornell, S., Dentener, F., Galloway, J., Ganeshram, R. S., Geider, R. J., Jickells, T., Kuypers, M. M., Langlois, R., Liss, P. S., Liu, S. M., Middelburg, J. J., Moore, C. M., Nickovic, S., Oschlies, A., Pedersen, T., Prospero, J., Schlitzer, R., Seitzinger, S., Sorensen, L. L., Uematsu, M., Ulloa, O., Voss, M., Ward, B. & Zamora, L. 2008. Impacts of atmospheric anthropogenic nitrogen on the open ocean. *Science,* 320**,** 893-897.

Ehhalt, D. H. & Schmidt, U. 1978. Sources and sinks of atmospheric methane. *Pure and Applied Geophysics,* 116**,** 452-464.

Eisma, D. & Kalf, J. 1987. Dispersal, concentration and deposition of suspended matter in the North Sea. *Journal of the Geological Society,* 144**,** 161-178.

Etheridge, D. M., Steele, L. P., Francey, R. J. & Langenfelds, R. L. 1998. Atmospheric methane between 1000 A.D. and present: Evidence of anthropogenic emissions and climatic variability. *Journal of Geophysical Research: Atmospheres,* 103**,** 15979-15993.

Farías, L., Castro-González, M., Cornejo, M., Charpentier, J., Faúndez, J., Boontanon, N. & Yoshida, N. 2009. Denitrification and nitrous oxide cycling within the upper oxycline of the eastern tropical South Pacific oxygen minimum zone. *Limnology and Oceanography,* 54**,** 132-144.

Feely, R. A., C.L. Sabine, T. Takahashi & Wanninkhof, R. 2001. Uptake and storage of carbon dioxide in the ocean: The global CO2 survey. *Oceanography,* 14**,** 18-32.

Ferry, J. G. & Lessner, D. J. 2008. Methanogenesis in marine sediments. *Annals of the New York Academy of Sciences,* 1125**,** 147-157.

Fofonoff, N. P. & Millard Jr, R. C. 1983. Algorithms for computation of fundamental properties of seawater. *Unesco technical papers in marine science*.

Forster, G., Upstill-Goddard, R. C., Gist, N., Robinson, C., Uher, G. & Woodward, E. M. S. 2009. Nitrous oxide and methane in the Atlantic Ocean between 50°N and 52°S: Latitudinal distribution and sea-to-air flux. *Deep-Sea Research Part II: Topical Studies in Oceanography,* 56**,** 964-976.

Freing, A., Wallace, D. W. R. & Bange, H. W. 2012. Global oceanic production of nitrous oxide. *Philosophical Transactions of the Royal Society B,* 367**,** 1245-1255.

Freing, A., Wallace, D. W. R., Tanhua, T., Walter, S. & Bange, H. W. 2009. North Atlantic production of nitrous oxide in the context of changing atmospheric levels. *Global Biogeochemical Cycles,* 23.

Fulweiler, R. W., Emery, H. E., Heiss, E. M. & Berounsky, V. M. 2011. Assessing the role of pH in determining water column nitrification rates in a coastal system. *Estuaries and Coasts,* 34**,** 1095-1102.

Galloway, J. N., Schlesinger, W. H., Levy Ii, H., Michaels, A. & Schnoor, J. L. 1995. Nitrogen fixation: Anthropogenic enhancement-environmental response. *Global Biogeochemical Cycles,* 9**,** 235-252.

Garcia, C. a. E., Sarma, Y. V. B., Mata, M. M. & Garcia, V. M. T. 2004. Chlorophyll variability and eddies in the Brazil–Malvinas Confluence region. *Deep-Sea Research Part II: Topical Studies in Oceanography,* 51**,** 159-172.

Gebco 2014. http://www.gebco.net/data_and_products/gridded_bathymetry_data/. *In:* (Gebco), G. B. C. O. T. O. (ed.).

Gordon, A. L. 1981. South Atlantic thermocline ventilation. *Deep-Sea Research Part A. Oceanographic Research Papers,* 28**,** 1239-1264.

Goreau, T. J., Kaplan, W. A., Wofsy, S. C., Mcelroy, M. B., Valois, F. W. & Watson, S. W. 1980. Production of NO_2^- and N_2O by nitrifying bacteria at reduced concentrations of oxygen. *Applied and Environmental Microbiology,* 40**,** 526 - 532.

Green, J. a. M., Simpson, J. H., Legg, S. & Palmer, M. R. 2008. Internal waves, baroclinic energy fluxes and mixing at the European shelf edge. *Continental Shelf Research,* 28**,** 937-950.

Grefe, I. 2013. *Concentration and isotopic composition of marine nitrous oxide, in particular the oxygen-17 isotope excess.* University of East Anglia.

Grefe, I. & Kaiser, J. 2014. Equilibrator-based measurements of dissolved nitrous oxide in the surface ocean using an integrated cavity output laser absorption spectrometer. *Ocean Science* 10**,** 501-512.

Grossart, H.-P., Frindte, K., Dziallas, C., Eckert, W. & Tang, K. W. 2011. Microbial methane production in oxygenated water column of an oligotrophic lake. *Proceedings of the National Academy of Sciences,* 108**,** 19657-19661.

Gruber, N. 2008. The marine nitrogen cycle: overview and challenges. *In:* Capone, D. G., Bronk, D. A., R., M. M. & Carpenter, E. J. (eds.) *Nitrogen in the marine environment,.* Elsevier Inc.

Grunwald, M., Dellwig, O., Beck, M., Dippner, J. W., Freund, J. A., Kohlmeier, C., Schnetger, B. & Brumsack, H.-J. 2009. Methane in the southern North Sea: Sources, spatial distribution and budgets. *Estuarine, Coastal and Shelf Science,* 81**,** 445-456.

Grunwald, M., Dellwig, O., Liebezeit, G., Schnetger, B., Reuter, R. & Brumsack, H.-J. 2007. A novel time-series station in the Wadden Sea (NW Germany): First results on continuous nutrient and methane measurements. *Marine Chemistry,* 107**,** 411-421.

GüLzow, W., Rehder, G., Schneider, B., V. Deimling, J. S. & Sadkowiak, B. 2011. A new method for continuous measurement of methane and carbon dioxide

in surface waters using off-axis integrated cavity output spectroscopy (ICOS): An example from the Baltic Sea. *Limnology and Oceanography Methods*

, 9**,** 176-184.

Gupta, A., Flora, J. R. V., Gupta, M., Sayles, G. D. & Suidan, M. T. 1994. Methanogenesis and sulfate reduction in chemostats—I. Kinetic studies and experiments. *Water Research,* 28**,** 781-793.

Gustafsson, B. & Stigebrandt, A. 1996. Dynamics of the freshwater-influenced surface layers in the Skagerrak. *Journal of Sea Research,* 35**,** 39-53.

Hahn, J. 1974. The North Atlantic Ocean as a source of atmospheric N_2O. *Tellus* 26**,** 160-168.

Hartmann, D. L., Klein Tank, A. M. G., Rusticucci, M., Alexander, L. V., BröNnimann, S., Charabi, Y., Dentener, F. J., Dlugokencky, E. J., Easterling, D. R., Kaplan, A., Soden, B. J., Thorne, P. W., Wild, M. & Zhai, P. M. 2013. Observations: Atmosphere and Surface. *In:* Stocker, T. F., Qin, D., Plattner, G.-K., Tignor, M., Allen, S. K., Boschung, J., Nauels, A., Xia, Y., Bex, V. & Midgley, S. K. (eds.) *Climate change 2013: the physical science basis. contribution of working group I to the fifth assessment report of the intergovernmental panel on climate change. .* Cambridge, United Kingdom and New York, NY, USA. : Cambridge University Press,.

Hedges, J. I., Keil, R. G. & Benner, R. 1997. What happens to terrestrial organic matter in the ocean? *Organic Geochemistry,* 27**,** 195-212.

Hickman, A. E., Moore, M., Sharples, J., Lucas, M. I., Tilstone, G. H., Krivtsov, V. & Holligan, P. M. 2012. Primary production and nitrate uptake within the seasonal thermocline of a stratified shelf sea. *Marine Ecology Progress Series,* 463**,** 39 - 57.

Hill, P. G., Mary, I., Purdie, D. A. & Zubkov, M. V. 2011. Similarity in microbial amino acid uptake in surface waters of the North and South Atlantic (sub-)tropical gyres. *Progress in Oceanography,* 91**,** 437-446.

Hinrichs, K.-U., Hayes, J. M., Sylva, S. P., Brewer, P. G. & Delong, E. F. 1999. Methane-consuming Archaebacteria in marine sediments. *Nature,* 398**,** 802-805.

Hirota, A., Ijiri, A., Komatsu, D. D., Ohkubo, S. B., Nakagawa, F. & Tsunogai, U. 2009. Enrichment of nitrous oxide in the water columns in the area of the Bering and Chukchi Seas. *Marine Chemistry,* 116**,** 47-53.

Holligan, P. M. 1981. Biological Implications of Fronts on the Northwest European Continental Shelf. *Philosophical Transactions of the Royal Society of London. Series A, Mathematical and Physical Sciences,* 302**,** 547-562.

Holt, J. & Umlauf, L. 2008. Modelling the tidal mixing fronts and seasonal stratification of the Northwest European Continental shelf. *Continental Shelf Research,* 28**,** 887-903.

Holzner, C. P., Amaral, H., Brennwald, M. S., Hofer, M., Klump, S. & Kipfer, R. 2005. Methane bubble streams in the Black Sea traced by dissolved noble gases. *Geophysical Research Abstracts,* 7.

Hovland, M., Judd, A. G. & Burke Jr, R. A. 1993. The global flux of methane from shallow submarine sediments. *Chemosphere,* 26**,** 559-578.

Huang, J., Golombek, A., Prinn, R., Weiss, R., Fraser, P., Simmonds, P., Dlugokencky, E. J., Hall, B., Elkins, J., Steele, P., Langenfelds, R., Krummel, P., Dutton, G. & Porter, L. 2008. Estimation of regional emissions of nitrous oxide from 1997 to 2005 using multinetwork measurements, a chemical transport model, and an inverse method. *Journal of Geophysical Research: Atmospheres,* 113**,** 2156-2202.

Inall, M., Gillibrand, P., Griffiths, C., Macdougal, N. & Blackwell, K. 2009. On the oceanographic variability of the North-West European Shelf to the West of Scotland. *Journal of Marine Systems,* 77**,** 210-226.

Isaksen, I. S. A. & Hov, O. 1987. Calculation of trends in the tropospheric concentration of O_3. OH, CO, CH_4 and NO_x. *Tellus,* 39**,** 271-285.

Jiang, X., Ku, W. L., Shia, R.-L., Li, Q., Elkins, J. W., Prinn, R. G. & Yung, Y. L. 2007. Seasonal cycle of N_2O: analysis of data. *Global Biogeochemical Cycles,* 21**,** GB1006.

Jones, R. D. 1991. Carbon monoxide and methane distribution and consumption in the photic zone of the Sargasso Sea. *Deep-Sea Research Part A. Oceanographic Research Papers,* 38**,** 625-635.

Karl, D. M., Beversdorf, L., Bjorkman, K. M., Church, M. J., Martinez, A. & Delong, E. F. 2008. Aerobic production of methane in the sea. *Nature Geoscience,* 1**,** 473-478.

Karl, D. M. & Tilbrook, B. D. 1994. Production and transport of methane in oceanic particulate organic matter. *Nature,* 368**,** 732-734.

Khalil, M. a. K. & Rasmussen, R. A. 1994. Global decrease in atmospheric carbon monoxide concentration. *Nature,* 370**,** 639-641.

Knittel, K. & Boetius, A. 2009. Anaerobic oxidation of methane: progress with an unknown process. *Annual Review of Microbiology,* 63**,** 311 - 334.

Kock, A., Schafstall, J., Dengler, M., Brandt, P. & Bange, H. W. 2012. Sea-to-air and diapycnal nitrous oxide fluxes in the eastern tropical North Atlantic Ocean. *Biogeosciences* 9**,** 957 - 964.

Kroeze, C., Mosier, A. & Bouwman, L. 1999. Closing the global N_2O budget: A retrospective analysis 1500-1994. *Global Biogeochemical Cycles,* 13**,** 1-8.

Krueger-Hadfield, S. A., Balestreri, C., Schroeder, J., Highfield, A., HelaouëT, P., Allum, J., Moate, R., Lohbeck, K. T., Miller, P., Riebesell, U., Reusch, T. B. H., Rickaby, R. E. M., Young, J. R., Hallegraeff, G., Brownlee, C. & Schroeder, D. C. 2014. Geno- tying an Emiliania huxleyi (Prymnesiophyceae) bloom event in the North Sea reveals evidence of asexual reproduction. *Biogeosciences Discussions,* 11**,** 4359–4408.

Kvenvolden, K. A. & Rogers, B. W. 2005. Gaia's breath-global methane exhalations. *Marine and Petroleum Geology,* 22**,** 579-590.

Lam, P., Lavik, G., Jensen, M. M., Van De Vossenberg, J., Schmid, M., Woebken, D., Gutiérrez, D., Amann, R., Jetten, M. S. M. & Kuypers, M. M. M. 2009. Revising the nitrogen cycle in the Peruvian oxygen minimum zone. *Proceedings of the National Academy of Sciences,* 106**,** 4752-4757.

Lamontagne, R. A., Swinnerton, J. W., Linnenbom, V. J. & Smith, W. D. 1973. Methane concentrations in various marine environments. *Journal of Geophysical Research,* 78**,** 5317-5324.

Large, W. G. & Pond, S. 1981. Open ocean momentum flux measurements in moderate to strong winds. *Journal of Physical Oceanography,* 11**,** 324-336.

Law, C. S. & Ling, R. D. 2001. Nitrous oxide flux and response to increased iron availability in the Antarctic Circumpolar Current. *Deep Sea Research Part II: Topical Studies in Oceanography,* 48**,** 2509-2527.

Law, C. S. & Owens, N. J. P. 1990a. Denitrification and nitrous oxide in the North Sea. *Netherlands Journal of Sea Research,* 25**,** 65-74.

Law, C. S. & Owens, N. J. P. 1990b. Significant flux of atmospheric nitrous oxide from the northwest Indian Ocean. *Nature,* 346**,** 826-828.

Le Quéré, C. & Saltzman, E. S. 2013. *Surface ocean-lower atmospheric processes,* Washington DC, American Geophysical Union.

Lefèvre, N. & Taylor, A. 2002. Estimating pCO_2 from sea surface temperatures in the Atlantic gyres. *Deep Sea Research Part I: Oceanographic Research Papers,* 49**,** 539-554.

Leifer, I. & Patro, R. K. 2002. The bubble mechanism for methane transport from the shallow sea bed to the surface: A review and sensitivity study. *Continental Shelf Research,* 22**,** 2409-2428.

Levipan, H. A., Quiñones, R. A., Johansson, H. E. & Urrutia, H. 2007. Methylotrophic methanogens in the water column of an upwelling zone with a strong gradient off central Chile. *Microbes and Environments,* 22**,** 268 - 278.

Linden, P. F. & Simpson, J. E. 1988. Modulated mixing and frontogenesis in shallow seas and estuaries. *Continental Shelf Research,* 8**,** 1107-1127.

Loder, J. W. & Wright, D. G. 1985. Tidal rectification and frontal circulation on the sides of Georges Bank. *Journal of Marine Research,* 43**,** 581-604.

Longhurst, A. R. 1998. *Ecological Geography of the Sea,* San Diago, California, US, Academic Press.

Löscher, C. R., Kock, A., Könneke, M., Laroche, J., Bange, H. W. & Schmitz, R. A. 2012. Production of oceanic nitrous oxide by ammonia-oxidising Archaea. *Biogeosciences,* 9**,** 2419-2429.

Mann, K. H. & Lazier, J. R. N. 2006. *Dynamics of Marine Ecosystems: Biological-Physical Interactions in the Oceans,* Victoria, Australia, Blackwell Publishing.

Mccandliss, R. R., Jones, S. E., Hearn, M., Latter, R. & Jago, C. F. 2002. Dynamics of suspended particles in coastal waters (southern North Sea) during a spring bloom. *Journal of Sea Research,* 47**,** 285-302.

Menon, S., Denman, K. L., Brasseur , G., Chidthaisong, A., Ciais, P., Cox, P. M., Dickinson, R. E., Hauglustaine, D., Heinze, C., Holland, E., Jacob , D., Lohmann, U., Ramachandran, S., Leite Da Silva Dias, P., Wofsy, S. C. & Zhang, X. 2007. Couplings between changes in the climate system and biogeochemistry. *In:* Solomon, S., Qin, D., Manning, M., Chen, Z., Marquis, M., Averyt, K. B., Tignor, M. & Miller, H. L. (eds.) *Climate change 2007: The physical science basis. Contribution of working group I to the fourth assessment report of the intergovernmental panel on climate change.* Cambridge, United Kingdom and New York, NY, USA: Cambridge University Press.

Miller, P. I., Xu, W. & Carruthers, M. 2014. Seasonal shelf-sea front mapping using satellite ocean colour and temperature to support development of a marine protected area network. *Deep Sea Research Part II: Topical Studies in Oceanography*.

Montzka, S. A., Fraser, P. J., Butler, J. H., Cunnold, D. M., Daniel, J. S., Derwent, R. G., Lal, S., Mcculloch, A., Oram, D. E., Reeves, C. E., Sanhueza, E., Steele, L. P., Velders, G. J. M., Weiss, R. F. & Rodolphe, Z. 2003. Chapter 1: Controlled substances and other source gases. *In:* Nohende Ajavon, A.-L., Albritton, D. L., Mégie, G. & Watson, R. T. (eds.) *Scientific Assessment of Ozone Depletion: 2002.* Geneva, Switzerland: World Meteorological Organization.

Montzka, S. A. & Reimann, S. 2011. Chapter 1: ozone-depleting sunstances (ODSs) and related chemicals. *In:* Ennis, C. A. (ed.) *Scientific assessment of ozone depletion: 2010, global ozone research and monitoring project.* Geneva, Switzerland: World Meteorological Organisation.

Moore, M. C., M., M. M., Achterberg, E. P., Geider, R. J., Laroche, J., Lucas, M. I., Mcdonagh, E. L., Pan, X., Poulton, A. J., Rijkenberg, M. J. A., Suggett, D. J., Ussher, S. J. & Woodward, E. M. S. 2009. Large-scale distribution of Atlantic nitrogen fixation controlled by iron availability. *Nature Geosci,* 2**,** 867-871.

Morell, J. M., Capella, J., Mercado, A., Bauzá, J. & Corredor, J. E. 2001. Nitrous oxide fluxes in Caribbean and tropical Atlantic waters: Evidence for near surface production. *Marine Chemistry,* 74**,** 131-143.

Mosier, A., Kroeze, C., Nevison, C., Oenema, O., Seitzinger, S. & Van Cleemput, O. 1998. Closing the global N_2O budget: Nitrous oxide emissions through the agricultural nitrogen cycle. *Nutrient Cycling in Agroecosystems,* 52**,** 225-248.

Muller-Karger, F. E., Mcclain, C. R. & Richardson, P. L. 1988. The dispersal of the Amazon's water. *Nature,* 333**,** 56-59.

Myhre, G., Shindell, D., BréOn, F.-M., Collins, W., Fuglestvedt, J., Huang, J., Koch, D., Lamarque, J.-F., Lee, D., Mendoza, B., Nakajima, T., Robock, A., Stephens, G., Takemura, T. & Zhang, H. 2013. Anthropogenic and natural radiative forcing. *In:* Stocker, T. F., Qin, D., Plattner, G.-K., Tignor, M., Allen, S. K., Boschung, J., Nauels, A., Xia, Y., Bex, V. & Midgley, P. M. (eds.) *Climate change 2013: The physical science basis. Contribution of working group I to the fifth assessment report of the intergovernmental panel on climate change.* Cambridge, United Kingdom and New York, NY, USA: Cambridge University Press.

Najjar, R. G. 1992. Marine biogeochemistry. *In:* Trenberth, K. E. (ed.) *Climate system modeling* Cambridge, UK: Cambridge University Press.

Naqvi, S. A., Naik, H., Jayakumar, D. A., Shailaja, M. S. & Narvekar, P. V. 2006. Seasonal oxygen deficiency over the western continental shelf of India *In:* Neretin, L. N. (ed.) *Past and Present Water Column Anoxia.* Springer Netherlands.

Naqvi, S. W. A., Bange, H. W., Farias, L., Monteiro, P. M. S., Scranton, M. I. & Zhang, J. 2010. Marine hypoxia/anoxia as a source of CH_4 and N_2O. *Biogeosciences,* 7**,** 2159 - 2190.

Naqvi, S. W. A., Bange, H. W., Gibb, S. W., Goyet, C., Hatton, A. D. & Upstill-Goddard, R. C. 2005. Biogeochemical ocean-atmosphere transfers in the Arabian Sea. *Progress in Oceanography,* 65**,** 116-144.

Naqvi, S. W. A., Jayakumar, D. A., Nair, M., Kumar, M. D. & George, M. D. 1994. Chemistry of the northern Indian Ocean nitrous oxide in the western Bay of Bengal. *Marine Chemistry,* 47**,** 269-278.

Naqvi, S. W. A. & Noronha, R. J. 1991. Nitrous oxide in the Arabian Sea. *Deep Sea Research Part A. Oceanographic Research Papers,* 38**,** 871-890.

Neef, L., Van Weele, M. & Van Velthoven, P. 2010. Optimal estimation of the present-day global methane budget. *Global Biogeochemical Cycles,* 24**,** GB4024.

Nevison, C., Butler, J. H. & Elkins, J. W. 2003. Global distribution of N_2O and the ΔN_2O-AOU yield in the subsurface ocean. *Global Biogeochemical Cycles,* 17.

Nevison, C. D., Lueker, T. J. & Weiss, R. F. 2004. Quantifying the nitrous oxide source from coastal upwelling. *Global Biogeochemical Cycles,* 18**,** GB1018.

Nevison, C. D., Weiss, R. F. & Erickson, D. J. 1995. Global oceanic emissions of nitrous oxide. *Journal of Geophysical Research,* 100**,** 15809-15820.

Nightingale, P. D., Malin, G., Law, C. S., Watson, A., Liss, P. S., Liddicoat, M. I., Boutin, J. & Upstill-Goddard, R. C. 2000. In situ evaluation of air-sea gas exchange parameterisations using novel conservative and volatile tracers. *Global Biogeochemical Cycles,* 14**,** 373-387.

Nisbet, E. G., Dlugokencky, E. J. & Bousquet, P. 2014. Methane on the Rise—Again. *Science,* 343**,** 493-495.

Oremland, R. S. & Polcin, S. 1982. Methanogenesis and sulfate reduction: competitive and noncompetitive substrates in estuarine sediments. *Applied and Environmental Microbiology,* 44**,** 1270 - 1276.

Oudot, C., Jean-Baptiste, P., Fourré, E., Mormiche, C., Guevel, M., Ternon, J.-F. & Le Corre, P. 2002. Transatlantic equatorial distribution of nitrous oxide and methane. *Deep-Sea Research Part I: Oceanographic Research Papers,* 49**,** 1175-1193.

Pachauri, R. K. & Meyer, L. A. 2014. IPCC, 2014: Climate Change 2014: Synthesis Report. *Contribution of working groups I, II and III to the fifth assessment report of the Intergovernmental Panel on Climate Change.* Geneva, Switzerland.

Pierotti, D. & Rasmussen, R. A. 1980. Nitrous oxide measurements in the eastern tropical Pacific Ocean. *Tellus,* 32**,** 56-72.

Pierrot, D., Neill, C., Sullivan, K., Castle, R., Wanninkhof, R., Lüger, H., Johannessen, T., Olsen, A., Feely, R. A. & Cosca, C. E. 2009. Recommendations for autonomous underway pCO2 measuring systems and data-reduction

routines. *Deep Sea Research Part II: Topical Studies in Oceanography,* 56**,** 512-522.

Pingree, R. D. 1980. Physical Oceanography of the Celtic Sea and English Channel. *In:* Banner, F. T., Colins, M. B. & Massie, K. S. (eds.) *The North-West European Shelf Seas: The Sea Bed and the Sea in Motion II. Physical and Chemical Oceanography, and Physical Resources.*

Pingree, R. D. & Mardell, G. T. 1985. Solitary internal waves in the Celtic Sea. *Progress in Oceanography,* 14**,** 431-441.

Podgrajsek, E., Sahlée, E. & Rutgersson, A. 2014. Diurnal cycle of lake methane flux. *Journal of Geophysical Research Biogeosciences,* 119**,** 236 - 248.

Portmann, R. W., Daniel, J. S. & Ravishankara, A. R. 2012. Stratospheric ozone depletion due to nitrous oxide: influences of other gases. *Philosophical Transactions of the Royal Society of London B: Biological Sciences,* 367**,** 1256-1264.

Poulton, A. J., Stinchcombe, M. C., Achterberg, E. P., Bakker, D. E., Dumousseaud, C., Lawson, H. E., Lee, G. A., Richier, S., Suggett, D. J. & Young, J. R. 2014. Coccolithophores on the North-West European Shelf: calcification rates and environmental controls. *Biogeosciences,* 11**,** 3919 - 3940.

Prather, M., Ehhalt, D., Dentener, F., Derwent, R., Dlugokencky, E., Holland, E., Isaksen, I., Katima, J., Kirchhoff, V., Matson, P., Midgley, P. & Wang, M. 2001. Chapter 4: Atmospheric chemistry and greenhouse gases. *In:* Houghton, J. T., Ding, Y., Griggs, D. J., Noguer, M., Van Der Linden, P. J., Dai, X., Maskell, K. & Johnson, C. A. (eds.) *Climate Change 2001: the scientific basis. Contribution of working group 1 to the third assessment report of the Intergovernmental Panel on Climate Change.* Cambridge University Press, Cambridge.

Prather, M. J., Holmes, C. D. & Hsu, J. 2012. Reactive greenhouse gas scenarios: Systematic exploration of uncertainties and the role of atmospheric chemistry. *Geophysical Research Letters,* 39**,** L09803.

Queste, B. Y., Fernand, L., Jickells, T. D. & Heywood, K. J. 2013. Spatial extent and historical context of North Sea oxygen depletion in August 2010. *Biogeochemistry,* 113**,** 53-68.

Rehder, G., Keir, R., Suess, E. & Pohlmann, T. 1998. The multiple sources and patterns of methane in North Sea waters. *Aquatic Geochemistry,* 4**,** 403-427.

Rhee, T. S., Kettle, A. J. & Andreae, M. O. 2009. Methane and nitrous oxide emissions from the ocean: A reassessment using basin-wide observations in the Atlantic. *Journal of Geophysical Research,* 114**,** 2156-2202.

Ribas-Ribas, M., Rerolle, V. M. C., Bakker, D. C. E., Kitidis, V., Lee, G., Brown, I., Achterberg, E. P., Hardman-Mountford, N. & Tyrrell, T. 2014. Intercomparison of carbonate chemistry measurements on a cruise in northwestern European shelf seas. *Biogeosciences,* 11**,** 4339-4355.

Rixen, T., Haake, B., Ittekkot, V., Guptha, M. V. S., Nair, R. R. & Schlüssel, P. 1996. Coupling between SW monsoon-related surface and deep ocean processes as discerned from continuous particle flux measurements and correlated satellite data. *Journal of Geophysical Research: Oceans,* 101**,** 28569-28582.

Rodhe, J. 1996. On the dynamics of the large-scale circulation of the skagerrak. *Journal of Sea Research,* 35**,** 9-21.

Santoro, A. E., Buchwald, C., Mcilvin, M. R. & Casciotti, K. L. 2011. Isotopic signature of N_2O produced by marine ammonia-oxidising Archaea. *Science,* 333**,** 1282-1285.

Schuster, U. & Watson, A. J. 2007. A variable and decreasing sink for atmospheric CO_2 in the North Atlantic. *Journal of Geophysical Research: Oceans,* 112**,** C11006.

Scranton, M. I. & Brewer, P. G. 1977. Occurrence of methane in the near-surface waters of the western subtropical North-Atlantic. *Deep-Sea Research,* 24**,** 127-138.

Scranton, M. I. & Mcshane, K. 1991. Methane fluxes in the southern North Sea: The role of European rivers. *Continental Shelf Research,* 11**,** 37-52.

Seitzinger, S. & Kroeze, C. 1998. Global distribution of nitrous oxide production and N inputs in freshwater and coastal marine ecosystems. *Global Biogeochemical Cycles,* 12**,** 93 -113.

Shakhova, N. & Semiletov, I. 2007. Methane release and coastal environment in the East Siberian Arctic shelf. *Journal of Marine Systems,* 66**,** 227-243.

Sharples, J., Tweddle, J. F., Mattias Green, J. A., Palmer, M. R., Kim, Y.-N., Hickman, A. E., Holligan, P. M., Moore, C. M., Rippeth, T. P., Simpson, J. H. & Krivtsov, V. 2007. Spring-neap modulation of internal tide mixing and vertical nitrate fluxes at a shelf edge in summer. . *Limnology and Oceanography,* 52**,** 1735-1747.

Siegenthaler, U. & Sarmiento, J. L. 1993. Atmospheric carbon dioxide and the ocean. *Nature,* 365**,** 119 - 125.

Simpson, J. H., Edelsten, D. J., Edwards, A., Morris, N. C. G. & Tett, P. B. 1979. The Islay front: Physical structure and phytoplankton distribution. *Estuarine and Coastal Marine Science,* 9**,** 713-IN1.

Simpson, J. H. & Sharples, J. 2012. *Introduction to the Physical and Biological Oceanography of Shelf Seas,* Cambridge, UK, Cambridge University Press.

Stigebrandt, A. 1983. A model for the exchange of water and salt between the Baltic and the Skagerrak. *Journal of Physical Oceanography,* 13**,** 411 - 427.

Stubbins, A., Uher, G., Kitidis, V., Law, C. S., Upstill-Goddard, R. C. & Woodward, E. M. S. 2006. The open-ocean source of atmospheric carbon monoxide. *Deep Sea Research Part II: Topical Studies in Oceanography,* 53**,** 1685-1694.

Suntharalingam, P. & Sarmiento, J. L. 2000. Factors governing the oceanic nitrous oxide distribution: Simulations with an ocean general circulation model. *Global Biogeochemical Cycles,* 14**,** 1944-9224.

Suntharalingam, P., Sarmiento, J. L. & Toggweiler, J. R. 2000. Global significance of nitrous-oxide production and transport from oceanic low-oxygen zones: A modeling study. *Global Biogeochemical Cycles,* 14**,** 1353-1370.

Svendsen, E., Bemtsen, J., Skogen, M., Ådlandsvik, B. & Martinsen, E. 1996. Model simulation of the Skagerrak circulation and hydrography during Skagex. *Journal of Marine Systems,* 8**,** 219-236.

Tang, K. W., Mcginnis, D. F., Frindte, K., Brüchert, V. & Grossart, H.-P. 2014. Paradox reconsidered: Methane oversaturation in well-oxygenated lake waters. *Limnology and Oceanography,* 59**,** 275-284.

Tarran, G. 2012. AMT22 cruise report. *Atlantic Meridional Transect (AMT).* Plymouth: Plymouth Marine Laboratory (PML).

Tett, P. B., Joint, I. R., Purdie, D. A., Baars, M., Oosterhuis, S., Daneri, G., Hannah, F., Mills, D. K., Plummer, D., Pomroy, A. J., Walne, A. W., Witte, H. J., Howarth,

M. J. & Lankester, R. 1993. Biological Consequences of Tidal Stirring Gradients in the North Sea [and Discussion]. *Philosophical Transactions of the Royal Society of London. Series A: Physical and Engineering Sciences,* 343**,** 493-508.

Tilbrook, B. D. & Karl, D. M. 1995. Methane sources, distributions and sinks from California coastal waters to the oligotrophic North Pacific gyre. *Marine Chemistry,* 49**,** 51-64.

Tomczak, M. & Godfrey, J. S. 1994. *Regional oceanography: An introduction,* New York, Elsevier.

Uher, G. 2006. Distribution and air–sea exchange of reduced sulphur gases in European coastal waters. *Estuarine, Coastal and Shelf Science,* 70**,** 338-360.

Upstill-Goddard, R. C., Barnes, J., Frost, T., Punshon, S. & Owens, N. J. P. 2000. Methane in the southern North Sea: Low-salinity inputs, estuarine removal, and atmospheric flux. *Global Biogeochemical Cycles,* 14**,** 1205-1217.

Upstill-Goddard, R. C., Barnes, J. & Owens, N. J. P. 1999. Nitrous oxide and methane during the 1994 SW monsoon in the Arabian Sea/northwestern Indian Ocean. *Journal of Geophysical Research: Oceans,* 104**,** 30067-30084.

Valentine, D. L., Blanton, D. C., Reeburgh, W. S. & Kastner, M. 2001. Water column methane oxidation adjacent to an area of active hydrate dissociation, Eel river Basin. *Geochimica et Cosmochimica Acta,* 65**,** 2633-2640.

Van Camp, L., Nykjaer, L., Mittelstaedt, E. & Schlittenhardt, P. 1991. Upwelling and boundary circulation off Northwest Africa as depicted by infrared and visible satellite observations. *Progress in Oceanography,* 26**,** 357-402.

Van De Graaf, A. A., Mulder A, De Bruijn, P., Jetten, M. S., Robertson, L. A. & Kuenen, J. G. 1995. Anaerobic oxidation of ammonium is a biologically mediated process. *Applied Environmental Microbiology,* 61**,** 1246-1251.

Van Der Maarel, M. J. E. C., Sprenger, W., Haanstra, R. & Forney, L. J. 1999. Detection of methanogenic Archaea in seawater particles and the digestive tract of a marine fish species. *Microbiology Letters,* 173**,** 189-194.

Veuger, B., Pitcher, A., Schouten, S., Sinninghe Damsté, J. S. & Middelburg, J. J. 2013. Nitrification and growth of autotrophic nitrifying bacteria and Thaumarchaeota in the coastal North Sea. *Biogeosciences,* 10**,** 1775-1785.

Walter, S., Bange, H. W., Breitenbach, U. & Wallace, D. W. R. 2006. Nitrous oxide in the North Atlantic Ocean. *Biogeosciences Discussions,* 3**,** 993-1022.

Walter, S., Bange, H. W. & Wallace, D. W. R. 2004. Nitrous oxide in the surface layer of the tropical North Atlantic Ocean along a west to east transect. *Geophysical Research Letters,* 31.

Wankel, S. D., Kendall, C., Pennington, J. T., Chavez, F. P. & Paytan, A. 2007. Nitrification in the euphotic zone as evidenced by nitrate dual isotopic composition: Observations from Monterey Bay, California. *Global Biogeochemical Cycles,* 21**,** GB2009.

Wanninkhof, R. 1992. Relationship between wind speed and gas exchange over the ocean. *J. Geophys. Res.,* 97**,** 7373-7382.

Ward, B. B., Kilpatrick, K. A., Novelli, P. C. & Scranton, M. I. 1987. Methane oxidation and methane fluxes in the ocean surface layer and deep anoxic waters. *Nature,* 327**,** 226-229.

Watson, R. T., Meira Filho, L. G., Sanhueza, E. & Janetos, A. 1992. Greenhouse gases: sources and sinks *In:* Houghton, J. T., Callander, B. A. & Varney, S. K. (eds.) *Climate Change 1992, the supplementary report to the IPCC scientific assessment.* Cambridge, Great Britain, New York, NY, USA, and Victoria, Australia.

Weiss, R. F. & Price, B. A. 1980. Nitrous oxide solubility in water and seawater. *Marine Chemistry,* 8**,** 347-359.

Weiss, R. F., Van Woy, F. A., Salameh, P. K. & Sepanski, R. J. 1992. Surface water and atmospheric carbon dioxide and nitrous oxide observations by shipboard automated gas chromatography: Results from expeditions between 1977 and 1990. *Other Information: DN: Environmental Sciences Division Publication No. 3987; PBD: Dec 1992.*

Westbrook, G. K., Thatcher, K. E., Rohling, E. J., Piotrowski, A. M., Palike, H., Osborne, A. H., Nisbet, E. G., Minshull, T. A., Lanoiselle, M., James, R. H., Huhnerbach, V., Green, D., Fisher, R. E., Crocker, A. J., Chabert, A., Bolton, C., Beszczynska-Moller, A., Berndt, C. & Aquilina, A. 2009. Escape of

methane gas from the seabed along the West Spitsbergen continental margin. *Geophysical Research Letters,* 36**,** L15608.

Wiesenburg, D. A. & Guinasso, N. L. 1979. Equilibrium solubilities of methane, carbon monoxide, and hydrogen in water and sea water. *Journal of Chemical & Engineering Data,* 24**,** 356-360.

Wilms, R., Sass, H., Köpke, B., Köster, J., Cypionka, H. & Engelen, B. 2006. Specific bacterial, archaeal, and eukaryotic communities in tidal-flat sediments along a vertical profile of several meters. *Applied and Environmental Microbiology,* 72**,** 2756–2764.

Wilson, D. F., Swinnerton, J. W. & Lamontagne, R. A. 1970. Production of carbon monoxide and gaseous hydrocarbons in seawater: relation to dissolved organic carbon. *Science,* 168**,** 1577-1579.

Wrage, N., Velthof, G. L., Van Beusichem, M. L. & Oenema, O. 2001. Role of nitrifier denitrification in the production of nitrous oxide. *Soil Biology and Biochemistry,* 33**,** 1723-1732.

Wyman, M., S, H. & C, B. 2013. Denitrifying Alphaproteobacteria from the Arabian Sea that express nosZ, the gene encoding nitrous oxide reductase, in oxic and suboxic waters. *Applied and Environmental Microbiology,* 79**,** 2670 - 2681.

Yoshinari, T. 1976. Nitrous oxide in the sea. *Marine Chemistry,* 4**,** 189-202.

Zhang, G., Zhang, J., Ren, J., Li, J. & Liu, S. 2008. Distributions and sea-to-air fluxes of methane and nitrous oxide in the North East China Sea in summer. *Marine Chemistry,* 110**,** 42-55.

Zhang, G. L., Zhang, J., Kang, Y. B. & Liu, S. M. 2004. Distributions and fluxes of methane in the East China Sea and the Yellow Sea in spring. *Journal of Geophysical Research,* 109.

Zhu-Barker, X., Cavazos, A. R., Ostrom, N. E., Horwath, W. R. & Glass, J. B. 2015. The importance of abiotic reactions for nitrous oxide production. *Biogeochemistry,* 126**,** 251-267.

Zubkov, M. 2013. AMT23 cruise report. *Atlantic Meridional Transect (AMT).* Plymouth Marine Laboratory (PML).

Appendix

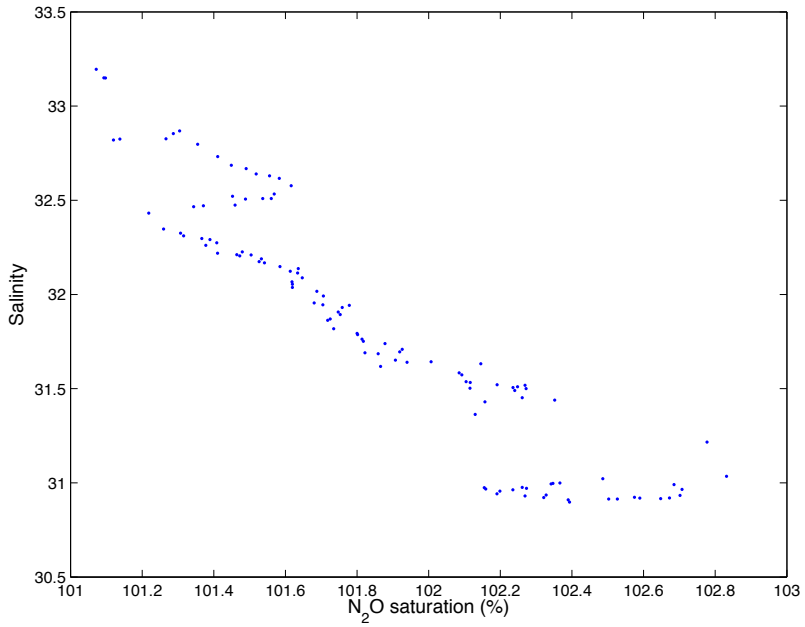

Figure 3.A 1: Negative correlation found between SSS and saturation N_2O in the yellow and cyan regions of the Skagerrak (r=-0.75 p≤0.05) (Figure 3. 23; Table 3. 2).

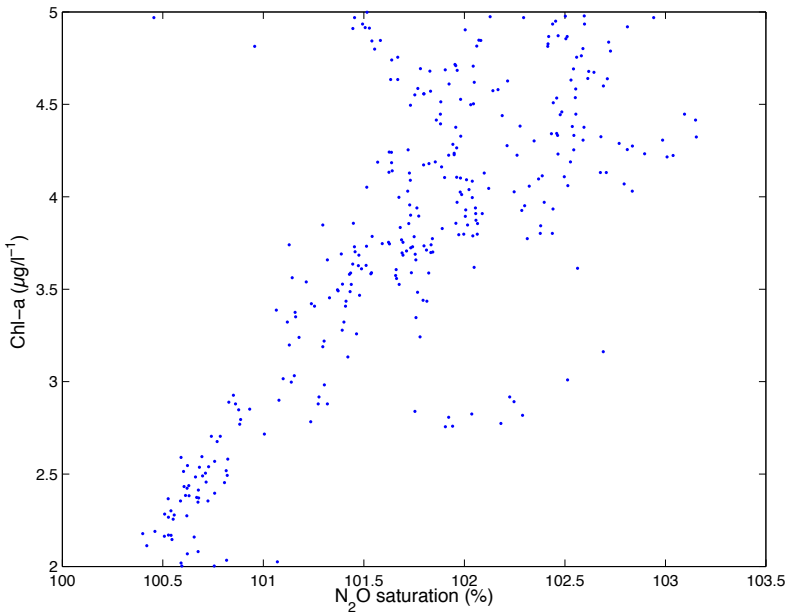

Figure 3.A 2: Positive correlation found between surface chl-a concentration (µg l^{-1}) and saturation for N_2O in the red region of the Skagerrak (r=0.78 p≤0.05) (Figure 3. 23; Table 3. 2).

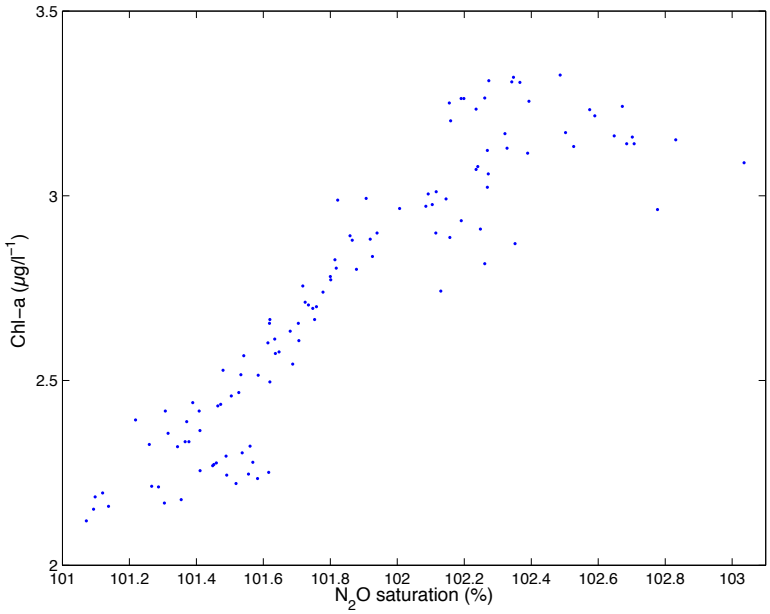

Figure 3.A 3: Positive correlation found between surface chl-a concentration (µg l^{-1}) and saturation for N_2O in the cyan region of the Skagerrak (r=0.91 p≤0.05) (Figure 3. 23; Table 3. 2).

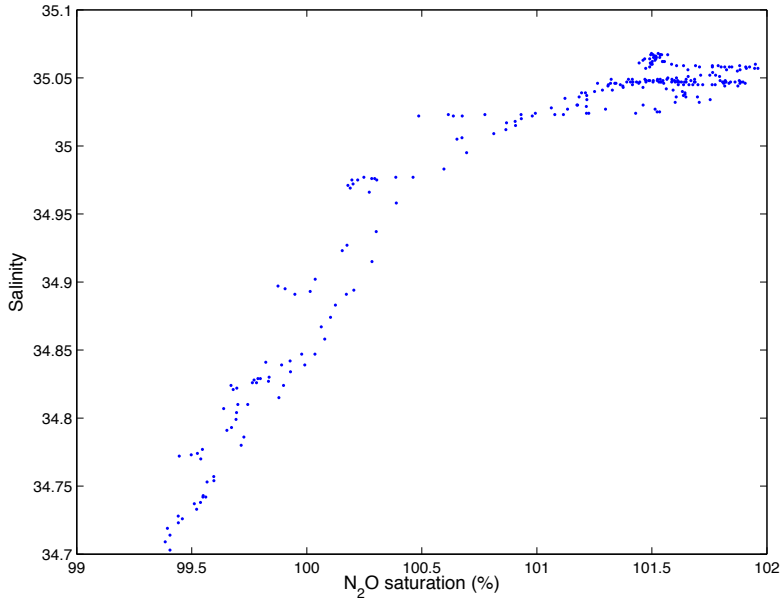

Figure 3.A 4: Positive correlation found between SSS and saturation for N_2O in the black region of the southern North Sea (r=0.93 p≤0.05) (Figure 3. 33; Table 3. 3).

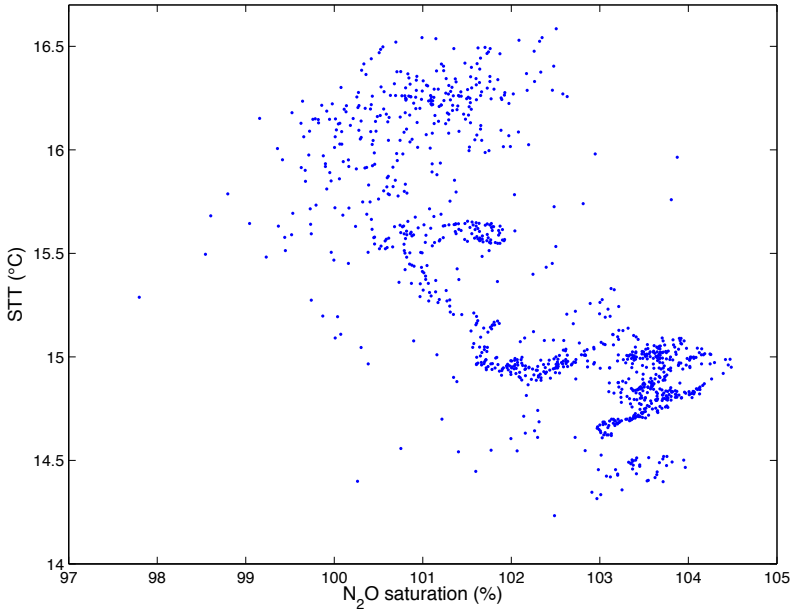

Figure 3.A 5: Negative correlation found between SST and saturation for N_2O in the red and blue regions of the southern North Sea (r=-0.73 p≤0.05) (Figure 3. 33; Table 3. 3).

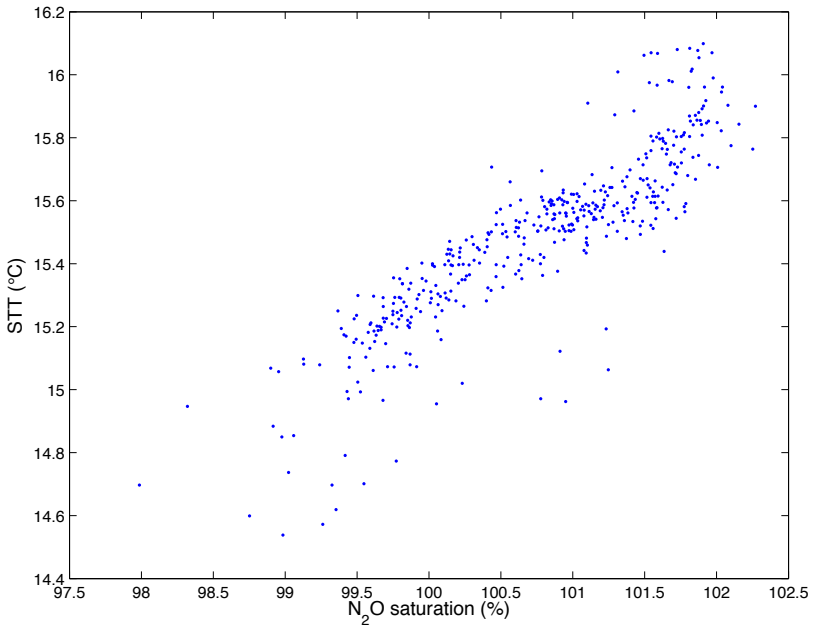

Figure 3.A 6: Positive correlation found between SST and saturation for N_2O in the magenta region of the southern North Sea (r=0.88 p≤0.05) (Figure 3. 33; Table 3. 3).

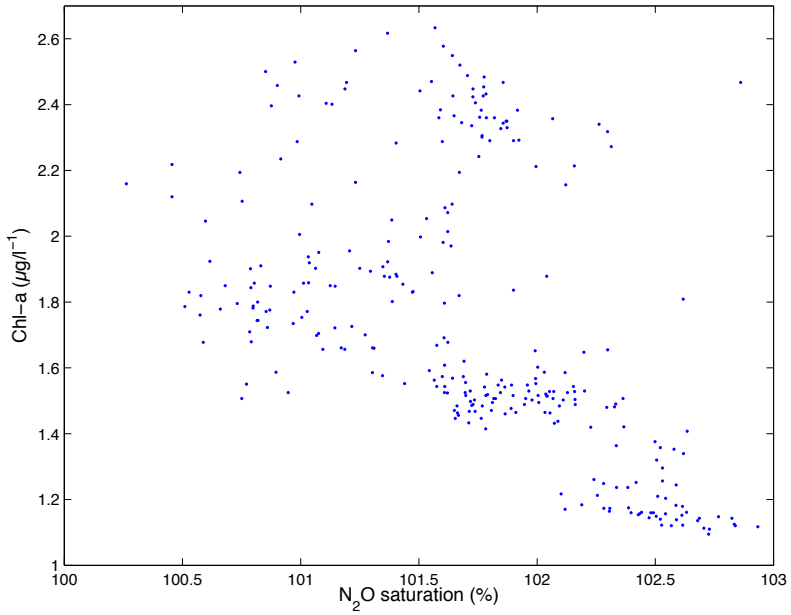

Figure 3.A 7: Negative correlation found between surface chl-a concentration and saturation for N_2O in the blue region of the southern North Sea (r=-0.67 p≤0.05) (Figure 3. 33; Table 3. 3).

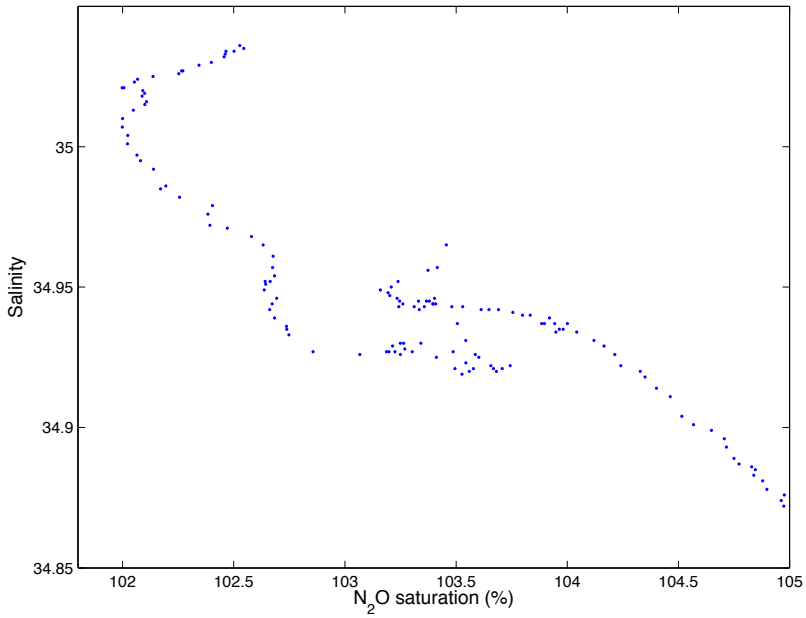

Figure 3.A 8: Negative correlation found between SSS and saturation for N_2O in the red region of the English Channel (r=-0.90 p≤0.05) (Figure 3. 38; Table 3. 4).

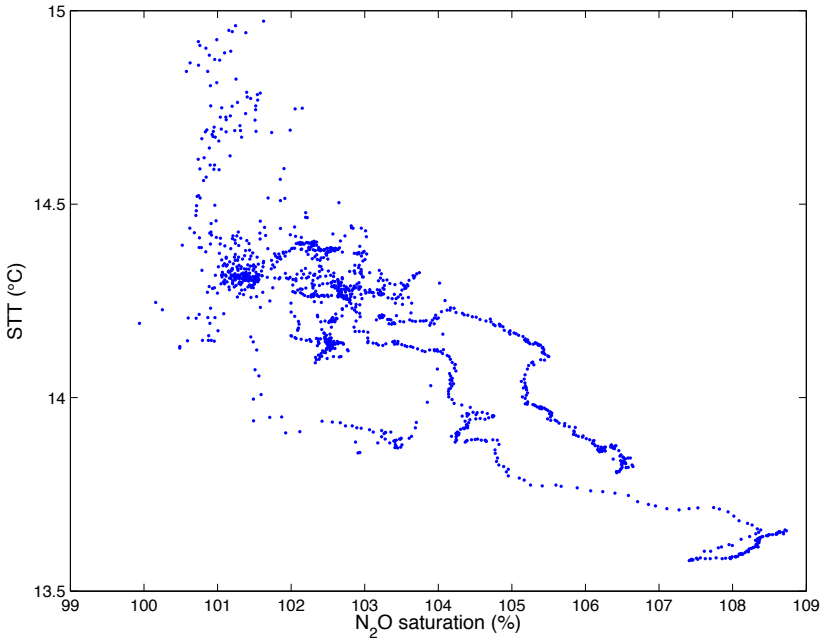

Figure 3.A 9: Negative correlation found between SST and saturation for N_2O in the green, black and red regions of the English Channel (r=-0.85 p≤0.05) (Figure 3. 38; Table 3. 4).

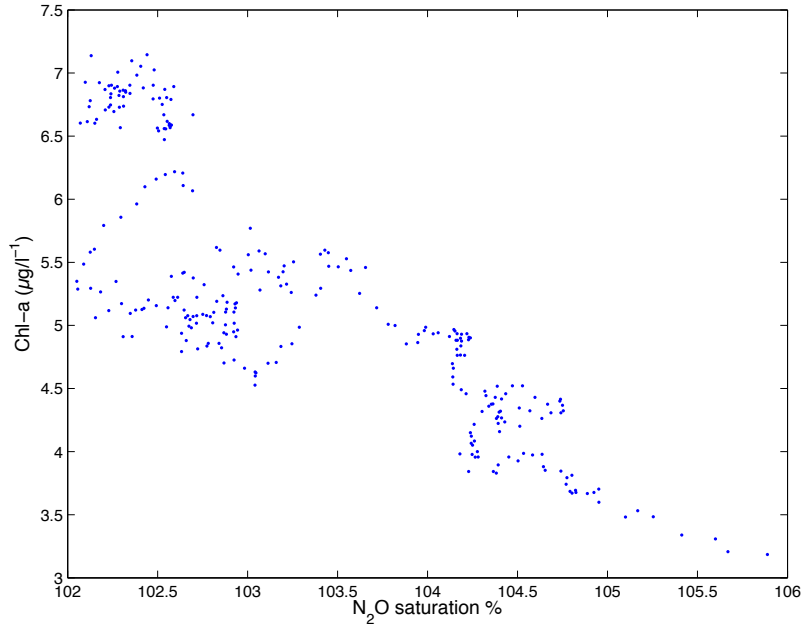

Figure 3.A 10: Negative correlation found between surface Chl-a concentration and saturation for N_2O in the green region of the English Channel (r=-0.86 p≤0.05) (Figure 3. 38; Table 3. 4).

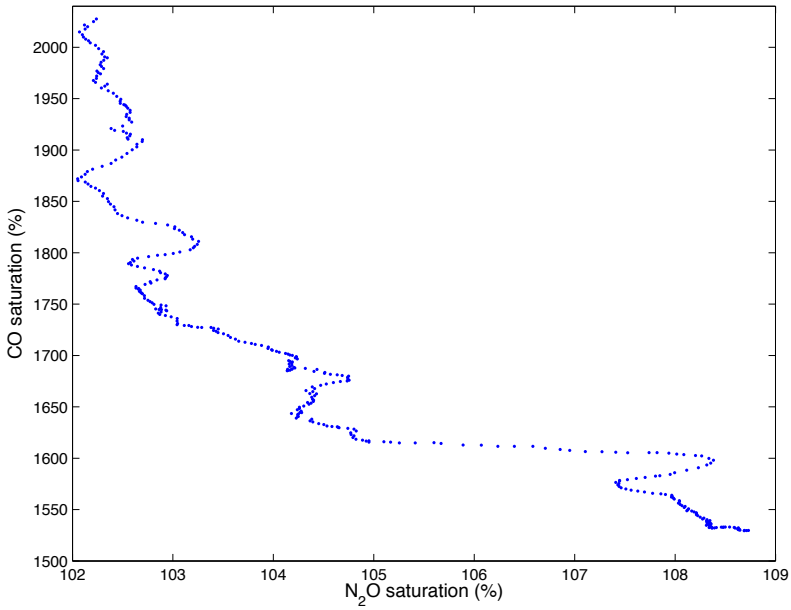

Figure 3.A 11: Negative correlation found between surface saturation for N_2O and CO in the green region of the English Channel (r=-0.88 p≤0.05) (Figure 3. 38; Table 3. 4).

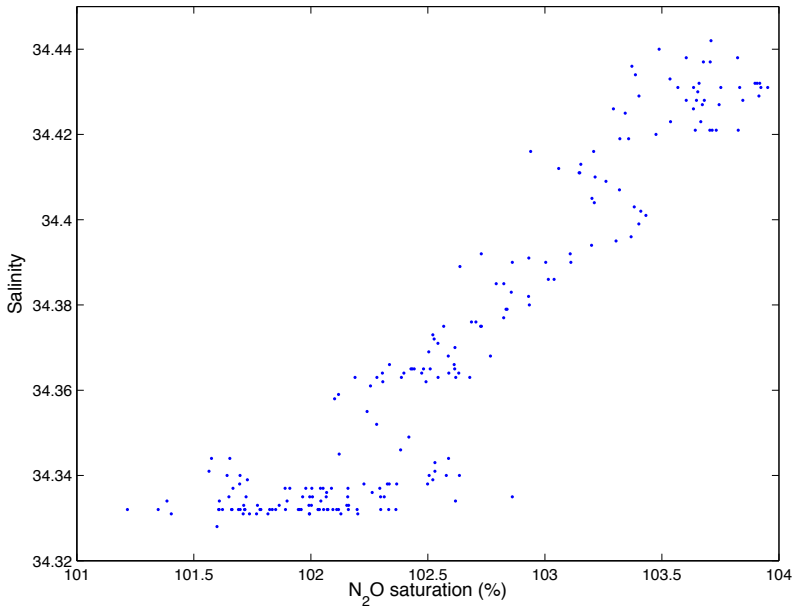

Figure 3.A 12: Positive correlation found between surface saturation for N_2O and salinity in the blue region of the southern North Sea (Flamborough-Helgoland frontal zone) (r=0.93 p≤0.05) (Figure 3. 42; Table 3. 5).

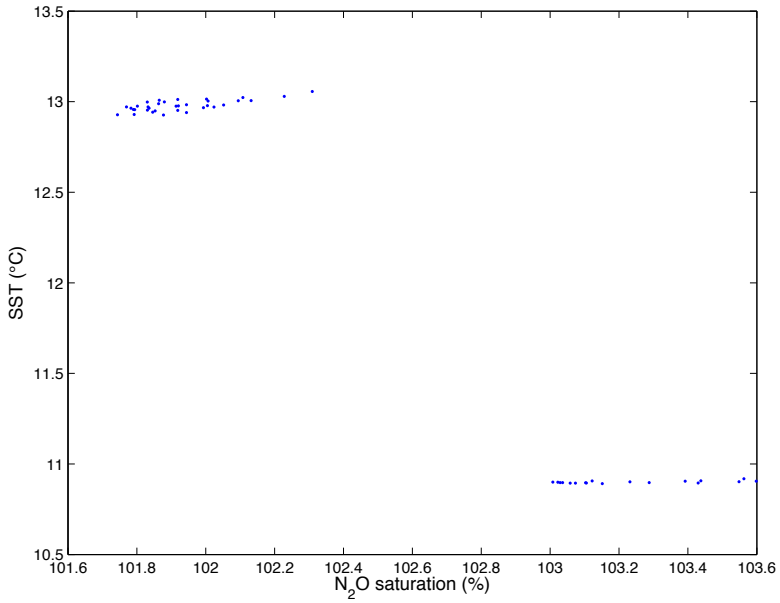

Figure 3.A 13: Rapid transition from a partially to fully mixed water column south of the Shetland Islands. The higher SST's and lower saturation for N_2O in surface waters were located in the partially mixed region and the cooler temperatures and higher saturation for N_2O in the fully mixed (Figure 3. 42: red region; Table 3. 5).

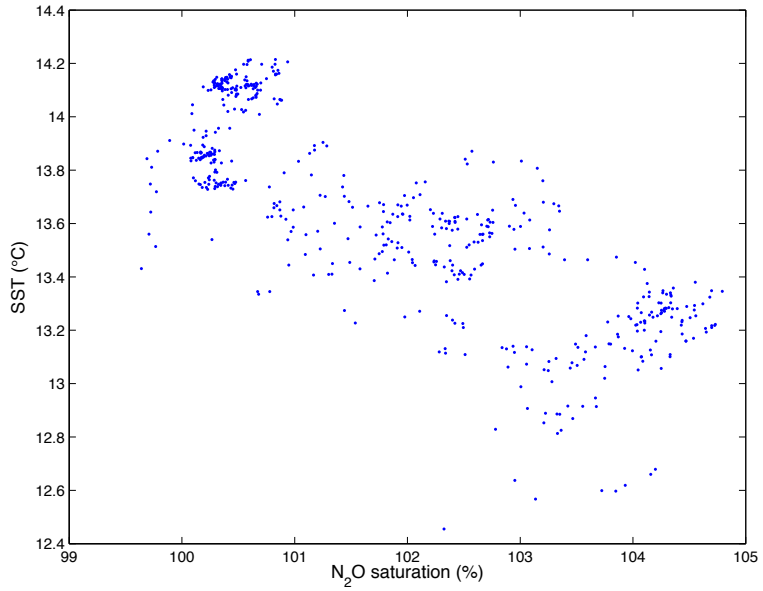

Figure 3.A 14: Negative correlation found between surface saturation for N_2O and SST in the cyan region off the SW coast of England (r=-0.80 p≤0.05) (Figure 3. 42; Table 3. 5).

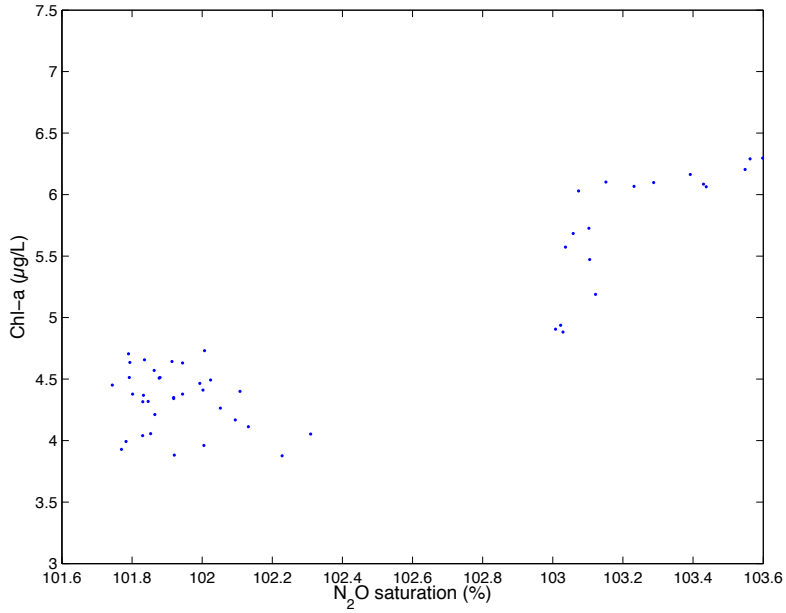

Figure 3.A 15: Rapid transition from a partially to fully mixed water column south of the Shetland Islands. The lower saturation for N_2O and lower surface concentration of chl-a were located in surface waters in the partially mixed region and the higher supersaturation for N_2O and higher chl-a concentrations found in the fully mixed (Figure 3. 42: red region; Table 3. 5).

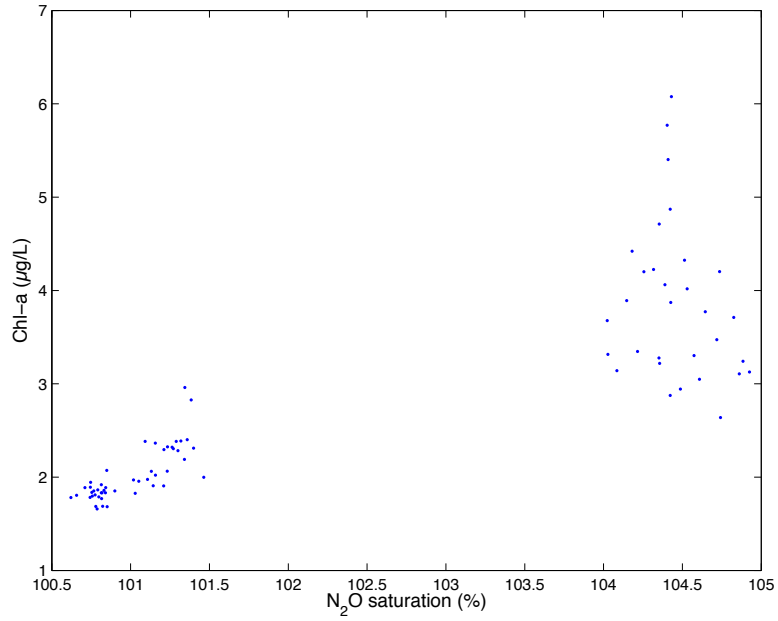

Figure 3.A 16: Rapid transition from a partially to fully mixed water column at St Georges Bank (Irish Sea). The lower saturation for N_2O and lower surface concentration of chl-a were located in surface waters in the partially mixed region and the higher saturation for N_2O and higher chl-a concentrations found in the fully mixed (Figure 3. 42: magenta region; Table 3. 5).

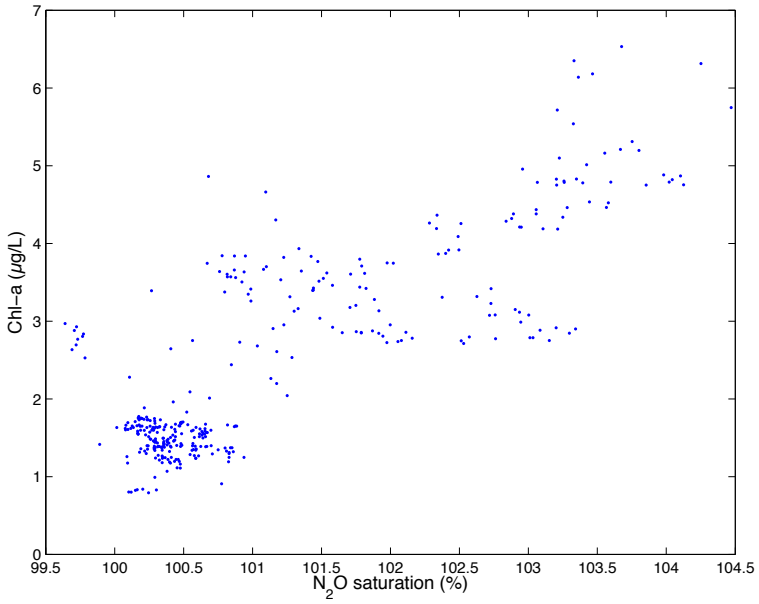

Figure 3.A 17: Positive correlation found between surface saturation for N_2O and surface chl-a concentration in the cyan region off the SW coast of England (r=0.83 p≤0.05) (Figure 3. 42; Table 3. 5).

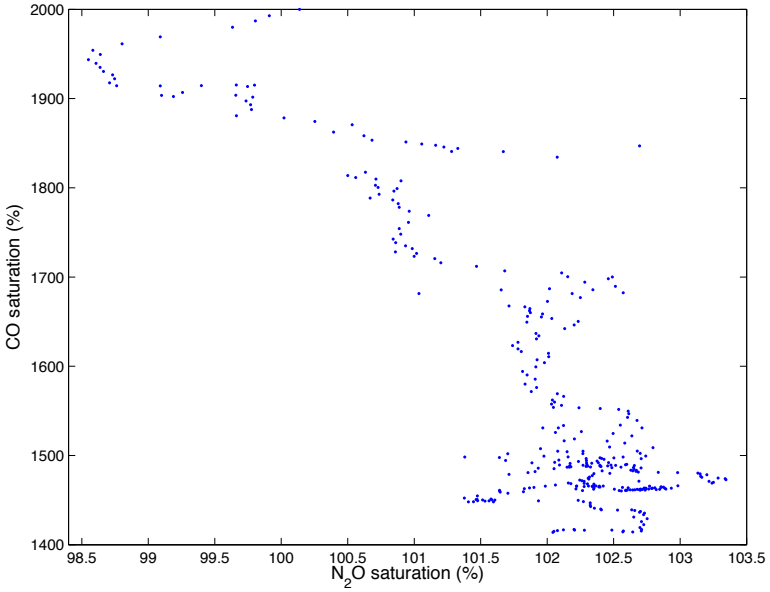

Figure 3.A 18: Negative correlation found between surface saturation for N_2O and CO in the green region off St Georges Bank (Irish Sea) (r=-0.80 p≤0.05) (Figure 3. 42; Table 3. 5).

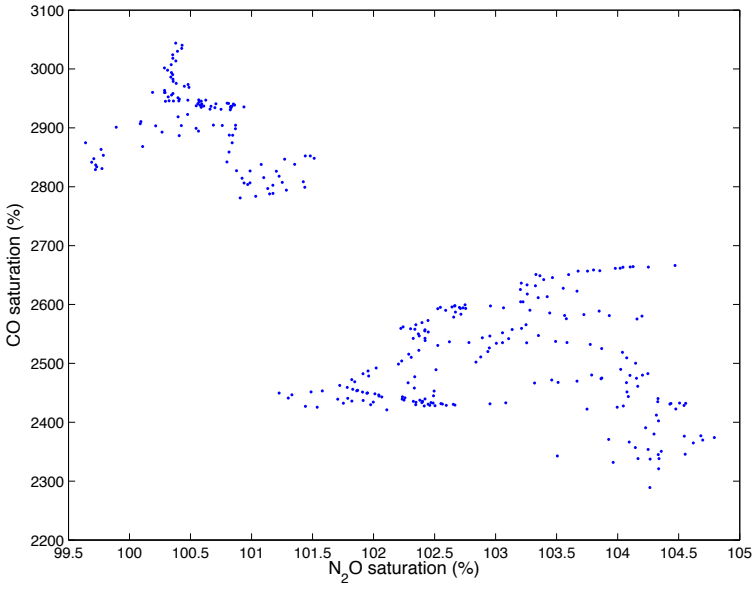

Figure 3.A 19: Rapid transition from a partially to fully mixed water column in the surface waters of the cyan region off the SW coast of England. The lower saturation for N_2O and higher saturation for CO were located in surface waters in the partially mixed region and the higher saturation for N_2O and lower saturation for CO found in the fully mixed (Figure 3. 42: cyan region; Table 3. 5).

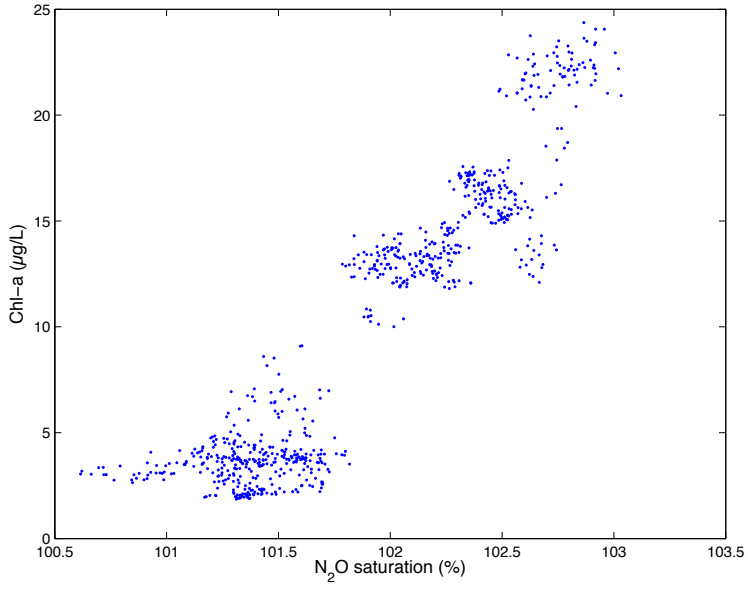

Figure 3.A 20: Positive correlation found between surface water saturation for N_2O and chl-a concentration in the green region (NE Atlantic) (r=0.93 p≤0.05) (Figure 3. 53; Table 3. 6).

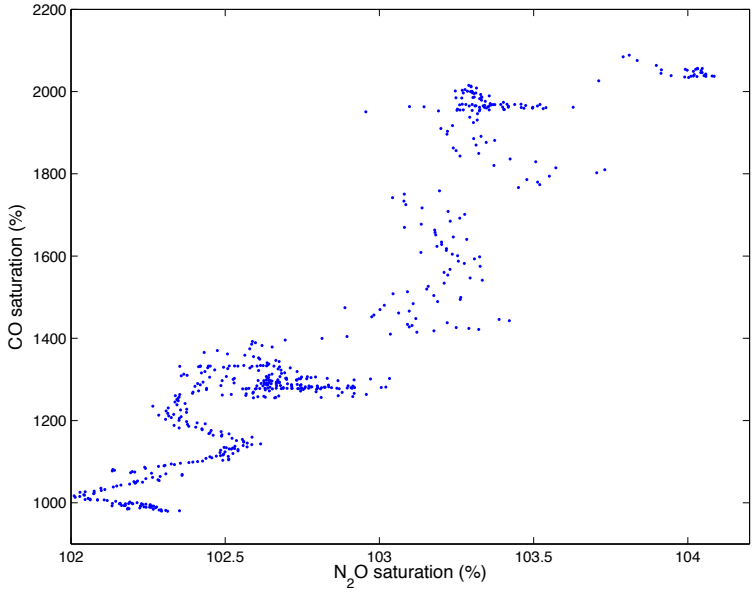

Figure 3.A 21: Positive correlation found between surface water saturation for N_2O and CO in the black region (NE Atlantic) (r=0.92 p≤0.05) (Figure 3. 53; Table 3. 6).

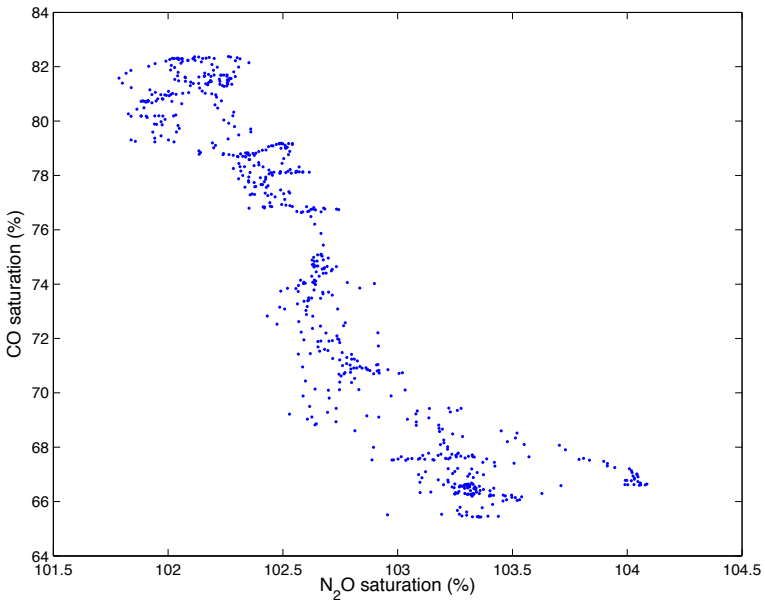

Figure 3.A 22: Negative correlation found between surface water supersaturation for N_2O and pCO_2 in the black region (NE Atlantic) (r=-0.91 p≤0.05) (Figure 3. 53; Table 3. 6).

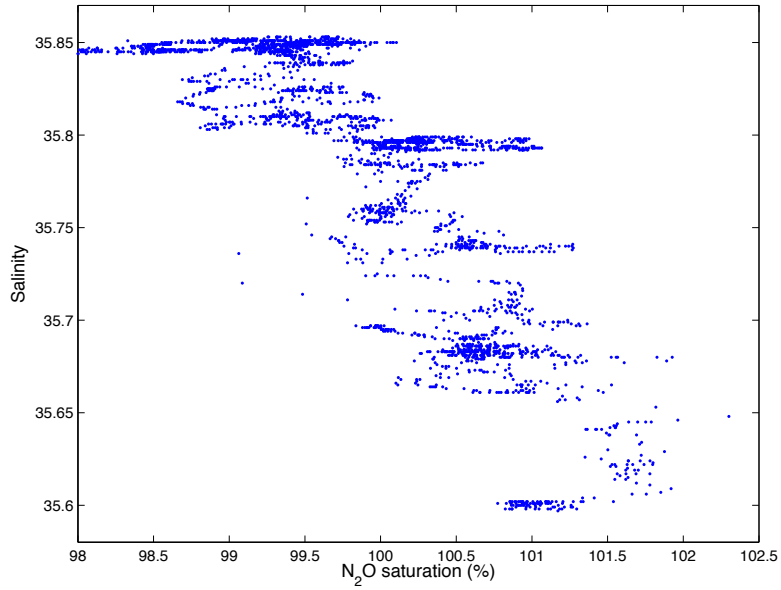

Figure 3.A 23: Negative correlation found between surface water saturation for N_2O and SSS in the red region of the Bay of Biscay (r=-0.78 p≤0.05) (Figure 3. 59; Table 3. 7).

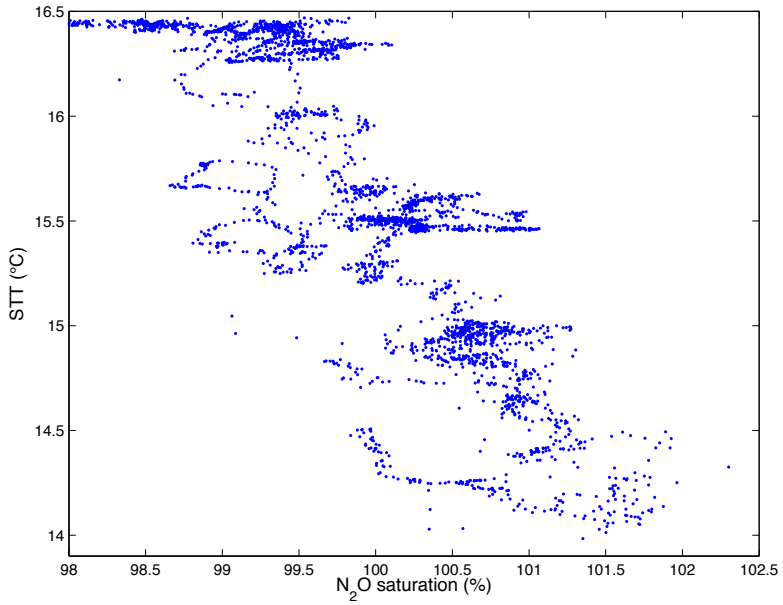

Figure 3.A 24: Negative correlation found between surface water saturation for N_2O and SST in the red region of the Bay of Biscay (r=-0.82 p≤0.05) (Figure 3. 59; Table 3. 7).

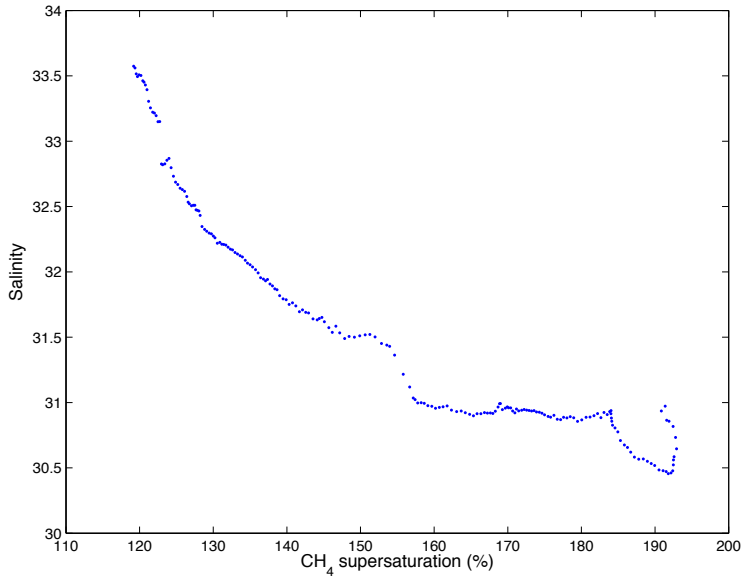

Figure 4.A. 1 A negative correlation found between surface water saturation for CH_4 and salinity in the magenta region of the Skagerrak (r=-0.94, p≤0.05) (Figure 4. 14; Table 4. 2).

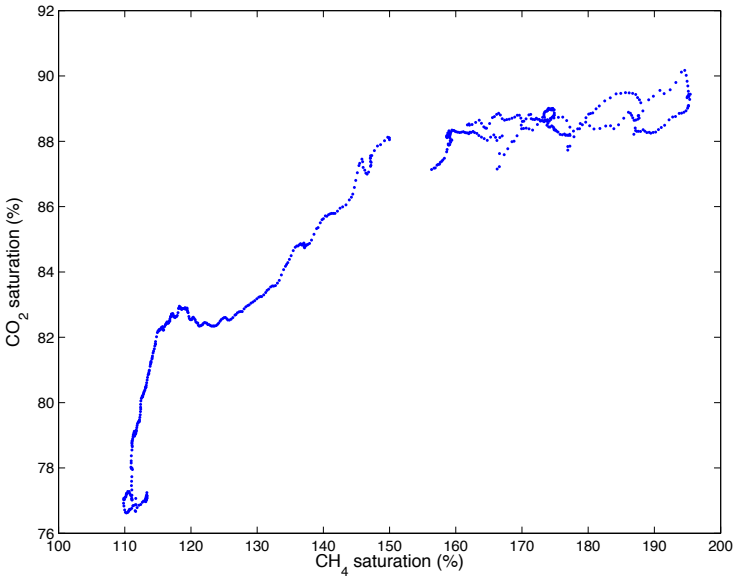

Figure 4.A. 2 A positive correlation found between surface water saturation for CH_4 and CO_2 in the green region of the Skagerrak (r=0.86, p≤0.05) (Figure 4. 14; Table 4. 2).

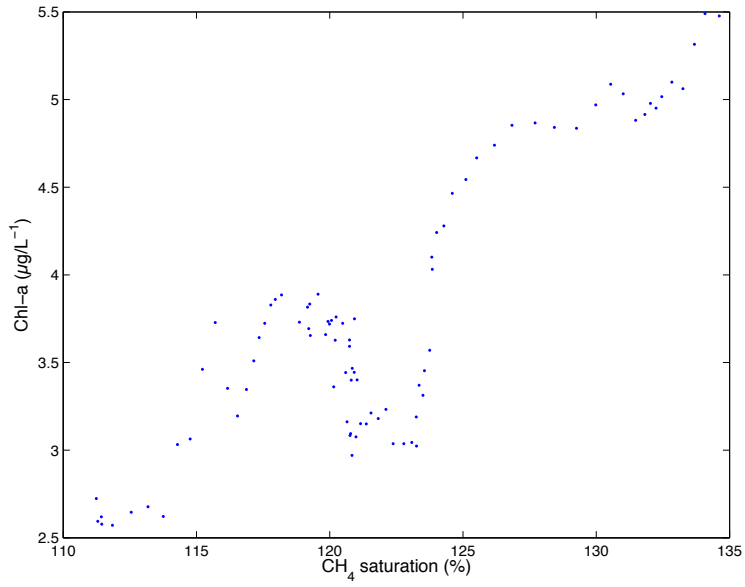

Figure 4.A. 3 A positive correlation found between surface water saturation for CH_4 and surface chl-a concentration in the blue region of the Skagerrak (r=0.87, p≤0.05) (Figure 4. 16; Table 4. 2).

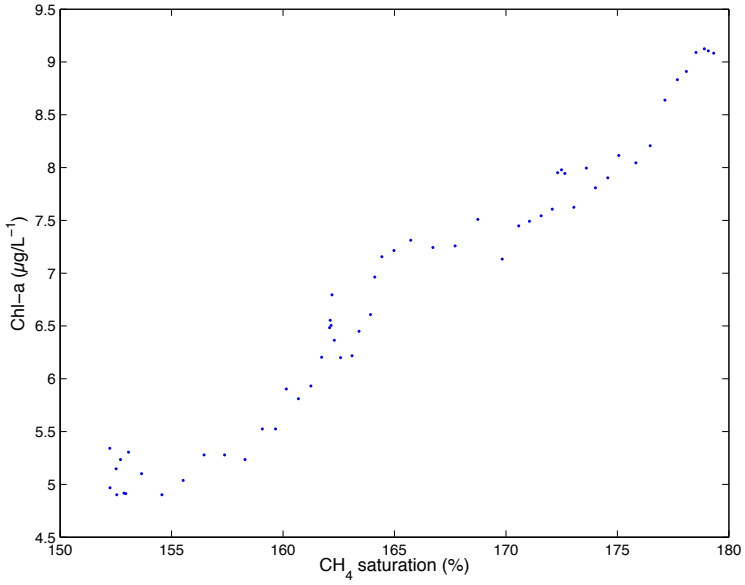

Figure 4.A. 4 A positive correlation found between surface water saturation for CH_4 and surface chl-a concentration in the red region of the Skagerrak (r=0.98, p≤0.05) (Figure 4. 16; Table 4. 2).

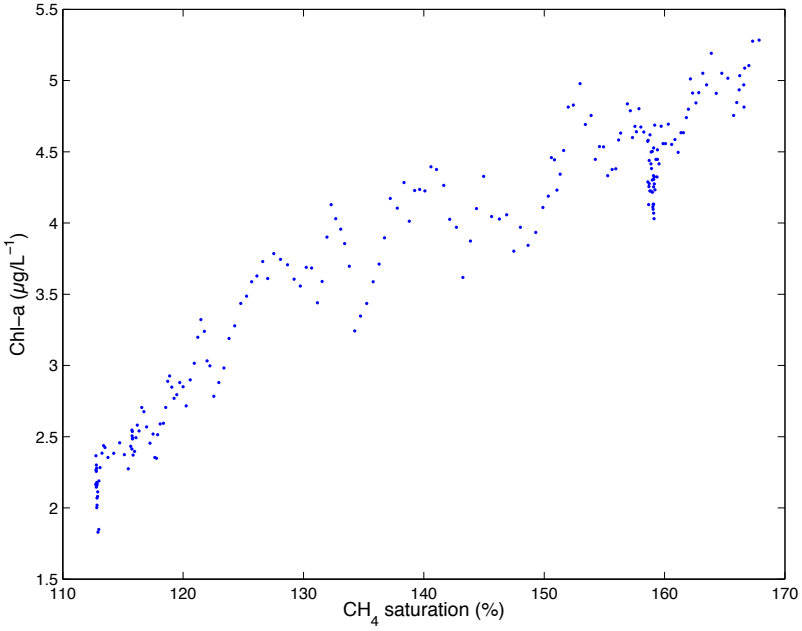

Figure 4.A. 5 A positive correlation found between surface water saturation for CH_4 and surface chl-a concentration in the green region of the Norwegian Trench (r=0.95, p≤0.05) (Figure 4. 16; Table 4. 2).

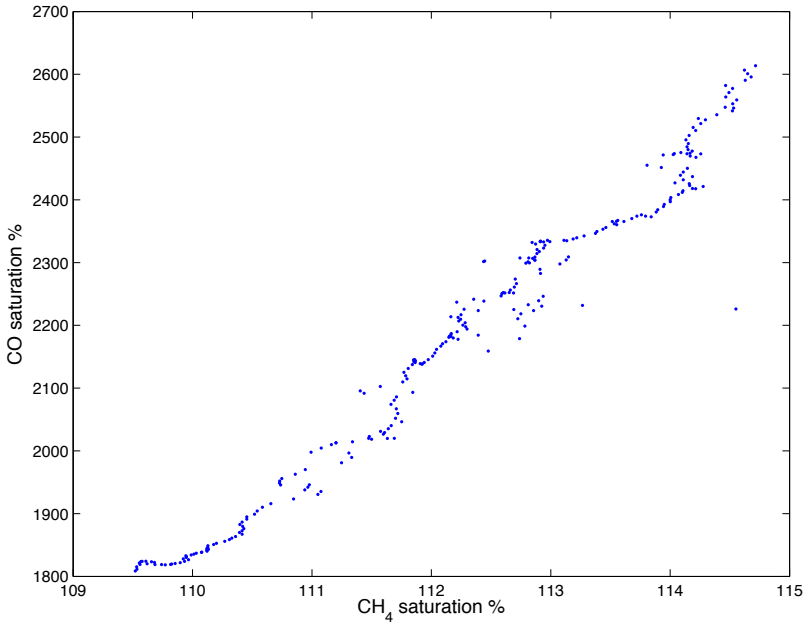

Figure 4.A. 6 A positive correlation found between surface water saturation for CH_4 and CO in the cyan region of the Skagerrak (r=0.96, p≤0.05) (Figure 4. 16; Table 4. 2).

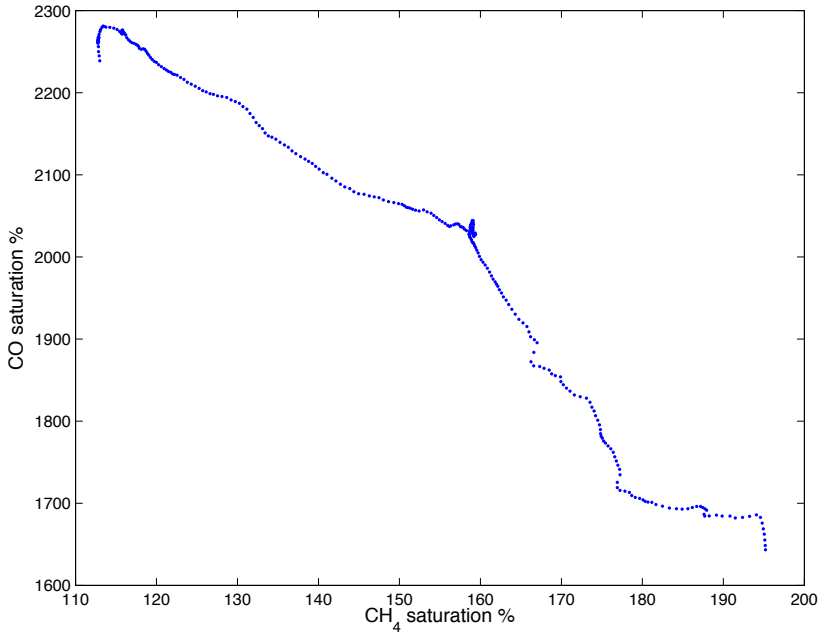

Figure 4.A. 7 A negative correlation found between surface water saturation for CH_4 and CO in the black and green region of the Norwegian Trench (r=-0.97, p≤0.05) (Figure 4. 16; Table 4. 2).

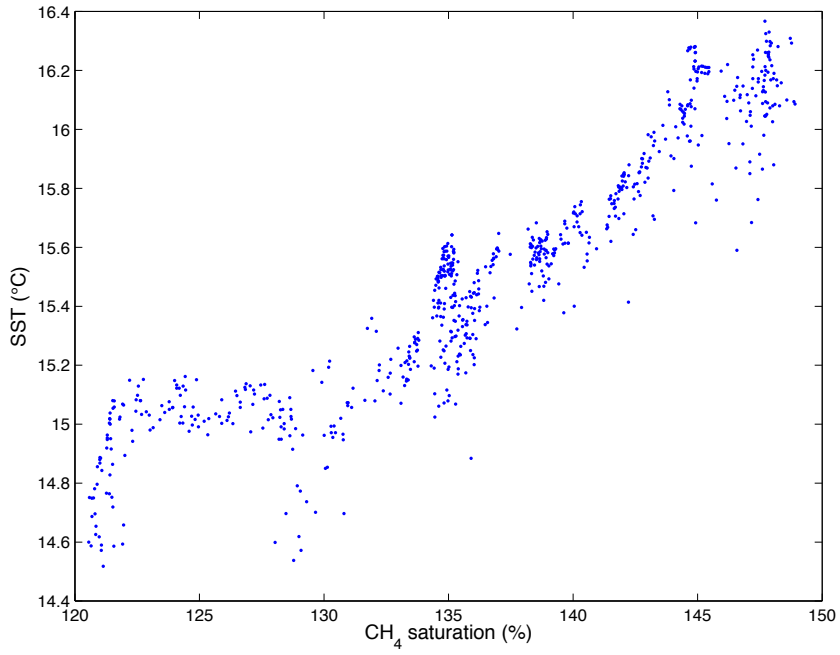

Figure 4.A. 8 A positive correlation found between surface water saturation for CH_4 and SST in the blue and green region of the southern/central North Sea (r=0.93, p≤0.05) (Figure 4. 22; Table 4. 3).

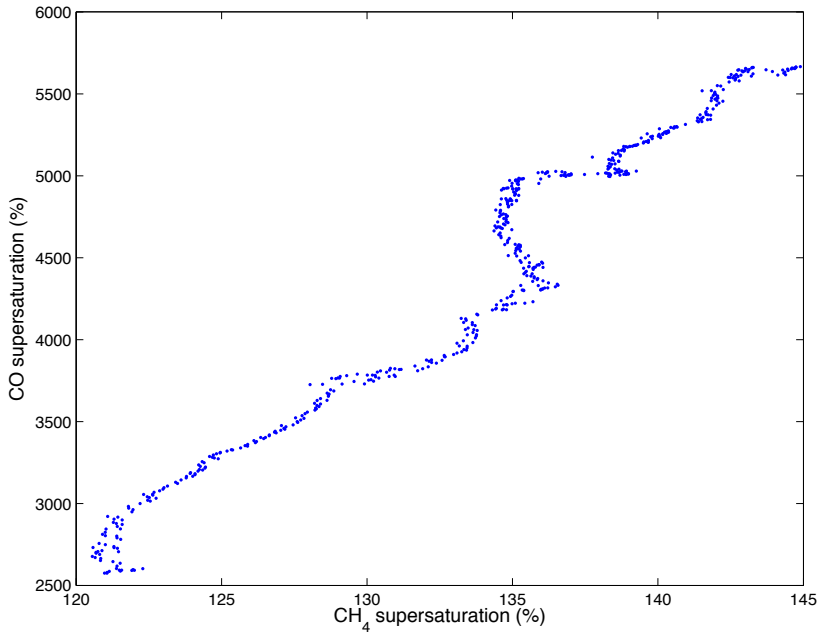

Figure 4.A. 9 A positive correlation found between surface water saturation for CH_4 and CO in the green region of the southern/central North Sea (r=0.98, p≤0.05) (Figure 4. 22; Table 4. 3).

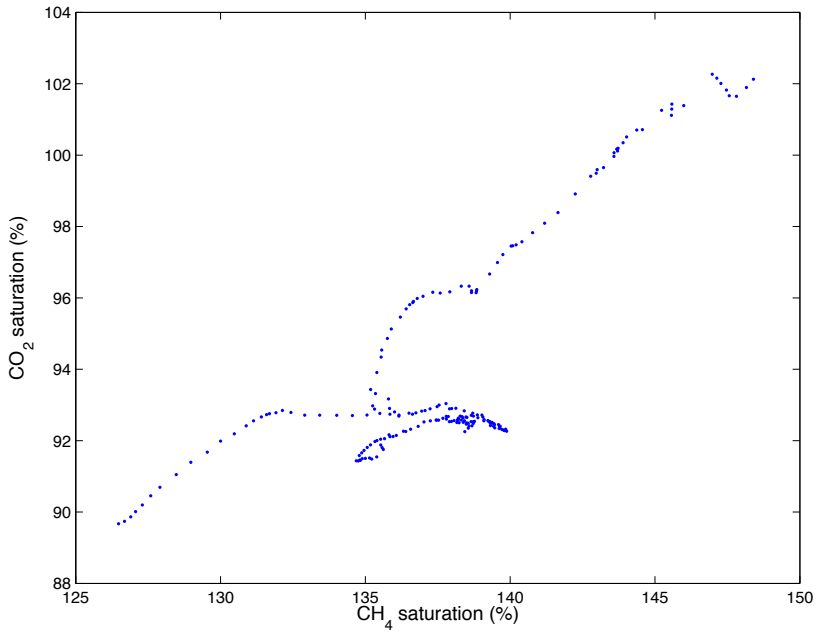

Figure 4.A. 10 A positive correlation found between surface water saturation for CH_4 and CO_2 in the magenta region of the southern/central North Sea (r=0.78, p≤0.05) (Figure 4. 22; Table 4. 3).

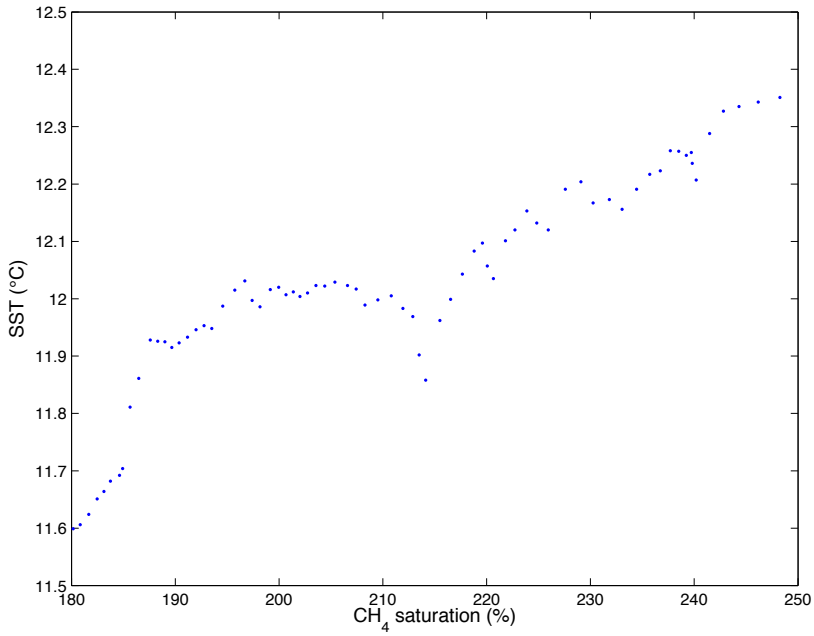

Figure 4.A. 11 A positive correlation found between surface water saturation for CH_4 and SST in the red region of the Irish Sea (r=0.66, p≤0.05) (Figure 4. 27; Table 4. 4).

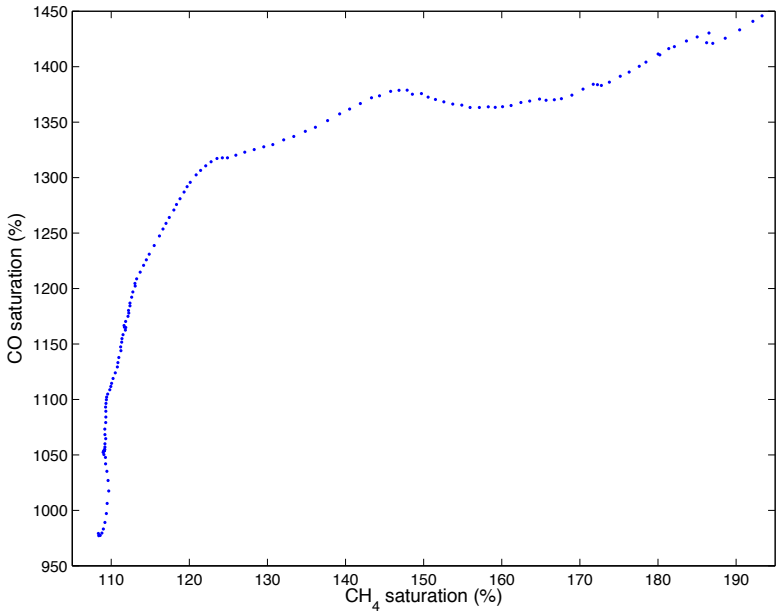

Figure 4.A. 12 A positive correlation found between surface water saturation for CH_4 and CO in the blue region of the Irish Sea (r=0.85, p≤0.05) (Figure 4. 27; Table 4. 4).

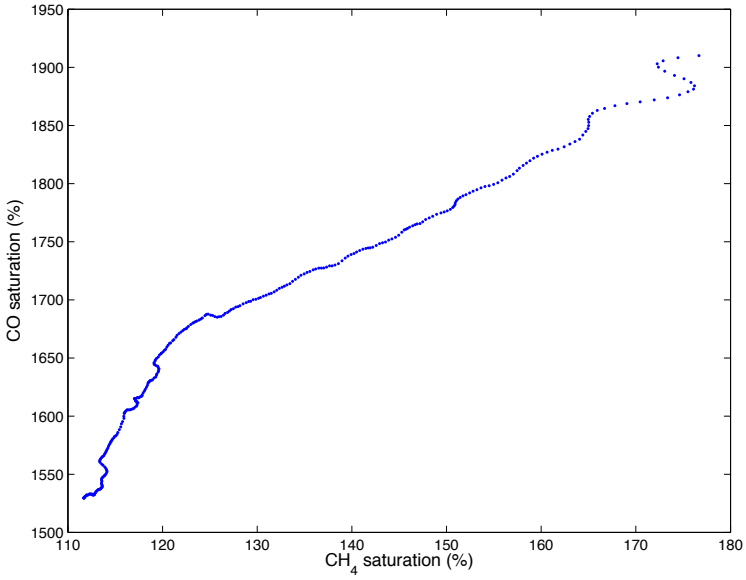

Figure 4.A. 13 A positive correlation found between surface water saturation for CH_4 and CO in the red region of the English Channel ($r=0.85$, $p \leq 0.05$) (Figure 4. 30; Table 4. 5).